SYNTHESIS AND PROPERTIES OF SOME RU(II) COMPLEXES CONTAINING TRIAZOLE LIGANDS

by

Renyi Wang

A Thesis presented to Dublin City University for the degree of Doctor in Philosophy.

Supervisor Dr. Johannes G. Vos.

School of Chemical Sciences
Dublin City University.

September 1991.

To my wife, Xia

Acknowledgements

First and foremost I wish to thank my supervisor, Dr. Han Vos, for his guidance, encouragement, and financial support during my postgraduate studies.

Thanks also to the following people:

Professor Russ Schmehl, for his guidance and support during my visit at Tulane University, New Orleans, U.S.A.;

All the academic staff in the Chemistry Department at DCU, in particular Professor Albert Pratt, Dr. Malcolm Smith and Dr. Conor Long for their help and for the use of the facilities;

Dr. Robert Forster for his generous help and instructions; Dr. Ronald Hage (Leiden University, The Netherlands) for synthesising most of the ligands used in this work and for his helpful advice; Dr. Jaap Haasnoot (Leiden) for his assistance with the 2D-COSY NMR measurements;

Ellie Ryan, Boris Fennema, Dr. Barbara Buchanan, Andrew Kelly, Alan Clarke, Andy Doherty, Helen Hughes, Fang Chen, Dr. Eileen Buckley, Dr. Michelle O'Conor, Dr. Donal Leech, Dr. Martin Telting-Diaz, Barry Crocock, Joe Bolger, Kieran McLoughlin, Aodhmar Cadogan, Carol Downey, Gerry Farrell, Dr. Paula Shearan, Dr. Graham Russell, and all other my fellow students at the Chemistry Department, DCU, for their help and friendship;

All the technical staff in the Chemistry Department: Teresa McDonnell, Mick Burke, Peig Ward, Ita Kinehan, Veronica Dobbyn, Fintan Keogh, Maurice Burke, Dawn Medforth, Hugh Gallagher, and Damien McGuirk for their assistance;

Delia Finnegan and Mamie Mulligan (DCU) for their help;

Dr. John Shaw (Tulane) for his time and help with the use of the laser and other equipment; Professor Mark Sulkes, Professor Andrew Waterhouse, Jianhua Liu, Arron Baba, Ronit Weigarden, Bill Lennon, Nancy Brady and Karen Bowers at Tulane for their help; Professor Max Roundhill and Professor Bill Alworth for access to the facilities at the Chemistry Department, Tulane University;

Dr. Mary Kelly-Vos for her kind help and for the proof reading of this thesis; Helen Hughes also for the proof reading;

Professor Dinyuan Gu, former President of Shanghai Institute of Electrical and Mechanical Engineering, China, not only for his instructions during my 7-year stay in the institute, but also for his help with obtaining my postgraduate opportunity at DCU;

My parents, my sister and brothers, for their encouragement and help;

Finally, my wife, Xia Chen, for her persistent encouragement, support and assistance.

This thesis has not been submitted as an exercise for a degree at this or any other university. Except as otherwise indicated, this work has been carried out by the author alone.

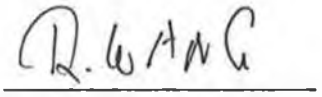

Renyi Wang

CONTENTS

Abstract.

Photophysical and photochemical properties of a series of Ru(II) complexes containing substituted 1,2,4-triazole ligands have been investigated. Photostability has been observed for a number of complexes containing triazoles. The photoreactivity for these complexes can be induced or inhibited by protonation or deprotonation of the triazole ring; Photoinduced linkage isomerism has been observed for the two isomers of $[Ru(bpy)_2(Hptr)]^{2+}$ (bpy = 2,2'-bipyridine; Hptr = 3-(pyridin-2-yl)-1,2,4-triazole). For $Ru(bpy)_2$ complexes containing pyrazyltriazole ligands, it is found that the nature of the emitting ^{3}MLCT state can be controlled by pH: when the triazole ring is changed from the protonated form to the deprotonated form, the LUMO is switched from bpy to pyrazyltriazoles. The emission lifetime for the two isomers of $[Ru(phen)_2(ptr)]^{+}$ (phen = 1,10-phenanthroline) is found to be much longer than their bpy- or dmb-based (dmb = 4,4'-dimethyl-2,2'-bipyridine) analogues and comparable to $[Ru(bpy)_3]^{2+}$. These phen-based two isomers are photostable. Significant oxygen quenching behaviour has been observed for these two isomers. Ru(II) complexes containing a pyridyltriazole ligand linked to a hydroquinone group have been synthesised and separated using semi-preparative HPLC. The compounds have been characterised using ^{1}H-NMR, UV-vis absorption, emission and electrochemistry. Preliminary photophysical studies show that for one of the coordination isomers, reductive quenching of the ^{3}MLCT state by the hydroquinone group is at best inefficient. For another isomer, where the hydroquinone group is coordinated, protonation results in an increase in emission lifetime, of which the value is much higher compared to the first isomer, where the hydroquinone is uncoordinated, and also longer compared to the corresponding dinuclear complex. Electrochemically induced proton transfer process has been observed for two Ru(II) complexes containing triazole ligands, where no external proton source is needed and the process can be most likely viewed as intramolecular.

Chapter I

Introduction: Natural and Artificial Photosynthesis

I.1 The natural photosynthetic process.

Photosynthesis is a process in which green plants and bacteria trap light energy and convert it into chemical energy [1]. It is no wonder that photosynthesis is of great importance to the humans as it produces the oxygen we breathe, as well as the oxygen we need to burn fuel. In addition, this biological process is the source of almost all our consumable energy. Coal, petroleum, natural gas, wood, and food all result from photosynthesis.

The energy content of the sunlight striking the surface of the earth is enormous, almost 7.2×10^{20} Kcal per year ——— roughly 25 times more than our proven resource of fossil fuel and uranium [2]. It is, of course, very attractive and very challenging to attempt to make more efficient use of solar energy through artificially built systems.

Artificial photosynthesis is a broad area, which includes several aspects such as photonitrogen fixation [3], photooxidation of water into O_2 [4], photoreduction of CO_2 into carbon hydrates [5], etc. However, photocleavage of water into H_2 and O_2 by solar energy is no doubt a most attractive strategy and has indeed become a main goal in the artificial synthesis studies [6]. Research on the photochemical molecular devices can also be considered as a

part of the artificial photosynthesis studies [7].

The work described in this thesis will deal with the synthetic inorganic and photoinorganic chemistry of ruthenium diimine complexes, an area of research which was aimed initially at the potential application of ruthenium complexes in the photosplitting of water. Ruthenium diimine complexes have been accredited as "an inorganic substitute for Chlorophyll-α in in-vitro photosynthesis" [8]. In the past few years this area has been extended to the study of chromophore-quencher or electron donor-acceptor assemblies [5, 7]. Most of the efforts have been concentrated on understanding the intramolecular energy transfer or electron transfer processes, which represent a key step in the understanding and mimicking of the natural photosynthesis [5, 7]. Research on natural photosynthesis and on artificial photosynthesis are so closely related that it is necessary to first give a brief description, on the nature on the photosynthetic processes.

I.1.1 Photosynthetic reaction centres.

Photosynthesis is primarily a photochemical process. The photochemistry of photosynthesis begins in complexes called photosynthetic reaction centres. These reaction centres have been used as model systems to study the fundamental processes by which plants and bacteria convert and store solar energy

as chemical free energy.

I.1.1.1 Green plants and cyanobacteria: PS I and PS II.

In green plants and cyanobacteria, photosynthesis occurs in two systems, each of which contains a different reaction centre, working in series. In one of them, known as photosystem I (PS I), oxidised nicotinamide adenine dinucleotide phosphate ($NADP^+$) is reduced to NADPH for use in a series of dark reactions called the Calvin cycle [9], in which carbon dioxide is converted into useful fuels such as carbohydrates and sugars. In the other half of the photosynthetic machinery of green plants, called photosystem II (PS II), water is oxidised to produce molecular oxygen [10].

I.1.1.2 Photosynthetic bacteria.

A different form of photosynthesis occurs in photosynthetic bacteria, which typically live at the bottom of ponds and feed on organic debris. Two main types of photosynthetic bacteria exist: purple and green. Neither type liberates oxygen from water. Instead, the bacteria feed on organic media or inorganic materials, such as sulfides, which are easier to reduce or oxidise than carbon dioxide or water [1].

I.1.2 Recent progress in studying photosynthetic reaction centres.

I.1.2.1 The X-ray structure of Rps. viridis.

The most exciting progress made in photosynthesis in the last decade was that the X-ray structure of a purple photosynthetic bacterium, Rhodopseudomonas (Rps.) viridis, was solved in 1984 [11]. It was also the first time that the complete structure of a membrane-bound protein was obtained in three dimensions. The breakthrough in determining the structure of Rps. viridis, provided a basis for study of the mechanism, by which solar energy is captured and converted.

The structure of the reaction centre in Rps. viridis (Fig. I.1) [11], like that of all other photosynthetic reaction centres [2], consists of two main systems: the protein and the donor-acceptor complex ("special pair"). The protein part is further made up of three distinct subunits. The donor-acceptor complex holds four bacteriochlorophylls, two bacteriopheophytins, two quinones and one iron atom in such a fashion that the whole structure shows approximately C_{2v} symmetry. The two quinones serve as electron acceptors involved in the beginning events of the photosynthesis, a proton-coupled electron transfer process (vide infra). This is also one of the reasons why synthetic systems, especially organic systems, designed for electron transfer studies often

contain quinones as excited state quenchers or electron acceptors [12-14].)

I.1.2.2 The electron transfer process in photosynthetic reaction centres in photosynthetic bacteria.

The initial event in the photosynthetic reaction centres during photosynthesis is the absorption of a photon, which subsequently induces intramolecular charge separation and electron transfer. The development of fast speed optical techniques (pico- or femto-second laser spectroscopy), together with other methods such as EPR (electron paramagnetic resonance) [15] and Stark effect spectroscopy [16-17], have made possible the detection of such very fast charge separation and migration processes. Several synthetic systems have also been prepared in efforts to elucidate the mechanism of the electron transfer in such biological systems. The beginning events in photosynthetic reaction centres can be described as follows [1-2, 12]:

During photosynthesis, sunlight is first collected by antenna, chlorophyll molecules, which pass the excitation along to the so-called "special pair", a bacteriochlorophyll dimer in the donor-acceptor complex. This excitation results in electron transfer from the special pair (electron donor), past a bacteriochlorophyll monomer, to a bacteriopheophytin intermediate about 11 Å away, a process that takes about

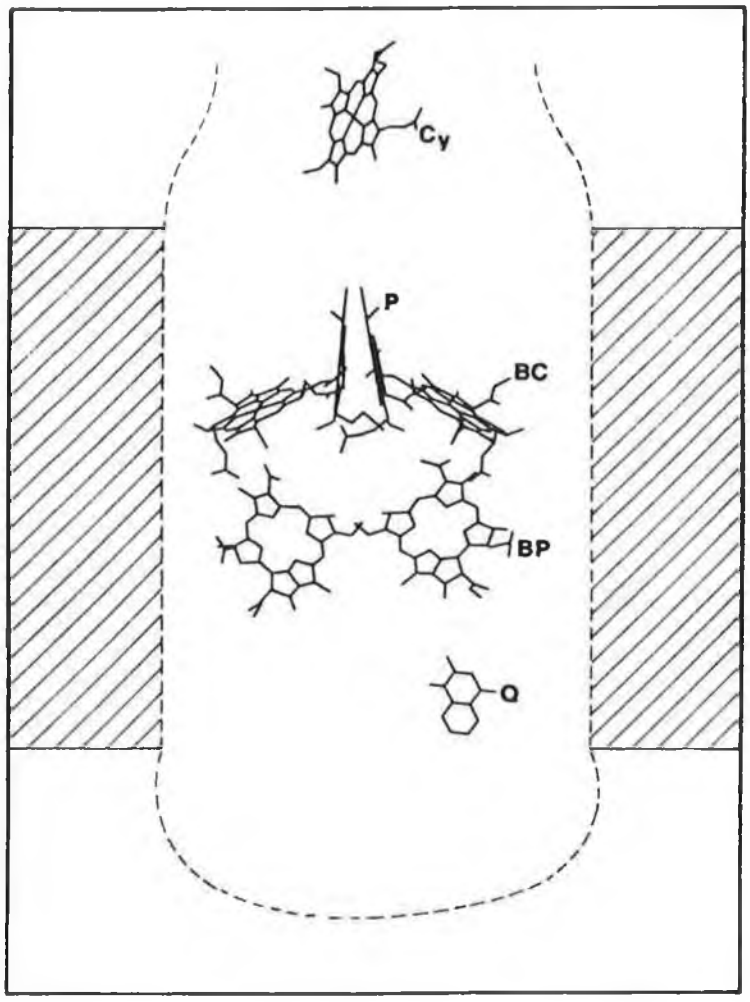

Fig. I.1 Arrangements of the chromophores in the reaction centre of Rps. Viridis, including bacteriochlorophyll special pair (P), bacteriochlorophyll momoner (BC), the bacteriopheophytin (BP), the quinone (Q), and the nearest heme group of the cytochrome (Cy). The shaded area and the dashed line schematically represent the membrane and the envelope of the protein matrix, respectively [7].

2.8 picoseconds. The electron is then transferred from the bacteriopheophytin to a ubiquinone molecule (terminal acceptor) and pumped across a phospholipid membrane in the cell [2, 12]. The reduced ubiquinone picks up two protons from the cytoplasm. Thus, the beginning event in the photosynthetic reaction centres is actually a proton-coupled electron transfer process.

Despite the progress made in the last ten years, the mechanism of the photosynthetic reaction centres is not yet completely understood. A most lively controversy which developed among researchers has been about how the electron is transferred from the special pair to the bacteriopheophytin in the reaction centre during the initial 2.8 picoseconds. This dispute, which has not yet been resolved, focussed on the role of the intervening bacteriochlorophyl monomer, which has an edge-to-edge distance of about 11 Å, and is located between the special pair and bacteriopheophytin [2, 12].

Electron transfer theory predicts that it would take 1000 x 2.8 picoseconds or even longer for an electron to travel 11 Å in vacuo [2, 12, 17]. In the photosynthetic centre, the bridging monomer and protein lie between the special pair and bacteriopheophytin. This intervening material must be somehow responsible for the rapid electron transfer. However at present the available theoretical models and the

experimental evidence can not unambiguously explain this very fast initial electron transfer process. There are a few other key questions to be answered such as why photosynthesis can operate with good quantum yield even at extremely low temperature, say, 2K or even less. The initial step of photosynthesis proceeds with a quantum yield of near unity (>0.95) [2]. The understanding of these questions will be, of course, extremely important for building up artificial systems which can operate in high quantum efficiency. It is expected that genetic engineering and chemical modification techniques will help in specifically defining and altering the structures of the photosynthetic reaction centres so that a complete elucidation of the charge separation and transfer processes can be eventually achieved.

I.1.2.3 Photosystem I and Photosystem II.

The structure of the PS II is somewhat similar to that of the synthetic reaction centre in purple photosynthetic bacteria. As mentioned in I.1.2.1 and I.1.2.2, significant progress has been made in the structure determination as well as the electron transfer process in purple photosynthetic bacteria, and thus many properties of the PS II reaction centre have been deduced in parallel. By contrast, the PS I reaction centre appears as a rather singular part, without any well known counterpart. Its equivalent can perhaps be found in the poorly-known green sulfur bacteria. Nevertheless, as in

all other photosynthetic centres, absorption of photons by PS I also induces the electron excitation of the pigments, which is then followed by a charge separation and transfer process [18-19].

Work carried out on Photosystem II, has shown that manganese is specially required for water oxidation to produce O_2 and that four manganese ions per PS II are required to achieve optimal rates [10].

If a dark-adapted sample of PS II is illuminated by short intense flashes of light, so that a single charge separation event takes place in each reaction centre per flash, the yield of O_2 is found to be maximal on the third flash and to oscillate with a periodicity of four thereafter [20-21]. To account for this result, Kok and co-workers [22] proposed that PS II cycles through five states during flash illumination. These intermediate oxidation states are referred to as S_i states ($i = 0 - 4$) with the subscript denoting the number of oxidising equivalents accumulated. A large body of evidence now supports Kok's model [23-25].

The structure of the manganese complex in PS II remains uncertain and the oxidation states of manganese in each of the S states remains unclear. Experimental results from EPR and EXAFS (extended X-ray absorption edge fine structure) have suggested an exchange-coupled tetranuclear complex in PS

II might be the most probable arrangement of the four manganese ions [10]. For instance, analysis of the EXAFS data of manganese in both the S_1 and S_2 states show a 2.7 A Mn-Mn distance [26-29], and indeed the Mn-Mn distance of about 2.7 A is found in numerous structurally characterised di-μ-oxo-bridged binuclear [30-31] and tetranuclear [32] manganese complexes. Different mechanisms have been proposed by several groups for oxygen evolution based on synthesised model compounds [23-24, 33-36]. Further biophysical studies as well as synthetic work are certainly needed to test the proposed mechanisms.

I.1.3 Concluding remarks.

The photosynthesis research consists of several independent areas which strongly influence each other. The common feature of the different photosynthetic reaction centres is that the beginning event is a photoinduced electron transfer process. The understanding of such very efficient charge separation and transfer processes is essential for the construction of artificial photosynthetic systems. On the other hand, research on natural photosynthesis is an area where chemistry plays an important role. Synthetic model compounds and the study of the photoinduced electron transfer and photochemical reactivity on these compounds have been useful for the elucidation of the working mechanisms in the natural photosynthetic systems.

I.2 The chemistry of Ru(II) complexes: towards artificial photosynthesis.

Research on artificial photosynthesis aims to design components which can mimic the natural photosynthetic system and even modify the properties of the latter in order to achieve the desired high efficiency conversion from solar energy into chemical energy. A purely synthetic system, should be able to offer the prospect of much greater flexibility and higher solar efficiencies, together with the possibility of tuning the chemistry for production of specific fuels and chemicals.

I.2.1 Photocleavage of water into H_2 and O_2.

As mentioned at the beginning of this chapter, photocleavage of water has been the main goal in the artificial photosynthesis area. This is simply because H_2 is an energy rich fuel, can be safely stored adsorbed to various porous metals, can be easily handled, and burns cleanly to regenerate the starting material without creating severe environmental polution problem [6]. To achieve such a solar energy driven cycle, first of all a photosensitiser is needed to harvest the photons emitted from the sun, as water itself has no electronic transition in the visible or near ultraviolet region. Secondly, the absorption of solar energy has to lead to an efficient charge separation and charge

transfer process, in order to produce the excited-state energy-enriched redox species. This strong redox species can be in turn coupled to other suitable redox couples or catalysts, to reduce water into H_2 and, ideally, oxidise water into O_2 simultaneously.

It can be easily seen that the whole strategy for photocleavage of water described here, is similar to the process found in the photosynthetic reaction centres. The so-called photosensitisers, function exactly the same as chlorophylls. The subsequent very fast charge separation and transfer process, needed to produce long-lived, energy enriched species, has already been ideally performed in the natural photosynthetic systems.

The light induced generation of strong oxidising/reducing agents can be described as

$$S \xrightarrow{h\nu} S^* \qquad \text{(I.1)}$$

$$S^* + A \longrightarrow S^+ + A^- \qquad \text{(I.2)}$$

or

$$S^* + A \longrightarrow S^- + A^+ \qquad \text{(I.3)}$$

where S is the photosensitiser, and A is a redox counterpart which can either be a stronger oxidant (as in eq. I.2) or a stronger reductant (as in eq. I.3) compared to the photoexcited S, S^* [37].

The photogenerated oxidising/reducing agents can then be used in the decomposition of water. For instance, if the reaction in eq. I.1 is achieved, then the next desired reactions are:

$$4S^{+} + 2H_2O \text{ ------> } 4S + 4H^{+} + O_2 \qquad (I.4)$$

$$2A^{-} + 2H_2O \text{ ------> } 2A + 2OH^{-} + H_2 \qquad (I.5)$$

The photocleavage of water involves a proton-coupled multielectron transfer process, and can be divided into two half-cell reactions:

$$H_2O + e^{-} \text{ -----> } 1/2\ H_2 + OH^{-} \qquad (I.6)$$

$$1/2\ H_2O \text{ -----> } 1/4\ O_2 + H^{+} + e^{-} \qquad (I.7)$$

At pH = 0, the reaction for hydrogen reduction has an electrochemical potential 0 V while for oxidation of water into oxygen the potential is 1.23 V (vs. normal hydrogen electrode, NHE) [38]. Obviously, any reducing agent which is able to reduce water should have a reduction potential more negative than 0 V vs. NHE at pH = 0. Similarily, for oxidising water, the oxidising agent should have an oxidation potential more positive than 1.23 V vs NHE at pH = 0.

I.2.2 Photophysical and photochemical properties of $[Ru(bpy)_3]^{2+}$.

As described in I.2.1, ideally, the principle light absorbing species will have the following qualities:

1. it can absorb an appreciable fraction of the solar spectrum that reaches the earth.
2. it possesses an excited lifetime of sufficient length to allow bimolecular photoprocesses to compete with all other deactivation processes, and
3. it can undergo excited-state electron transfer reactions with suitable quenching species.

Although synthetic porphyrins have been used as photosensitisers in artificial systems [7, 38-39], the most extensively studied photosensitisers during the last 15 years have been the complex $[Ru(bpy)_3]^{2+}$ (bpy = 2,2'-bipyridine), and its derivatives and analogues [5, 8, 37-38, 40-41].

$[Ru(bpy)_3]^{2+}$ fulfils the requirements for a photosensitiser quite well. Firstly, along with having an intraligand π ---> π^* electronic absorption centered around 280 nm, $[Ru(bpy)_3]^{2+}$ has a broad electronic transition in the visible region around 450 nm. Secondly, the excited state of $[Ru(bpy)_3]^{2+}$ is sufficiently long

(680 ns in water at room temperature). Thirdly, $[Ru(bpy)_3]^{2+}$ has adjacent ground-state redox forms, e.g., $[Ru(bpy)_3]^{+}$ and $[Ru(bpy)_2]^{3+}$. Furthermore, $[Ru(bpy)_3]^{2+}$ becomes both a stronger oxidant and a better reductant in the excited state, which can undergo energy quenching or electron transfer quenching (either oxidative or reductive). For instance, oxidative quenching by paraquat (PQ^{2+}) [5],

$$[Ru(bpy)_3]^{2+} \text{ -----> } [Ru(bpy)_3]^{2+*} \quad (I.8)$$

$$[Ru(bpy)_3]^{2+*} + PQ^{2+} \text{ -----> } [Ru(bpy)_3]^{3+} + PQ^{+} \quad (I.9)$$

$$[Ru(bpy)_3]^{3+} + PQ^{+} \text{ -----> } [Ru(bpy)_3]^{2+} + PQ^{2+} \quad (I.10)$$

provides a basis for the conversion of visible light energy into a transiently stored redox pair. The above mentioned properties of $[Ru(bpy)_3]^{2+}$ make it an attractive candidate for a solar energy transfer system. An extensive ground-state synthetic chemistry is available to prepare families of related complexes to optimise the photophysical properties.

The successful utilisation of $[Ru(bpy)_3]^{2+}$ and related complexes in a practical energy conversion system relies on the understanding of their properties, especially, in the excited states. In 1959, the emission from $[Ru(bpy)_3]^{2+}$ was firstly discovered by Paris and Brandt [42]. The possibility for $[Ru(bpy)_3]^{2+}$ to undergo excited state

quenching processes by using different quenchers was first reported by Adamson's group [43-44]. The results indicate the potential use of this complex in an energy conversion system. The assignment of the electronic absorption and emission spectra, has been the subject of a long controversy [41, 45]. At present it is generally agreed that for $[Ru(bpy)_3]^{2+}$ the population and decay of the excited-states involve several processes, as described in Fig. I.2.

$[Ru(bpy)_3]^{2+}$ has a ground state electronic configuration of $d\pi^6$ (t_{2g} in O_h symmetry) [41]. The absorption spectrum of $[Ru(bpy)_3]^{2+}$ exibits an intense absorption band at 450 nm with a molecular extinction coefficient (ϵ) of 14600 $M^{-1}cm^{-1}$, which has been assigned to a metal-to-ligand charge transfer (MLCT) transition [45]:

$$\underset{(d\pi^6)}{[Ru^{II}(bpy)_3]^{2+}} \text{ -----> } \underset{(d\pi^5)(\pi^*)^1}{[Ru^{III}(bpy)_2(bpy^{\cdot -})]^{2+*}} \quad \text{(I.11)}$$

This electron transition state is largely singlet in character, but fast intersystem crossing (ISC) occurs from a singlet (^{1}MLCT) to a triplet state (^{3}MLCT) with an efficiency of unity [45]. Emission from the triplet state to the ground state (k_r) or radiationless deactivation (k_{nr}) can take place [41]. Another deactivation pathway is population of the metal centered (^{3}MC) excited states,

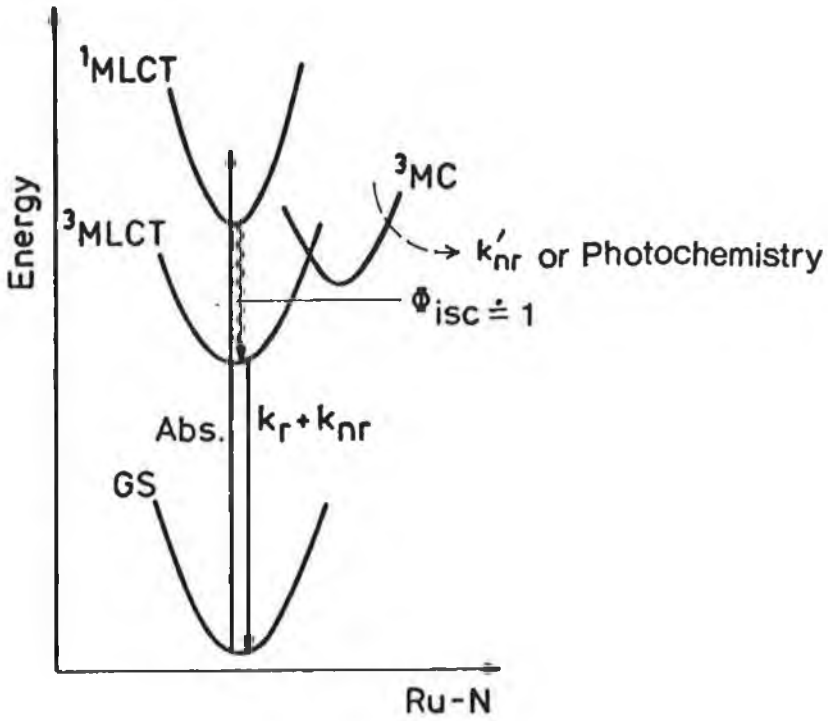

Fig. I.2. Photophysical decay pathway of $[Ru(bpy)_3]^{2+}$.

where the excited electron is pumped into Ru(II) centered antibonding orbitals (e_g^* in O_h symmetry), as described in eq. I.12:

$$(d\pi^5)(\pi^*)^1 \text{ -----> } (d\pi^5)(d\pi^*)^1 \qquad \text{(I.12)}$$
$$^3\text{MLCT} \qquad\qquad ^3\text{MC (d-d)}$$

The population of the ^{3}MC state will cause a distortion of the electronic configuration and, as a consequence, gives rise to either radiationless deactivation (k_{nr}') or to photodecomposition of the complex [41, 45].

It should be pointed out that the emitting state (^{3}MLCT) illustrated in Fig. I.2 for $[Ru(bpy)_3]^{2+}$ (as for its analogues) is actually a composite of at least four states [50-52]. This has been supported by molecular orbital calculations as well as evidenced by temperature dependent life time measurements. The four low lying states share a common $(d\pi)^5(\pi^*)^1$ electronic configuration, but they are mixed to different extents with the lowest excited singlet states (^{1}MLCT). The energy levels and decay characteristics of these four emitting states are different. The energy spacings among the three lowest states are small (10-100 cm^{-1}) so that they can be populated thermally with a large probability and can be equilibrated at room temperature (Boltzman equilibrium) [41, 45, 46-48]. At room temperature, photophysical properties can be treated , to a

good approximation, as arising from a single emitting state. This 'single state', as illustrated in Fig. I.2 (^{3}MLCT), has therefore the averaged properties of the three components. The energy gap to the fourth state is larger ($\doteq$600 cm^{-1} above the lowest state). Because of its greater singlet character (due to larger spin-orbit coupling), the fourth emitting state has a considerabely shorter lifetime [52]. As mentioned earlier, at room temperature the ^{3}MC state can be thermally populated and, as a result, the transition from the low-lying emitting states to this fourth emitting state is completely masked. However, direct evidence was obtained for the existence of the fourth emitting state from temperature dependent emission polarisation experiments [49]. The existence of the high lying emitting state and the ^{3}MC state and their relationship will be discussed in more detail in Chapter IV.

$[Ru(bpy)_3]^{2+}$ has a rich redox chemistry in the ground state. One electron can be removed from the t_{2g} orbital of Ru(II) (oxidation). The empty π^* orbitals of the ligand can receive up to three electrons (reduction). Upon photoexcitation, it becomes a stronger oxidant and also a better reductant. The excited state redox potentials can be estimated from ground state potentials and emission energy [45]:

$$E^{0'}[Ru(bpy)_3^{2+*/+}] = E^{0'}[Ru(bpy)_3^{2+/+}] + E_{em} \quad (I.13)$$

$$E^{0'}[Ru(bpy)_3^{3+/2+*}] = E^{0'}[Ru(bpy)_3^{3+/2+}] - E_{em} \quad (I.14)$$

The excited-state potentials can also be directly measured by electron transfer quenching experiments, provided that the formal potentials of the quenchers are known.

The redox properties of $[Ru(bpy)_3]^{2+}$ in the ground state and excited state are [41]:

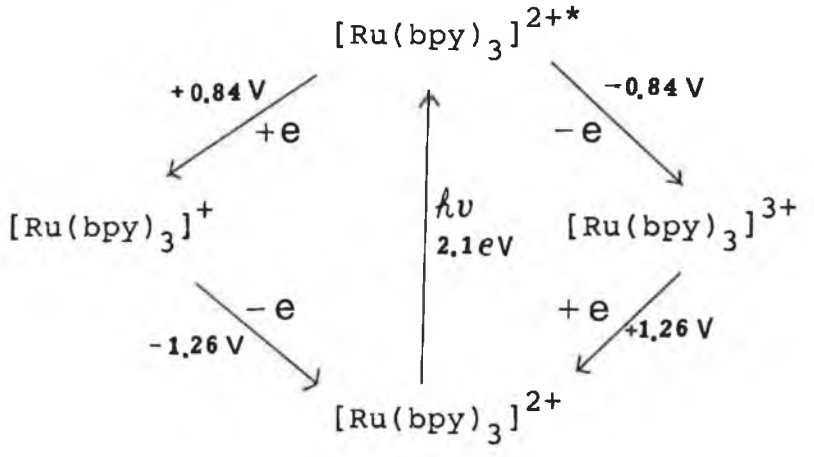

Fig. I.3 Ground-state and excited-state redox properties of $[Ru(bpy)_3]^{2+}$ (V vs. SCE) [41].

In the excited state, $[Ru(bpy)_3]^{2+}$ should be able to either oxidise water into O_2 or reduce water into H_2 thermodynamically. For practical applications, kinetic problems have to be considered and often an extra electron donor or acceptor with suitable electrochemical potential is coupled to $[Ru(bpy)_3]^{2+*}$, in order to achieve H_2 and/or O_2 production from water. One of the schemes proposed by Gratzel et al. is shown in Scheme I for

simultaneous production of H_2 and O_2 [50]:

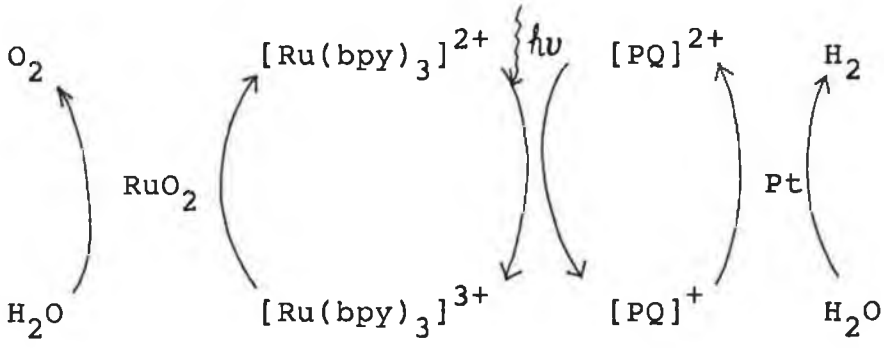

Scheme I Simultaneous catalytic photo-decomposition of Water into H_2 and O_2.

I.2.3 Synthetic design and tuning of the photophysical and photochemical properties of the Ru(II) complexes.

The photophysical and photochemical properties described in section I.2.2 have shown that $[Ru(bpy)_3]^{2+}$ is not an ideal photosensitiser for the photocleavage of water. The main drawback of this complex is that its ^3MC level can be easily populated at room temperature. Population of the d-d state provides an alternative pathway for the decay of the emitting states. Furthermore, ligand loss can be induced, since occupation of an excited electron in the metal centered antibonding orbital (e_g^*) leads to a large distortion of the electronic configuration [45].

As the ^3MC (d-d) state is normally populated from the ^3MLCT state, one approach to avoid the photochemical

lability is to make the ^{3}MC state inaccessible by increasing the ^{3}MLCT - ^{3}MC energy gap.

There are two ways to reach this goal. Firstly, one may increase the ^{3}MC energy level by using strong σ-donating ligands to coordinate Ru(II) instead of bpy. Higher ligand strength should increase the orbital splitting between the t_{2g} and e_g^*. If the ^{3}MLCT level remains approximately the same then the gap between ^{3}MLCT and ^{3}MC energy levels will be increased. However, a significant increase in the σ-donating ability of the ligands will certainly destabilise the t_{2g} level, and as a result the gap between t_{2g} and ^{3}MLCT will decrease, which means that the emission energy will decrease. An alternative choice to isolate the ^{3}MC state from the ^{3}MLCT state is to lower the ^{3}MLCT energy level. This can be done by introducing ligands which possess π^* energy level lower than that of bpy.

However, a significant decrease in emission energy is not always desired, as it will lead to a decrease in emission quantum yields and excited lifetimes. The energy gap law [51] predicts that the non-radiative decay rate should increase linearly with the decrease of emission energy, as the non-radiative decay process can be virtually considered as an intramolecular electron transfer process occurring in the "Marcus inverted region" [52]. Therefore the isolation

of the ^{3}MC states from the emitting states often has to compromise the possible decrease in the emission lifetime, which is crucial for an efficient excited state redox reaction to occur.

With the availability of an extensive range of organic bidentate ligands (more than 200 polypyridyl type bidentate ligands have been reported in two recent reviews [41,53]), in principle three types of Ru(II) complexes can be made: i) $[Ru(L\text{-}L)_3]^{2+}$; ii) $[Ru(L\text{-}L)_{3-n}(L\text{-}L')_n]^{2+}$; and iii) $[Ru(L\text{-}L)(L\text{-}L')(L\text{-}L'')]^{2+}$. All the ligands cited in this thesis are shown in Fig. I.4. Complexes of type i) and type ii) are most commonly studied. Complexes of type iii), due to synthetic difficulties, are relatively rare, although a few examples have been reported [54-56].

In the literature most attention has been paid to the complexes containing at least one ligand with a π^* level lower than that of bpy. Ligands of this type are, for instance, 2,2'-bipyrazine (bpz), 2,2'-bipyrimidine (bpm), 2,2'-biquinoline (biq), and their derivatives [55-69]. Unfortunately, strong π-accepting ligands of this type are often very weak σ-donors. Therefore homoleptic complexes made from these ligands in general have very low ligand fields. Although the ^{3}MLCT energy can be decreased, the ^{3}MLCT - ^{3}MC gap will not necessarily increase due to the

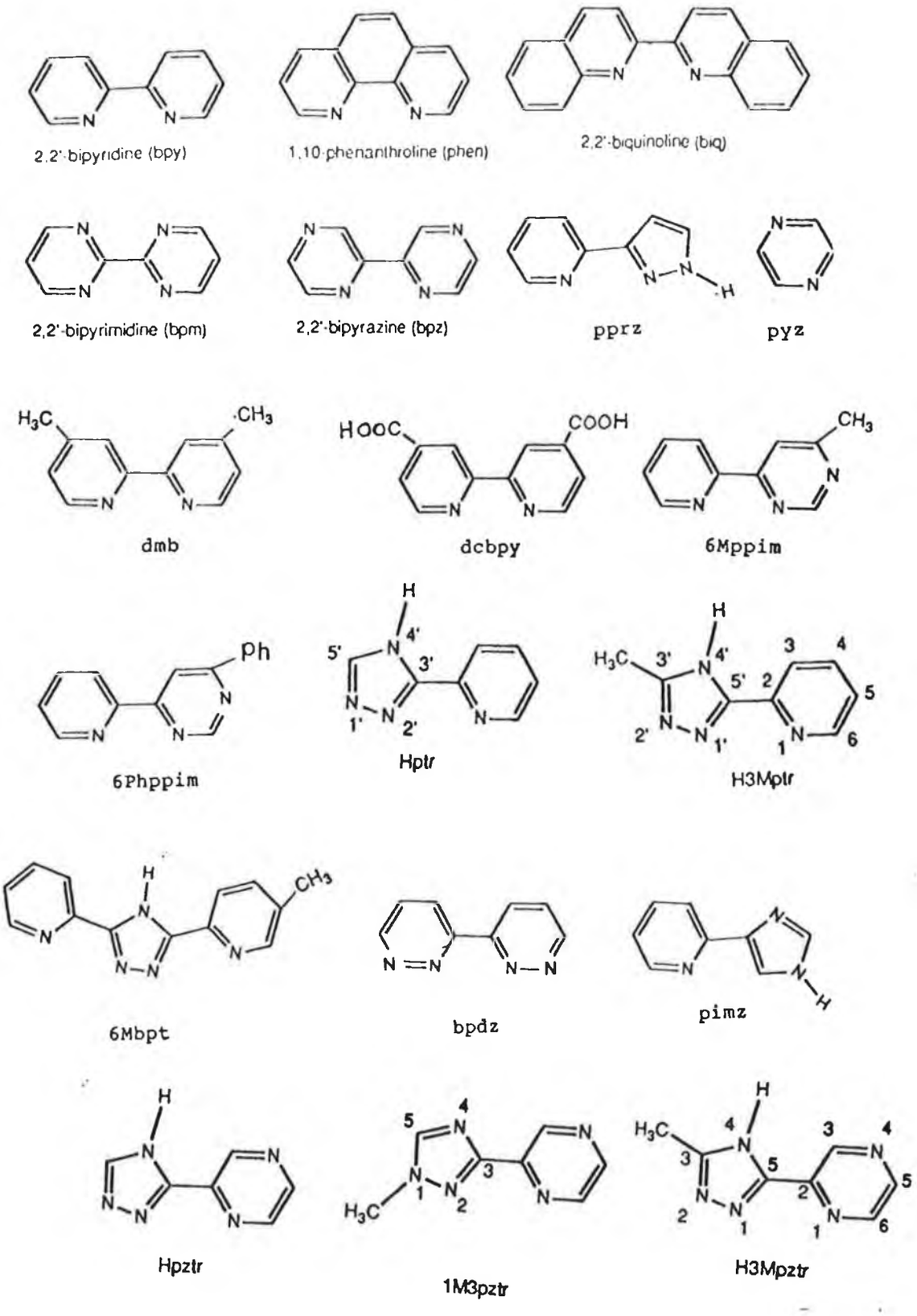

Fig. I.4 Ligands cited in the text. (to be continued in next page.)

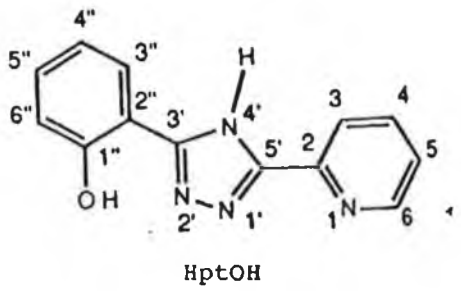

HptOH

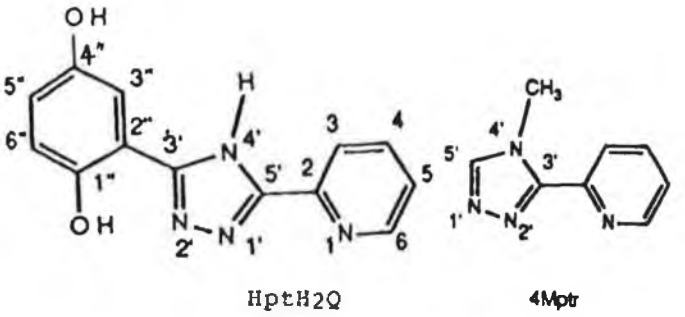

HptH2Q 4Mptr

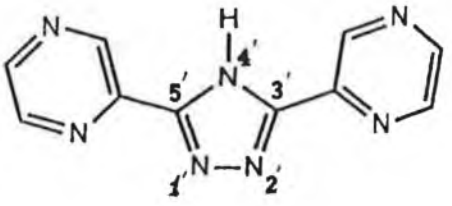

Hbpzt

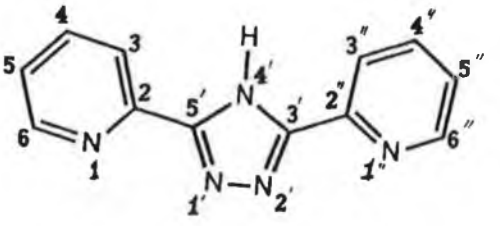

Hbpt

ppyz = 3-pyridin-2-yl-pyrazole.
dmb = 4,4'-dimethyl-2,2'-bipyridine.
dcbpy = 4,4'-dicarboxyl-2,2'-bipyridine.
6mppim = 6-methyl-4-(2-pyridyl)pyrimidine.
6phppim = 6-phenyl-4-(2-pyridyl)pyrimidine.
Hptr = 3-(pyridin-2-yl)-1,2,4-triazole.
H3Mptr = 3-methyl-5-(pyridin-2-yl)-1,2,4-triazole.
4Mptr = 4-methyl-5-(pyridin-2-yl)-1,2,4-triazole.
6Mbpt = 3-(6-methyl-pyridin-2-yl)-5-(pyrin-2-yl)-
1,2,4-triazole
bpdz = 3,3-bipyridazine.
pimz = 2-(2-pyridyl)imidazole.
Hpztr = 3-(pyrazin-2-yl)-1,2,4-triazole.
1M3pztr = 1-methyl-3-(pyrazin-2-yl)-1,2,4-triazole.
H3Mpztr = 3-methyl-5-(pyrazin-2-yl)-1,2,4-triazole.
HptOH = 3-(2-phenol)-5-(pyrazin-2-yl)-1,2,4-triazole.
HptH2Q = 3-(1,4-dihydroxy-2-phenol)-5-(pyridin-2-yl)-
1,2,4-triazole.
pyz = pyrazine.
Hbpzt = 3,5-bis(pyrazin-2-yl)-1,2,4-triazole.
Hbpt = 3,5-bis(pyridin-2-yl)-1,2,4-triazole.

Fig. I.4 (continued) Ligands cited in the text.

small t_{2g} - e_g^* splitting. The ligand field can be enhanced by making mixed chelates $[Ru(bpy)_n(L\text{-}L)_{3-n}]^{2+}$. Photochemical ligand loss has been indeed eliminated for several complexes of this type [56, 69].

A second class of the Ru(II) complexes, which received less attention than they should have, are those containing strong σ-donating ligands [70-86]. Ligands of this type, for instance, are 2-(pyridin-2-yl)-imidazole) (pimz) [70-73], 2-(pyridin-2-yl)-pyrazole) (pprz) [74-76], and 3-(pyridin-2-yl)-1,2,4-triazole (Hptr) [77-86]. As mentioned earlier, the advantage of the strong σ-donating property is that the gap between t_{2g} and e_g^* can be increased. On the other hand, these ligands are generally weaker π-acceptors. This will cause a blue shift in the absorption maxima, which narrows the visible light collecting region. Weak π-acceptors will increase the emission energy of the ^{3}MLCT state, which will have to be controlled carefully otherwise the ^{3}MC - ^{3}MLCT gap will decrease again. A better design is again to make heteroleptic complexes of the type $[Ru(bpy)_{3-n}(L\text{-}L)_n]^{2+}$, so that the strong σ -donating property can be maintained while the lowest π^* energy level is still bpy based. For most of these complexes the emission energy is slightly lower than that of $[Ru(bpy)_3]^{2+}$. Photostability is observed for some of these complexes [82, 87].

It is very important to note that for a large number of complexes uncoordinated free nitrogen atoms in the ligands can undergo a protonation/deprotonation process, and this can further alter their σ-donating and π-accepting properties [77-80, 83-103] For solution species, the possibility of making the d-d states inaccessible by adjusting the pH has not been appreciated until very recently [87], and this will be discussed in detail in Chapter IV and Chapter V.

Cage-type ligands, e.g., three bidentate diimine ligands linked together, have been used to encapsulate Ru(II), based on the idea that such a rigid matrix might be able to prevent ligand dissociation occurring (from ^{3}MC level), while the non-radiative decay (from ^{3}MLCT level) which occurs by releasing excited-state energy via the pyridyl ring based stretching vibration, might be hindered to a certain extent. Some of these cage-type complexes have been recently synthesised, and indeed they show longer emission lifetime as well as much higher (10^4 times!) photochemical stability than $[Ru(bpy)_3]^{2+}$ [104-106].

Another approach to elimimate the ^{3}MC state by synthetic design is to turn to the third transition series where, in complexes of Os(II), the splitting between the $d\pi$ and $d\sigma^*$ levels is 30% greater than for Ru(II) when coordinated to the same ligands [5, 45]. The $d\pi$ ---> $d\sigma^*$ energy gap for Os(II) complexes are so high that the ^{3}MC state is

inaccessible at room temperature except for some unusual cases [5]. By contrast, for polypyridyl complexes of the third-row element Fe(II), the $d\pi$ ---> $d\sigma^*$ separation is 30% smaller than the Ru(II) analogues. The d-d state is even lower in energy compared to the MLCT level, and therefore the photophysics of these complexes is dominated by the d-d level. Thus, complexes of Fe(II), in principle, have not been of value in energy conversion applications [5, 45].

I.2.4 Concluding remarks.

$[Ru(bpy)_3]^{2+}$ and numerous related Ru(II) polypyridyl complexes have been studied during the last 10-15 years, because of their potential applications in the photocleavage of water, based on the discovery of the promising photophysical and photochemical properties of $[Ru(bpy)_3]^{2+}$. However, synthetic design and photophysical studies of these complexes have not only led to the development of such an artificial solar energy conversion system but also enriched the whole field of photoinorganic chemistry.

A number of questions concerning the photophysical properties of the Ru(II) complexes have been successfuly answered. For instance, the relationship between emission energy and nonradiative decay rate (energy gap law) [52], the relation between the emission energy and radiative decay rate [45],

and the multiple emitting states [46-48], have been investigated and understood. Optimisation of the functions of the Ru(II) complexes has been largely centered on the efforts towards the isolation of the photochemically labile ^{3}MC state from the ^{3}MLCT state. However, the control of the radiative decay rate and elimination of the population of the ^{3}MC state by the design of the coordinating ligands have not been completely achieved yet.

Studies on the Ru(II) complexes have also been extended into other areas. This has largely relied on the emission properties of the Ru(II) complexes. The Ru(II) based chromophore-quencher assemblies have been used as model systems to study spatial controlled charge separation and migration processes [5, 107-108]. (This is an area of great relevance to both natural and artificial photosynthesis research, see Chapter VII.) The Ru(II) based chromophores have also been used in studying electron transfer processes in biological systems [109-110]. The application of Ru(II) complexes in selective photocleavge of DNA or RNA [111-112], immunoassay techniques [113], and photosensitisation and photocatalysis on semiconductors [114-117], have received much attention.

Since the discovery of the Creutz-Taube ion [118], mixed-valence complexes, including ruthenium based complexes, have been the subject of much attention [119-120, 123, 133,

139-140]. In the area of supramolecular photochemistry [7], where organic systems play a major role, inorganic systems including Ru(II) and Os(II) based dinuclear and polynuclear complexes began to receive much attention. A large number of such complexes have been prepared for studying photoinduced electron transfer or energy transfer processes [80-82, 119-138]. This is also an area closely related to photosynthesis studies [7]. Very recently, several structurally novel and important helical and double helical metal complexes have been synthesised [141-149], including one Ru(II)-based example [149]. These complexes, apart from their fundamental importance and relevance to biological systems, are considered to be promising candidates for constructing photochemical molecular devices [7].

I.3 Bridging the gap between natural and artificial photosynthesis.

Bridging the gap between natural photosynthesis and artificial photosynthesis is based on, of course, an understanding of the structure and properties of the natural photosynthetic center, as well as the detailed chemistry of the artificial synthetic system which is used to achieve the equivalent function of the natural system.

It is exciting to see that such a bridge is being built. The key role has been played by research on electron transfer

processes. As noted in Section I.1, a large portion of the research on the photosynthetic reaction centres has been focused on photoinduced intramolecular electron transfer processes. It is the very efficient photoinduced charge separation followed by charge transfer that allows the production of strong redox reagents, which in turn reduce CO_2 into carbohydrate and also oxidise H_2O into O_2. Apart from studies on the isolated and purified real or modified biological systems [109-110], several Ru(II) based chromophores have been linked to proteins as models for intramolecular transfer studies [38, 150-151]. It is also interesting to note that the intramolecular control of the photo-induced electron transfer has led to the design of artificial reaction centers which can essentially reduce CO_2 or oxidise H_2 [5].

For the oxidation of water, substantial similarity exists between ruthenium based oxo complexes and photosystem II. For instance, Meyer and co-workers [152] found that an oxo-bridged ruthenium dimer can function as a catalyst for the electrochemical oxidation of water. The reduction of this ruthenium oxo complex is proved to be a proton-coupled electron transfer process. Recently, a process of this type is also reported for a manganese oxo compound (a PS II model complex) [153-154].

Another interesting aspect which has received considerable

attention in recent years is to mimic the photosynthetic reaction centers by using membranes and other thin films. Some chromophore-quencher assemblies have been incorporated into membranes, micelles, vesicles or other self-organised systems [7].

In 1982, the "Marcus inverted region" effect [155-156] in electron transfer reactions was for the first time observed by Closs, Miller, and co-workers [157] on a series of organic chromophore-quencher assemblies. This work is of great importance for understanding the natural photosynthetic processes [2, 12]. On the other hand, Meyer and co-workers, provided clear results in 1982, demonstrating that for a series of Ru(II) and Os(II) complexes, non-radiative excited-state decay rate decreases linearly with the increase of emission energy of the chromophores. This work essentially provides a special case for the "inverted region", as non-radiative decay can be virtually considered as an intramolecular electron transfer process [52].

I.3 Scope of the thesis.

The work to be described in this thesis largely involves photophysical and photochemical properties of some Ru(II) complexes containing various substituted 1,2,4-triazoles. This work is a part of a wider research programme on the triazole-containing mononuclear, dinuclear and polynuclear

complexes [66, 77-89, 101-103, 135-138].

The most important features of these triazole ligands are:

1. In general they are stronger σ-donors but weaker π-acceptors than bpy. These properties can be tuned by different substituents on the triazoles.
2. The uncoordinated free nitrogen atoms on the triazoles can undergo protonation and deprotonation processes, which will further alter the σ-donating and π-accepting properties of the ligands.

Compared to the work on the Ru(II) complexes containing at least one low-lying π^* ligand, research on the complexes containing strong σ-donor ligands is relatively rare. Detailed photophysical and photochemical studies are necessary for the understanding and control of the excited-state properties of these complexes.

The experimental procedures, which include synthesis and physical measurements, are given in Chapter II. Chapter III contains a brief description of the modification of the working conditions for the HPLC separation of Ru(II) complexes. In Chapter IV, a detailed photophysical and photochemical investigation is reported, on the two coordination isomers of the complex $[Ru(bpy)_2(Hptr)]^{2+}$ (for ligand structure see Fig. I.4). This study is focussed

on how protonation and deprotonation processes affect excited-state lifetimes and photochemical reactivity. In Chapter V, the effects of ligand variation and second-sphere perturbation on the photophysical properties of a series of triazole-containing Ru(II) complexes are described. Chapter VI reports on the synthesis, characterisation and photophysical studies of several new Ru(II) complexes containing a pyridyltriazole ligand substituted with a hydroquinone group. The aim of this work is to prepare a chromophore-quencher assembly in which the intramolecular electron transfer process can be studied. In Chapter VII, the electrochemically induced proton transfer processes in Ru(II) complexes containing triazoles are described.

In addition, a project on the electrochemistry of a redox polymer $[Ru(bpy)_2PVP_{10}Cl]Cl$ is carried out. This work belongs to a different system and therefore it is omitted from the thesis. A copy of the publication based on this work is enclosed (Appendix II).

Considerable efforts have also been made on computer interfacing and programming. Selected computer programs relevant to the work described in this thesis (square wave voltammetry and pK_a titration data analysis) are listed in Appendix III.

Chapter II

Experimental

II.1 Synthesis and purification of ruthenium complexes.

Except for bpy and phen (1,10-phenanthroline), all the organic heterocyclic bidentate ligands used in this work were synthesised by Dr. Ronald Hage (Leiden University, The Netherlands) according to modified literature methods [88-89]. These ligands include Hptr, H3Mptr, Hpt, and $HptH_2Q$.

The following ruthenium complexes used in this work were also synthesised by Dr. Ronald Hage:
$[Ru(bpy)_2(bpt)]PF_6$ and $[\{Ru(bpy)_2\}_2(bpt)](PF_6)_3$ [80];
$[Ru(bpy)_2(6Mbpt)]PF_6$ and $[\{Ru(bpy)_2\}_2(6Mbpt)](PF_6)_3$ [86];
$[Ru(bpy)_2(bpzt)]PF_6$ and $[\{Ru(bpy)_2\}_2(bpzt)](PF_6)_3$ [89].
$[Ru(bpy)_2(Hpztr)](PF_6)_2$ ($N^{2'}$ and $N^{4'}$ bound isomers) [103];
$[Ru(bpy)_2(1M3pztr)]PF_6$ and $[Ru(bpy)_2(1M5pztr)]PF_6$ [103].

$[Ru(phen)_2(ptr)]PF_6$ ($N^{2'}$ and $N^{4'}$ bound isomers) and $[Ru(phen)_2(3Mptr)]PF_6$ were synthesised by Eleanor M. Ryan (Dublin City University) [158].

The structures and full names of the ligands mentioned above are presented in Fig. I.4.

$[Ru(bpy)_2(ptH_2Q\text{-}1)]PF_6.2H_2O$ (1)

Cis-$[Ru(bpy)_2Cl_2].2H_2O$ [159] (520 mg, 1 mmol) was heated with the ligand $HptH_2Q$ (304 mg; 1.2 mmol) in 50 ml ethanol/H_2O (1:1 v/v) in a 50 ml flask under reflux for 6 h. The solvent was then removed by rotary evaporation. The product was redissolved in 10 ml water and added into an aqueous NH_4PF_6 (conc.) solution. The precipitate was collected by filtration and washed with 50 ml water (in small portions) and then with 20 ml diethylether. Yield 530 mg (60%). Analytical HPLC showed the formation of three products. The three products were separated and isolated by semi-preparative HPLC as described in II.2.8.2. The first fraction collected was evaporated to dryness by rotary evaporation. (A small amount of NH_4PF_6 was added into the solution beforehand.) The solids were dissolved in acetone and filtered once, and then recrystallised twice in acetone/water (1:1 v/v) containing drops of conc. NaOH (pH = 6-7). Anal. Found: C, 46.69; H, 3.23; N, 13.31 %. Calcd. for $[Ru(bpy)_2(ptH_2Q\text{-}1)]PF_6.2H_2O$: C, 46.76; H, 3.45; N, 13.22%.

$[Ru(bpy)_2(ptH_2Q\text{-}2)]PF_6$ (2)

The second fraction separated from (1) using semi-preparative HPLC was isolated and recrystallised as described for (1). Anal. Found: C, 48.61; H, 3.45; N, 15.79 %. Calcd. for $[Ru(bpy)_2(ptH_2Q\text{-}2)]PF_6$: C, 48.83; H, 3.10; N, 13.81 %.

$[\{Ru(bpy)_2\}_2(ptH_2Q)](PF_6)_3$ **(3)**

Electrochemistry indicated that the third fraction separated from (1) and (2) was a dinuclear complex. This complex was then synthesised directly. Cis-$[Ru(bpy)_2Cl_2].2H_2O$ (1145 mg; 2.2 mmol) was dissolved in 50 ml ethanol/water (2:1 v/v) and then heated with the $HptH_2Q$ ligand (253 mg; 1 mmol; added in three portions over 6 h) under reflux. The reaction took in total 24 h. The product was then isolated as described for (1). The small amount (<20%) of mononuclear species formed was removed using semi-preparative HPLC. The desired last fraction was then isolated, again as described for (1). Recrystallisation took place in acetone/water (1:1 v/v) containing drops of conc. NaOH (pH = 6-7). Yield (300 mg; 30%). Anal. Found: C, 41.60; H, 2.76; N, 11.89%. Calcd. for $[\{Ru(bpy)_2\}_2ptQ](PF_6)_3$: C, 42.02; H,2.73; N, 11.09%.

The following complexes were synthesised and purified according to literature or modified literature methods:

Cis-$[Ru(bpy)_2Cl_2].2H_2O$ [159] **(4)**

$RuCl_3.3H_2O$ (7.8 g; 30 mmol), bpy (9.4 g; 60 mmol) and LiCl (8.4 g; 198 mmol) were heated under reflux in 50 ml DMF for 8 h. After cooling, 250 ml acetone was added to the purple solution. After leaving the solution for 4 h at -20 ^0C, the dark purple crystals were collected by filtration. The product was washed with 100 ml cold water (in portions)

and 50 ml diethylether, and then dried in vacuo. Yield: 12.1 g (78%).

$[Ru(bpy)_2(Hptr)](PF_6)_2$ (two isomers) [84-85] (5)

Cis-$[Ru(bpy)_2Cl_2].2H_2O$ (520 mg; 1 mmol) was heated under reflux with Hptr the ligand (343 mg; 1.2 mmol) for 6 h in 50 ml ethanol/water (1:1 v/v). The solvent was removed by rotary evaporation. The remaining solid was dissolved in 10 ml water and dropped into an aqueous NH_4PF_6 (conc.) solution. The precipitate was filtered and washed with 50 ml water (in small portions) and then with 20 ml diethylether. Yield 626 mg (74%). The complex contained two geometrical isomers [88-89], which were separated by semi-preparative HPLC as described in section II.2.8.2. After separation, a small amount of solid NH_4PF_6 was added into the two fractions. The two solutions were then evaporated to dryness. The products were dissolved in acetone and filtered. Recrystallisation took place in acetone/H_2O (1:1 v/v) containing drops of conc. HCl.

$[Ru(bpy)_2(ptr)]PF_6.3H_2O$ (two isomers) [84-85] (6)

This compound was synthesised and separated as described for (5), except that at last the two isomers were recrystallised in acetone/water (1:1) containing drops of conc. NaOH.

$[Ru(bpy)_2(ptOH)]PF_6.CH_3COCH_3$ [83] (7)

Cis-$[Ru(bpy)_2Cl_2].2H_2O$ (520 mg; 1 mmol) was heated

under reflux with the Hpt ligand (286 mg; 1.2 mmol) in 50 ml ethanol/water (1:1 v/v) for 6 h. After evaporation to dryness, the solid was dissolved in 5 ml of water and precipitated in an aqueous NH_4PF_6 (conc.) solution. The precipitate was washed with 50 ml cold water (in small portions) and then with 20 ml diethylether. The compound was further purified by recrystallisation from acetone/water (1:1 v/v) containing drops of conc. NaOH. Yield 500 mg (60%).

$[Ru(bpy)_2(3Mptr)]PF_6.4H_2O$ [79] **(8)**

This complex was prepared as described for (7). Yield 500 mg (60%).

$[Ru(bpy)_2(H3Mptr)](PF_6)_2.H_2O$ [79] **(9)**

This complex was prepared as described for (8) except that the recrystallisation took place in acetone/water (1:1 v/v) containing drops of conc. HCl. Yield 550 mg (60%).

II.2 **Physical measurements.**

II.2.1 Electronic spectra.

UV-vis spectra were obtained using either a Shimadzu UV-240 spectrophotometer or a Hewlett Packard 8451 diode array spectrophotometer. Extinction co-efficients are accurate up to 5% .

Emission spectra were obtained on a Perkin-Elmer LS-5 luminescence spectrometer equipped with a red sensitive Hamamatsu R928 detector, using an emission slit width of 10 nm at room temperature and of 2.5 nm at 77 K. The emission spectra recorded in Tulane University were obtained on a Spex Industries Model IIIC fluorescence spectrometer equipped with a 450-W Xe Arc lamp and cooled PMT housing. The spectra were not corrected for the photomultiplier response.

For absorption and room temperature emission measurements the samples were dissolved in CH_3CN, while for 77 K emission measurements the solvent used was 4:1 EtOH:MeOH. Typically 10 μl Et_2NH or CF_3COOH were added to about 10 ml sample solutions to ensure protonation/deprotonation.

II.2.2 Ground state and excited state pK_a titrations.

The ground state pK_a was measured by monitoring the UV-vis absorption intensity as a function of pH. Similarly, the excited state acid-base equilibria were measured by monitoring the emission intensity as a function of pH. The excitation wavelength for the emission titration was chosen from an appropriate isosbestic point determined from the absorption titration curve. The spectra were recorded on the instruments described in II.2.1.

The samples to be measured were first dissolved in ca. 1 ml

acetonitrile (HPLC grade) and then added into 150-200 ml of Britton-Robinson buffer (0.04 M boric acid, 0.04 M acetic acid, and 0.04 M phosphoric acid). The pH of the solutions was adjusted by adding NaOH or H_2SO_4 solutions and measured using a Corning 240 digital pH meter.

The ground state pK_a value and emission titration inflection point pH_i value were obtained by using a program which was developed for a BBC-microcomputer (see Appendix II).

II.2.3 Nuclear magnetic resonance spectroscopy.

All the ^{1}H-NMR spectra were recorded on a Bruker WM-300 MHz spectrophotometer (Leiden University, The Netherlands). The solvent used is $(CD_3)_2CO$ or $(CD_3)_2CO/D_2O$. pH is adjusted by adding NaOD or DCl into $(CD_3)_2CO/D_2O$. All the chemical shifts are relative to TMS.

II.2.4 Elemental analysis.

All the elemental analyses were carried out in University College Dublin.

II.2.5 Emission and photoanation quantum yields.

II.2.5.1 Emission quantum yields.

Emission quantum yields were measured at room temperature by using a Spex Industries Model 111C fluorescence spectrometer as described in II.2.2.

The samples were dissolved in CH_3CN and 10 μl CF_3COOH or Et_2NH was added to 5 ml solutions to ensure protonation/deprotonation. The absorbance of all solutions was matched at 0.5 ODU at excitation wavelength 440 nm. The solutions were degassed with nitrogen for 30 min., prior to measurements and a blanket of N_2 was maintained during the measurements. Emission measurements were made at 90^0 relative to excitation and the data were not corrected for the response of the photomultiplier tube (PMT). Quantum yields were calculated from the integrated emission spectra relative to $[Ru(bpy)_3]^{2+}$ in CH_3CN (ϕ_{em} = 0.062 [160]).

II.2.5.2 Photoanation quantum yields.

Photoanation quantum yields were measured using the same solutions for photolysis in the presence of anions (see II.2.7.1) while the absorbance at the excitation wavelength (468 nm, the most intense line from the Xe arc lamp) was adjusted so that it was matched at 0.40 ODU. The solutions were degassed in the same way as for emission quantum yield measurements. The emission intensity was monitored at 650 nm as a function of time.

The emission intensity decreased linearly, especially at the beginning of the photolysis (typically < 100 seconds, only <10% conversion to product), and the ratio of the slopes calculated from the linear regression data were used to determine the photoanation quantum yields relative to $[Ru(bpy)_3]^{2+}$.

II.2.6 Emission lifetime measurements.

II.2.6.1 Room temperature and 77 K lifetime measurements.

The lifetimes were obtained with a Laser Photonics LN 1000 MegaPlus Nitrogen laser (Wavelength 337 nm, pulsewidth 600 picosecond) as excitation source. The laser beam was passed through a Scott UG-11 coloured glass filter. Emitted light from the sample was collected at 90^0 from the incident excitation beam, filtered with a glass filter which has a cutoff wavelength either at 454 or 590 nm, imaged onto the entrance slit of a GCA/McPherson EU-700 monochromator and then detected with a Hamamatsu R777 PMT in a Pacific Instruments 3150 PF holder. The PMT output was captured using a HP54111D digitiser (limited to 8 bit vertical resolution). Triggering was accomplished by splitting off a fraction of laser beam to saturate a photodiode. Experiments were controlled by a Hewlett-Packard 9826 microcomputer interfaced to a HP 6940B multiprogrammer.

Lifetime data were analysed by using a nonlinear least squares fit to exponential decay with a base line correction. The fitting program uses a modified Marquart algorithm for least squares minimisations [161].

For pH dependent lifetime measurements, the samples were predissolved in ca 200 μl CH_3CN and then added into 150 ml Britton-Robinson Buffer. The pH was adjusted as described in II.2.2 and measured using a Extech 651 digital pH meter.

For room temperature lifetime measurements 1-cm pyrex luminescence cells were used while for 77 K measurements pyrex tubes (diammeter 2 mm) cooled in a quartz windowed ESR type liquid nitrogen Dewar were used.

For the samples having pH < 7, the lifetime data were recorded on a time correlated single photon counting system employing a mode locked, cavity dumped Ar^+ laser for excitation (doubled dye output at 295 nm) [162].

II.2.6.2 Temperature dependent lifetime measurements.

The samples were dissolved in 4:1 EtOH/MeOH, and 10 μl Et_2NH or CF_3COOH was added to a 10 ml sample solution to ensure deprotonation/protonation.
Sample solutions sealed in 0.2 cm x 3 cm cylindrical tubes, after being freeze-pump-thaw degassed for at least 6 cycles,

were placed in a home built copper sample holder and mounted to an Air Products Dixplex cryostat, which was thermostatted by a DTC-2 digital temperature controller using a Pt resistance thermometer attached to the heat-exchange block of the cryostat. An independent Pt thermister attached to the tip of the sample cell was employed for temperature measurement. The position of the cryostat, once adjusted, was not altered during the subsequent measurements. Samples were equilibrated for 20 minutes at each temperature.

II.2.7 Photolysis.

II.2.7.1 Photolysis in TBAB/CH_2Cl_2 monitored by UV-vis absorption spectroscopy.

Solutions for photolysis of the protonated complexes were prepared by mixing equal volumes of the protonated complexes (10^{-5} M) and tetrabutylammonium bromide (6.0×10^{-3} M) in CH_2Cl_2 in a 1-cm pyrex luminescence cell. In the case of the deprotonated samples, 10 μl of Et_2NH was added to the solutions prepared as above. All the preparations were performed in the dark and all the solutions were deaerated by bubbling with solvent saturated N_2 for 15 minutes. Absorption spectra were measured as a function of time during photolysis using a Hewlett Packard 8541A diode array spectrophotometer. The N_2 bubble degassed sample solutions in sealed pyrex glass cells were mounted in a fixed

position by using a Model EU-701-11 Heath Sample Cell Module. The photolysis was achieved by using an Ealing Universal broad band Xe Arc Lamp (250 W). The light was focused onto the glass window of the cell module, while UV and infra-red irradiation were filtered by using Schott GC 400 and Corning 4-71 glass filters and passing the excitation beam through a water bath (5cm path).

II.2.7.2 Photolysis in CH_2Cl_2 or TBAB/CH_2Cl_2- monitored by HPLC.

The preparation of solutions for photolysis in TBAB/CH_2Cl_2 and the apparatus used are the same as described as as in II.2.7.1 except that an analytic HPLC system (see II.2.8) was used for monitoring the photolysis processes.

II.2.8 High performance liquid chromatography (HPLC).

II.2.8.1 The analytical HPLC system.

Analytical HPLC experiments were carried out using a Waters HPLC system, which consists of a 990 photodiode array detector, a model 6000 A HPLC pump, a 20 μl injector loop and a μPartisil SCX radical PAK cartridge mounted in a radial compression Z module. The system was controlled by a NEC APC

III computer.

The detection wavelength used was 280 or 290 nm, which corresponds to the most intense band in the absorption (π---> π^* transition) for all the ruthenium complexes studied in this work. The mobile phase was 80:20 $CH_3CN:H_2O$ containing 0.08 M $LiClO_4$. For photolysis of $[Ru(bpy)_2(H3Meptr)]^{2+}$, 0.09 M $LiClO_4$ was used to reduce the retention time. The flow rate used was 2.5 ml/min.

II.2.8.2 The semi-preparative HPLC system.

Semi-preparative HPLC was carried out using an Applied Chromatography Service pump (either Model RR/066 or Model 353), a 1 ml injection loop and a Magnum 9 Partisil cation exchange column (10 mm x 25 cm). The mobile phase used for separating the two isomers of $[Ru(bpy)_2(ptr)]^+$ was 80:20 $CH_3CN:H_2O$ containing 0.08 M $LiClO_4$. For all other complexes, the mobile phase used was 80:20 $CH_3CN:H_2O$ containing 0.1 M KNO_3.

II.2.9 Column chromatography.

Column chromatography was applied when purification of the ruthenium complexes was carried out at Tulane University, as there was no semi-preparative HPLC apparatus available. The working conditions were developed based on the preliminary

results obtained by Ryu and Schmehl [163] (See Chapter III). The stationary phase used was controlled-pore glass beads (Sigma), while the mobile phase used was CH_3CN/H_2O (80:20 v/v) containing 0.025-0.1 M KNO_3 (for eluting mononuclear species) and 0.5 M or saturated KNO_3 (for eluting the dinuclear species). A semi-preparative scale separation was achieved when a ϕ2 cm x 10 cm column was combined with a 1 ml injector loop and a medium-pressure pump. The fractions separated were then checked by UV-vis spectroscopy. After isolation the different fractions were examined on a HPLC system and it was shown that the separation quality achieved on the controlled-pore glass beads column was satisfactory.

II.2.10 Electrochemistry.

II.2.10.1 General conditions.

HPLC grade CH_3CN dried over molecular sieves 4 A or EM Science CH_3CN distilled over CaH_2 was used in all the electrochemical measurements. 0.1 M home made tetraethylammonium perchlorate (TEAP) or AR grade tetrabutylammonium perchlorate was used as electrolyte. A 3 mm diameter Teflon shrouded glassy carbon electrode was used as working electrode and a platinum foil as auxilary electrode. The reference electrode used was either a Ag/AgCl (saturated with KCl) electrode or a saturated calomel electrode. The electrochemical cell was a conventional

three-compartment cell. Solution was degassed for 20 min. with nitrogen in advance if the ligand based reduction, which was normally at a potential range below 0 V (vs SCE), were to be measured.

II.2.10.2 Cyclic voltammetry.

Cyclic Voltammetry (CV) was carried out using either an Edt ECP 133 Potentio/Galvanostat together with a JJ PL3 X-Y recorder, or an EG&G PAR Model 173 potentiostat equipped with a Model 176 current follower, a Model 175 Universal programmer, and a Hewlett-Packard Model 7015B x-y recorder. Scan rate: 100 mV/sec.

II.2.10.3 Differential pulse voltammetry.

Differential pulse voltammetry (DPV) was carried out on an EG&G Model 264A Polarographic Analyser together with an EG&G 2000 X-Y recorder. Scan rate 5 mV/sec. Peak height for each potential pulse: 20 mV.

II.2.10.4 Square wave voltammetry.

Square wave voltammetry was carried out on an EG&G Model 273 Potentio/Galvanostat interfaced to BBC microcomputer and linked with an Epson HI-80 Plotter/Printer. Pulse height: 50 mV. Potential increment: 4 mV. Frequency 25 Hz. (For the

computer software see Appendix III).

II.2.11 Spectroelectrochemistry.

II.2.11.1 UV-vis spectroelectrochemistry.

Home made (either quartz or pyrex glass) thin layer cells were used for spectroelectrochemical studies. The working electrode was a platinum grid inserted into the thin layer part of the cell. The reference (Ag/AgCl) and auxiliary (platiunum wire) electrodes were placed in the solution at the top part of the cell (an electrolysis solution reservoir). The ruthenium compounds were predissolved in the electrolyte (CH_3CN containing 0.1 M TEAP or TBAP) and then transferred into the thin layer cell.

The solution was degassed by passing through a stream of N_2 for 20 min and a blanket of N_2 was present over the solution throughout the whole experiments. The working electrode was held at each potential for 20 min (in order to ensure a complete electrolysis of the solution in the thin layer part) before any spectra were recorded. The potentiostats used were the same as those for cyclic voltammetry (see II.2.10.2). The UV-vis spectrophotometers used were the same as those described in II.2.1.

II.2.11.2 Emission spectroelectrochemistry.

The sample solutions were prepared in the same way as described in II.2.11.1. The thin layer cell was held in 45^0 relative to the incident excitation laser beam. The laser beam reflected from the thin layer cell was then filtered by a quartz cell containing nitromethane, which was located just in front of the entrance slit of the monochrometer. The emission lifetime was measured after the working electrode was held at each potential for 20 min. The potentiostat and emission lifetime equipment were the same as described in II.2.10.2 and II.2.6.1.

Chapter III

Investigation of Working Conditions for the HPLC Separation and Isolation of Ruthenium Diimine Complexes.

III.1 Introduction.

III.1.1 The application of HPLC in inorganic systems.

High performance liquid chromatography (HPLC), has been applied extensively to the separation of numerous organic and biochemically active compounds, while its application in inorganic chemistry has been relatively limited [164].

The first report on the HPLC separation of organometallic compounds appeared in 1969 [165]. For coordination compounds the first detailed separation using reverse-phase ion-pair chromatography (RP-IPC) was reported by Valently and Behnken in 1972 [166].

Starting in 1980, O'Laughlin and co-workers [167-168] published a series of papers on the separation of complexes of $[M(bpy)_3]^{2+}$ (M = Ru, Ni, Fe, etc). Both RP-IPC and ion-exchange chromatography were examined. The best separation was achieved by using a cation exchange column (μ-Partisil-SCX) and a mobile phase of 4:1 CH_3CN/H_2O containing 0.06 M $HClO_4$. Of interest is that even though the column used was an ion-exchange type column, the separation mechanism was found to be dominated by partition of the paired ions (in this case positively charged metal chelates and negatively charged perchlorate ions) between the

stationary and mobile phases.

Reverse-phase ion-pair HPLC, was applied also by a few groups for the separation of ruthenium diimine coordination compounds. For instance, Creutz and Sutin's group, as well as Meyer's group, separated some ruthenium coordination compounds using a C18 (ODS-3) column. A mixture of THF (tetrahydrofuran) and aqueous acetates was used as mobile phase with sodium octasulfonate as the ion-pair reagent [169-170]. The HPLC system, combined with a single-wavelength UV-vis detector, was also used to monitor photochemical reactions [170]. However, this system has a few drawbacks. Firstly, the acetates used in the mobile phase are potential coordination ions, therefore ligand exchange reactions often occur during separation processes, which complicates the analysis of the photochemical reaction products. Secondly, resolution between complexes carrying the same positive charge was sometimes not achieved [170].

The first systematic investigation of HPLC separation of ruthenium bis(bpy) compounds of the type $[Ru(bpy)_2(L\text{-}L')]^{n+}$ and $[Ru(bpy)_2(L)(L')]^{n+}$ (n=1,2) (L-L' = bidentate ligands; L or L' = monodentate ligands) was carried out in this laboratory [171-172]. When combined with a photodiode array detector, the HPLC technique has also been applied to monitor photochemical reactions [171]. For most Ru(II) compounds investigated the best separation was

achieved using a cation-exchange column (μ-Partisil-SCX) and a mobile phase which consists of 4:1 CH_3CN/H_2O and 0.08 M $LiClO_4$. These conditions are very similar to those reported by O'Laughlin for the separation of tris(bpy) compounds of different transition metals [167]. Further extention of the technique has been successfully made to separate reaction products and even photochemical reaction intermediates on a semi-preparative scale [84, 87, 173]. Thus, compounds of the type $[Ru(bpy)_2(L\text{-}L')]^{n+}$ or $[Ru(bpy)_2(L)(L')]^{n+}$ (n=1,2) can be separated completely, something which would be very difficult to achieve using ordinary column chromatography or recrystallisation techniques.

III.1.2 The importance of HPLC separation in ruthenium chemistry.

For the ruthenium coordination compounds, a high purity is required, especially for photophysical studies. For example, when a mixture of mononuclear and dinuclear compounds is formed during synthesis, it is of great importance to ensure a complete separation between these species before any photochemical and photophysical measurements are carried out. Very often the dinuclear complexes are weaker emitters compared to their mononuclear counterparts. If a complete separation is not achieved, then the emission from a dinuclear complex can be masked by that from its parent

mononuclear complex [89]. If two isomeric species (resulting from different coordination mode) exist, they also have to be completely separated otherwise correct lifetime data can never be obtained for each species. HPLC techniques have made such separations possible.

HPLC techniques can also be used to probe photochemical reactions. For ruthenium bis(bpy) compounds photo-substitution reactions are often very complex, as a number of intermediates can be involved. These intermediates can be unstable, and difficult to identify. As mentioned earlier, a HPLC system combined with a photodiode array detector, has made possible not only a quick and well resolved separation but also a spectroscopic analysis for each separated species.

III.1.3 Problems to be solved.

As described above, a HPLC system has been developed in this laboratory for the separation of ruthenium complexes. However, there are still a few problems remaining. The first problem is that for some of the compounds with charge > 2+, which are normally dinuclear species, the retention time is too long (> 15 min) and a large peak distortion and tailing (>10 min) are often observed. This causes a large consumption of solvent especially when the separation is conducted on a semi-preparative scale. The second problem is that after isolation of the fractions from semi-preparative

HPLC, it is very difficult to remove all the perchlorate ions when a compound of the type $[Ru(bpy)_2(L\text{-}L')](PF_6)_n$ or $[Ru(bpy)_2(L)(L')](PF_6)_n$ is desired. The products obtained were usually a mixture of $[Ru(bpy)_2(L\text{-}L')]^n(PF_6)_n$ and $[Ru(bpy)_2(L\text{-}L')]^n(ClO_4)_n$ (or $[Ru(bpy)_2(L)(L')]^n(PF_6)_n$ and $[Ru(bpy)_2(L)(L')]^n(ClO_4)_n$. This is, of course, a disadvantage because elemental analysis becomes almost impossible for the compounds separated and isolated from semi-preparative HPLC. Thus, it is necessary (1) to find proper working conditions for reducing the retention time for the dinuclear species while maintaining a good separation between mononuclear and dinuclear compounds, and (2) to find a proper ion-pair reagent which can replace the perchlorate ion.

III.2 Results and discussion.

The compounds chosen to optimise the HPLC separations are a series of ruthenium dinuclear complexes and their parent mononuclear complexes (for ligand structures see Fig. I.4):

$[Ru(bpy)_2(bpzt)]PF_6$ and $[\{Ru(bpy)_2\}_2(bpzt)](PF_6)_3$;
$[Ru(bpy)_2(bpt)]PF_6$ and $[\{Ru(bpy)_2\}_2(bpt)](PF_6)_3$;
$[Ru(bpy)_2(6Mbpt)]PF_6$ and $[\{Ru(bpy)_2\}_2(6Mbpt)](PF_6)_3$.

All the complexes were purified in advance by conventional column chromatography and recrystallisation.

In order to optimise the HPLC system for the separation of the mononuclear complexes from their related dinuclear complexes, three variables were examined: the column, the solvent and the concentration of the ion-pair reagent.

III.2.1 μ-Bondpack C18 Column.

A μ-bondpack C18 column was tested as an alternative column for separations under reverse-phase conditions. Different solvents and their mixtures in different ratios (CH_3OH, CH_3CN and H_2O) were examined. The ion-pair reagent, if used, was 0.08 M $LiClO_4$. In all cases, the separation was very poor for these complexes and no further investigation was carried out.

III.2.2 Cation-exchange column: retention time as a function of the ion-pair reagent concentration.

Using a μ-Partisil SCXcation exchange column, at a fixed $LiClO_4$ concentration (0.08 M), the retention time as a function of the solvent ratio (CH_3CN/H_2O) was examined but no improved separation was achieved for the ruthenium complexes investigated. However, the retention time as a function of the concentration of $LiClO_4$ at a fixed solvent ratio (CH_3CN/H_2O 4:1 v/v) has a significant influence on the elution and separation processes.

$[Ru(bpy)_2(bpzt)]^+$ and $[\{Ru(bpy)_2\}_2(bpzt)]^{3+}$. Listed in Table III.1 are the results obtained from sample A and sample B. The main product in sample A is $[Ru(bpy)_2(bpzt)]^+$, while that in sample B is $[\{Ru(bpy)_2\}_2(bpzt)]^{3+}$. HPLC shows that although the complexes had been purified using conventional column chormatography, the mononuclear complex contains a small amount of dinuclear species (see Fig. III.1). Meanwhile, the dinuclear complex contains some of the mononuclear species.

Table III.1 HPLC separation of $[Ru(bpy)_2(bpzt)]^+$ and $[\{Ru(bpy)_2\}_2(bpzt)]^{3+}$; Retention time as a function of the concentration of $LiClO_4$. Solvent: CH_3CN/H_2O (4:1 v/v).

$LiClO_4$(M)	Retention Time (min.)	
	sample A	sample B
0.08	2.5, 9.4, 18.5	9.9, 18.5
0.09	2.4, 8.8, 15.2	9.1, 14.2
0.10	2.4, 8.8, 12.2	9.1, 11.4
0.12	8.0	8.4
0.15	2.2, 5.5[d], 7.2	5.3[d], 7.3
0.18	2.2, 5.1[d], 11.1	4.8[d], 11.5

d: dinuclear complex; retention time reversed.

For instance, when the mobile phase contains 0.09 M $LiClO_4$,

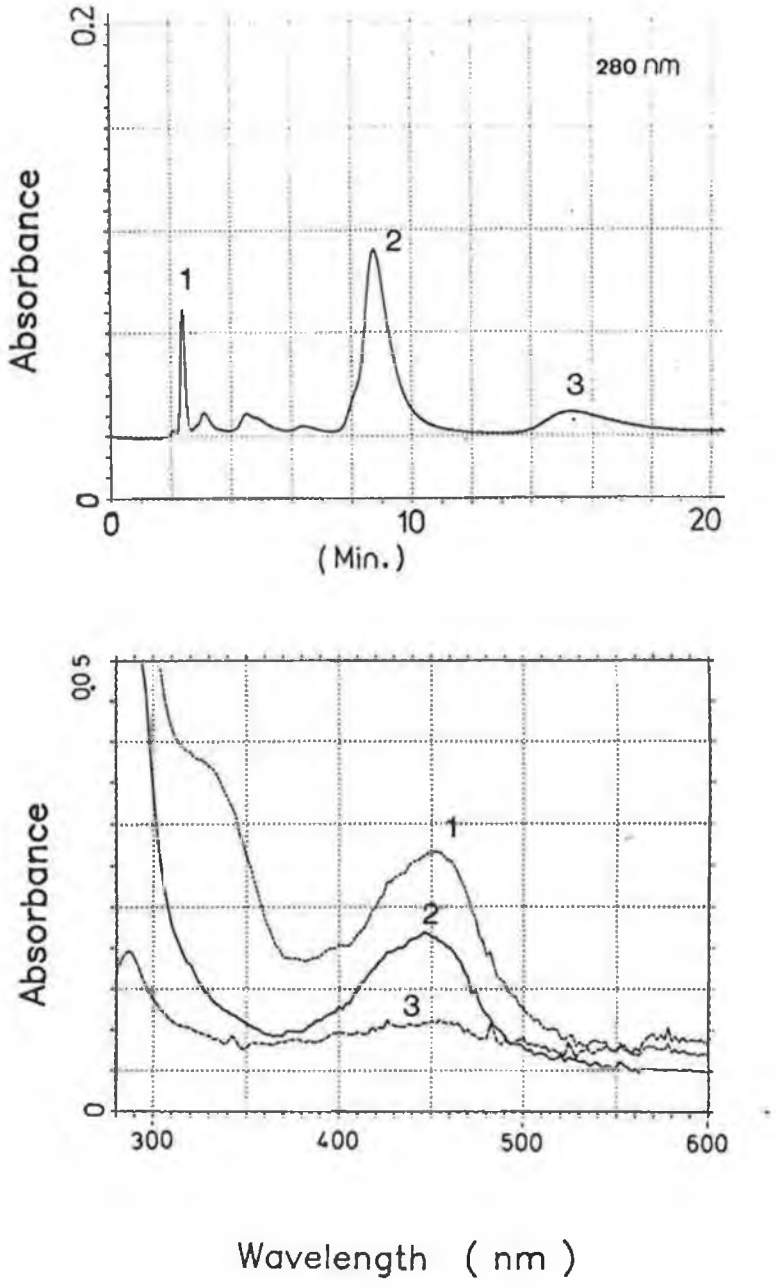

Fig. III.1 Chromatogram for sample A and UV-vis spectrum for each peak. $LiClO_4$ concentration : 0.09 M in CH_3CN/H_2O (4:1 v/v).

the chromatogram of the mononuclear species shows three well resolved peaks (Fig. III.1). Compared to the chromatogram for the dinuclear complex, the peak at 8.8 min. is corresponding to the mononuclear complex while the peak at 15.2 min. is corresponding to the dinuclear complex. The UV-vis spectrum of the very first peak, at 2.4 min., rules out any cis-dichloro- or monochloro- ruthenium complex (Fig. III.1). The short retention time for this first peak also suggests that it is unlikely to be a dinuclear complex. Thus, another mononuclear isomer is most likely responsible for the first peak.

Similar very short retention times are also found for other mononuclear complexes carrying a 1+ charge. For instance, under the same condition, the retention time for $[Ru(bpy)_2(ptOH)]^+$ is ca. 1.8 min. (for ligand structure see Fig. I.4).

From the structure of the bridging ligand bpzt (Fig. I.4), it can be seen that the Ru(II) centre can be bound to a nitrogen of the pyrazyl ring and a nitrogen on the triazole ring. However, there are two nitrogens on the triazole ring ($N^{1'}$ and $N^{4'}$) available for coordination. Thus, the formation of two coordination isomers is possible. The UV-vis absorption spectra for the first two peaks are not identical (Fig. III.1), which further supports this point.

The second fraction has been characterised using NMR, and the data indicates that the Ru(II) center is bound via $N^{1'}$ of the triazole ring [86]. If the first fraction is indeed another isomer then the Ru(II) center should be bound via $N^{4'}$ of the triazole ring. No further isolation and characterisation of this first fraction has been carried out. However, it is interesting that the same elution order is also found for another similar compound $[Ru(bpy)_2(ptr)]^+$ (for ligand structure see Fig. I.4), where the $N^{4'}$ bound isomer elutes before the $N^{2'}$ bound one [84].

The retention time for the first peak, is affected very little by the change of the $LiClO_4$ concentration. For both the $N^{1'}$ bound mononuclear complex and dinuclear complex, the retention time is reduced when the $LiClO_4$ concentration is increased from 0.08 M to 0.09 M.

Further increase of the concentration of $LiClO_4$ up to 0.10 M causes very little change in retention time for the mononuclear complex, while the retention time for the dinuclear complex still decreases (Fig. III.2A and III.2B). When $LiClO_4$ is increased to 0.12 M, the retention time for the $N^{1'}$ bound mononuclear complex and that for the dinuclear complex become the same so no separation is obtained. More interestingly, at 0.15 M $LiClO_4$ a reversed behaviour was observed. That is, the dinuclear compound

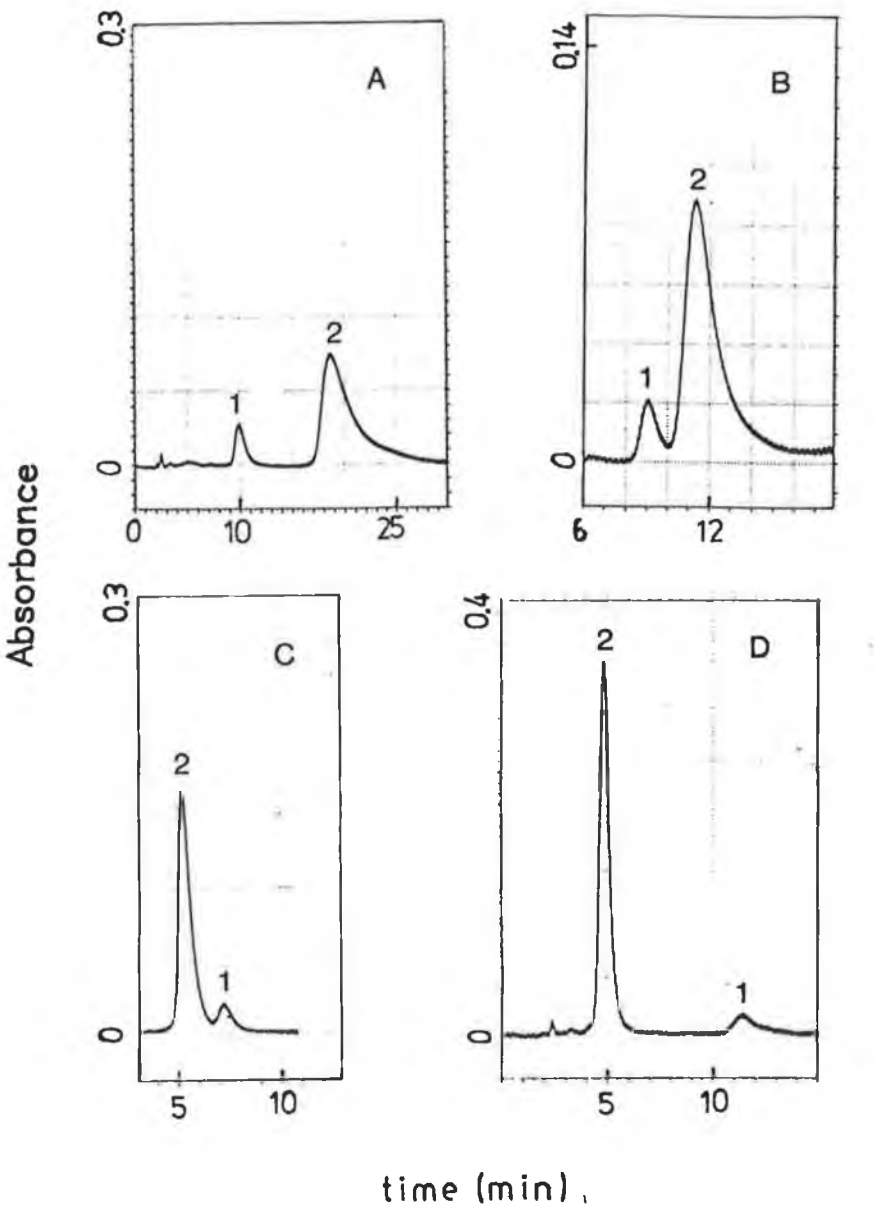

Fig. III.2 Sample B. The effect of ion-pair reagent concentration on the separation process. $LiClO_4$ concentration (from 1 to 4): 0.08 M, 0.10, 0.15 M and 0.18 M in CH_3CN/H_2O (4:1 v/v).

1 --- $[Ru(bpy)_2(bpzt)]^+$;

2 --- $[\{Ru(bpy)_2\}_2(bpzt)]^{3+}$.

elutes before the $N^{1'}$ bound mononuclear complex (Fig. III.2C). Further increase of the $LiClO_4$ to 0.18 M results in further decrease in retention time for the dinuclear complex, while the retention time for the $N^{1'}$ bound mononuclear complex is increased (Fig. II.2D).

Clearly, a mixed mechanism affects the separation process. When the $LiClO_4$ concentration < 0.15 M, the increase of the $LiClO_4$ concentration reduces the retention time for all three species, but certainly the effect on the dinuclear complex is more significant than for the mononuclear complex. The elution order suggests that an ion exchange mechanism might dominate the separation process [174]. It is likely that the species which carries a higher positive charge would be retained longer on the stationary phase by electrostatic interactions.

The reversed elution order at a higher concentration of $LiClO_4$ (> 0.15 M) and the decrease of the retention time for the $N^{1'}$ bound mononuclear complex at 0.18 M $LiClO_4$ indicates that a partition mechanism becomes dominant at higher $LiClO_4$ concentrations [174]. In this case the ion-pair reagent is so concentrated that all the positively charged Ru(II) species are "tightly" paired by the perchlorate ions. Ion exchange can hardly take place under such conditions. Why the dinuclear complex species shows a stronger affinity to the mobile phase (or weaker affinity to

the stationary phase) is at present not understood. Nevertheless, from the above results it is clear that a good separation with reasonable retention time can be achieved using $LiClO_4$ at a concentration either 0.10 M or 0.15 M.

$[Ru(bpy)_2(bpt)]^+$ and $[\{Ru(bpy)_2\}_2(bpt)]^{3+}$. The results obtained for sample C (main product: $[Ru(bpy)_2(bpt)]^+$) and sample D (main product: $[\{Ru(bpy)_2\}_2(bpt)]^{3+}$) are shown in Table III.2. In this case, for both mononuclear and

Table III.2 HPLC separation of $[Ru(bpy)_2(bpt)]^+$ and $[\{Ru(bpy)_2\}_2(bpt)]^{3+}$; Retention time as a function of the concentration of $LiClO_4$. Solvent: CH_3CN/H_2O (4:1 v/v).

$LiClO_4$(M)	Retention time (min)	
	sample C	sample D
0.08	5.8, 7.5(sh.)	7.5
0.09	5.2	5.3(sh.), 5.8
0.10	4.4	4.5
0.12	4.0[d], 4.7	3.9
0.15	3.0[d], 4.0	2.9
0.18	2.8[d], 4.4	2.8

d: dinuclear complex; retention time reversed.

dinuclear compounds the retention time is quite short (< 8 min.) even at 0.08 M $LiClO_4$. HPLC carried out at a higher $LiClO_4$ concentration (> 0.12 M) shows that the mononuclear complex contains a considerable amount (ca. 30%) of the dinuclear complex (Fig. III.3B - D), but at a lower concentration of $LiClO_4$ there is no separation at all between these two species (Fig. III.3A).

As observed for $[Ru(bpy)_2(bpzt)]^+$ and $[\{Ru(bpy)_2\}_2(bpzt)]^{3+}$, the reversed elution order behaviour is also observed. However, this reversion starts at a lower $LiClO_4$ concentration (0.12 M), which is reasonable as the retention time for the bpt-bridged dinuclear complex is much shorter than that for $[\{Ru(bpy)_2\}_2(bpzt)]^+$. The results indicate that if the retention time for a compound is less than 10 min., special attention should be paid to the working conditions of the HPLC system, as there would be a possibility that the mononuclear and the dinuclear complexes have a similar retention time. The separation of the mononuclear complex from the dinuclear complex and its dependence on the concentration of $LiClO_4$ is presented in Fig. III.3.

$[Ru(bpy)_2(6mbpt)]^+$ and $[\{Ru(bpy)_2\}_2(6mbpt)]^{3+}$. The results obtained on sample E (main product: $[Ru(bpy)_2(6mbpt)]^+$) and sample F (main product: $[\{Ru(bpy)_2\}_2(6mbpt)]^{3+}$) are listed in Table III.3.

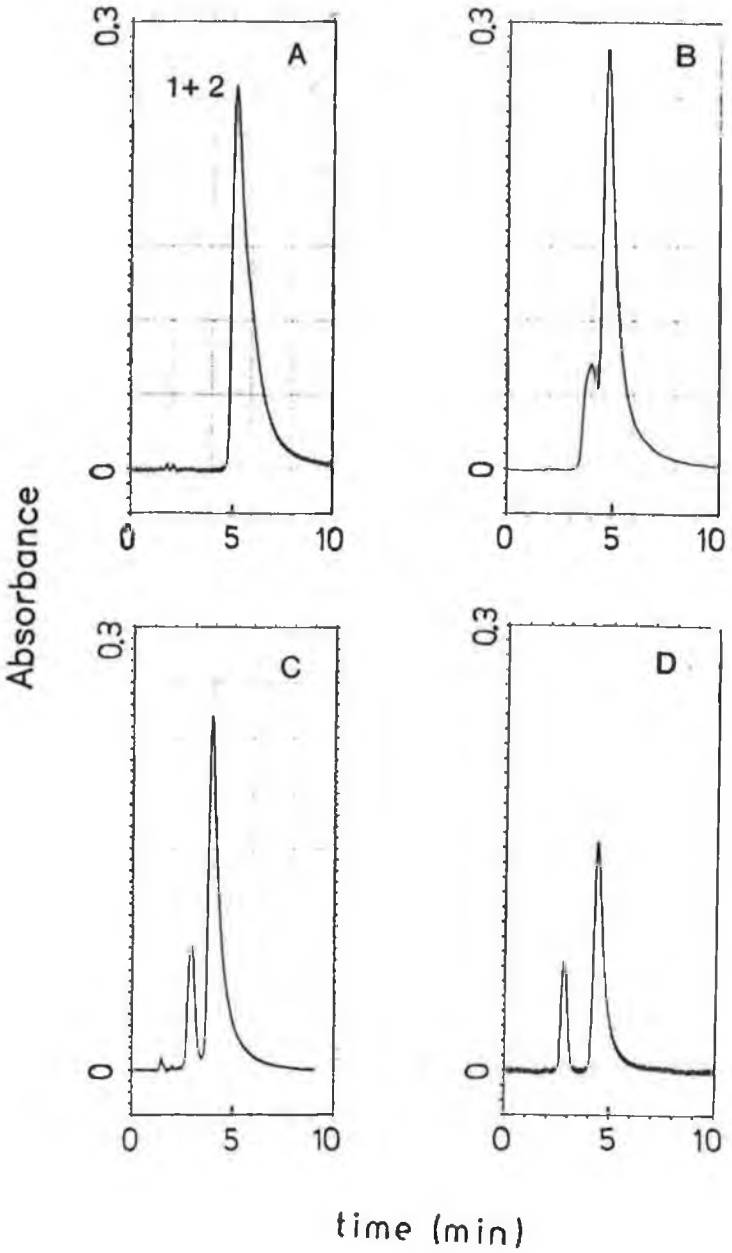

Fig. III.3 Sample C. The effect of ion-pair reagent concentration on the separation process. $LiClO_4$ concentration (from 1 to 4): 0.09 M, 0.12, 0.15 M and 0.18 M in CH_3CN/H_2O (4:1 v/v). For experimental details see text.

1 --- $[Ru(bpy)_2(bpt)]^+$;

2 --- $[\{Ru(bpy)_2\}_2(bpt)]^+$.

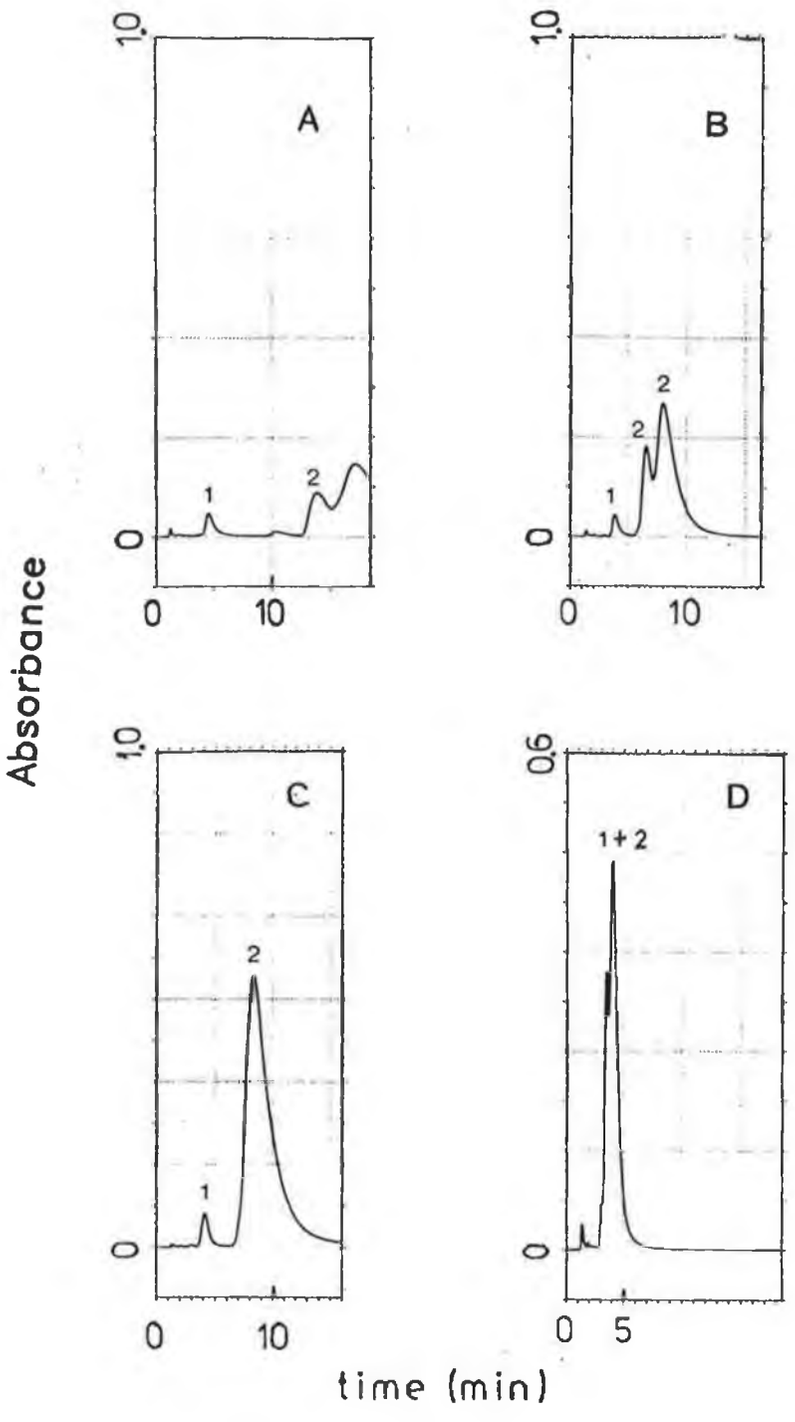

Fig. III.4 Sample F. The effect of ion-pair reagent concentration on the separation process. $LiClO_4$ concentration (from 1 to 4): 0.09 M, 0.12, 0.15 M and 0.18 M in CH_3CN/H_2O (4:1 v/v).

1 --- $[Ru(bpy)_2(6Mbpt)]^+$;

2 --- $[\{Ru(bpy)_2\}_2(6Mbpt)]^{3+}$.

Table III.3 HPLC separation of $[Ru(bpy)_2(6Mbpt)]^+$ and $[\{Ru(bpy)_2\}_2(6Mbpt)]^{3+}$; Retention time as a function of the concentration of $LiClO_4$. Solvent: CH_3CN/H_2O (4:1 v/v).

$LiClO_4$ (M)	Retention time (min)	
	sample E	sample F
0.08	4.8	5.8, 26.9, 32.8
0.09	4.2	4.6, 13.8, 16.8
0.10	4.3	4.6, 11.9, 14.8
0.12	3.7	3.9, 6.6, 8.0
0.15	3.8	4.2, 8.4
0.18	3.1	3.0(sh.), 3.5, 4.0

The chromatograms for sample F show three peaks at all $LiClO_4$ concentrations except for 0.15 M (see Fig. III.4). Compared to the chromatograms obtained for sample E, the first peak can be attributed to the mononuclear complex, while the second and third peaks are most probably due to dinuclear species. The UV-vis spectra for the second and third peaks are very similar, therefore, they might be due to different geometrical dinuclear isomers [80].

At 0.08 M $LiClO_4$, the retention times for the second and third peaks are very long (> 25 min. !). Upon increasing the

$LiClO_4$ concentration, the retention time for the dinuclear species is significantly reduced, while that for the mononuclear complex is affected much less. The second and third peaks overlap when the $LiClO_4$ concentration reaches 0.15 M, but are split again at higher centrations. No reversed behavior of the retention time is observed in this case.

III.2.3 KNO_3 as an ion-pair reagent.

The idea to use KNO_3 to replace $LiClO_4$ as an ion-pair reagent for HPLC separations is based on the results obtained on controlled-pore glass bead column chromatography (CPGBC). The CPGBC technique has been used to separate several ruthenium diimine complexes [163], and the retention time for the complexes of different size and charges strongly depends on the concentration of KNO_3 in the mobile phase (CH_3CN/H_2O, 4:1 v/v). It has been found that at 0.1 M KNO_3 or lower concentration, the complexes with lower charge (1+ or 2+) can be separated, while the dinuclear complexes (usually carrying charge > 2+) are retained on the top of the column. By increasing KNO_3 concentration up to 1 M or even higher, the dinuclear complexes can be removed from the column.

KNO_3 is a good candidate as an ion-pair reagent to replace $LiClO_4$ for the semi-preparative HPLC system, as it can be

removed from the desired ruthenium complexes after HPLC separations. By applying the conditions used for GCBCC to the cation-exchange coulmn, a similar separation quality was achieved. For instance, reaction of cis-$[Ru(bpy)_2Cl_2].2H_2O$ and $HptH_2Q$ ligand generally results in three products (see section II.1). These products have been successfully separated on a semi-preparative HPLC system using a mobile phase of CH_3CN/H_2O (4:1, v/v) containing 0.1 M KNO_3. The retention time for all three components (one of which has been proved to be a dinuclear species) is less than 10 min.. For different compounds the KNO_3 concentration should be slightly altered, in order to achieve the best separation with reasonable retention time.

II.3 Concluding remarks.

From the above results several conclusions can be drawn:

1. On the analytical HPLC system, the separation of dinuclear ruthenium complexes from their parent mononuclear species strongly depends on the $LiClO_4$ concentration. The retention time for the dinuclear species can be reduced significantly by increasing the concentration of $LiClO_4$. Even though the optimum concentration of $LiClO_4$ will vary between different compounds and can not be completely predicted, it normally falls into the region 0.12 to 0.15 M.

2. When both mononuclear and dinuclear complexes have a similar retention time (this will only happen when the dinuclear species has a retention time shorter than 8 to 10 min.), it is particularly worthwhile to examine the effect of the ion-pair reagent concentration.

3. For semi-preparative HPLC, KNO_3 can be used to replace $LiClO_4$ as an ion-pair reagent. As KNO_3 can be removed from the desired product after HPLC separation, the products can be isolated more easily as PF_6^- salts.

Chapter IV

pH Control of Nonradiative Relaxation, Photoinduced Linkage Isomerism and Ligand Substitution in Ru(II) Complexes Containing Pyridyltriazoles

Introduction.

For $[Ru(bpy)_3]^{2+}$, relaxation of the emissive metal-to-ligand charge transfer (^{3}MLCT) state exhibits a temperature dependence in 150-300 K range. This behaviour has been ascribed to a thermally activated population of the metal centered excited state (^{3}MC) which decays more rapidly than the ^{3}MLCT state [45]. In the ^{3}MC excited state, an antibonding, metal centered orbital (e_g^* in O_h symmetry) [45] is occupied and this is expected to lead to a significant distortion along the Ru-N bonding axis. Therefore, population of the ^{3}MC state often results in ligand loss, especially in the presence of coordinating anions such as halides [45].

Such photochemical reactions were investigated first by Van Houten and Watts [175] in 0.1 M HCl at temperatures between 313 and 368 K. The photosubstitution of $[Ru(bpy)_3]^{2+}$ was shown to be thermally activated, with a quantum yield of 10^{-3} to 10^{-5} depending upon conditions. The reaction involves a ligand field level (^{3}MC) which lies 3600 cm^{-1} above the lowest ^{3}MLCT level.

In 1982, Durham et al. [176], further investigated the temperature dependent emission lifetime and photochemistry of $[Ru(bpy)_3]^{2+}$ in dichloromethane. A substantial difference between aqueous and CH_2Cl_2 solutions is that

salts of $[Ru(bpy)_3]^{2+}$ are completely ion-paired in the latter. It was found that irradiation of $[Ru(bpy)_3]X_2$ (X = Cl^-, Br^-, and NCS^-) always gives rise to $[Ru(bpy)_2X_2]$ as a final product (eq. IV.1):

$$[Ru(bpy)_3]X_2 \xrightarrow[CH_2Cl_2]{h\upsilon} [Ru(bpy)_2X_2] + bpy \qquad (IV.1)$$

When the photolysis was carried out in the presence of NCS^-, there is clear evidence that the loss of a bpy ligand occurs in a stepwise manner. It has been proposed that a monodentate intermediate $[(bpy)_2Ru(NCS)bpy]^+$ is formed during the reaction. This intermediate is very unstable and, within minutes, reacts thermally at room temperature with NCS^- to give $[Ru(bpy)_2(NCS)_2]$. The overall mechanism in CH_2Cl_2 can be ascribed by eq. IV.2:

$$[Ru(bpy)_3]X_2 \xrightarrow[CH_2Cl_2]{h\upsilon} [(bpy)_2Ru(X)(bpy)]X$$
$$[(bpy)_2Ru(X)(bpy)]X \xrightarrow[CH_2Cl_2]{h\upsilon} [Ru(bpy)_2(X)_2] + bpy \qquad (IV.2)$$

Such photosubstitutional reactivity of $[Ru(bpy)_3]^{2+}$, although may be of some synthetic use, is certainly a drawback for the utilisation of this complex in solar energy conversion systems. In the past ten years, much work has been devoted to Ru(II) polypyridyl complexes. By changing the coordinating ligands, the redox properties and excited state photophysical properties of Ru(II) complexes can be

altered. However, the alteration and control of photophysical properties is much more difficult than those of ground state redox properties. As described in Chapter I, a photostable complex with a non-accessible ^{3}MC state usually shows a small temperature dependence of the emission lifetime. Up to 1989, among numerous ruthenium diimine complexes synthesised in different groups, only about 10 (!) were found to exhibit small temperature dependence of the emission liftimes and photostability against lignad substitution [56, 69, 129].

To isolate the ^{3}MC state from the ^{3}MLCT state, the energy gap ^{3}MLCT - ^{3}MC should be enlarged as much as possible. The energy level of a ^{3}MC state and of a ^{3}MLCT state depend on the σ-donating and π-accepting properties of the coordinated ligands. Strong σ-donating ligands tend to increase the ^{3}MC energy level but the t_{2g} - ^{3}MLCT energy gap may decrease because the electron density denoted from these ligands will destabilise the t_{2g} energy level. Good π-accepting ligands may also serve to enlarge the ^{3}MLCT - ^{3}MC gap, but again the t_{2g} - ^{3}MLCT energy gap will be decreased. The t_{2g} - ^{3}MLCT gap in a spin-orbit coupled system will determine the excited state lifetime and quantum yield. The energy gap law [52] predicts that the non-radiative decay rate of the excited-state increases linearly with the decrease in emission energy. It is obvious that a compromise has to be found between the

isolation of the ^{3}MC state and the inevitable decrease of the emission lifetime, as for energy conversion applications the excited state lifetime has to be long enough to undergo electron or energy transfer processes. The synthetic control of ^{3}MLCT - ^{3}MC energy gap and ^{3}MLCT energy level simultaneously is, therefore, very difficult. At present, there is no quantitative theory available which can effectively direct the design of ligands with which the Ru(II) complexes can be made with both an inaccessible ^{3}MC level and a long lifetime.

For the Ru(II) complexes containing ligands with non-coordinated atom(s) that can be protonated such as nitrogen, the photophysical and photochemical properties of the complexes can be further altered by pH. This is because the σ-donating and π-accepting properties of the ligands can be changed by protonation/deprotonation. In fact, it has been shown that upon protonation/deprotonation of the coordinated ligands, the redox potentials, the absorption and emission energies can be changed appreciably [77-86, 88-103].

However, the acid-base chemistry of Ru(II) diimine complexes has not so far concerned itself with the effect of protonation/deprotonation on the photochemical reactivity. Most of the work has been concentrated on the ground-state metal-to-ligand interactions, on the determination of the ligand involved in the emitting states, and on the dynamic

aspect of the excited-state proton transfer process. These aspects of the acid-base chemistry of the Ru(II) complexes will be discussed further in Chapter V.

In this chapter, the protonation/deprotonation effect on the photophysical and photochemical properties of $[Ru(bpy)_2(Hptr)]^{2+}$ will be described. This complex contains two coordination isomers [84-85], and the structures of the two isomers are presented in Fig. IV.1.

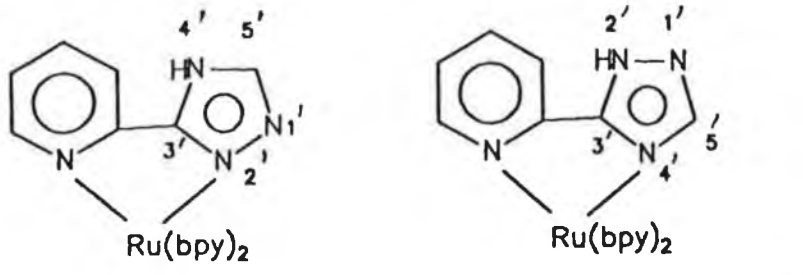

$[Ru(bpy)_2(Hptr\text{-}2)]^{2+}$ $[Ru(bpy)_2(Hptr\text{-}4)]^{2+}$

Fig. IV.1 The structures of the two coordination isomers of $[Ru(bpy)_2(Hptr)]^{2+}$.

Previous studies have shown that the ground-state redox potentials, the absorption and emission energies for the two isomers are not identical [84-85]. The redox and photophysical properties of these two isomers are affected not only by the coordination mode but also by the protonation of the non-coordinated nitrogen. Acid-base chemistry shows

that the two isomers have shown ground-state pK_a values differing in about two pH units [85]. Preliminary photophysical studies suggest that at room temperature for both isomers the deprotonated forms have higher emission quantum yields and longer emission lifetimes than thier protonated analogues in Britton-Robinson buffer [85]. In this work, a detailed photophysical study on the two isomers will be described, which will focuse on the excited-state decay and photochemical reactivity associated with and controlled by protonation and deprotonation.

IV.2 Results and Discussion.

IV.2.1 General properties of the two isomers of $[Ru(bpy)_2(Hptr)]^{2+}$.

From Fig. IV.1 it is clear that on the triazole ring there are two nitrogens potentially available for coordination ($N^{2'}$ and $N^{4'}$). The formation of the two coordination isomers was found to be of approximately 1:1 ratio, according to HPLC analysis of the mixture obtained from synthesis [84-85, 171]. Injection of a mixture of the two isomers onto the cation exchange column (for working conditions see Chapter II) yields two very well resolved peaks. The coordination mode for each isomer has been elucidated by proton NMR [84]. In this text, the $N^{2'}$ bound isomer will be referred to $[Ru(bpy)_2(Hptr\text{-}2)]^{2+}$ and $N^{4'}$ bound

isomer $[Ru(bpy)_2(Hptr\text{-}4)]^{2+}$. The absorption and emission energies, together with the electrochemical potentials, are listed in Table IV.1.

Several conclusions can be drawn from Table IV.1. First, the Hptr ligand, either in protonated or in deprotonated form, is a stronger σ-donor and π-acceptor compared to bpy. This is reflected by the lower energy in absorption maxima and lower Ru(II/III) oxidation potentials for the two isomers compared to that of $[Ru(bpy)_3]^{2+}$. That the Hptr ligand is a weaker π-acceptor compared to bpy is also reflected by its very negative reduction potential (Table IV.1). The Hptr ligand is much more difficult to reduce than bpy, indicating that the LUMO (π^* energy) level for Hptr (or ptr^-) is higher than that of bpy in the two coordination isomers. Thus for both $[Ru(bpy)_2(Hptr\text{-}4)]^{2+}$ (or $[Ru(bpy)_2(ptr\text{-}4)]^{+}$) and $[Ru(bpy)_2(Hptr\text{-}2)]^{2+}$ (or $[Ru(bpy)_2(ptr\text{-}2)]^{+}$ the emission observed orginates from bpy based π^* orbitals [85].

IV.2.2 Evidence of the two factors governing the excited state decay: energy gap law and ^{3}MC state population.

The room temperature and low temperature (110 K) lifetimes for the two isomers in protonated form and deprotonated forms are listed in Table IV.2. Assuming that the efficiency for

Table IV.1 Absorption, emission and electrochemical data for Ru(II) complexes containing pyridyltriazoles.

	λ_{max}[a], nm (log e)	λ_{em}, nm		$E^{0'}$ (V vs SCE)[e]			
		RT[a]	77 K[b]	Ru(II/III)	Ligand based		
$[Ru(bpy)_2(Hptr\text{-}4)]^{2+}$	452 (4.05)	616	580	1.20	-1.47	-1.72	-2.25
$[Ru(bpy)_2(ptr\text{-}4)]^{+}$	488 (3.97)	678	607	0.90	-1.51	-1.78	
$[Ru(bpy)_2(Hptr\text{-}2)]^{2+}$	444 (4.11)	611	577	1.14	-1.49	-1.73	-2.25
$[Ru(bpy)_2(ptr\text{-}2)]^{+}$	484 (4.04)	677	607	0.83	-1.49	-1.74	
$[Ru(bpy)_2(H3Mptr)]^{2+}$	438 (----)	615	587	1.20	-1.55	-1.88	-2.27
$[Ru(bpy)_2(3Mptr)]^{+}$	488 (----)	713	610	0.80	-1.48	-1.74	
$[Ru(bpy)_3]^{2+}$	452 (1.29)c	608c	582d	1.26	-1.35	-1.55	-1.80

a. Measured in CH_3CN. The protonation and deprotonation were ensured by adding CF_3COOH and Et_2NH.

b. Measured in 4:1 ethanol/methanol. Protonation and deprotonation were ensured by adding conc. HCl or NaOH.

c. Measured in CH_3CN [69].

d. Measured in 4:1 ethanol/methanol [69].

e. Measured in CH_3CN containing 0.1 M TEAP by differential pulse voltammetry [84].

Table IV.2 Emission lifetimes at room temperature and at 110 K obtained on the Ru(II) complexes containing pyridyltriazoles.

	τ, ns[a] 298 K	τ, ns[b] 110 K	ϕ_{em}[d] ($x10^4$)	k_r ($x10^{-4}s^{-1}$)
$[Ru(bpy)_2(Hptr\text{-}4)]^{2+}$	2	3548	7.3	3.7
$[Ru(bpy)_2(ptr\text{-}4)]^{+}$	205	1570	63	3.1
$[Ru(bpy)_2(Hptr\text{-}2)]^{2+}$	5	3635	4.3	8.6
$[Ru(bpy)_2(ptr\text{-}2)]^{+}$	142	2436	30	2.1
$[Ru(bpy)_2(H3Mptr)]^{2+}$	9	4517	5.5	6.1
$[Ru(bpy)_2(3Mptr)]^{+}$	46	2334	11	2.4
$[Ru(bpy)_3]^{2+}$	860[c]	5210[e]	620[f]	6.0

a. Measured in CH_3CN.

b. Measured in 4:1 ethanol/methanol.

c. Ref. 64.

d. Measured in 298 K in CH_3CN.

e. Ref. 177.

f. Ref. 160.

^{1}MLCT ---> ^{3}MLCT intersystem crossing is unity [45], the emission quantum yields (ϕ_{em}) and radiative decay rate constants (k_r) calculated according to eq. IV.3 [45] are also listed in the Table.

$$k_r = \phi_{em}\, \tau^{-1} \qquad \text{(IV.3)}$$

(τ stands for the emission lifetime at room temperature.) The data show that the emission decay processes are very complex. At room temperature, the lifetimes for the protonated complexes are much shorter than those of the deprotonated ones. However, at 110 K an opposite behaviour was observed: both protonated isomers show longer emission lifetimes.

That at low temperature the protonated isomers have longer lifetimes might be explained by the "energy gap law" [52]. Upon protonation, the ligand (Hptr) becomes a better π-acceptor but a weaker σ-donor compared to the deprotonated form. As a consequence, the t_{2g} orbitals are stabilised, and the t_{2g} - ^{3}MLCT energy gap is increased. Indeed the protonated species have higher emission energy (see Table IV.1). According to the energy gap law, the nonradiative decay rate for the protonated species should decrease relative to that for the deprotonated ones. In other words, the protonated complexes should have longer emission lifetimes.

Room temperature data, however, indicate that the changes in the emission lifetime with the protonation of the triazole ring are not governed by the energy gap law. The lifetimes for both isomers decrease upon protonation. Furthermore, emission lifetime and quantum yield data show that radiative decay rates change by little more than a factor of two upon protonation of the complexes. Thus, the bulk of the observed change is in the nonradiative relaxation rates of the two isomers and, most likely, the nonradiative relaxation is via another competing pathway: the thermally activated population of a ^{3}MC state close in energy to the ^{3}MLCT state (vide supra). This ^{3}MC state is much more difficult to populate at very low temperature (< 150 K) [52].

As described above, upon protonation the coordinated pyridyltriazole ligand becomes a weaker σ-donor and better π-acceptor. The weaker σ-donating ability causes a smaller splitting of t_{2g} - e_g^* energy gap, while increased π^*-accepting ability reduces the t_{2g} - ^{3}MLCT gap. Both changes in metal-ligand interaction upon protonation should serve to decrease the energy gap between the ^{3}MLCT and ^{3}MC states. Therefore protonation of the complex favours the population of the ^{3}MC state, which undergoes fast non-radiative decay. On the other hand, for the deprotonated isomers, the ^{3}MLCT - ^{3}MC energy gap is much larger, as the negatively charged pyridyltriazole ligand is a stronger σ-donor and the t_{2g} - e_g^* energy gap is increased.

Therefore, the ^{3}MC state is more difficult to populate, and this is reflected by the longer emission lifetimes.

IV.2.2 Temperature dependent emission lifetime behaviour.

The temperature dependence of the luminescence lifetime of both $N^{2'}$ and $N^{4'}$ isomers was examined in 4:1 ethanol/methanol solutions. Results over the temperature range 110 K to 290 K are shown in Fig. IV.2. Both isomers exhibit a much stronger temperature dependence in their protonated forms. The data were fit by assuming that the excited state decay consists of a temperature independent intrinsic decay from the ^{3}MLCT state and a single thermally activated nonradiative decay process (eq. IV.4) [45].

$$1/\tau_{obs} = k_0 + k'\exp(-E_a/RT) \qquad \text{(IV.4)}$$

The first term is the sum of the temperature independent radiative and non-radiative decay (eq. IV.5) [45]:

$$k_0 = k_{nr} + k_r \qquad \text{(IV.5)}$$

Other approaches have been used in treating temperature dependent lifetimes of related Ru(II) diimine complexes, in particular, additional parameters are frequently included to fit data obtained in the solvent-glass transition region (110-130 K for 4:1 ethanol:methanol) [41]. With the

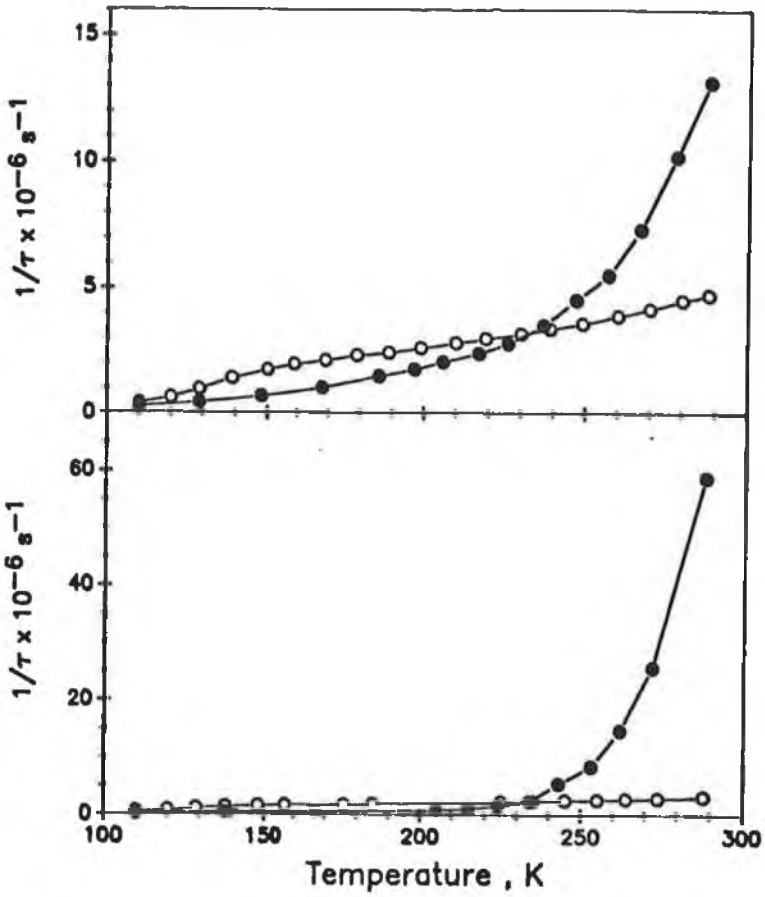

Fig. IV.2 Emission lifetime as a function of temperature in 4:1 ethanol/methanl.

A --- $[Ru(bpy)(Hptr\text{-}2)]^{2+}$ (●);

$[Ru(bpy)(ptr\text{-}2)]^{+}$ (o);

B --- $[Ru(bpy)(Hptr\text{-}4)]^{2+}$ (●);

$[Ru(bpy)(ptr\text{-}4)]^{+}$ (o);

exception of $[Ru(bpy)_2(ptr\text{-}2)]^+$ the data can be adequately fit without employing the solvent parameters. Results of data fit to eq. IV.4 are given in Table IV.3; parameters for $[Ru(bpy)_2(ptr\text{-}2)]^+$ were obtained by fitting data obtained at temperature above the glass transition temperature (>150 K) using eq. IV.4.

Activation parameters obtained for complexes having ^{3}MLCT states usually fall into one of two categories: (a) small activation energies (< 800 cm^{-1}) and low prefactors (< 10^9 s^{-1}) or (b) large activation energies (> 2000 cm^{-1}) and large prefactors (> 10^{11} s^{-1}) [45]. In the second case the activation process has been ascribed to population of the ^{3}MC state. If the ^{3}MLCT and ^{3}MC states are in equilibrium, the measured "activation energy" corresponds to the energy gap between the two states [45, 56]. If relaxation of the ^{3}MC state is rapid relative to crossover from the ^{3}MC state back to the ^{3}MLCT state, the measured E_a represents the activation energy for ^{3}MLCT - ^{3}MC internal conversion. Since the process is viewed as an electron transfer in a strongly coupled system, the prefactor is expected to be large (10^{13} - 10^{14} s^{-1}). When both the activation barrier and prefactor are small, interpretation of data is less clear. Complexes exibiting this behaviour are typically unreactive to photosubstitution and it is unlikely that population of the ^{3}MC state occurs [45, 56, 69]. The low prefactor also suggests the process

involves the population of a state only weakly coupled to the ^{3}MLCT state. Based on these observations and molecular orbital calculations, Kober and Meyer have postulated that this activated process corresponds to the population of a MLCT state of largely singlet character [45].

From the activation parameters obtained for the two isomers in both protonated and deprotonated forms in (4:1) ethanol/methanol, it appears that only $[Ru(bpy)_2(Hptr\text{-}4)]^{2+}$ has a prefactor and activation barrier common to complexes having the E_a values which can be interpreted as the activation barriers from the ^{3}MLCT state to the ^{3}MC state. The deprotonated forms of both isomers have low prefactors and small activation barriers characteristic of photoinert complexes. $[Ru(bpy)_2(Hptr\text{-}2)]^{2+}$ exhibits intermediate behaviour; however, the prefactor of $6x10^{10}$ s^{-1} and 1700 cm^{-1} "activation barrier" are not unreasonable for ^{3}MLCT and ^{3}MC states in equilibrium [56]. If the assumption is made that the ^{3}MLCT and ^{3}MC states are in equilibrium then the observed activation energies can be taken to be the ^{3}MLCT - ^{3}MC gap for $[Ru(bpy)_2(Hptr\text{-}2)]^{2+}$.

Further analysis can be made based on the comparison of rate constants illustrated in Scheme II.

Scheme II

$$GS \xrightarrow{h\upsilon} {}^1MLCT \xrightarrow{\phi_{ISC}\doteq 1} {}^3MLCT$$

$${}^3MLCT \xrightarrow{k_1} GS \quad (k_1 = k_r + k_{nr})$$

$${}^3MLCT \underset{k_{-2}}{\overset{k_2}{\rightleftharpoons}} {}^3MC$$

$${}^3MC \xrightarrow{k} \text{photochemistry}$$

$${}^3MC \xrightarrow{k_3} GS$$

Using the rate constants defined in Scheme II, steady state approximation for the ^3MC state formation leads to the expression in eq. IV.6 for the lifetime of the ^3MLCT emitting state (see appendix I):

$$1/\tau = k_1 + k_2(k_3 + k_4)/(k_{-2} + k_3 + k_4) \quad (IV.6)$$

In eq. IV.6, $k_1 = k_r + k_{nr}$, which can be considered to be temperature independent; The second term deals with the ^3MC state and is temperature dependent (eq. IV.7) [56, 176]:

$$k_2(k_3 + k_4)/(k_{-2} + k_3 + k_4) = k'\exp(-E_a/RT) \quad (IV.7)$$

For this term, there are two limiting cases. In the first, $k_{-2} >> (k_3 + k_4)$, then

$$(k_3 + k_4)/(k_2/k_{-2}) = k'\exp(-E_a/RT) \quad (IV.8)$$

In this limit, the back electron transfer from the ^3MC

level (e_g^*; Ru(II)) to the ^{3}MLCT state (π^*; ligand) is very fast compared to the ^{3}MC decay (k_3) and photochemistry (k_4). So the ^{3}MC state is in equilibrium with the ^{3}MLCT state before any ^{3}MC decays take place. If this limiting case is valid, the experimental rate constants and E_a are complex and can not be interpreted in a definite way. The difficulty arises from that the ^{3}MC state is not spectroscopically observable and k_3 and k_4 are probably parallel processes which are impossible to differentiate. However, it is probably safe to assume that the exponential term is dominated by the energy gap between the ^{3}MC and ^{3}MLCT state [56, 176]. For $[Ru(bpy)_2(Hptr\text{-}2)]^{2+}$, the prefactor k'($6.0\times10^{10}$ s^{-1}) and E_a (1710 cm^{-1}) can be considered to belong to this limiting case [56, 176].

In the second limiting case, $k_{-2} << (k_3 + k_4)$, eq IV.7 becomes eq. IV.9:

$$k_2 = k'\exp(-E_a/RT) \qquad \text{(IV.9)}$$

In this limit the ^{3}MLCT - ^{3}MC transition becomes an irreversible surface crossing, as the subsequent decay from the ^{3}MC state is probably very fast. So the E_a is the activation energy for this surface crossing. The preexponential factor k' becomes the rate constant for the population of the ^{3}MC state. For $[Ru(bpy)_2(Hptr\text{-}4)]^{2+}$, the k' ($9.2\times10^{13}$ s^{-1}) and E_a (2860 cm^{-1}) values can

be classified into this second limiting case [56, 176].

By combining redox and luminescence data, approximate relative state energies for the protonated and free base forms of each complex can be represented as shown in Fig. IV.3. The relative ground state energies are obtained from the Ru(II/III) potentials [84], while the approximate ^{3}MLCT state energies are obtained from the room temperature luminescence maxima [84]. The ^{3}MC state energies can not be determined directly, but can be approximated from activation parameters obtained from temperature dependent luminescence lifetimes [129].

The activation energy for populating the ^{3}MC state for the deprotonated species can not be determined from the temperature dependent emission lifetime data. A rough estimate can be made according to the t_{2g} - e_g^* gap values obtained for the protonated complexes. For protonated forms, the energy gap between t_{2g} and e_g^* can be estimated using eq. VI.10 [129]:

$$E_{(t_{2g}-e_g^*)} = E_{em} + E_a(^3\text{MLCT}-^3\text{MC}). \qquad \text{(IV.10)}$$

For deprotonated complexes, due to the stronger -donating ability of the ligand (ptr^-), the splitting between t_{2g} and e_g^* levels is expected to be much larger. The exact values for the the energy gap between t_{2g} and e_g^* are

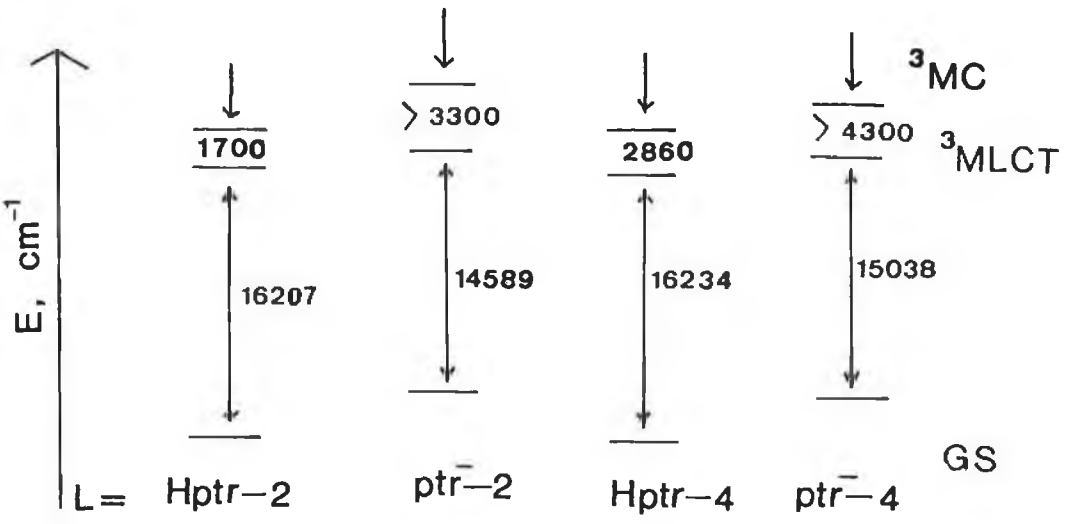

Fig. IV.3 The relative energy levels for $Ru(bpy)_2$ complexes containing ligand L.

unknown, so for calculation purpose it is assumed that this energy gap is the same for both protonated and deprotonated complexes in order to calculate the minimum values of the ^{3}MLCT - ^{3}MC energy gap for the deprotonated complexes. For $[Ru(bpy)_2(ptr\text{-}4)]^+$ the ^{3}MLCT-^{3}MC energy difference obtained using this approximation is 4300 cm^{-1} while for $[Ru(bpy)_2(ptr\text{-}2)]^+$ a gap of 3300 cm^{-1} is obtained. Because of the assumption made above these values are only minimum ones. The data indicate that for $[Ru(bpy)_2(ptr\text{-}4)]^+$ the energy gap will be > 4300 cm^{-1} and that of $[Ru(bpy)_2(ptr\text{-}2)]^+$ > 3300 cm^{-1}. Further assuming that prefactors for populating the ^{3}MC state are similar for protonated and deprotonated complexes, the efficiency of population of ^{3}MC states (η_{ic}) will be much smaller.

The internal conversion efficiency for the population of the ^{3}MC state (η_{ic}) can be calculated using eq. IV.11 [56, 129]:

$$\eta_{ic} = \frac{k'\exp(-E_a/RT)}{k_0 + k'\exp(-E_a/RT)} \qquad \text{(IV.11)}$$

Calculated values of η_{ic} for the protonated and the deprotonated complexes are listed in Table IV.3. For the deprotonated complexes values of η_{ic} are also calculated from the parameters given in Table IV.3 (k_0, k' and

Table IV.3 Activation parameters from temperature dependent emission lifetimes[a]; photoantion quantum yields (ϕ_p).

	k_0, s^{-1}	k', s^{-1}	E_a, cm^{-1}	η_{ic}	ϕ_p[b]
$[Ru(bpy)_2(Hptr-4)]^{2+}$	$6.1x10^6$	$9.2x10^{13}$	2860	0.94	0.0437
$[Ru(bpy)_2(ptr-4)]^{+}$	$1.6x10^6$	$3.1x10^7$	600	0.050(0.52)[c]	0
$[Ru(bpy)_2(Hptr-2)]^{2+}$	$1.6x10^6$	$6.0x10^{10}$	1710	0.91	0.0385
$[Ru(bpy)_2(ptr-2)]^{+}$	$1.7x10^6$	$4.7x10^7$	550	0.004(0.66)[c]	0

a. Measured in 4:1 ethanol/methanol.

b. measured in CH_2Cl_2 containing 3 mM TBAB; values are relative to $[Ru(bpy)_3]^{2+}$.

c. Internal conversion to state other than the ^{3}MC excited state. See text.

E_a). These values represent the efficiency for the population of a state other than the ^{3}MC state (which decays faster than the ^{3}MLCT state [129]. The relative energy levels for the two isomers in protonated and deprotonated forms are illustrated in Fig. IV.3.

IV.2.4 Photoanation reactions.

One measure of the validity of the above description of the excited-state decay is the susceptibility of the complexes to photoanation in non-polar solvents. For $[Ru(bpy)_3]^{2+}$ and numerous other Ru(II) diimine complexes, photolysis in the presence of coordination anions (e.g. halides or NCS^-) results in a loss of one of the three bidentate ligands and formation of bis halo- or bis NCS^- complexes. This photoanation process does not occur readily for complexes having ^{3}MC states which are not accessible from the ^{3}MLCT states [56, 69, 129].

Therefore the deprotonated isomers are expected to be much more photochemically stable against photosubstitutional reactions upon photolysis in the presence of coordination ions in CH_2Cl_2. Indeed these deprotonated species were found to be unusually photoinert. Even upon prolonged (>8 h) photoexcitation no evidence of photoanation was observed This high stability against photochemical reaction is, of course, desired for energy conversion applications. But it

should be noticed that the lifetimes for both isomers in deprotonated form are significantly lower compared to $[Ru(bpy)_3]^{2+}$, which might mainly result from the decrease in emission energy (energy gap law).

The photostability of the deprotonated isomers is consistent with the excited state decay behaviour; for the deprotonated isomers, the ^3MC state is inaccessible at room temperature. In contrast, the protonated complexes are photochemcally labile (vide infra) due to the fact the ^3MC state can be easily populated. Thus, the photosubstitutional ability of these two isomers can be controlled simply by adjusting the pH of the solution.

As expected, photolysis of either $[Ru(bpy)_2(Hptr\text{-}4)]^{2+}$ or $[Ru(bpy)_2(Hptr\text{-}2)]^{2+}$ in CH_2Cl_2 containing Br^- results in the formation of a cis-dibromo complex. The photolyses monitored by UV-vis spectroscopy are presented in Fig. IV.4. The results on $[Ru(bpy)_3]^{2+}$ are also presented for comparison. Fig. IV.4 shows that for $[Ru(bpy)_3]^{2+}$, photolysis results in a clean conversion to $[Ru(bpy)_2Br_2]$ (λ_{max} 548 nm [69]). For $[Ru(bpy)_2(Hptr\text{-}4)]^{2+}$, three isosbestic points are maintained through most of the photolysis, but for $[Ru(bpy)_2(Hptr\text{-}2)]^{2+}$ clearly more than two species are present in solution during the photolysis. The observed loss of isosbestic points suggests that some product other than

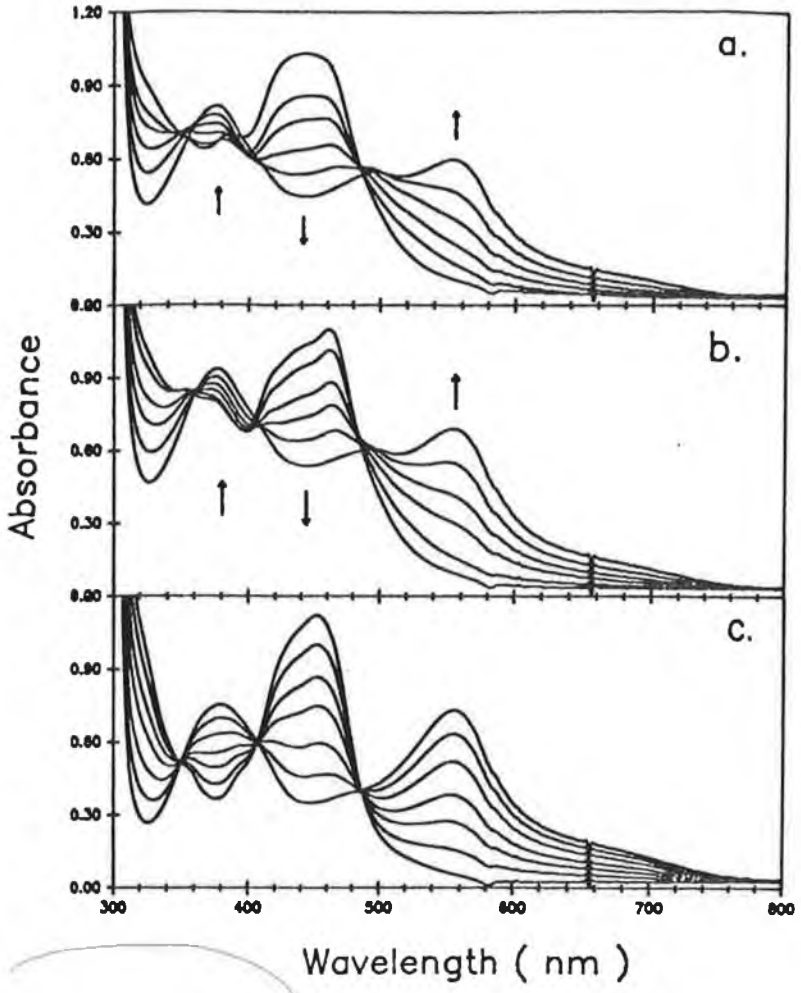

Fig. IV.4 Photolysis of (a) $[Ru(bpy)_2(Hptr\text{-}2)]^{2+}$, (b) $[Ru(bpy)_2(Hptr\text{-}4)]^{2+}$ and (c) $[Ru(bpy)_3]^{2+}$ in CH_2Cl_2 containing 3 mM TBAB.

$[Ru(bpy)_2Br_2]$ is formed during the photolysis.

In order to examine the photoprocess of the protonated complexes in 3 mM TBAB/CH_2Cl_2 in more detail, aliquots taken during photolysis were examined by HPLC using photodiode array spectrophotometric detection. HPLC traces taken before and at three times during photolysis of $[Ru(bpy)_2(HPtr\text{-}2)]^{2+}$ are shown in Fig. IV.5 and spectra of the fractions obtained are shown in Fig. IV.6. In Fig. IV.5, peak 1 is attributed to CH_2Cl_2. Peak 2 is due to the starting material $[Ru(bpy)_2(Hptr\text{-}2)]^{2+}$ while peaks 3-5 are due to photolysis products. UV-vis aborption spectra for peak 3-5 are identical and are all characteristic of $[Ru(bpy)_2Br_2]$ (Fig. IV.6). This peak splitting behaviour is not understood at present. But it is worth pointing out that when only $[Ru(bpy)_2Cl_2]$ is injected into the HPLC system similar peak splitting behaviour is also observed. Peak 6 is due to the free ligand dissociated from the complex. Peak 7 is due to a small amount of $[Ru(bpy)_2(Hptr\text{-}4)]^{2+}$ formed during photolysis, which might be responsible for the loss of the isosbestic points in the UV-vis absorption spectra (Fig. IV.6). A more detailed investigation and discussion of this linkage isomerism will be given in next section.

The photolysis of $[Ru(bpy)_2)(Hptr\text{-}4)]^{2+}$ in TBAB/CH_2Cl_2 monitored by HPLC is presented in Fig. IV.7.

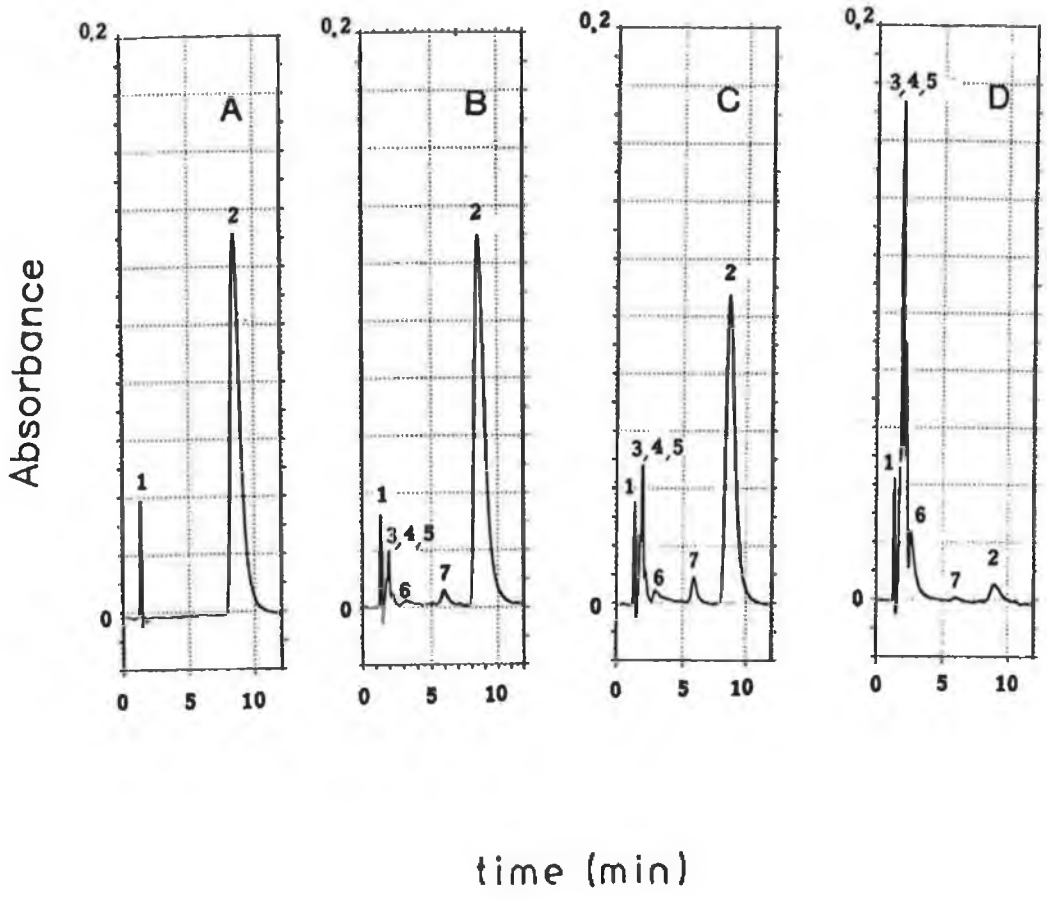

Fig. IV.5 Photolysis of $[Ru(bpy)_2(Hptr\text{-}2)]^{2+}$ in TBAB/CH_2Cl_2. From A to D: 0, 1.5, 2.5, 4.1 min. irradiation. Monitored at 280 nm.

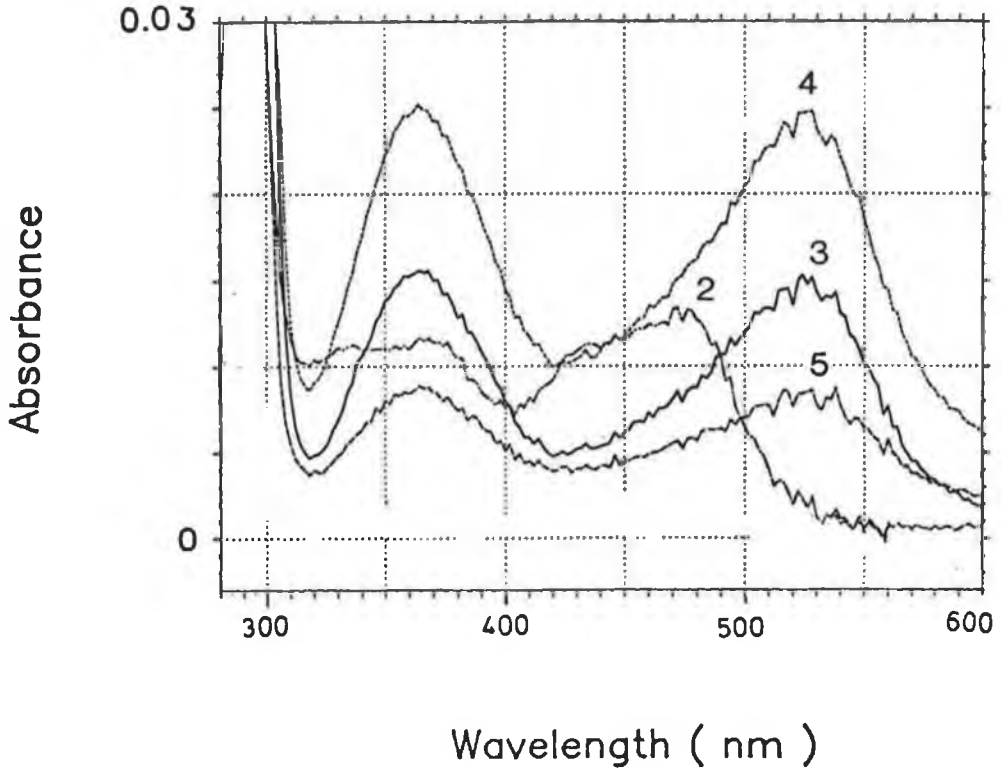

Fig. IV.6 UV-vis absorption spectra obtained for the fractions during photolysis of $[Ru(bpy)_2(Hptr\text{-}2)]^{2+}$. The numbering of the peaks (2-5) are corresponding to the numbering for the chromagram peaks (2-5) in Fig. IV.5.

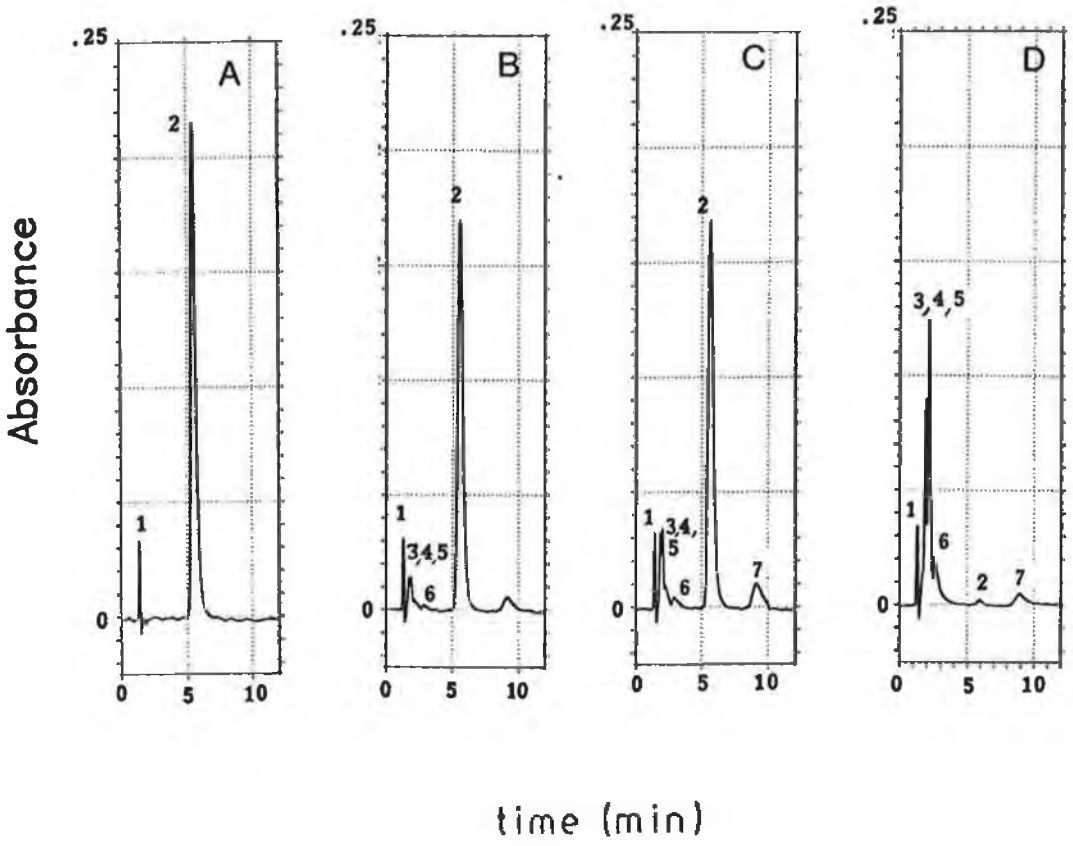

Fig. IV.7 Photolysis of $[Ru(bpy)_2(Hptr\text{-}4)]^{2+}$ in CH_2Cl_2 containing 3 mM TBAB. From A to D: 0, 1, 3, 170 min..

The UV-vis absorption spectra for the different fractions are shown in Fig. IV.8. It can be seen that the photolysis process is very similar to that found for $[Ru(bpy)_2(Hptr\text{-}2)]^{2+}$, which involves the formation of $[Ru(bpy)_2Br_2]$ as a final product. Again, a small amount of the other isomer, $[Ru(bpy)_2(Hptr\text{-}2)]^{2+}$ is formed during the photolysis.

The photosubstitutional reaction observed for the two protonated isomers, together with their temperature dependent lifetime data, strongly suggest that the competing pathway for nonradiative relaxation is the thermally activated population of the ^3MC state close in energy to the ^3MLCT state. In the studies of the effect of protonation on the excited-state behaviour of $[Ru(bpy)_2(CN)_2]$, Scandola and co-workers postulated that protonation of the complex results in a decrease in the ^3MLCT - ^3MC gap and a subsequent increase in the nonradiative relaxation rate [178]. In the case of the pyridyltriazole complexes, protonation results in an increase in the emission energy and the decrease in the ^3MLCT -^3MC energy gap. Therefore the photosubstitution most likely results from a facile internal conversion to a ^3MC state which rapidly relaxes to the ground state.

The photoanation quantum yields (Table IV.3) indicate that for both isomers the photoanation process is less efficient than for $[Ru(bpy)_3]^{2+}$. The E_a for populating the ^3MC

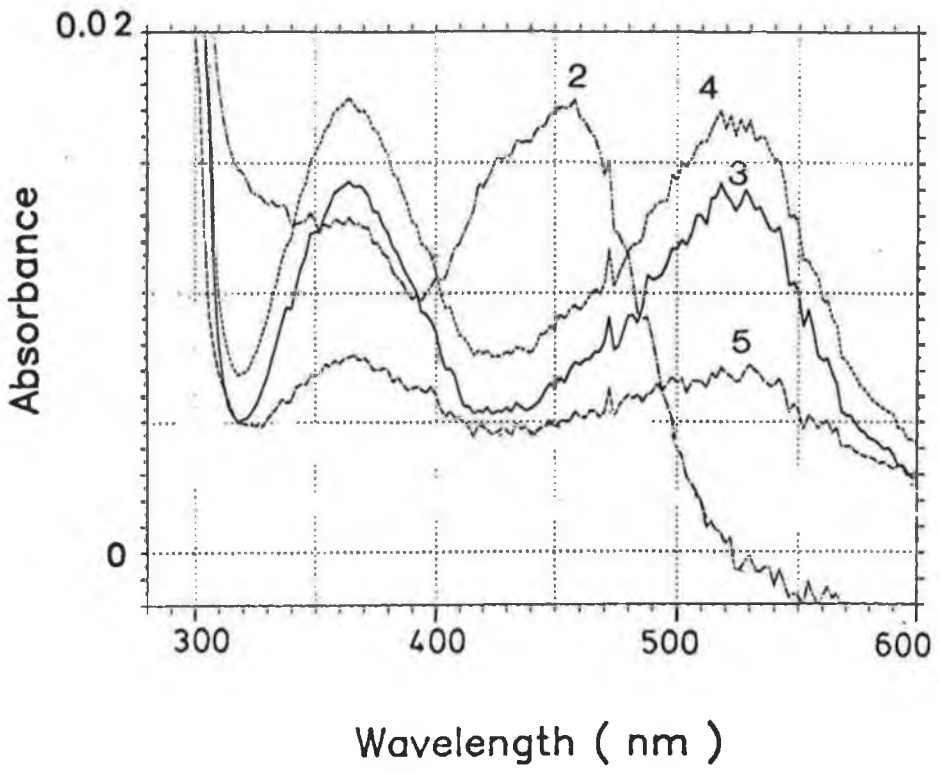

Fig. IV.8 UV-vis absorption spectra obtained for the fractions during photolysis of $[Ru(bpy)_2(Hptr\text{-}4)]^{2+}$. The numbering of the peaks (2-5) are corresponding to the numbering for the chromagram peaks (2-5) in Fig. IV.7.

level from the ^{3}MLCT level is 2860 cm^{-1} for $[Ru(bpy)_2(Hptr\text{-}4)]^{2+}$, which is lower than that for $[Ru(bpy)_3]^{2+}$ (3600 cm^{-1} in CH_2Cl_2 [177]). This suggests that population of the ^{3}MC state is not the rate determining step during the photoanation process. The low efficiency of the photoanation for the two isomers might be due to the slow kinetics for the ligand loss subsequent to the population of the ^{3}MC state.

In a related study, the photoanation behaviour of $[Ru(bpy)_2(bpt)]^+$ and the dinuclear complex $[\{Ru(bpy)_2\}_2bpt]^{3+}$ was recently reported by Balzani, Vos and co-workers [82]. The mononuclear complex is photoinert and has activation parameters for nonradiative decay similar to those of $[Ru(bpy)_2(ptr\text{-}2)]^{2+}$ ($k' = 6.5 \times 10^7$ s^{-1} and E_a = 660 cm^{-1} in 4:5 propionitrile: butyronitrile). The dinuclear complex exhibits photophysical characteristics and photoanation behaviour similar to $[Ru(bpy)(Hptr\text{-}2)]^{2+}$. The photoreactivity of $[\{Ru(bpy)_2\}_2bpt]^+$ is attributed to the population of a ^{3}MC state because the ligand field strength of the bpt^- ligand decrease upon coordination of the second metal center (analogous to the protonation effect to a certain extent). The same behaviour is observed upon protonation of the coordinated ptr^- ligands.

IV.2.5 Photoinduced linkage isomerism.

Photolysis of $[Ru(bpy)_2(Hptr\text{-}2)]^{2+}$ in CH_2Cl_2 in the absence of Br^- results in a partial (80%) conversion to $[Ru(bpy)_2(Hptr\text{-}4)]^{2+}$. Fig. IV.9 shows HPLC traces obtained at several times during the photolysis of $[Ru(bpy)_2(Hptr\text{-}2)]^{2+}$ in CH_2Cl_2. Irradiation of $[Ru(bpy)_2(Hptr\text{-}4)]^{2+}$ under the same conditions results in the formation of small amount of $[Ru(bpy)_2(Hptr\text{-}2)]^{2+}$ (20%). Prolonged irradiation (> 2 h) leads to a slight decomposition of the complex (Fig. IV.10). With $[Ru(bpy)_2(Hptr\text{-}2)]^{2+}$, no decomposition was found during prolonged irradiation. It is interesting that upon photolysis equilibrium is always reached at the ratio 4:1 $[Ru(bpy)_2(Hptr\text{-}4)]^{+}$: $[Ru(bpy)_2(Hptr\text{-}2)]^{2+}$, no matter which isomer is started with.

Such photoinduced linkage isomerism, has not been observed before for other Ru(II) diimine complexes. The only similar case is the photoracemisation of $[Ru(bpy)_3]^{2+}$ reported by Porter's group [179]. This unusual photoisomerism behaviour observed for the two isomers might be of some fundamental interest and deserves a more detailed discussion here.

First, the photoisomerism indicates that upon photoexcitation a monodentate intermediate is formed. The nitrogen which remains coordinated is the nitrogen on the pyridine ring of

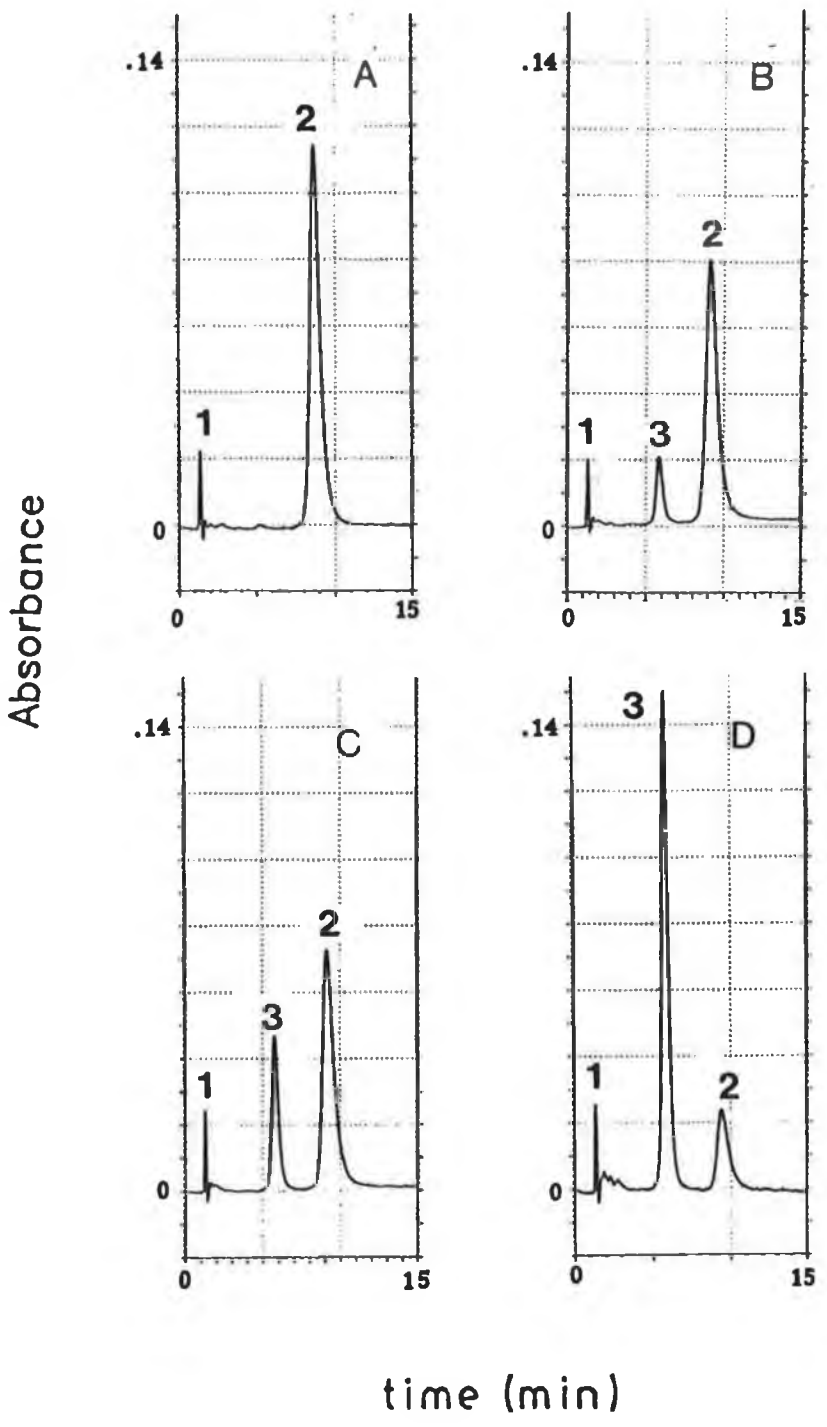

Fig. IV.9 Photolysis of $[Ru(bpy)_2(Hptr\text{-}2)]^{2+}$ in CH_2Cl_2. From A to D: 0, 10, 20 and 200 min..
1 --- CH_2Cl_2. 2 --- $[Ru(bpy)_2(Hptr\text{-}2)]^{2+}$. 3 --- $[Ru(bpy)_2(Hptr\text{-}4)]^{2+}$.

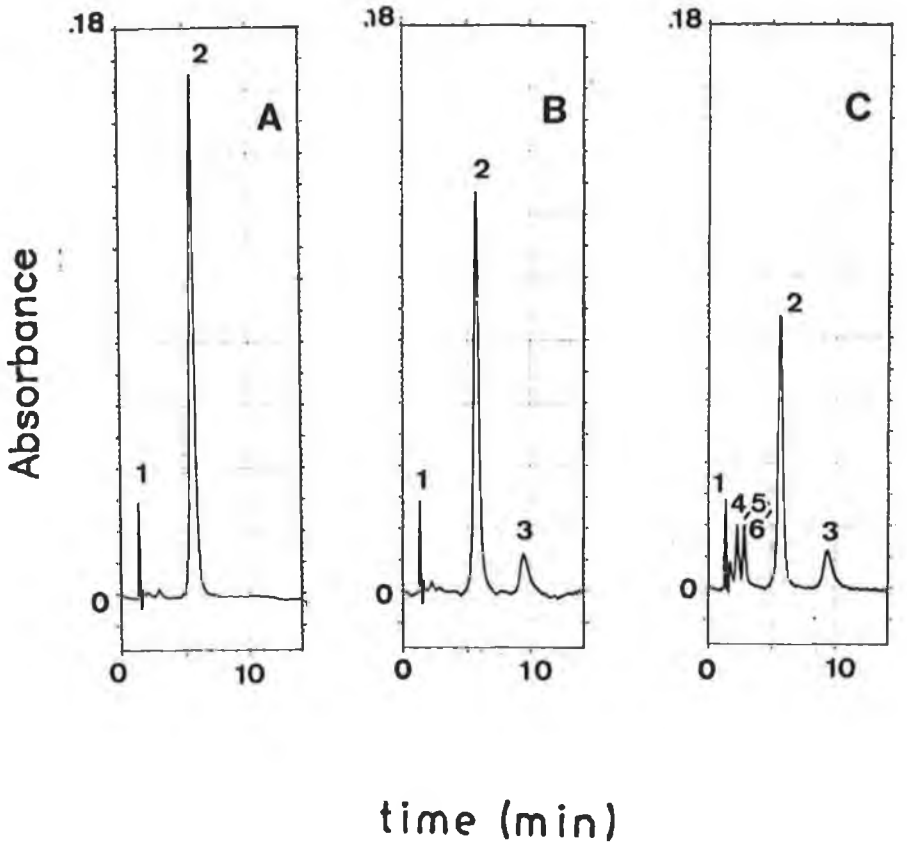

Fig. IV.10 Photolysis of $[Ru(bpy)_2(Hptr\text{-}4)]^{2+}$ in CH_2Cl_2. From A to C: 0, 30, 120 min..
1 --- CH_2Cl_2. 2 --- $[Ru(bpy)_2(Hptr\text{-}4)]^{2+}$. 3 --- $[Ru(bpy)_2(Hptr\text{-}2)]^{2+}$. 4,5 --- unidentified photoproducts. 6 --- free ligand.

the Hptr ligand. The formation of a monodentate complex and the "self-annealing" process were only observed before for $[Ru(bpy)_3]^{2+}$ in H_2O [41], but not in organic solvent. For other mixed-ligand Ru(II) complexes, no such behaviour has ever been reported.

Second, the photoisomerism might be resposible, at least partially, for the deviation from the isosbestic points on the UV-vis absorption spectra during the photolysis in the presence of additional coordination ions (Br^-). It is also conceivable that a monodentate form of the pyridyltriazole complex $[Ru(bpy)_2(Hptr)(Br^-)]^+$ is formed. Fig. IV.11 illustrates the chemistry of the ^3MC state of $[Ru(bpy)_2(Hptr\text{-}2)]^{2+}$ for photoinduced linkage isomerism and photoanation.

Finally, the population of the ^3MC state is probably not the rate-limiting step in the whole photoisomerisation process because of the following reasons:

As $N^{2'}$ should be a stronger donor, it causes a larger splitting between the t_{2g} and e_g^* levels in $[Ru(bpy)_2(Hptr\text{-}2)]^{2+}$ complex relative to that in $[Ru(bpy)_2(Hptr\text{-}4)]^{2+}$. It is then expected that the activation energy for the population of the ^3MC state from the ^3MLCT state is higher for $[Ru(bpy)_2(Hptr\text{-}2)]^{2+}$.

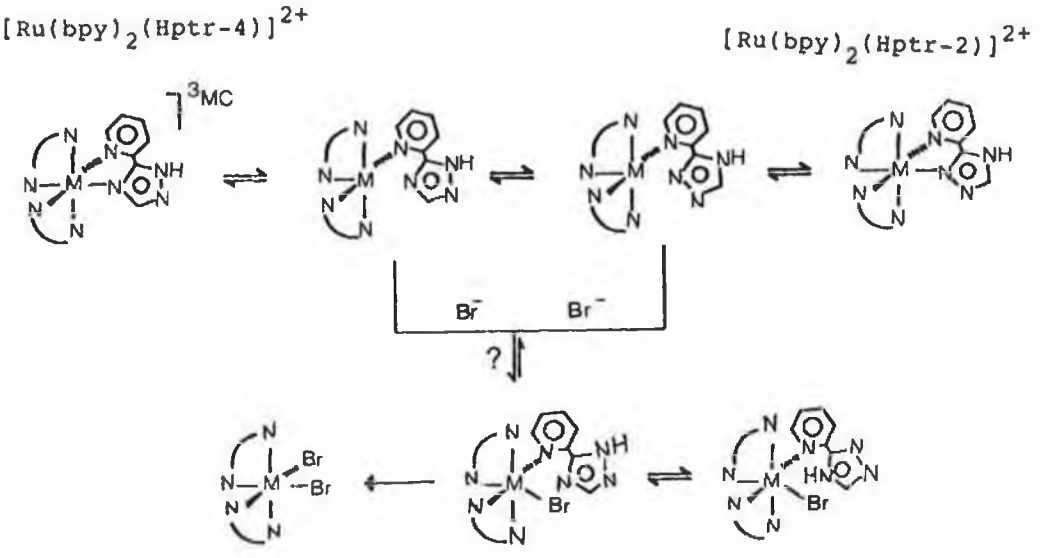

Fig. IV.11 Proposed mechanism of photoinduced isomerism and photoanation.

However, according to temperature dependent lifetime data, "E_a" for $[Ru(bpy)_2(Hptr\text{-}2)]^{2+}$ is 1710 cm^{-1}, much lower than that of $[Ru(bpy)_2(Hptr\text{-}4)]^{2+}$, E_a = 2860 cm^{-1}. Compared to the results on other diimine complexes [41], E_a 2860 cm^{-1} can be reasonably accounted for the activation energy for the ^{3}MC-state population from the ^{3}MLCT state. But the 1710 cm^{-1} value obtained for $[Ru(bpy)_2(Hptr\text{-}2)]^{2+}$ seems to be rather low for this "activation barrier", and is more likely corresponding to the energy gap between the ^{3}MLCT and ^{3}MC levels when they are in equilibrium (see Fig. IV.12). If the ^{3}MC state population is the rate-limiting step for photoisomerisation process, the predominant product would be $[Ru(bpy)_2(Hptr\text{-}2)]^{2+}$. Obviously this is not the case here.

The complex $[Ru(bpy)_2(Hptr\text{-}2)^{2+}$ has a higher activation energy for population of the ^{3}MC state (the exact energy is unknown), so it is less easy to reach the ^{3}MC state. However, relative to the ^{3}MC state decay and photochemistry process, the ^{3}MC-state population from the ^{3}MLCT level is probably very efficient and fast. In other words, the "lifetime" of the ^{3}MC state and the kinetic barrier for the formation of the monodentate species and self-annealing might determine the rate of the whole photochemical process. The "lifetime" of the ^{3}MC state for $[Ru(bpy)_2(Hptr\text{-}2)]^{2+}$ is longer than that of $[Ru(bpy)_2(Hptr\text{-}2)]^{2+}$, which is

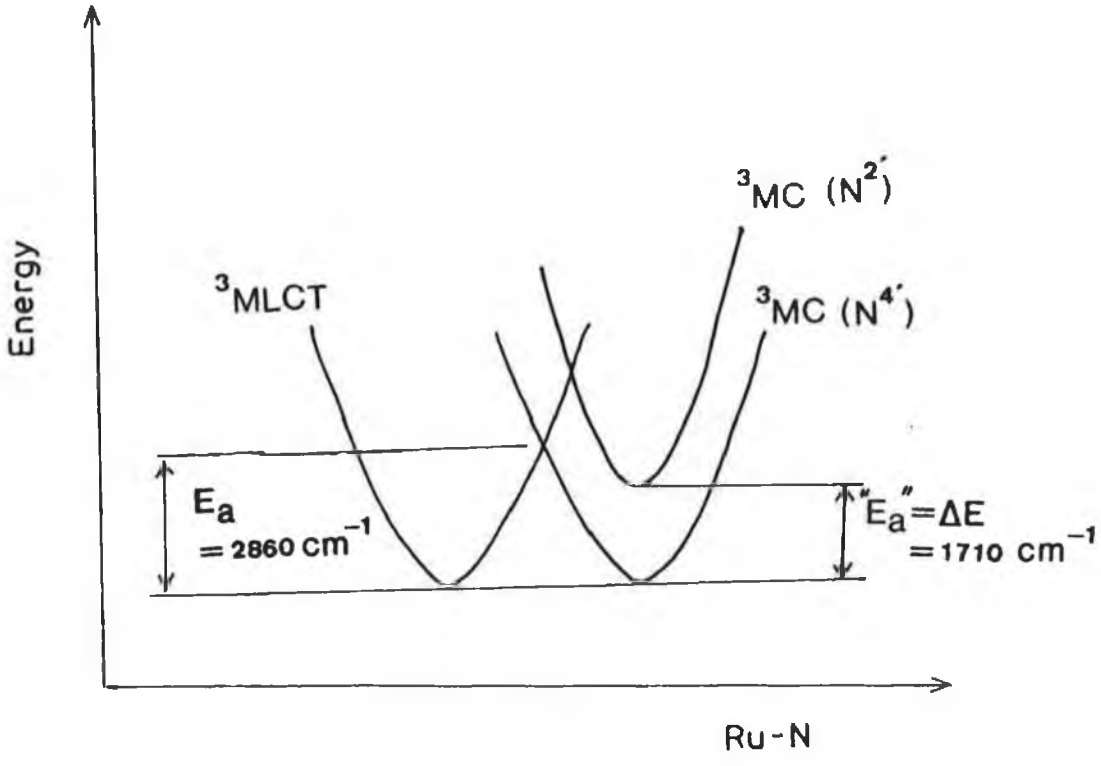

Fig. IV.12 Schematic interpretation of the "E_a" data ontained from the temperature dependent emission lifetime fittings. The ^{3}MLCT level is roughly the same for the two isomers according to their very close emission enegies (Table IV.1).

evidenced by the temperature dependent emission lifetime data, as the equilibrium is most likely established between the ^{3}MLCT and ^{3}MC states acoording to the small "E_a" value. The reason why the photoisomerism product ratio is always 4:1 $[Ru(bpy)_2(Hptr\text{-}4)]^{2+}$: $[Ru(bpy)_2(Hptr\text{-}2)]^{2+}$ is now clear: $[Ru(bpy)_2(Hptr\text{-}2)]^{2+}$ has more chance to form and remain a monodentate species. Plus the fact that $N^{4'}$ (or $N^{1'}$) is easier to protonate so that a relative ease for photo-switching of $[Ru(bpy)_2(Hptr\text{-}2)]^{2+}$ to $[Ru(bpy)_2(Hptr\text{-}4)]^{2+}$ is not unreasonable.

In another study recently reported in this group [173], photoexcitation of the complex $[Ru(bpy)_2(4Mptr)]^{2+}$ in CH_3CN results in the formation of a monodentate intermediate $[Ru(bpy)_2(4Mptr)(CH_3CN)]^{2+}$, which is detected and isolated by HPLC. NMR suggests that for the monodentate complex, the Ru(II) center is bound via the nitrogen of the triazole ring of the H4Mptr ligand. This means that during photolysis, the nitrogen on the pyridine part of the H4Mptr ligand is more labile. However, for $[Ru(bpy)_2(Hptr\text{-}4)]^{2+}$ and $[Ru(bpy)_2(Hptr\text{-}2)^{2+}$, photoisomerism suggests that in the monodentate intermediate species, the Ru(II) has to be bound via the nitrogen on the pyridine part of the Hptr ligand in order to achieve the switching of the coordination mode. In other words, the nitrogen on the triazole ring is more labile compared to that

on the pyridine part of the Hptr ligand.

IV.2.7 The photophysics and photochemistry of $[Ru(bpy)_2(H3Mptr)]^{2+}$.

There are several reasons for examining the complex $[Ru(bpy)_2(H3Mptr)]^{2+}$ (for ligand structure see Fig. I.4). First, the electron-donating CH_3- group on the triazole ring in H3Mptr ligand should make the whole ligand a better -donor compared to the Hptr ligand. This might be reflected from the difference in the photophysical properties. A larger splitting between the t_{2g} and e_g^* levels would be expected for $[Ru(bpy)_2(H3Mptr)]^{2+}$. Secondly, only one isomer was isolated for $[Ru(bpy)_2(H3Mptr)]^{2+}$, and X-ray crystallography reveals that the coordination of Ru(II) is via $N^{1'}$ of the H3Mptr ligand. It would be interesting to examine whether upon photoexcitation another isomer ($N^{4'}$ bound) can be formed. The general properties of this complex have been presented in Table IV.2.

The emission lifetime of this compound, as observed for the two isomers of $[Ru(bpy)_2(Hptr)]^{2+}$, is pH dependent (Table IV.2). The low temperature data indicate that the excited-state decay also follows the energy gap law (the protonated species shows a longer lifetime at 77 K). At room temperature, the ^{3}MC state dominates the nonradiative decay

process, and the protonated species show a shorter lifetime compared to the deprotonated species. Thus, the protonated species is expected to be more photochemically labile compared to the deprotonated one.

The photolysis of $[Ru(bpy)_2(H3Mptr)]^{2+}$ in CH_2Cl_2 monitored by HPLC strongly suggests that another isomer is formed. The results are presented in Fig. IV.13. The UV-vis spectra for each species obtained by photodiode array detection are shown in Fig. IV.14. In Fig. IV.13, it can be seen upon photolysis a new peak (peak 3) grows up. The spectra of the two fractions are not identical (Fig. IV.14). It is, therefore, most likely that the photolysis product is another isomer, where Ru(II) is bound via $N^{4'}$ of the H3Mptr. The photoisomerism found for this complex implies that the photolysis product is not produced in a thermoinduced but a photoinduced reaction, as from synthesis (thermal reaction) only one product is formed, which is bound via $N^{1'}$. This also supports the fact that the switching between $[Ru(bpy)_2(Hptr-4)]^{2+}$ and $[Ru(bpy)_2(Hptr-2)]^{2+}$ is also a photoinduced process, which is orginated from the ^{3}MC state populated thermally from the ^{3}MLCT state.

The photolysis in the presence of TBAB of the deprotonated form $[Ru(bpy)_2(3Mptr)]^{+}$ did not yield any products. As expected, for the protonated complexes, photolysis in $TBAB/CH_2Cl_2$ yields $[Ru(bpy)_2Br_2]$ as a final product.

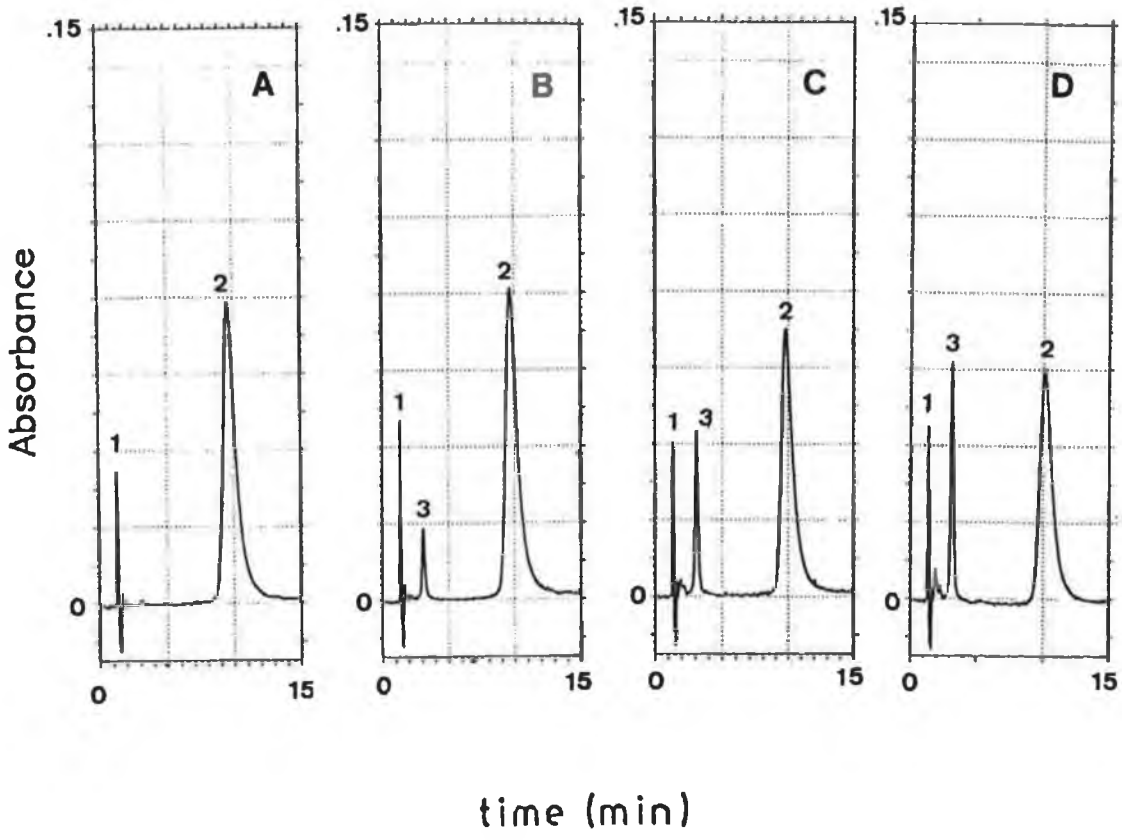

Fig. IV.13 Photoinduced isomerism of $[Ru(bpy)_2(H3Mptr)]^{2+}$ in CH_2Cl_2. From A to D: 0, 10, 25 and 105 min. irradiation.

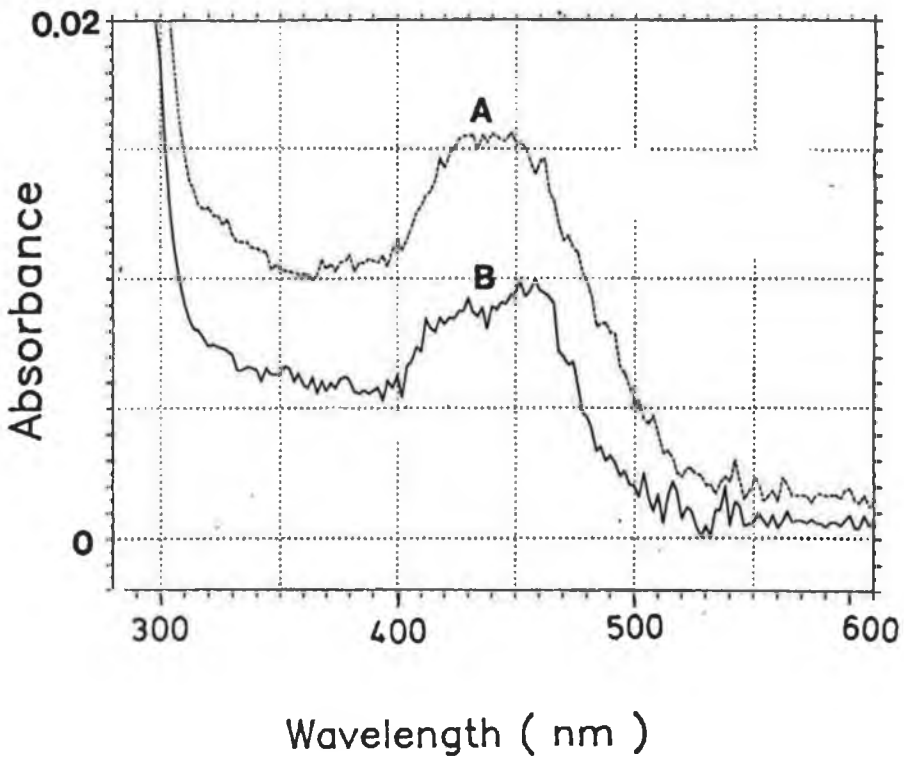

Fig. IV.14 **Uv-vis absorption spectra of the two fractions during photolysis of $[Ru(bpy)_2(H3Mptr)]^{2+}$ in CH_2Cl_2.**

A --- $[Ru(bpy_2(H3Mptr)]^{2+}$ (starting material);

B --- photoproduct.

The photolysis monitored by UV-vis spectroscopy is presented in Fig. IV.15). The isosbestic points are not maintained through the whole photolysis, again possibly due to the participation of the photoisomerisation process.

VI.7 Concluding Remarks.

Temperature dependent and pH dependent emission lifetime measurements show that for $[Ru(bpy)_2(Hptr\text{-}2)]^{2+}$ and $[Ru(bpy)_2(Hptr\text{-}4]^{2+}$ the excited-state decay follows the energy gap law at low temperature, while at near room temperature the ^3MC state populated from the ^3MLCT state dominates the whole non-radiative process. In deprotonated form, both isomers do not efficiently populate this state at or below room temperature. As a result the deprotonated isomers are photochemically inert.

Protonated complexes are photochemically labile due to the population of the ^3MC state. Photolysis of either isomer of $[Ru(bpy)(Hptr)]^{2+}$ in CH_2Cl_2 results in a linkage isomerism; equilibrium is established at 4:1 $[Ru(bpy)_2(Hptr\text{-}4)]^{2+}$ to $[Ru(bpy)_2(Hptr\text{-}2)]^{2+}$. From kinetic analysis the photoswitching and the product ratio between the two isomers can be interpreted in terms of different efficiency for the decay from the ^3MC state. The rate limiting step is not at the population of ^3MC state from the ^3MLCT state.

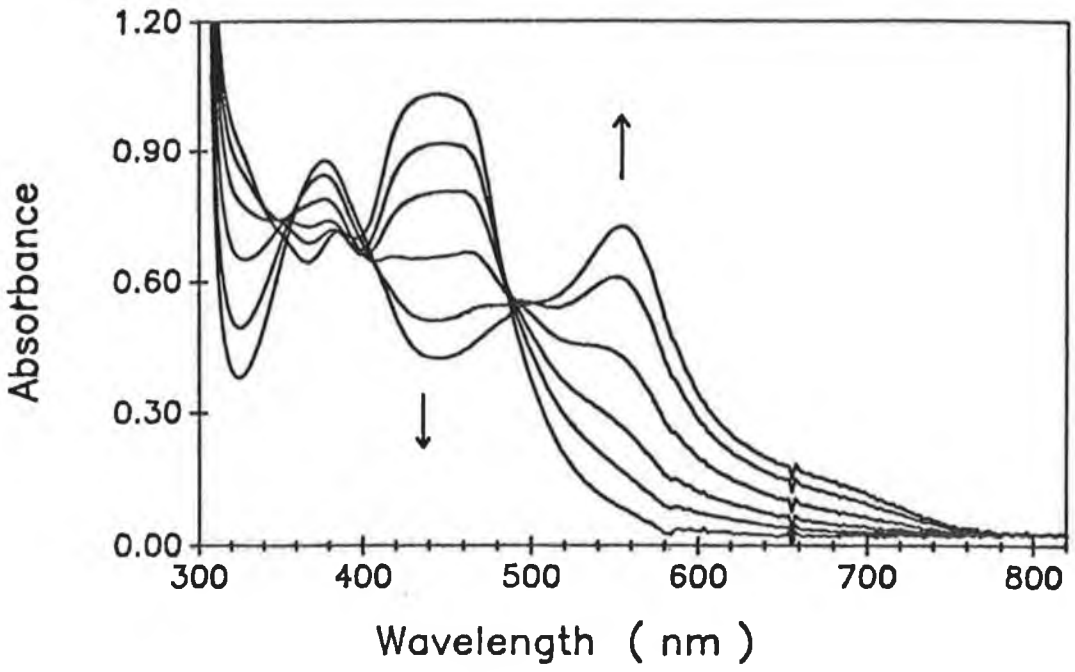

Fig. IV.15 Photolysis of $[Ru(bpy)_2(H3Mptr)]^{2+}$ in 3 mM TBAB/CH_2Cl_2 monitored by UV-vis spectroscopy.

In the presence of coordinating anions photoanation occurs to yield the cis-anion complex with a loss of pyridyltriazole. The photoanation involves an intermediate, which is confirmed by the photoisomerisation. The complex $[Ru(bpy)_2(H3Mptr)]^{2+}$ shows very similar photophysical behaviour to that of $[Ru(bpy)_2(Hptr)]^{2+}$. The photoisomerisation of this complex suggests that the isomer formation is photoinduced, as by thermal reaction only one product is obtained. The basic form of both isomers of $[Ru(bpy)_2(Hptr)]^{2+}$ and $[Ru(bpy)_2(H3Mptr)]^{2+}$ are all inert to photosubstitution in 3 mM TBAB/CH_2Cl_2 at room temperature. Thus, the substitutional lability can be controlled by controlling protonation of the complexes in the ground state.

Appendix I. Derivation of eq. IV.6.

According to Scheme II,

$$k_1 = k_{nr} + k_r$$

$$-d[^3MLCT]/dt = k_1[^3MLCT] + k_2[^3MLCT] - k_{-2}[^3MC] \quad (1)$$

following steady state approximation,

$$d[^3MC]/dt = k_2[^3MLCT] - k_{-2}[^3MC] - k_3[^3MC] - k_4[^3MC] = 0$$

$$\therefore \quad [^3MC] = k_2[^3MLCT]/(k_{-2} + k_3 + k_4) \quad (2)$$

Combine (1) and (2), then

$$-d[^3MLCT]/dt = [^3MLCT][k_1 + k_2 - k_{-2}.k_2/(k_{-2} + k_3 + k_4)]$$

$$= [^3MLCT][k_1 + k_2(k_3 + k_4)/(k_{-2} + k_3 + k_4)]$$

Further,

$$1/\tau = k = k_1 + k_2(k_3 + k_4)/(k_{-2} + k_3 + k_4). \quad (IV.6)$$

Chapter V

The Effect of First Coordination Sphere and "Second-Sphere" Perturbations on the Photophysical Properties of Ru(II) Complexes Containing Triazole Ligands

V.1 Introduction.

The ^{3}MC state, which can be thermally activated from the ^{3}MLCT state, has been a major limitation to the use of Ru(II) polypyridyl complexes as photosensitisers in energy conversion systems. As described in chapter I, the most straight forward synthetic method to make "^{3}MC-state free" compounds is to turn to Os(II) complexes. For Os(II)-bpy or -phen complexes, where 10 D_q is 30% larger than that for Ru(II) compounds, the ^{3}MC state is not accessible at room temperature, and excited-state lifetimes are nearly temperature independent [45].

However, there are several reasons why Ru(II) polypyridyl complexes still represent potentially superior photosensitisers. First, Ru(II) ^{3}MLCT excited states are longer lived than the Os(II) analogues. For equivalent cases where excited-state energies are the same, the lifetimes of Ru(II) ^{3}MLCT states are usually longer by a factor of 3 [45]. Second, an extensive synthetic chemistry exists for Ru(II), and the preparative conditions involved are less demanding [5, 45]. Furthermore, the synthetic chemistry to ligand-bridged multinuclear complexes and chromophore-quencher assemblies is better known, which is attractive in terms of the potential application of these complexes in solar energy conversion systems [5, 45].

To eliminate the ^{3}MC excited state and/or to modify other redox and photophysical properties of Ru(II) diimine complexes, there are several methods, which can be divided into two main classes. Firstly, one can alter the chemical environment of the Ru(II) center by changing the first coordination sphere, i.e., by replacement of the coordinating ligands. Secondly, one can alter the properties of a given Ru(II) complex by so-called "second-sphere perturbation" [180]. The second-sphere perturbation is not associated with coordination. Instead, it is associated with intermolecular interactions between the complex and solvent, protons, paired ions, etc. In other words, Ru(II) complexes may exhibit different chemical or physical properties without adding or losing any coordinating ligands. A very clear case of second-sphere perturbation has been given in Chapter IV, where the photochemical reactivity of the Ru(II) complexes can be controlled by protonation and deprotonation of a coordinated ligand.

Much work has been carried out in the past ten years on tuning the photophysical properties of Ru(II) complexes by ligand modification [41]. The ligands introduced generally belong to either of two classes compared to bpy: 1) better π-acceptors but weaker σ-donors (class I); or 2) better σ-donors but weaker π-acceptors (class II). The different effects of such ligands on the ^{3}MLCT state and redox properties have been described in Chapter I. There are some

additional points to be mentioned here.

First, in Ru(II) diimine-based mixed-ligand complexes, class I ligands are involved in ^{3}MLCT states so they are called chromophore ligands. In contrast, class II ligands, because of their higher π^*-energy levels, are normally not involved in the ^{3}MLCT emitting process, so they are called non-chromophore or spectator ligands [180]. One of the most direct methods to test whether a ligand is involved in the emitting process is Resonance Raman spectroscopy [102]. Another method is to compare the ground-state and excited-state pK_a values provided the ligand is protonatable [180]. It should be noted that the so-called "spectator ligands" are by no means irrelevant to the photophysical properties of Ru(II) complexes. Their stronger σ-donating and weaker π-accepting ability can substantially alter the photophysical properties of such complexes, in particular, emission energies, excited-state lifetimes and ^{3}MC state energy levels.

Second, although to isolate the ^{3}MC state from the ^{3}MLCT state and so to obtain photostable complexes have been the main aim of synthetic modification of Ru(II) complexes, there are only a few complexes (about 12-14) synthesised so far possessing such desired photostability. Most of these photostable complexes are Ru(II) polypyridyl compounds containing at least one bidentate good π-accepting ligand

(class I). These compounds include $[Ru(bpy)_2(bpyz)]^{2+}$ and $[Ru(bpy)_2(bpym)]^{2+}$ reported by Meyer's group [69], $[Ru(L)_3]^{2+}$ (L = 6Mppim, 6phppim, bpdz; for structures see Fig. I.4) by Tazuke's group [69] and $[Ru(dmb)_2(decb)]^{2+}$ and $[Ru(dmb)(decb)_2]^{2+}$ reported by Schmehl's group [129]; In complexes containing class II ligands only four have shown small temperature dependence of the emission lifetime and high photostability. These complexes are, all based on triazole ligands, $[Ru(bpy)_2(bpt)]^{+}$ [82], $[Ru(bpy)_2(3Mptr)]^{+}$, and the two linkage isomers of $[Ru(bpy)_2(ptr)]^{+}$ (Chapter IV).

The discovery of the above-mentioned photostable Ru(II) compounds, clearly shows that in principle the ^{3}MC state can be removed from the ^{3}MLCT state by ligand variations. It should be pointed out that the photostability of the four complexes containing class II ligands mentioned above is due to a combination of ligand tuning and "second-sphere" perturbation (vide infra).

The energy gap between the ^{3}MLCT and the ^{3}MC states can be increased in a number of ways. The energy of the ^{3}MLCT state largely depends on two factors: 1) the energy of the π^* orbital of the chromophore ligand and 2) the stabilisation of the Ru(II) $d\pi$ orbitals by a combination of σ and π properties of the introduced ligand [41]. However, there is no useful model nor sufficient experimental data

available to predict quantitatively how the energy of the ^{3}MC state varys with the coordinating ligands [45].

"Second-sphere" perturbation provides an alternative way to modify the photophysical properties of the Ru(II) complexes. For instance, protonation/deprotonation of coordinated ligands can change not only ground-state redox potentials but also excited-state properties such as emission energy and emission lifetime. An example has been given in Chapter IV, where the two isomers of $[Ru(bpy)_2(ptr)]^+$ are photochemically stable, contrary to their protonated counterparts which are photochemically labile.

Protonation of Ru(II) complexes can some time even change the origin of the emitting state. A very interesting case has been reported by Peterson and Demas [95, 181]. For the complex $[Ru(bpy)_2(CN)_2]$, emission occurs from the ^{3}MLCT state. In concentrated sulfuric acid at 77 K, where the excited species is protonated, another type of emission takes over. Based on the spectrum structure, lifetime and its similarity with the emission of the free ligand bpy, the emission of the complex in sulfuric acid is assigned as a ligand-centered π--->π^* phosphoresence [85, 181]. A similar behaviour was also reported by Balzani's group for the complex $[Ru(biq)_2(CN)_2]$ [185].

Proton-transfer processes are also a good probe for

determining the interaction between Ru(II) and coordinated ligands and the nature of the ^{3}MLCT emitting state. In general, coordinated ligands have lower pK_a values than free ligands. This is caused by electron donation from the ligand to the Ru(II) center. However, an exceptional case has been reported by Taube's group [97]. For the complex $[Ru(NH_3)_5(pyz)]^{2+}$, the pyz ligand (see Fig. I.4) was found to be more basic upon coordination. This is attributed to an extraordinarily strong backdonation of electron density from the Ru(II) t_{2g} orbitals to the unoccupied π^* orbitals of the pyz ligand. An unusually short Ru-N(pyz) bonding distance, revealed from X-ray crystallographic data, supports this assumption [97]. This is an important discovery, as it implies that the energy level of the t_{2g} orbital is affected not only by the σ-donating ability but also the π-accepting ability of the ligands.

The excited-state pK_a, pK_a^*, is a good probe for determining which ligand is directly involved in the emission process. For mixed-ligand Ru(II) complexes, if the basicity of a coordinated ligand in the excited-state increases, the excited electron is thought to be localised on this ligand, and it is therefore directly involved in the emission process of the complex. If, however, the excited state basicity decreases, the ligand is not expected to be involved in the emitting process, but acts as a spectator ligand. This can be explained by assuming that when an electron is excited from

the t_{2g} orbital to a chromophore ligand π^* orbital, then the increased positive charge on the Ru(II) center will withdraw more electron density from the spectator ligand. In other words, the electron density on the spectator ligand decreases when the complex is excited, so that its pK_a^* decreses compared to that in ground state [95, 181].

The first example of excited-state acid-base chemistry in Ru(II) complexes was reported by Wrighton and co-workers for $[Ru(bpy)(dcbpy)]^{2+}$ (Fig. V.1) [90-91].

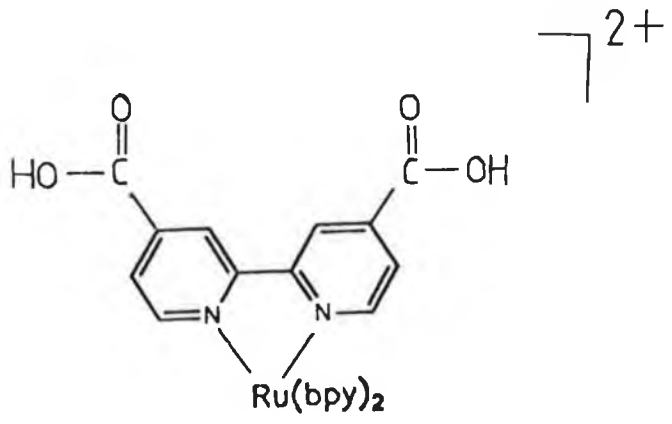

Fig. V.1 $[Ru(bpy)_2(dcbpy)]^{2+}$.

The pK_a^* value for this complex was found to be increased relative to that in ground state, so it was concluded that the lowest unoccupied molecular orbital (LUMO) is dcbpy based. Upon photoexcitation the dcbpy ligand becomes more basic, therefore the complex that is deprotonated in the ground state can be protonated in the excited state. Indeed,

at a pH sightly higher than the pK_a, where the ground-state complex is deprotonated, upon excitation an emission characteristic of protonated complex was observed. This means that photoinduced proton transfer from solvent to the complex takes place without deactivation of the emitting state. For this complex, Wrighton's group observed only one step proton-transfer equilibrium. Later, Shimizu's group found that both monoprotonated and doubly protonated species can be detected by careful titration, i.e., two separate proton-transfer steps were confirmed [94].

Much work has been carried out, after Wrighton's pioneering work, on the acid-base chemistry of Ru(II) diimine complexes [77, 79-80, 83, 85, 92-103]. But it has not been appreciated until very recently that protonation and deprotonation of the coordinated ligands can be used for controlling the photochemical reactivity of Ru(II) complexes (see Chapter IV). Another interesting point is that the excited-state proton transfer in Ru(II) complexes might be of some resemblance to the beginning event in the natural photosynthetic process. It is known that in the photosynthetic reaction centers of photosynthetic bacteria, photon absorption by chlorophylls (photosensitisers) causes a charge separation and then an intramolecular electron-transfer process, which ends up with the reduction of the ubiquinone (electron acceptor) coupled with protonation (see Chapter I). Thus, the beginning event in

the photosynthetic reaction centers is actually a proton-coupled intramolecular electron-transfer process. In Ru(II) complexes, upon excitation an electron is pumped from the Ru(II)-based t_{2g} orbital to the ligand-based π^* orbital, which leads to the protonation of the ligand in the excited state at an appropriate pH range (in the case that the low-lying π^* ligand is protonatable). This might also be considered to be a proton-coupled intramolecular electron-transfer process (or a charge separation process as the distance between the donor and acceptor is very short).

Another example of second-sphere perturbation is solvent interaction. Experimental evidence is available to suggest that in protic solvents, especially H_2O or CH_3OH, high frequency ν(O-H) modes at 3500 cm^{-1} can play a role as energy acceptor in non-radiative decay processes. Meyer's group observed that for $[Ru(bpy)_3]^{2+}$ the emission lifetime can vary from 0.48 to 0.94 μs over a range in solvents from CH_2Cl_2 to propylene carbonate [45, 56]. The photoanation quantum yield ϕ_p has also been shown to be extremely solvent dependent. For $[Ru(bpy)_3]Cl_2$, ϕ_p is less than 2.1×10^{-5} in 0.1 M HCl while $\phi_p = 0.100$ in CH_2Cl_2 [56]. The rate of reorientation of the dipole moment for a given solvent also affects the excited-state relaxation process of a solute. For instance, the ground-state electron configuration for $[Ru(bpy)_3]^{2+}$ has a symmetry of D_3 and a dipole moment μ of 0 D. In the MLCT

excited state $[Ru(III)(bpy^{-\cdot})(bpy)_2]^{2+}$ (symmetry C_{2v}), the dipole moment becomes 13 D, which is significant in terms of solvent-solute interactions [45, 183]. The effect of the solvent dipole orientation on the excited-state energy of Ru(II) diimine complexes can be most clearly observed at the glass-to-fluid transition region of the solvent. In a rigid glass, the solvent dipoles are immobile on the time scale of the excited-state, and therefore can not respond to the change in electronic configuration between the ground-state and excited-state, with as a result an increase in the emission energy. At higher temperatures, the solvent continues to soften and, when it reaches the fluid state, the solvent dipoles are free to reorient in response to the change in electronic structure and thus the emission energy decreases. The emission energy of $[Ru(bpy)_3]^{2+}$ also tends to decrease as the static dielectric constant of the solvent increases [45]. This again shows that the excited state is preferentially stabilised relative to the ground state by the surrounding solvent dipoles. However, the microscopic origions of the solvent shifts observed in emission energy are not fully understood [45].

The photophysical properties of Ru(II) complexes can also be altered through ion-pairing. An example was reported by Meyer and co-workers, where lifetime values for $[Ru(bpy)(bpyz)_2]^{2+*}$ in CH_3CN were shown to decrease linearly with added $[Cl^-]$ [56]. In contrast, the lifetime

of $[Ru(bpy)_3]^{2+}$ shows no $[Cl^-]$ dependence but photochemistry does occur [56]. This suggests that for $[Ru(bpy)_3]^{2+}$ the kinetics for the ^3MC decay and photoanation is so fast that $[Cl^-]$ has no effect on the emission lifetime. For $[Ru(bpy)_2(bpyz)]^{2+}$, the ^3MLCT and ^3MC states are dynamically coupled, and Cl^- interacts with the complex within the time scale of the ^3MC state thus influencing the ^3MLCT lifetime. On the other hand, electron-transfer reductive quenching of the ^3MLCT excited state by Cl^- is another possible reason for the observed decrease in the emission lifetime. Such quenching has been evidenced, from laser flash photolysis data, for a similar complex $[Ru(bpyz)_3]^{2+*}$ [184].

Other aspects of the second-sphere perturbation to the photophysical properties of Ru(II) complexes include metalation of the coordinated ligands [185], and incorporation of Ru(II) complexes into micelles or other self-organised media and host-guest systems [182].

The results to be reported in this chapter largely deal with the changes in photophysical properties of the Ru(II) diimine complexes caused by ligand variations and by second-sphere perturbation. The photophysical and photochemical properties of three types of Ru(II) complexes are described: 1) $[Ru(bpy)_2(ptOH)]^+$; 2) $[Ru(bpy)_2(HL)]^{2+}$ where HL stands for pyrazyltriazole ligands; and 3) $[Ru(phen)_2(ptr)]^+$ and

$[Ru(dmb)_2(ptr)]^+$. All the ligand structures have been presented in Fig. I.4. It can be seen that the $ptOH^-$ ligand is actually the ptr^- ligand substituted with a phenol group on the triazole ring. Another interesting feature is that this complex can potentially undergo multi-step proton transfer, which might have some effects on its ^{3}MLCT- and/or ^{3}MC-state properties. The type 2) complexes are interesting as pyrazyltriazoles are actually the combination of class I and class II ligands. These ligands can be protonated so that the properties of the complexes can be easily probed by proton-transfer equilibria. Finally, for the type 3) complexes, where bpy is replaced either by phen or by dmb in the complex $[Ru(bpy)_2(ptr)]^+$, a strong ligand variation effect is expected.

V.2 Results and Discussion.

V.2.1 Acid-base chemistry and its effect on the photophysical properties in the complex $[Ru(bpy)_2(ptOH)]^{\pm}$.

V.2.1.1 General.

X-ray crystallagraphy (Fig. V.2) and proton NMR data show that the coordination of the Ru(II) center is via $N^{1'}$ of the triazole ring [83]. The $N^{4'}$-bound isomer was not found

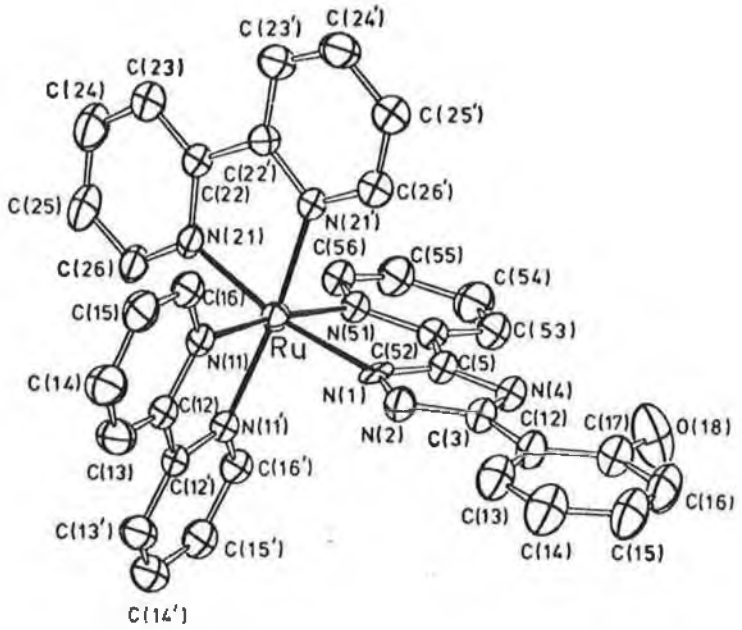

Fig. V.2 ORTEP drawing (30% probablity) of the $[Ru(bpy)_2(ptOH)]^+$ [83].

from the product obtained. The absence of the $N^{4'}$-bound isomer is most likely due to steric reasons. If $N^{4'}$ is coordinated to the Ru(II) center, the coordination environment would be more crowded due to the phenol group. The phenol group is expected to serve as an electron-withdrawing group. This is just opposite to another complex $[Ru(bpy)_2(3Mptr)]^+$, where the methyl substituent acts as an electron-donating group (see Fig. V.3).

V.2.1.2 Acid-base equilibria of the free ligand.

As expected, three stepwise acid-base equilibria are observed for the free ligand HptOH. Typical ground-state absorption titration results are shown in Fig. V.4. All the spectra changes vs. pH are reversible. For all three equilibria, well defined isosbestic points are present in the spectra. The corresponding $\Delta A/\Delta A_{tot}$ vs. pH curves are shown in Fig. V.5. For each equilibrium the limiting pH range is indicated by the plateaus on the top and bottom of the titration curves. From the inflection points, three pK_a values are determined:

Between pH 9-13 (Fig. V.4A and V.5A), the acid-base equilibrium (pK_a = 11.6) can be assigned to the protonation of the phenol group [186]. The next step (pK_a = 6.0) can be explained by the protonation of the triazole ring (Fig. V.4B and Fig. V.5B). It can be seen that the pK_a value for

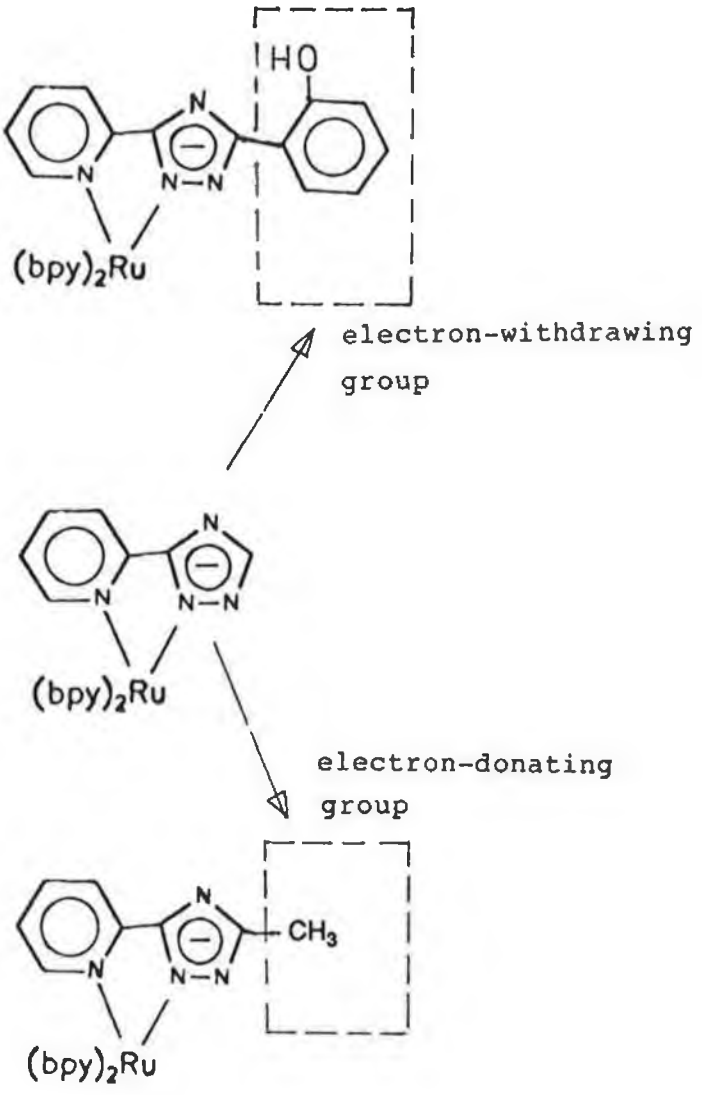

Fig. V.3 Modification of the structure of the ptr^- ligand by substituted groups.

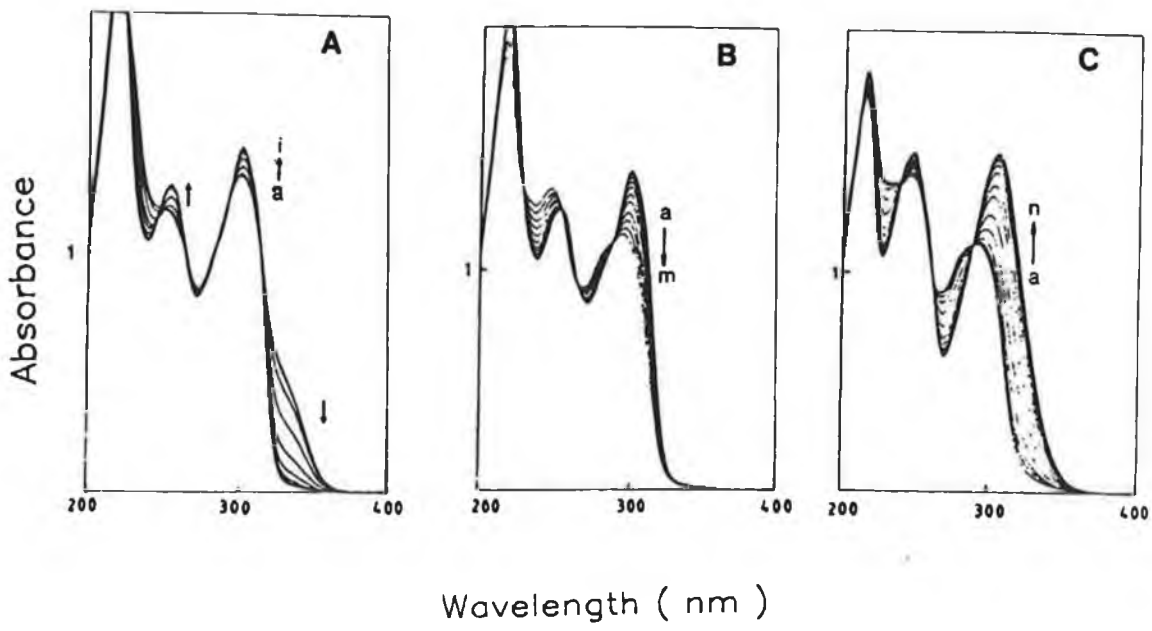

Fig. V.4 pH dependence of the absorption spectrum of HptOH in an aqueous Britton-Robinson buffer. For curves A from (a) to (i): pH = 12.13, 11.99, 11.559, 11.10, 10.57, 9.99, 9.41, 8.96, 8.43; B from (a) to (m): pH = 8.25, 8.00, 7.61, 7.36, 7.06, 6.82, 6.63, 6.43, 6.25, 6.03, 5.86, 5.67, 5.46 and C from (a) to (n): pH = 4.48, 4.29, 4.12, 3.85, 3.5, 3.25, 2.97, 2.78, 2.51, 2.32, 2.13, 1.96, 1.80, and 1.56.

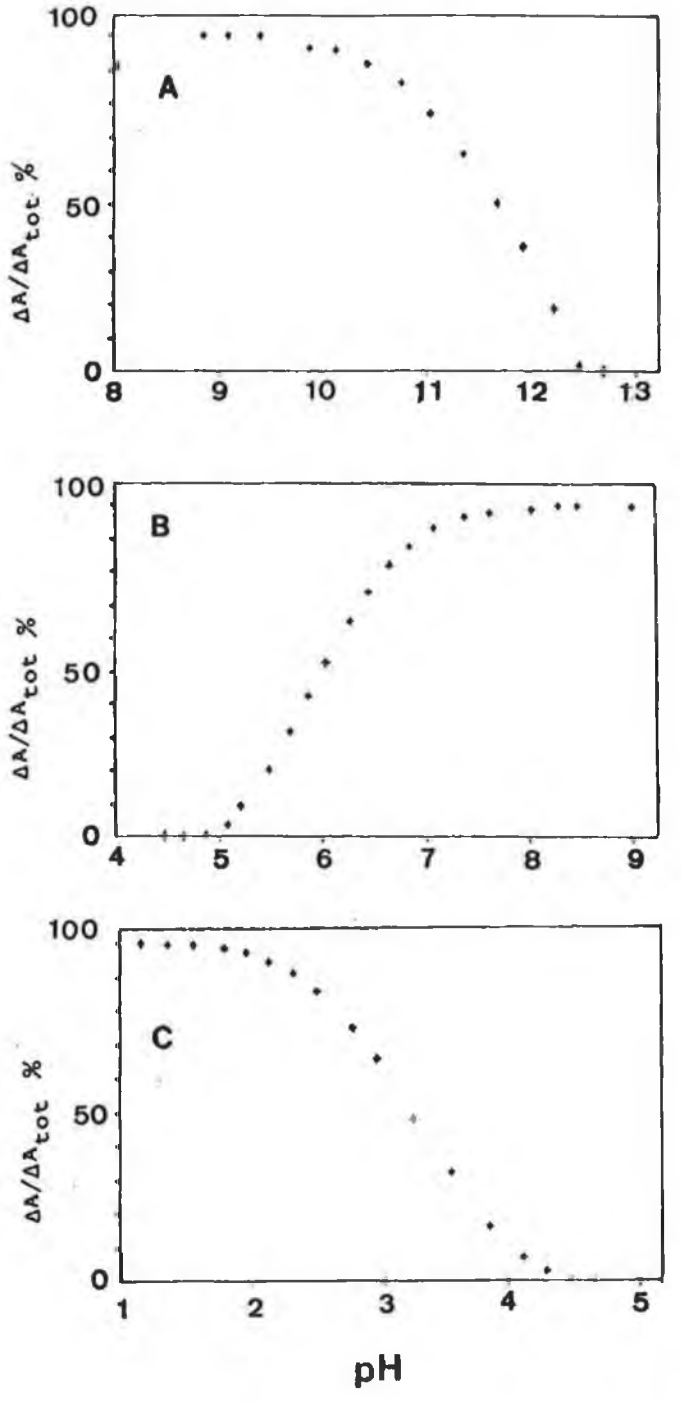

Fig. V.5 Reletive absorbance vs. pH for the ligand HptOH, corresponding to Fig. V.4. All the intensity data are taken at 300 nm.

the triazole ring is significantly lower than that for the ligand Hptr, where a pK_a(acid) value of 9.2 was found [85]. The stronger acidity of the HptOH ligand compared to Hptr indicates that the phenol group does serve as an electron-withdrawing group. It is also known that the pK_a(acid) of H3Mptr is 9.8 [85], which is slightly higher than that of Hptr (9.2), indicating that the methyl group acts as an electron-donating group. Finally, a pK_a of 3.2 was found in the last equilibrium between pH 1-5 (Fig. V.4C and Fig. V.5C). This value is similar to that obtained for the Hptr ligand, where pK_a(base) was found to be 3.3 [85]. This suggests that the distribution of the electron density in the pyridine ring is not significantly affected by the phenol group. On the other hand, this value is lower than that of the pyridine (pK_a 5.3) [186], which might be caused by the electron-withdrawing effect of the neighbouring triazole ring. Although the last protonation step is thought to have occured on the pyridine moiety in the HptOH ligand, hydrogen-bridge formation to the adjacent triazole N-atom is also possible. The three proton-transfer equilibria are depicted in Fig. V.6.

V.2.1.3 Acid-base equilibria of the complex.

The pH dependence of the absorption spectrum of the complex is given in Fig. V.7. The results clearly show the presence of two different equilibria: one between pH 1 and 8, with

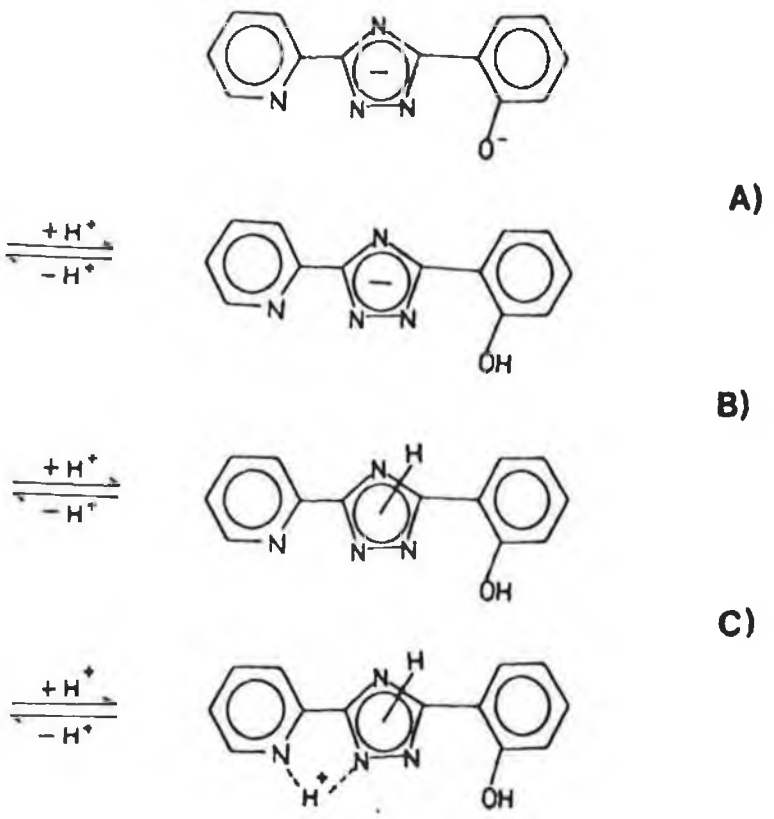

Fig. V.6 Multi-step protonation/deprotonation processes of the free ligand HptOH.

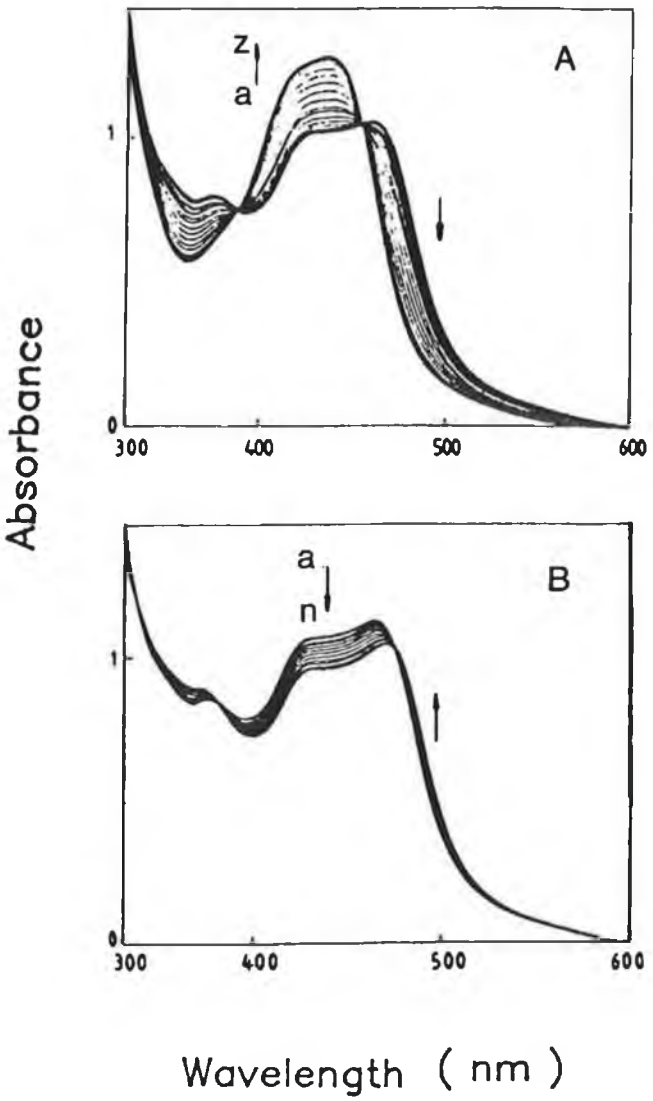

Fig. V.7 pH dependence of the absorption spectrum of $[Ru(bpy)_2(HptOH)]^{2+}$ (10^{-4} M) in an aqueous buffer. For curves A (a) to (z): pH = 7.35, 7.16, 6.95, 6.72, 6.56, 6.35, 6.07, 5.83, 5.56, 5.31, 5.06, 4.84, 4.61, 4.43, 4.21, 4.09, 3.89, 3.69, 3.49, 3.29, 3.10, 2.80, 2.58, 2.37, 2.15, 1.92 and B (a) to (n): pH = 9.54, 9.87, 10.23, 10.56, 10.85, 11.07, 11.27, 11.48, 11.70, 11.93, 12.14, 12.34, 12.54, and 12.76.

isosbestic points at 385 and 455 nm; and the second one above pH 8, with isosbestic points at 385 and 473 nm. The corresponding $\Delta A/\Delta A_{tot}$ vs. pH curves are shown in Fig. V.8.

By comparison with other similar systems, the first proton equilibrium observed for the complex (pK_a 3.7) is assigned to the protonation of the triazole ring [85]. The coordinated ligand (pK_a = 3.7) is more acidic than the free ligand (pK_a = 6.0) by about 2 orders of magnitude. On the other hand, the acidity of the phenol group of the free ligand (pK_a = 11.6) has little change upon coordination (pK_a = 11.2). The increased acidity of the triazole ring after coordination can be attributed to the σ-donor property of the ligand. The metal t_{2g} to ligand π^* electron back-donation is not as significant as the σ-electron donation from the ligand to the Ru(II) center. The rather small reduction in pK_a of the phenol group (about 0.5 pH units) points to a very limited interaction between the phenol group and the coordinating part of the ligand.

The MLCT absorption maximum for the complex shifts to a lower energy with increasing pH. Similar results were also found for other $Ru(bpy)_2(II)$ complexes containing pyridyltriazole ligands [77, 79-80, 83-85]. For the complex $[Ru(bpy)_2(ptOH)]^+$, the negative charge present on the triazole ring enhances the σ-donating ability of the ligand.

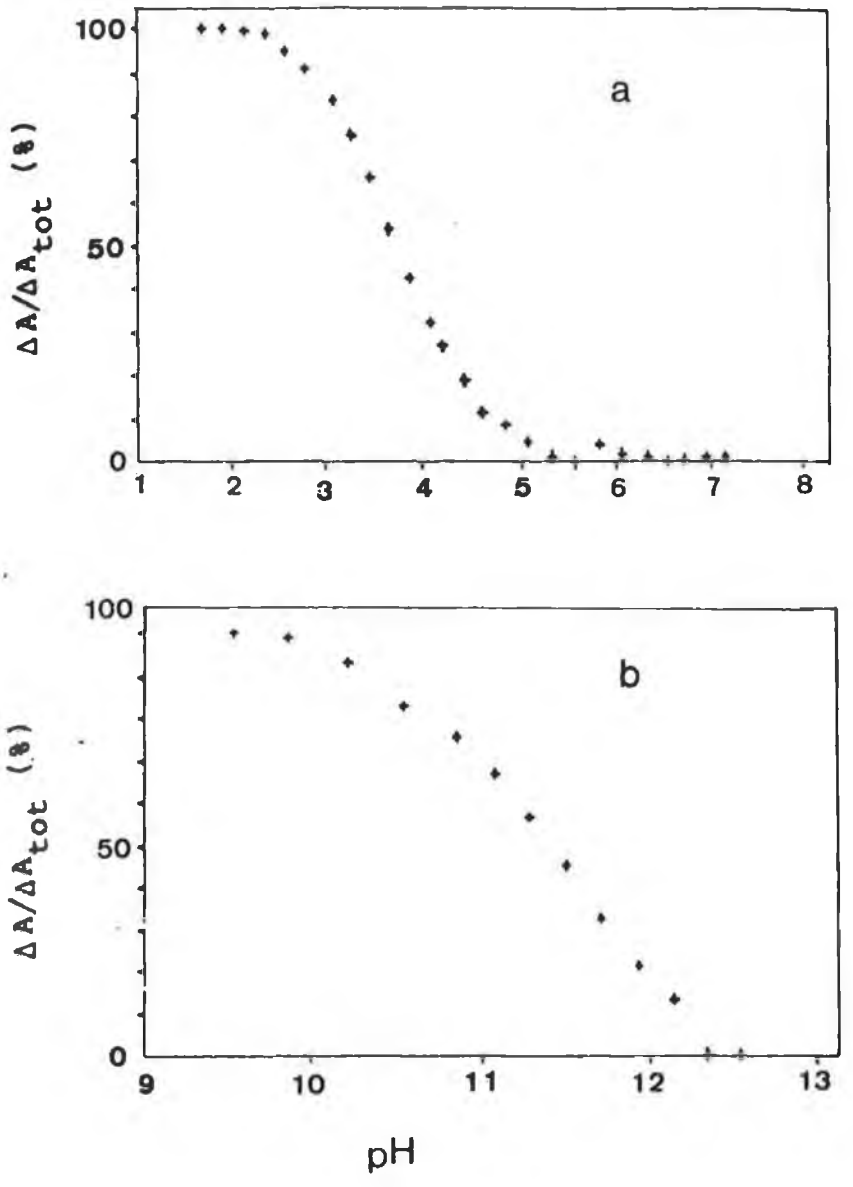

Fig. V.8 Relative absorbance vs. pH for the complex $[Ru(bpy)_2(HptOH)]^{2+}$ (corresponding to Fig. V.7). All the intensity values are taken at 440 nm.

This results in the destabilisation of the Ru(II) t_{2g} level. Therefore the energy, which is needed to excite an electron from the t_{2g} orbital to the ligand π^* orbital (based on bpy, vide infra), is reduced.

The effect of the pH on the emission properties of the complex was also investigated. The pH dependence of the emission is given in Fig. V.9. The relative emission intensity vs. pH is given in Fig. V.10. Between pH 0-7, the first protonation equilibrium is observed. With increasing pH, the emission maximum shifts to a lower energy while the emission intensity increases (Fig. V.9A). This result is similar to that observed for the complex $[Ru(bpy)_2(ptr\text{-}2)]^+$ [85]. That the emission maximum shifts to lower energies upon increasing pH is due to the destabilisation of the Ru(II) t_{2g} level and, as a consequence, the reduction of the t_{2g}-^{3}MLCT energy gap. The decrease of the emission intensity with an increase of the acidity of the solution is probably due to a thermally populated ^{3}MC state and proton-induced quenching [92]. In the second equilibrium, between pH 7-14, the emission maximum further shifts to lower energies upon increasing the pH. This suggests that the deprotonation of the phenol group also increases the σ-donating ability of the ligand. However, it was found that in this pH domain, the emission intensity decreases with the increase of pH, which is not understood at this stage.

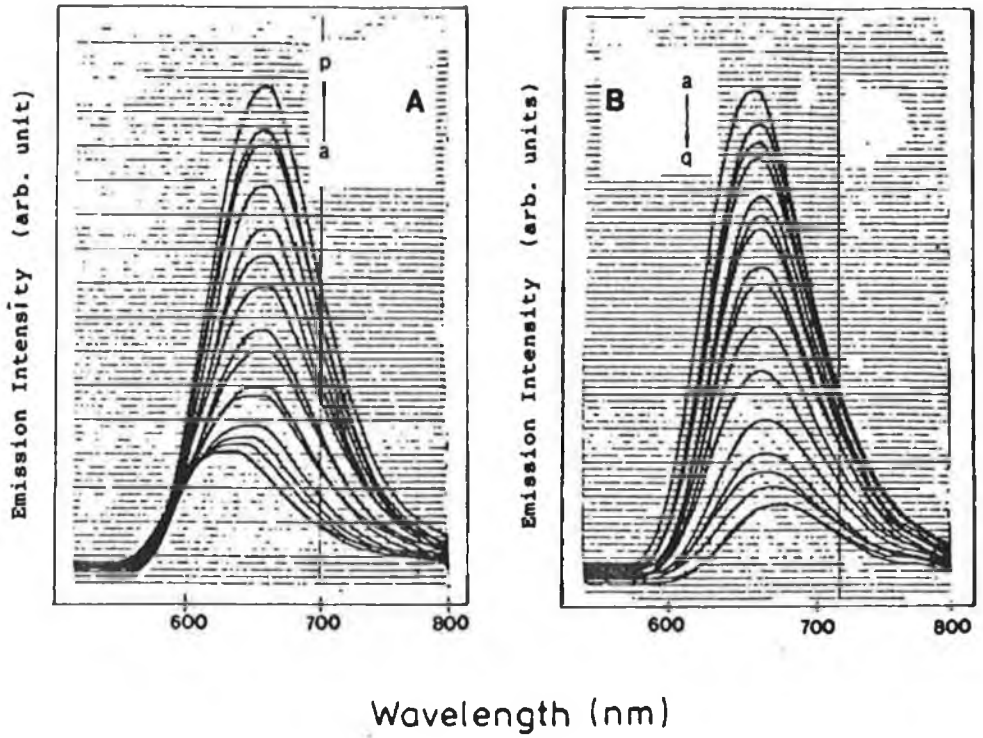

Fig. V.9 pH dependence of the emission spectrum of $[Ru(bpy)_2(HptOH)]^{2+}$ (10^{-4} M) in Britton-Robinson buffer. For curves (a) to (p): pH = 0.44, 0.86, 1.31, 1.52, 1.74, 1.96, 2.20, 2.48, 2.74, 3.03, 3.34, 3.61, 3.91, 4.24, 4.54, 5.71 and B (a) to (q): pH = 7.75, 8.90, 9.38, 9.79, 10.31, 10.54, 10.70, 10.93, 11.11, 11.30, 11.55, 11.83, 12.06, 12.32, 12.54, 12.75, and 12.95.

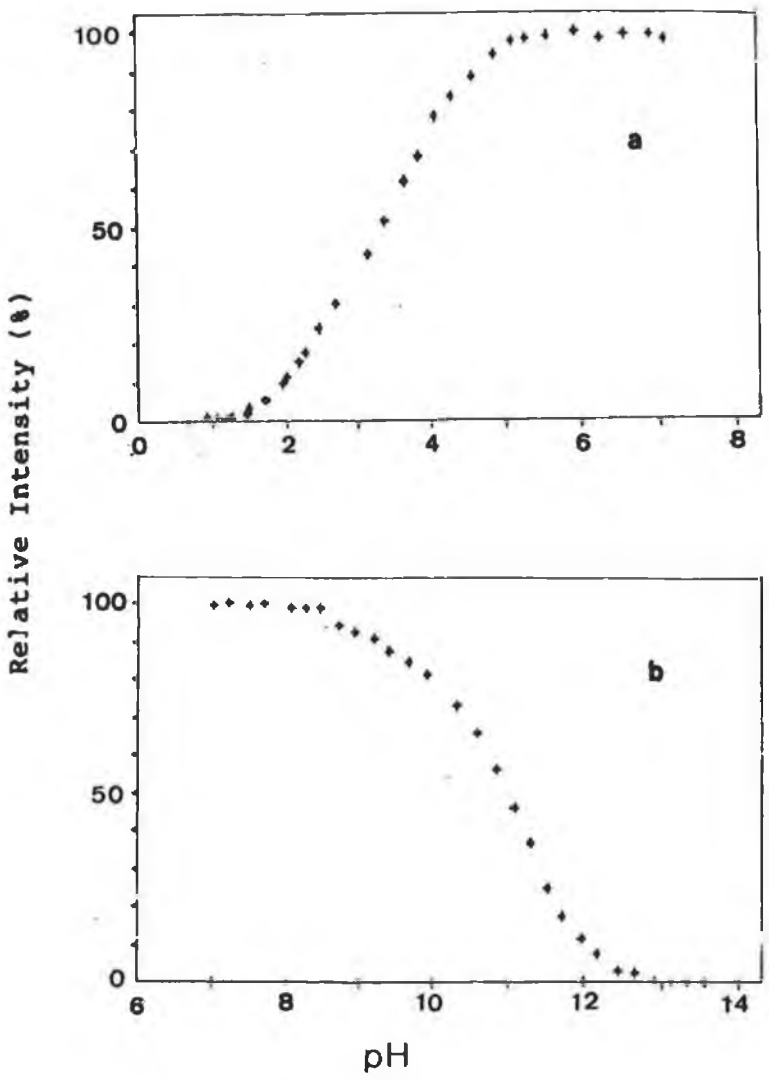

Fig. V.10 Relative emission intensity vs pH for the complex $[Ru(bpy)_2(HptOH)]^{2+}$. (corresponding to Fig. V.9).

Assuming the entropy changes accompanying protonation are minimal from the ground state to the excited state, the pK_a^* can be calculated on the basis of the Forster cycle (eq. V.1) [187]:

$$pK_a^* = pK_a + \frac{0.625}{T}(\nu_b - \nu_a) \qquad (V.1)$$

where ν_a and ν_b are the energies in wave numbers (cm^{-1}) of the 0-0 transition of the acid and base forms, respectively. The best evaluation of the 0-0 energy should come from a detailed analysis of the vibrational structure by low temperature emission spectra fitting, as demonstrated by Meyer and co-workers [188-189].

The pK_a^* can also be determined from the excited-state emission titration data and emission lifetimes using eq. V.2 [187]:

$$pK_a^* = pH_i + \log(\tau_a/\tau_b) \qquad (V.2)$$

where pH_i is the inflection point in the emission titration curve and τ_a and τ_b are the excited-state lifetimes for the protonated and deprotonated forms, respectively.

The pK_a^* values calculated using the two equations, together with the lifetime values and ground-state pK_a values, are listed in Table V.1. Compared to the values

obtained for the ground-state pK_a's, it is clear that the excited-state is more acidic than the ground-state. This indicates that the $ptOH^-$ (or HptOH) ligand is not directly involved in the excited-state chemistry of the compound, but the photophysical properties of the complex are bpy-based. Excitation creates an effective Ru(III) state which results in an increased electron donation from the spectator ligand, as observed for other related pyridylazole ligands [85, 88-89]].

It is interesting that the difference between the ground-state and excited-state pK_a values (pK_a - pK_a^*) for deprotonation of the triazole ring is in the following order (see Table V.1):

$$[Ru(bpy)_2(HptOH)]^{2+} < [Ru(bpy)_2(Hptr\text{-}2)]^{2+} < [Ru(bpy)_2(H3Mptr)]^{2+}$$

This is expected, as relative to Hptr (or ptr^-) ligand, the HptOH (or $ptOH^-$) ligand is a weaker σ-donor due to the electron-withdrawing effect of the phenol group. In contrast, H3Mptr (or $3Mptr^-$) ligand is a better σ-donor due to the electron-donating property of the methyl group. This results in the different magnitude of the electron-donation from these ligands to the ruthenium center when the complexes are photoexcited.

In chapter IV it has been shown that the two isomers of $[Ru(bpy)_2(ptr)]^+$ and $[Ru(bpy)_2(3Mptr)]^+$ are

photochemically stable. Results obtained from preliminary photolysis experiments shown that, despite of the reduced o-donor ability of $ptOH^-$ compared to ptr^-, the $[Ru(bpy)(ptOH)]^+$ complex is still photochemically very stable. In CH_2Cl_2 containing 3 mM TBAB and 10^{-4} M $[Ru(bpy)_2(ptOH]^+$, broad band irradiation (> 430 nm) up to 3 h yields no photochemical reaction. This suggests that the ^3MC state energy is still at a higher level and remains inaccessible at room temperature. It is expected that for this complex (in deprotonated form) the temperature dependence of the emission lifetime will be very small.

The results obtained for $[Ru(bpy)_2(ptOH)]^+$ show that the presence of the phenol group on the triazole ring only has very small effects on the photophysical properties of the complex. The difference is reflected from their different basicities in both ground state and excited state. Like the two isomers of $[Ru(bpy)_2(ptr)]^+$ and $[Ru(bpy)(3Mptr)]^+$, $[Ru(bpy)_2(ptOH)]^+$ is also photostable and its emission lifetime is very close to the value obtained on $[Ru(bpy)_2(ptr\text{-}2)]^+$. Finally, the emission intensity and maximum of the complex are pH dependent, which indicates that protonation and deprotonation of the spectator ligand do affect the ^3MLCT emitting process which is originated from the bpy-based π^* orbitals.

V.2.3 $Ru(bpy)_2$(II) complexes containing pyrazyltriazoles: pH control of the nature of the ^{3}MLCT emitting state.

V.2.2.1 General.

In this section, the photophysical properties of the complexes $[Ru(bpy)_2(HL)]^{2+}$ will be discussed, where HL stands for Hpztr, H3Mpztr, and 1M3pztr. The structures of these complexes are presented in Fig. V.11.

The complex $[Ru(bpy)_2(Hpztr)]^{2+}$ has two coordination isomers. Using semi-preparative HPLC the two isomers have been separated and isolated [89, 103]. The coordination mode for each of the isomers has been elucidated using proton NMR [89, 103]. Depending on the nitrogen via which the Ru(II) center is bound, the two isomers are denoted as $[Ru(bpy)_2(Hpztr\text{-}4)]^{2+}$ (first fraction collected from HPLC) and $[Ru(bpy)_2(Hpztr\text{-}2)]^{2+}$ (second fraction), respectively (see Fig. V.11). For $[Ru(bpy)_2(H3Mpztr)]^{2+}$, only one isomer was obtained from the product, and the proton NMR data reveal that the Ru(II) center is coordinated via $N^{1'}$ of the triazole ring [89, 103] (see Fig. V.11). For $[Ru(bpy)_2(1M3pztr)]^{2+}$, again only one product was found. Proton NMR data suggest that in this compound the Ru(II) center is bound via $N^{4'}$ of the triazole ring [89, 103] (see Fig. V.11). This is also attributed to the steric hinderance

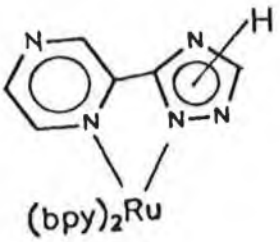

$[Ru(bpy)_2(Hpztr\text{-}2)]^{2+}$

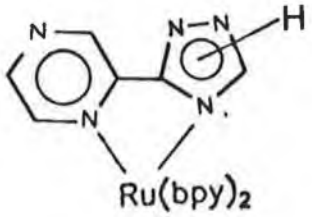

$[Ru(bpy)_2(Hpztr\text{-}4)]^{2+}$

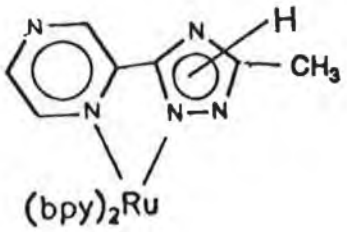

$[Ru(bpy)_2(H3Mpztr)]^{2+}$

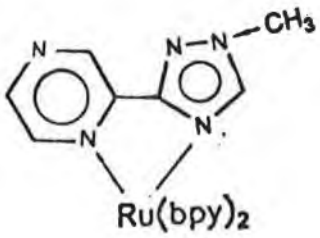

$[Ru(bpy)_2(1M3pztr)]^{2+}$

Fig. V.11 $Ru(bpy)_2$ complexes containing pyrazyltriazoles.

of the methyl group on the $N^{1'}$ position [89, 103].

Pyrazyltriazoles combine the properties of both class I and class II ligands. Pyrazine and bipyrazine are known as better π-accepting but weaker σ-donating ligands compared to bpy [56, 92, 97]. Triazole and pyridyltriazoles, in contrast, are stronger σ-donating but weaker π-accepting ligands compared to bpy [85, 88-89, 101]. Interestingly, $[Ru(bpy)_2(ptr)]^+$ and $[Ru(bpy)_2(bpyz)]^{2+}$ complexes have both shown to be photostable [56, 87, and Chapter IV]. It is therefore interesting to see what type of behaviour will be observed for the pyrazyltriazole complexes. In this section, the photophysical properties of these complexes have been probed by a study of proton transfer reactions and emission lifetimes.

V.2.2.2 Ground-state acid-base properties.

The two isomers of $[Ru(bpy)_2(Hpztr)]^{2+}$ and $[Ru(bpy)_2(H3Mpztr)]^{2+}$, in principle, can be protonated on both the triazole ring and the pyrazine ring, as shown in eq. V.3:

$$[Ru(bpy)_2(L)]^+ \underset{-H^+}{\overset{+H^+}{\rightleftharpoons}} [Ru(bpy)_2(HL)]^{2+} \underset{-H^+}{\overset{+H^+}{\rightleftharpoons}} [Ru(bpy)_2(H_2L)]^{3+}$$

pK_a(acid) pK_a(base)

(V.3)

For $[Ru(bpy)_2(1M3pztr)]^{2+}$, naturally only the pyrazine ring can be protonated (see Fig. V.11).

The protonation of the pyrazine ring is independent of the coordination mode of the triazole ring. For all four compounds the absorption maximum originally observed at about 450 nm disappears upon protonation of the pyrazine ring and two new bands appear at 400 and 530 nm [102]. Resonance Raman spectra have shown that the lowest energy band can be described as a Ru(II) ---> π^* (H_2L) transition [89, 102], which suggests that the LUMO is based on the pyrazyltriazole ligand. Using UV-vis spectroscopy, a pK_a(base) of -1.8 has been obtained for all four complexes [89, 102-103], a value which is typical for a pyrazine protonation [92].

Also in the pH range 2-7 the absorption spectra of all the compounds, except for $[Ru(bpy)_2(1M3pztr)]^{2+}$, are pH dependent. The fact that for the compound $[Ru(bpy)_2(1M3pztr)]^{2+}$ no variation of the absorption spectrum with pH was observed in this pH range, clearly indicating that the spectral changes for the other three are related to the acid-base properties of the triazole group.

The ground-state absorption titration results for $[Ru(bpy)_2(Hpztr\text{-}2)]^{2+}$ and $[Ru(bpy)_2(Hpztr\text{-}4)]^{2+}$ are presented in Fig. V.12 and Fig. V.13. A remarkable feature of these results is the small effect that deprotonation of

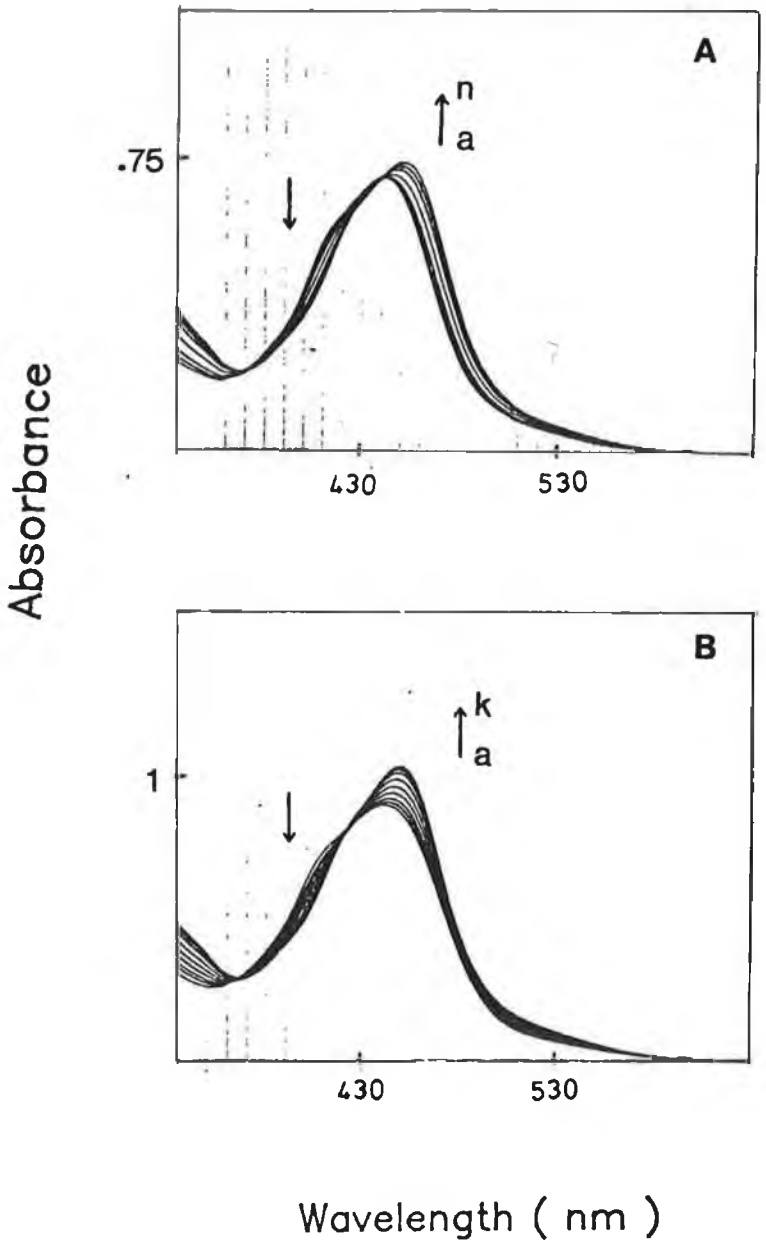

Fig. V.12 pH dependence of the absorption spectrum for A) $[Ru(bpy)_2(pztr\text{-}4)]^+$ and B) $[Ru(bpy)_2(pztr\text{-}2)]^+$ (10^{-4} M). A) curves a-n pH = 1.91, 2.39, 2.84, 3.05, 3.39, 3.86, 4.28, 4.73, 5.22, 5.64, 5.98, 6.38, 6.80, 7.30 and B) a-k pH = 1.21, 2.89, 3.19, 3.50, 3.76, 4.08, 4.46, 4.91, 5.58, 6.20, 7.04.

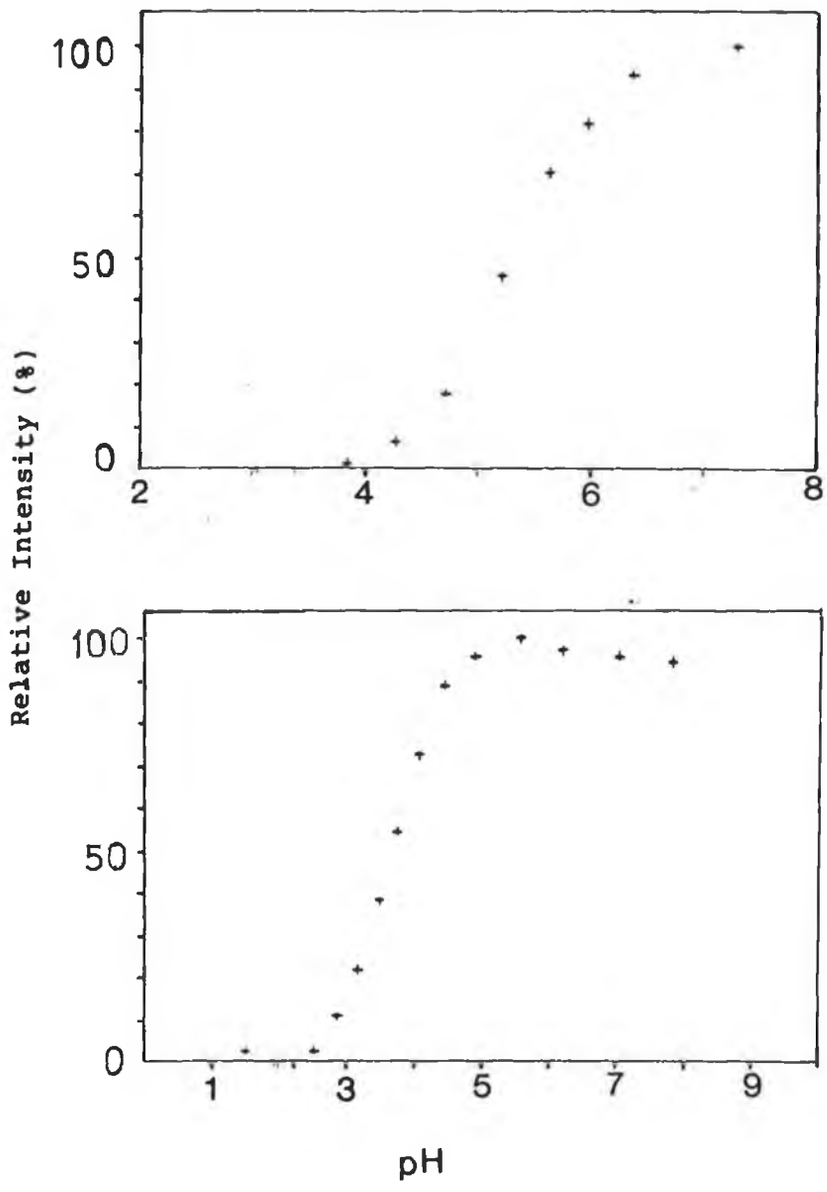

Fig. V.13 Relative intensity vs. pH for A) $[Ru(bpy)_2(Hpztr\text{-}4)]^{2+}$ at 440 nm and B) $[Ru(bpy)_2(Hpztr\text{-}2)]^{2+}$ at 450 nm.

Table V.2 pK_a and pK_a^* values for the $Ru(bpy)_2(II)$ complexes containing pyrazyltriazoles measured in Britton-Robinson buffer.

	pK_a [a]	pH_i	pK_a^* [b]	pK_a^* [c]	E_{em}, nm
$[Ru(bpy)_2(H_2pztr\text{-}4)]^{3+}$	-1.8[e]	2.5			
$[Ru(bpy)_2(Hpztr\text{-}4)]^{2+}$	5.3(8.7)	5.5	5.4	4.8	596[d]
$[Ru(bpy)_2(pztr\text{-}4)]^{+}$					603[d]
$[Ru(bpy)_2(H_2pztr\text{-}2)]^{3+}$	-1.8[e]	2.0			
$[Ru(bpy)_2(Hpztr\text{-}2)]^{2+}$	3.7(8.7)	3.9	3.8	3.4	612[d]
$[Ru(bpy)_2(pztr\text{-}2)]^{+}$					618[d]
$[Ru(bpy)_2(H_25Mpztr)]^{3+}$	-1.8[e]	2.4			
$[Ru(bpy)_2(H5Mpztr)]^{2+}$	4.2(9.4)	4.4	4.4	3.8	620[d]
$[Ru(bpy)_2(5Mpztr)]^{+}$					627[d]
$[Ru(bpy)_2(H1M3pztr)]^{2+}$	-1.8[e]	3.2			
$[Ru(bpy)_2(1M3pztr)]^{+}$					575[d]
$[Ru(bpy)_2(Hptr\text{-}4)]^{2+}$	5.7(9.2)	5.1	4.2	3.1	580
$[Ru(bpy)_2(ptr\text{-}4)]^{+}$					607
$[Ru(bpy)_2(Hptr\text{-}2)]^{2+}$	4.1(9.2)	2.8	2.2	1.4	577
$[Ru(bpy)_2(ptr\text{-}2)]^{+}$					607

a. Data in parentheses are obtained for free the ligands.
b. Calculated using eq. V.2 (Forster cycle).
c. Calculated using eq. V.3 (lifetimes).
d. Measured in 4:1 ethanol/methanol at 77 K [89, 103].
e. Measured in conc. H_2SO_4 [89, 103].

the triazole ring has on the absorption spectrum. The ground-state pK_a values for the free ligands and for the complexes are listed in Table V.2.

The pK_a values for deprotonation of the triazole ring are very similar to those obtained on the pyridyltriazole-containing analogues (Table V.2). Also, the $N^{2'}$ bound isomer is more basic than the $N^{4'}$ bound one, indicating that the $N^{2'}$ is a better σ-donor. In $[Ru(bpy)_2(H3Mpztr)]^{2+}$, where the Ru(II) is bound via $N^{1'}$, the presence of the electron-donating methyl group does make the ligand slightly more basic compared to $[Ru(bpy)_2(Hptr\text{-}2)]^{2+}$ (Fig. V.11). All these results are very similar to those obtained on the pyridyltriazole analogues.

V.2.2.3 Excited-state acid-base properties.

The excited-state acidity has been investigated by a study of the pH dependence of the emitting properties of the compounds. These emission titrations were carried out by excitation into the appropriate isosbestic points. Two examples of the emission titration for $[Ru(bpy)_2(Hpztr\text{-}2)]^{2+}$ and $[Ru(bpy)_2(H3Mpztr)]^{2+}$ are presented in Fig. V.14 and Fig. V.15.

At very low pH values the emission intensity for all four

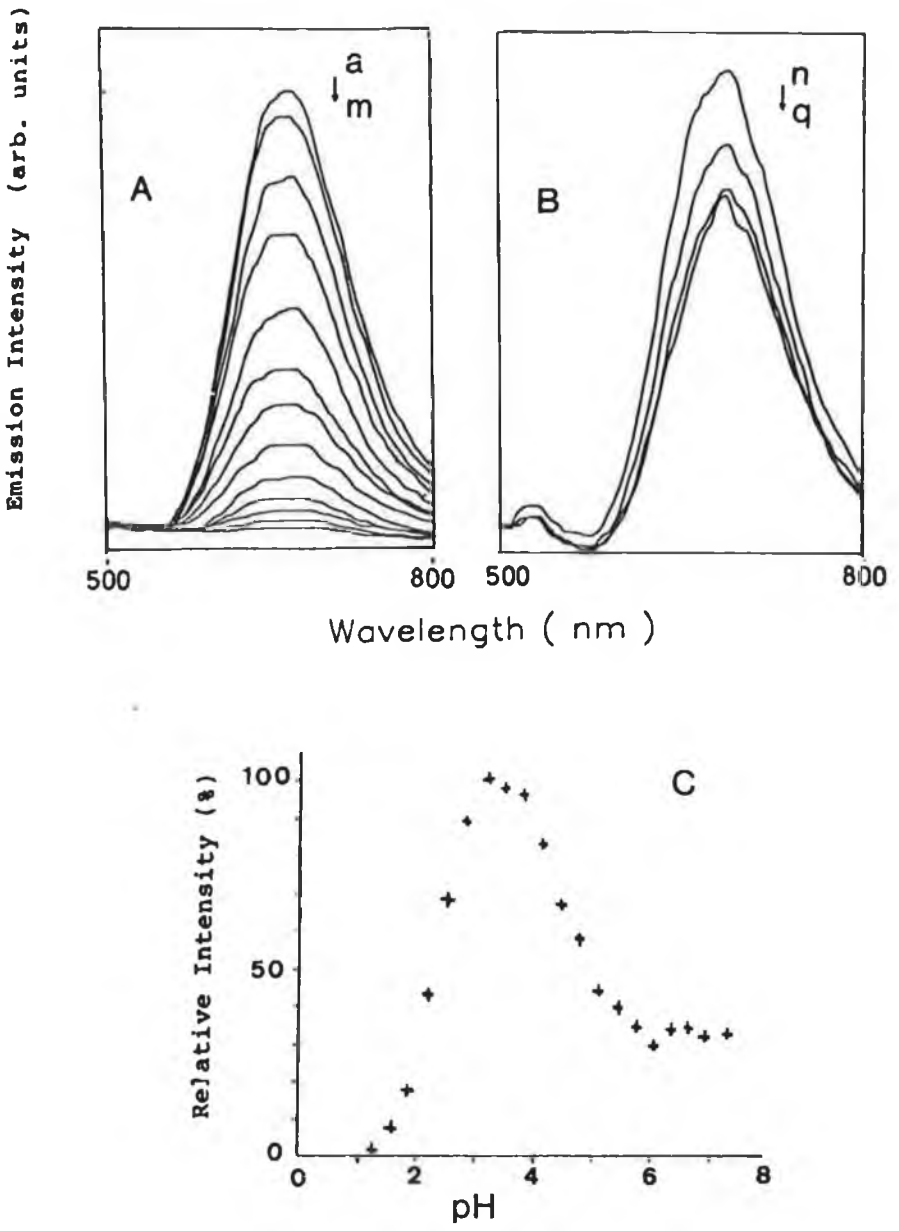

Fig. V.14 A and B: pH dependence of the emission spectrum for $[Ru(bpy)_2(Hpztr\text{-}2)]^{2+}$; for curves a-m pH 2.95 to 0.2; n-q pH = 3.67 to 4.90. C) relative emission intensity vs. pH.

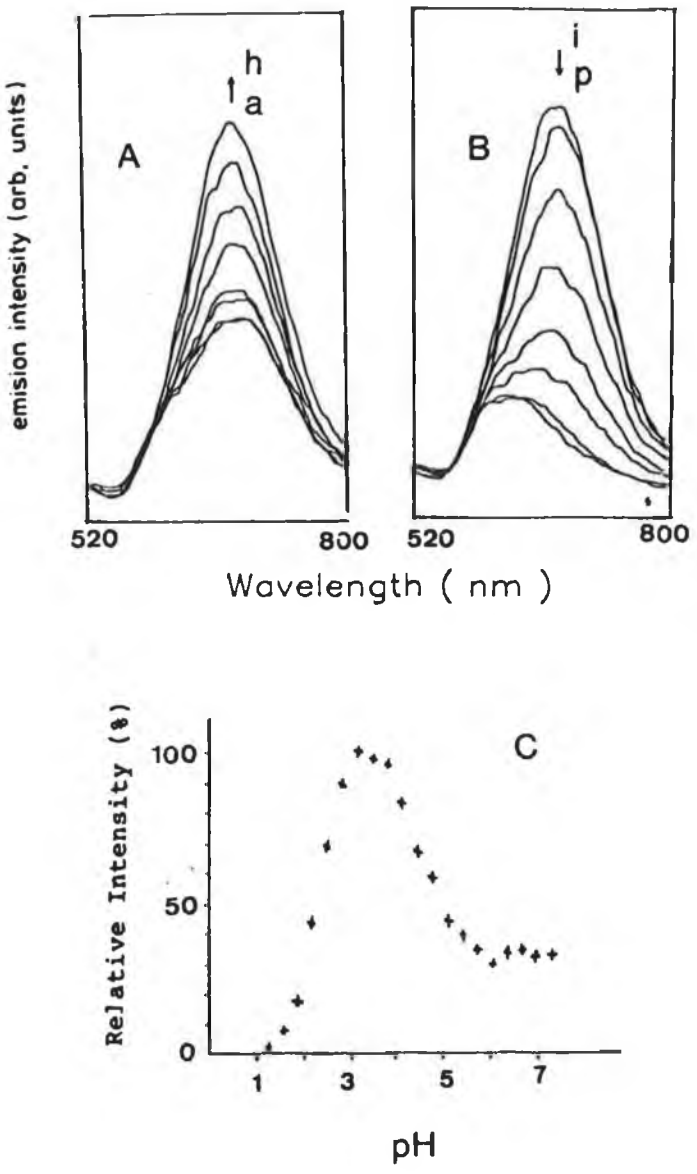

Fig. V.15 A and B: pH dependence of emission spectrum for $[Ru(bpy)_2(H3Mpztr)]^{2+}$; for curves a-h pH = 6.07 to 3.84; i-p pH 3.18 to 0.94. C: relative emission intensity vs. pH.

compounds is negligible. The luminesence becomes stronger when the pH is increased until a maximum intensity is reached at about pH 3. For $[Ru(bpy)_2(Hpztr\text{-}4)]^{2+}$, $[Ru(bpy)_2(Hpztr\text{-}2)]^{2+}$, and $[Ru(bpy)_2(H3Mpztr)]^{2+}$ the emission intensity decreases between pH 3 and pH 6 (Fig. V.14-15). For $[Ru(bpy)_2(1M3pztr)]^{2+}$ no decrease in the emission intensity is observed in this pH range. This is again consistent with the absence of a triazole N-H group in this compound.

There are a number of possible reasons for the absence of emission when the pyrazine ring is protonated. First, the protonation of the pyrazine ring may lower the π^* energy level with the result that the emission lifetime and quantum yield of the doubly protonated complexes are decreased because of the smaller t_{2g} - ^{3}MLCT energy gap (energy gap law). Also, a weak emission, if any, occuring at low energies might be beyond the detecting limit of the photomultiplier tube (900 nm).

Second, the irreversible proton bonding to the pyrazine ring might contribute, to a certain extent, to the deactivation of the emitting states, as N-H stretching vibration can serve as an excited-state energy receptor. This type of behaviour has been found for several other Ru(II) diimine complexes by Lever, De Mesmeaker and Kalyanasundarum's groups [92-93, 98].

The emission lifetimes for the protonated and deprotonated species are measured in CH_3CN and Britton-Robinson buffer, respectively. The results are in Table V.3. Except for $[Ru(bpy)_2(1M3ptr]^{2+}$, all the compounds show longer emission lifetimes (more than a factor of 10) in CH_3CN than in aqueous buffer. This might be explained by that an extra energy trapping O-H vibration mode in aqueous solution contributes to the excited-state decay. The solvent dependence of the emission lifetimes seems much more significant in these complexes compared to the two isomers of $[Ru(bpy)_2(ptr)]^+$ (see Table V.2), and this is not understood at present.

The lifetime for $[Ru(bpy)_2(1M3pztr)]^+$ in buffer is similar to those observed for other three complexes. In CH_3CN, however, the excited-state lifetime becomes very short (< 5 ns), and the reason is again unclear at this stage.

Based on the ground-state pK_a values, the 77 K emission energies, the pH_i values obtained from emission titration results and the emission lifetimes, the pK_a^* values can be calculated for the compounds investigated. The data have been presented in Table V.2. As no emission is observed when the pyrazine ring is protonated, the excited-state lifetimes can not be measured for the doubly protonated complexes. Therefore the pK_a^* (base) values are not obtained for

Table V.3 Room temperature emission lifetimes of $Ru(bpy)_2$ complexes containing pyrazyltriazoles.

	$\tau_{(298\ K)}$[a], ns	
	CH_3CN	B.R. Buffer
$[Ru(bpy)_2(Hpztr\text{-}4)]^{2+}$	b	14
$[Ru(bpy)_2(pztr\text{-}4)]^{+}$	227	12
$[Ru(bpy)_2(Hpztr\text{-}2)]^{2+}$	b	15
$[Ru(bpy)_2(pztr\text{-}2)]^{+}$	215	18
$[Ru(bpy)_2(H3Mpztr)]^{2+}$	b	12
$[Ru(bpy)_2(3Mpztr)]^{+}$	145	16
$[Ru(bpy)_2(1M3pztr)]^{2+}$	< 5	23
$[Ru(bpy)_2(Hptr\text{-}4)]^{2+}$	2	2
$[Ru(bpy)_2(Hptr\text{-}4)]^{+}$	205	117
$[Ru(bpy)_2(Hptr\text{-}2)]^{2+}$	5	9
$[Ru(bpy)_2(ptr\text{-}2)]^{+}$	142	90

a. N_2-degassed for 10 min. before each measurement.

b. Emission lifetimes not available due to the difficulty in controlling the acidity in CH_3CN.

these compounds.

A few conclusions can be drawn from the pH_i and pK_a^* values in Table V.2. First, although the pK_a^* values for deprotonation of the pyrazine ring are not available, the pH_i values (2.4-3.2) for the pyrazine ring suggest that the complexes are at least four orders of magnitude more basic than in the ground state (pK_a = -1.8 for the triazole ring in the free ligands). This points to an indication that between pH 0-3, where the triazole ring is protonated, the LUMO is pyrazyltriazole-based, which is consistent with the results obtained from Resonance Raman experiments [89, 102].

Second, when the triazole ring is changed from the protonated form to the deprotonated form, the LUMO in the complexes is switched to bpy-based π^* orbitals. This is reflected by the slightly lower pK_a^*(acid) values compared to the ground-state pK_a(acid) values. The schematic relative energy levels for this proton-induced LUMO switching is presented in Fig. V.16.

Finally, the difference between the pK_a and pK_a^* values for deprotonation of the triazole ring are very small. This is due to the opposite σ-donor and π-acceptor effects of the pyrazyl and triazole groups. The strong σ donating ability of the triazole ring (especially when deprotonated) is always compensated by the strong π-accepting ability of the pyrazine

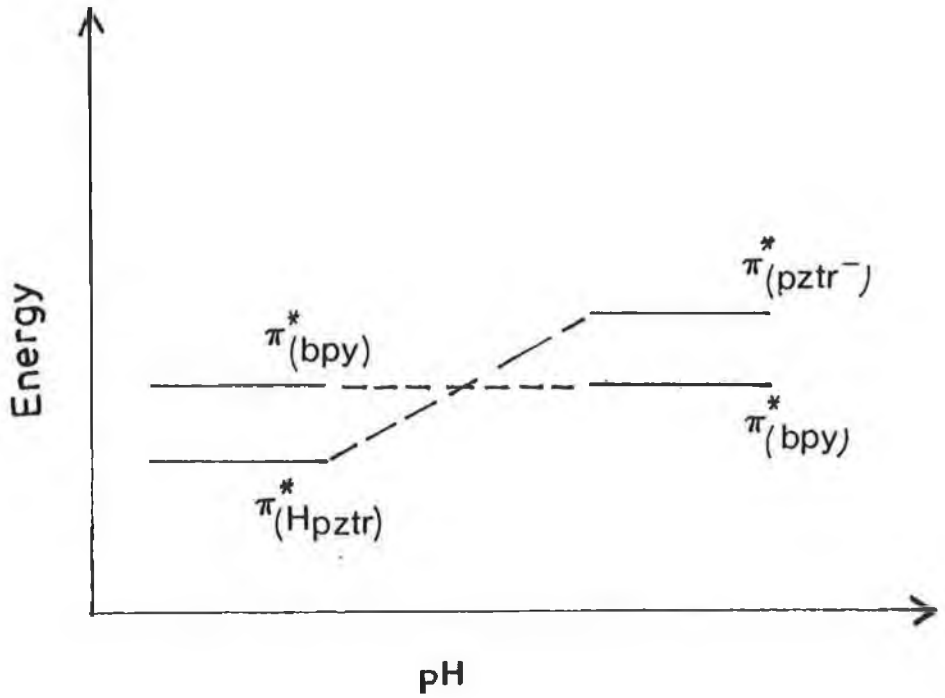

Fig. V.16 pH control of the LUMO in $Ru(bpy)_2$ complexes containing pyrazyltriazoles.

ring, and vice versa. The small shift in absorption and emission maxima in the complexes upon deprotonation of the triazole ring supports this suggestion. Also, the very small decrease of the pK_a^* values for deprotonation of the triazole ring in the complexes suggests that while the excited electron is clearly located on the pyrazyltriazole ligand when protonated, the major part of this electron density is present on the pyrazine ring.

Photolysis in CH_2Cl_2 containing 3 mM TBAB has been carried out for $[Ru(bpy)_2(1M3pztr)]^{2+}$, $[Ru(bpy)_2(Hpztr-2)]^{2+}$ $[Ru(bpy)_2(H3Mpztr)]^{2+}$ and their deprotonated analogues. The reactions were monitored using UV-vis absorption spectroscopy. At the same concentration (10^{-4} M), all the complexes undergo photochemical reactions giving rise to $[Ru(bpy)_2Br_2]$ as a final product. There is no substantial difference in the reaction rate between the protonated and deprotonated species except for $[Ru(bpy)_2(H3Mpztr)]^{2+}$, where photosubstitution occurs much faster than for its deprotonated analogue $[Ru(bpy)_2(3Mpztr)]^{+}$. Within 30 min. the reaction goes to completion for $[Ru(bpy)_2(H3Mpztr)]^{2+}$. Prolonged irradiation of $[Ru(bpy)_2(3Mpztr)]^{+}$ for up to 3 h, however, only leads to less than 20% conversion of the starting material to the photolysis product.

lifetime measurements.

The results clearly show that both ligand variation and second-sphere perturbation can alter the photophysical properties of Ru(II) diimine complexes. The combination of the features of both class I and class II ligands does make the pyrazyltriazole-containing complexes quite unique in their excited-state behaviour. The second-sphere perturbation also plays an important role: firstly, solvents have a large effect on the the excited-state lifetimes; secondly and more interestingly, the LUMO can be switched from pyrazyltriazoles to bpy by deprotonation of the triazole ring. This is a case similar to that observed by Demas' group and Balzani's group on the complexes $[Ru(bpy)_2(CN)_2]$ [181] and $[Ru(biq)_2(CN)_2]$ [182].

V.2.3 $Ru(phen)_2$ and $Ru(dmb)_2$ complexes containing pyridyltriazoles: ligand and solvent effects on the emission lifetime and oxygen quenching.

V.2.3.1 General.

In this section, the effect of a change of diimine ligands on the photophysical properties are described. Two types of complexes are examined: $Ru(phen)_2(Hptr)]^{2+}$ and $[Ru(dmb)_2(Hptr)]^{2+}$. As observed for $[Ru(bpy)_2(Hptr)]^{2+}$, for each of these two complexes there

exist two coordination isomers (Fig. V.17). The two isomers for each of the complexes are separated using semi-preparative HPLC [158]. The coordination modes have been elucidated using proton NMR spectroscopy [158]. For $[Ru(phen)_2(Hptr\text{-}4)]^{2+}$ and $[Ru(dmb)_2(Hptr\text{-}4)]^{2+}$ (first fractions isolated from HPLC), the Ru(II) center is bound via $N^{4'}$; while for $[Ru(phen)_2(Hptr\text{-}2)]^{2+}$ and $[Ru(dmb)_2(Hptr\text{-}2)]^{2+}$ (second fractions) the Ru(II) center is bound via $N^{2'}$ (Fig. V.17).

As decribed in Chapter IV, the two isomers of $[Ru(bpy)_2(ptr)]^{+}$ exhibit very high stability against photosubstitution compared to $[Ru(bpy)_3]^{2+}$. The emission lifetimes of the two isomers are, however, about twice as short as that for $[Ru(bpy)_3]^{2+}$ and this limits the application of these compounds as photosensitisers. By replacing bpy by phen or dmb the lifetimes of the complexes might be altered. In fact, some bis-phen based complexes have been reported to have longer emission lifetimes than that of $[Ru(bpy)_3]^{2+}$. [41].

To evaluate the relative σ-donating and π-accepting abilities of phen, dmb and bpy ligands, it is useful to compare the Ru(II/III) oxidation potentials and first ligand-based reduction potentials of complexes containing these ligands (Table V.4).

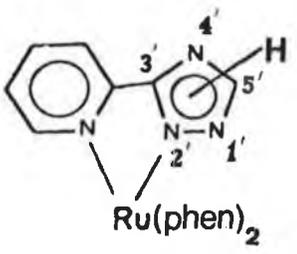

$[Ru(phen)_2(Hptr\text{-}2)]^{2+}$

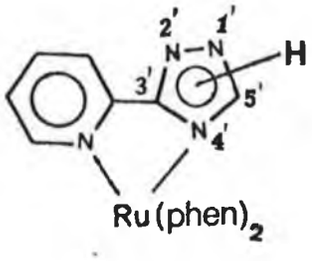

$[Ru(phen)_2(Hptr\text{-}4)]^{2+}$

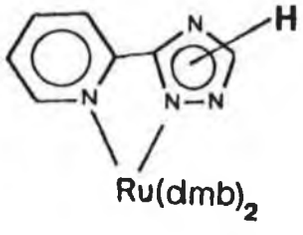

$[Ru(dmb)_2(Hptr\text{-}2)]^{2+}$

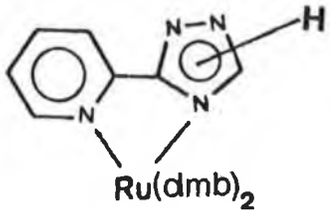

$[Ru(dmb)_2(Hptr\text{-}4)]^{2+}$

Fig. V.17 Coordination isomers of $Ru(phen)_2$ and $Ru(dmb)_2$ complexes containing the ptr^- (or Hptr) ligand.

Table V.4. Emission energy and electrochemical data for Ru(II) complexes containing bpy, phen and dmb ligands.

	E_{em}[a] 298 K, nm	$E^{o'}$ (V vs. SCE)[b] Ru(II/III)	first reduction (ligand-based)
[c] $[Ru(phen)_2(Hptr\text{-}4)]^{2+}$	611	1.19	-1.51
[c] $[Ru(phen)_2(ptr\text{-}4)]^{+}$	651	0.84	-1.64
[c] $[Ru(phen)_2(Hptr\text{-}2)]^{2+}$	607	1.18	---
[c] $[Ru(phen)_2(ptr\text{-}2)]^{+}$	663	0.86	-1.51
[c] $[Ru(dmb)_2(Hptr\text{-}4)]^{2+}$	624	1.08	-1.49
[c] $[Ru(dmb)_2(ptr\text{-}4)]^{+}$	667	0.72	-1.75
[c] $[Ru(dmb)_2(Hptr\text{-}2)]^{2+}$	621	1.08	-1.59
[c] $[Ru(dmb)_2(ptr\text{-}2)]^{+}$	674	0.75	-1.63
$[Ru(bpy)_2(Hptr\text{-}4)]^{2+}$	616	1.20	-1.47
$[Ru(bpy)_2(ptr\text{-}4)]^{+}$	678	0.90	-1.51
$[Ru(bpy)_2(Hptr\text{-}2)]^{2+}$	611	1.14	-1.49
$[Ru(bpy)_2(ptr\text{-}2)]^{+}$	677	0.83	-1.49
$[Ru(bpy)_3]^{2+}$ [69]	620	1.26	-1.35
$[Ru(phen)_3]^{2+}$ [190]	604	1.27	-1.35
$[Ru(dmb)_3]^{2+}$ [129]	618	1.10	-1.46

a. Measured in CH_3CN.

b. Measured using differential pulse voltammetry in CH_3CN containing 0.1 M TEAP.

c. Ref. 158.

For $[Ru(L)_3]^{2+}$ complexes (L = bpy, phen, dmb), the Ru(II/III) oxidation potentials and first reduction potentials are almost identical for phen- and bpy- based complexes [69, 190]. However, $[Ru(dmb)_3]^{2+}$ has quite different redox potentials (see Table V.4). The more negative ligand-based reduction potential [129] indicates that dmb is a weaker π-acceptor compared to bpy and phen. The electron-donating effect of the methyl group, on the other hand, is expected to make dmb a better σ-donor. The stronger σ-donating but weaker π-accepting properties of dmb indeed leads to a lower oxidation potential of $[Ru(dmb)_3]^{2+}$ [129].

In mixed-ligand complexes, replacing one of the diimine ligands with Hptr leads to lower Ru(II/III) oxidation potentials in both the protonated and deprotonated forms (see Table V.4). This can be explained by the stronger σ-donor but weaker π-acceptor properties of the Hptr (or ptr^-) ligand. There are no significant differences in Ru(II/III) oxidation potentials between the $N^{2'}$ and $N^{4'}$ isomers. However, the two isomers of $[Ru(dmb)_2(ptr)]^+$ still have lowest oxidation potentials. The two isomers of $[Ru(phen)_2(ptr)]^+$ have lower Ru(II/III) oxidation potentials than their $[Ru(bpy)_2(ptr)]^+$ analogues, suggesting that the perturbation caused by the triazole ligand in the two types of complexes is not equivalent.

V.2.3.2 Excited-state lifetimes and photostability.

The emission maxima and emission lifetimes at room temperature for the dmb- and phen-based Ru(II) complexes are listed in Table V.5.

An attractive feature of the two isomers of $[Ru(phen)_2(ptr)]^+$ is that they have much longer lifetimes than their $[Ru(bpy)_2(ptr)]^+$ analogues. In CH_3CN, the emission lifetime is 898 ns for $[Ru(phen)_2(ptr\text{-}4)]^+$ and 673 ns for $[Ru(phen)_2(ptr\text{-}2)]^+$. These values are comparable to the that reported for $[Ru(bpy)_3]^{2+}$ (680 ns) [190] and longer than that of $[Ru(phen)_3]^{2+}$ (460 ns) [190] in the same solvent. The emission energies of the two isomers of $[Ru(phen)_2(ptr)]^+$ are slightly higher than those reported for the $[Ru(bpy)_2(ptr)]^+$ analogues. It will be shown later for all these deprotonated complexes, the ^3MC - ^3MLCT energy gap is large, suggested from their photostability. Thus the non-radiative decay from the ^3MC level is not a dominant pathway for the excietd-state deactivation, and the longer emission lifetimes observed for phen-containing complexes can be explained by the energy gap law.

For the two isomers of $[Ru(dmb)_2(ptr)]^+$ have emission lifetimes and emission energies close to those found for the two isomers of $[Ru(bpy)_2(ptr)]^+$.

Table V.5 Room temperature emission lifetimes of $Ru(phen)_2$ and $Ru(dmb)_2$ complexes containing pyridyltriazole ligand.

	$\tau_{(298\ K)}$, ns	
	CH_3CN[a]	B.R. Buffer[b]
$[Ru(phen)_2(Hptr\text{-}4)]^{2+}$	5	8
$[Ru(phen)_2(ptr\text{-}4)]^{+}$	898(81)	499
$[Ru(phen)_2(Hptr\text{-}2)]^{2+}$	5	6
$[Ru(phen)_2(ptr\text{-}2)]^{+}$	673(80)	428
$[Ru(dmb)_2(Hptr\text{-}4)]^{2+}$	5	11
$[Ru(dmb)_2(ptr\text{-}4)]^{+}$	180(57)	95
$[Ru(dmb)_2(Hptr\text{-}2)]^{2+}$	5	7
$[Ru(dmb)_2(ptr\text{-}2)]^{+}$	133(55)	80
$[Ru(bpy)_2(Hptr\text{-}4)]^{2+}$	2	2
$[Ru(bpy)_2(ptr\text{-}4)]^{+}$	205(82)	117
$[Ru(bpy)_2(Hptr\text{-}2)]^{2+}$	5	9
$[Ru(bpy)_2(ptr\text{-}2)]^{+}$	142(60)	90
$[Ru(bpy)_3]^{2+}$ [69]	680	
$[Ru(phen)_3]^{2+}$ [190]	460	
$[Ru(dmb)_3]^{2+}$ [129]	931 (in CH_2Cl_2)	

a. N_2-degassed for 10 min. before each measurement; data in parentheses are recorded in air-saturated solution.

b. N2-degassed for 10 min. before each measurement; The data recorded in air-saturated solution are only about 10% shorter and omitted here.

The excited-state pK_a^* values have been calculated using the lifetime data obtained for these complexes (Table V.6). The values calculated using the Forster cycle and using emission lifetimes are very similar. In the excited state all the complexes become more acidic than in the ground state, indicating that the ptr^- (or Hptr) ligand is not directly involved in the ^{3}MLCT emitting process but acts as a spectator ligand. The $N^{4'}$-bound isomers are more basic in the ground state compared to the $N^{2'}$-bound isomers. This suggests that the $N^{2'}$ is a better o-donor, which is consistent with the results obtained on the two isomers of $[Ru(bpy)_2(ptr)]^+$ (see Table V.6).

Preliminary photolysis in 3 mM TBAB/CH_2Cl_2 has been carried out for all the four complexes in deprotonated form. $[Ru(dmb)_2(ptr\text{-}4)]^+$ is very stable against photosubstitution. After 3 h irradiation no reaction was observed. For $[Ru(dmb)_3(ptr\text{-}2)]^+$, a slight photodecomposition was observed, but the reaction rate is very slow. For a 10^{-4} M sample, 3 h irradiation only leads to a decomposition less than 4%. Under the same conditions, the photosubstitution for $[Ru(bpy)_3]^{2+}$ completes within 30 min.

The results obtained on the two isomers of $[Ru(phen)_2(ptr)]^+$ are similar to those obtained for $[Ru(dmb)_2(ptr)]^+$. After 3 h irradiation only less than

Table V.6 pK_a and pK_a^* values for the $Ru(phen)_2$ and $Ru(dmb)_2$ complexes containing the pyridyltriazole ligand measured in Britton-Robinson buffer.[a]

	pK_a	pH_i	pK_a^{*b}	pK_a^{*c}	E_{em}[d], nm
$[Ru(phen)_2(Hptr\text{-}4)]^{2+}$	5.8	5.6	4.0	3.8	573
$[Ru(phen)_2(ptr\text{-}4)]^{+}$					603
$[Ru(phen)_2(Hptr\text{-}2)]^{2+}$	4.3	3.8	2.3	1.9	568
$[Ru(phen)_2(ptr\text{-}2)]^{2+}$					600
$[Ru(dmb)_2(Hptr\text{-}4)]^{2+}$	6.1	5.9	4.7	5.0	586
$[Ru(dmb)_2(ptr\text{-}4)]^{+}$					609
$[Ru(dmb)_2(Hptr\text{-}2)]^{2+}$	4.4	3.4	2.2	2.6	585
$[Ru(dmb)_2(ptr\text{-}2)]^{+}$					616
$[Ru(bpy)_2(Hptr\text{-}4)]^{2+}$	5.7	5.1	4.2	3.1	580
$[Ru(bpy)_2(ptr\text{-}4)]^{+}$					607
$[Ru(bpy)_2(Hptr\text{-}2)]^{2+}$	4.1	2.8	2.2	1.4	577
$[Ru(bpy)_2(ptr\text{-}2)]^{+}$					607

a. The pK_a, pH_i, and E_{em} values for the phen- and dmb-containing complexes are taken from Ref. 158.

b. Calculated using eq. V.2 (Forster cycle).

c. Calculated using eq. V.3 (emission lifetimes used are the values measured in buffer; see Table V.5).

d. Measured in 4:1 ethanol/methanol at 77 K.

3% of the starting material undergoes photosubstitution.

The photostability of these complexes most likely results from the large ^{3}MLCT - ^{3}MC energy gap, as found earlier for $[Ru(bpy)_2(ptr)]^+$. The strong σ-donating ability of the ptr^- ligand causes a large splitting between t_{2g} and e_g^* levels. Therefore the ^{3}MC state becomes difficult to populate from the ^{3}MLCT state even at room temperature.

$[Ru(bpy)_3]^{2+}$ and $[Ru(phen)_3]^{2+}$ have been shown to be photochemically labile [175-176]. The much higher photostability observed for the two isomers of $[Ru(phen)(ptr)]^+$, together with their long emission lifetimes, suggests that these bis(phen) triazole complexes might be very promising candidates for use in energy conversion systems and photochemical molecular devices.

V.2.3.3. Oxygen quenching of the ^{3}MLCT excited state.

Another striking observation is that $[Ru(phen)_2(ptr\text{-}4)]^+$ and $[Ru(phen)_2(ptr\text{-}2)]^+$ are very sensitive to oxygen quenching (Table V.5). For $[Ru(phen)_2(ptr\text{-}4)]^+$, the emission lifetime in CH_3CN is 10 times longer in degassed solution than in air-saturated solution (898 vs 81 ns). For $[Ru(phen)_2(ptr\text{-}2)]^+$, the emission lifetime is about 7 times longer in degassed CH_3CN (673 vs 80). For $[Ru(bpy)_2(ptr)]^+$ and $[Ru(dmb)_2(ptr)]^+$ complexes, the

emission lifetimes are only 1-2 times longer in degassed CH_3CN (Table V.5). In aqueous buffer such quenching is not found for the phen-based complexes, so the unusual oxygen quenching behaviour is also solvent dependent. For all the dmb-based and bpy-based isomers, the lifetimes are increased less than 10% upon degassing.

Although oxygen quenching of the emitting excited-state is a well documented phenomena for Ru(II) diimine complexes [191-194], such a significant quenching observed for the two isomers of $[Ru(phen)_2(ptr)]^+$ is rather unusual. The most dramatic oxygen quenching for other Ru(II) complexes reported so far is that observed for $[Ru(phen)_3]^{2+}$ absorbed on fumed silica, where the lifetime is at maximum enhanced by a factor of 6 when oxygen pressure is decreased from 800 to 0 mmHg. Based on this observation, Demas and his co-workers have developed an approach for constructing O_2 sensors [193]. If the quenching mechanism follows Stern-Volmer kinetics (i.e. the kinetics for binding O_2 and metal complexes together is not a rate-limiting step), then the concentration of oxygen can be monitored simply by measuring the emission intensity or emission lifetime of the Ru(II) complexes. Obviously, the two isomers of $[Ru(phen)_2(ptr)]^{2+}$ also have the potentials for the application in constructing O_2 sensors.

V.3 Concluding remarks.

The results described in this chapter show that the photophysical properties of Ru(II) complexes can be tuned by ligand variation (first coordination sphere perturbation) and by solvent effect and protonation/deprotonation of the coordinated ligands (second-sphere perturbation).

For the $[Ru(bpy)_2(ptOH)]^+$ complex, the multi-step acid-base proton-transfer equilibria in both the ground and the excited states have been clearly resolved. The presence of an electron-withdrawing phenol group on the triazole ring reduces the basicity of the pyridyltriazole ligand. However, the ^3MC state is still not accessible at room temperature for this complex, as suggested by its high photostability against photosubstitution. This implies that the σ-donor and π-acceptor ability of the $ptOH^-$ ligand is still comparable to that of ptr^-, and substitution of a phenol group on the triazole ring only has a fine-tuning effect on the photophysical properties in the complex.

For the $Ru(bpy)_2$ complexes containing pyrazyltriazoles, the most interesting behaviour is that when the triazole ring is changed from the protonated form to the deprotonated form, the LUMO is switched from the pyrazyltriazole-based σ^* orbital to the bpy-based π^* orbital. This is one of the few cases, where the origin of the emitting state can be

altered and controlled by the second-sphere perturbation [95, 181]. That both the protonated and deprotonated complexes are photochemically labile suggests that the ^{3}MLCT - ^{3}MC energy gap is changed very little upon deprotonation/protonation. This may result from the combination effect of the different σ and π abilities of the pyrazine ring and triazole ring. The σ ability of the triazole ring (especially when deprotonated) is effectively compensated by the π ability of the pyrazine ring, so that the t_2g - e_g^* gap is always small and the ^{3}MC state can be easily populated from the ^{3}MLCT state at room temperature.

For the two isomers of $[Ru(dmb)_2(ptr)]^+$, the electron-donating effect of the methyl group does make the ground-state redox potentials differ from those of the $[Ru(bpy)_2(ptr)]^+$ analogues, but the excited-state properties are changed by a very small amount. A more substantial change in the photophysical properties caused by ligand variation and solvent, however, was observed for the two isomers of $[Ru(phen)_2(ptr)]^+$ relative to their $[Ru(bpy)_2(ptr)]^+$ analogues. The long emission lifetimes of the deprotonated two isomers compared to their bpy-based analogues can be explained by the energy gap law, as non-radiative decay from the ^{3}MC state is not a dominant pathway for the excited state. The emission lifetimes for the two isomers of $[Ru(phen)_2(ptr)]^{2+}$ are similar to that

for $[Ru(bpy)_3]^{2+}$, but the photostability is much higher for the former. This suggests that the phen-based pyridyltriazole complexes might be promising photosensitisers for the application in solar energy transfer systems and photochemical molecular devices. Finally, the significant quenching of the ^{3}MLCT state observed for the two isomers of $[Ru(phen)_2(ptr)]^{2+}$, points to the fact that they might be promising candidates for constructiong oxygen gas sensors.

Chapter VI

Synthesis, Characterisation and Physical Properties of $Ru(bpy)_2$ Complexes Containing a Pyridyltriazole Ligand Linked to a Hydroquinone Group

VI.1 Introduction.

In the photosynthetic reaction centres of purple photosynthetic bacteria, photon absorption of chlorophylls induces a charge separation within the so-called "special pair" and a subsequent intramolecular electron transfer. The electron migrates from the special pair, along the electron-transport chains within the membrane, and eventually reaches the acceptor, ubiquinone. The ubiquinone is then reduced and simultaneously protonated [2]. In fact, in other photosynthetic reaction centres (e.g. Photosystem II), the fundamental process in the beginning event for solar energy conversion is also photoinduced electron transfer from a donor, either through space or through bridging chains, to an acceptor. In this manner, highly exoergic redox sites are generated, where CO_2 can be reduced or H_2O can be oxidised by the aid of suitable enzymes [1, 10, 18-19].

Inspired by the natural photosynthetic systems, a large body of interesting electron donor-acceptor molecules have been prepared [5, 7]. The elucidation of the crystal structure of the reaction centre in a purple synthetic bacterium [11] certainly stimulated the growing of this area. Most of such synthetic molecules are based on porphyrins and metalloporphyrins [57]. Quinone groups are often used as electron-acceptors and excited-state quenchers, and they are separated from electron donors or chromophores via either

rigid or flexible chains [5, 7]]. In the past few years, transition metal complexes, especially Ru(II) and Re(I) based complexes, have been utilised to serve as light-harvesting groups or chromophores in the chromophore-quencher assemblies [5, 7].

There are a number of reasons for building and examining such artificially designed chromophore-quencher or donor-acceptor assemblies. First, the study of such artificial systems is an attempt towards a better understanding of the natural photosynthetic systems. In natural photosynthetic reaction centres, the factors which affect the electron transfer processes are very difficult to isolate and control. For instance, the charge-transport chains are structurally flexible proteins so that the distance between electron donor and acceptor is not well defined. Thus the distance effect on the electron transfer processes is not easy to examine and control [109, 110]. In synthetic systems, however, spatial control of the electron transfer process is less difficult [5].

It has been mentioned in Chapter I that very efficient charge separation and transfer processes are probably due to the "Marcus inverted region" effect [12]. Charge recombination and back electron transfer are virtually thermal processes, and they might be so exothermic that fall into the Marcus inverted region. In this region the more exothermic the

reaction, the slower the reaction rate. Therefore, these back reactions can not compete with the photoinduced forward reactions. Although the Marcus theory was published thirty years ago [155-156], clear supporting evidence was not obtained until 1982, when Closs, Miller and co-workers examined a series of artificially designed organic electron donor-acceptor molecules [13, 157]. In the past a few years transition metal complex based chromophores have been adopted into the similar synthetic systems. The strong absorbance in the near-UV and visible region and ^{3}MLCT based excited-states allow transition metal complexes to function as light-harvesting reagents and chromophores. Very recently, Meyer and co-workers have reported clear evidence for electron transfer in the Marcus inverted region in inorganic systems based on Ru(II) and Re(I) complexes [195].

Synthetic systems might also be able to mimic the functions of the natural photosynthetic systems. The increasing interest in the development of such artificial photosynthetic systems (or photochemical molecular devices) and optical electronic materials, has resulted in a rapidly growing area of "supramolecular photochemistry" [7, 196].

Although the majority of the work in this area has been associated with organic systems [196], the transition metal complexes based systems also received attention [5, 197]. In Meyer's group, several chromophore-quencher assemblies have

been studied. The chromophores are generally Ru(II) or Re(I) polypyridyl complex units, which are linked with organic electron-accepting or energy-accepting groups using spacially defined chains [5]. Elliot, Kelly and co-workers [107], also reported a series of studies on the electron transfer in tris(2,2'-bipyridine)-ruthenium(II) complexes linked with the diquart-based quenchers (diquart = N,N'-diquarternary-2,2'-bipyridium salt). The distance between chromophore and quencher is varied by changing the number of the bridging methylene units. Schanze and Sauer [108], prepared and characterised a series of molecules in which the Ru(II) polypyridyl chromophore is linked to a p-benzoquinone moity via a peptide bridge. They prepared the Ru(II)-peptide-hydroquinone assemblies first, and then chemically oxidised the hydroquinone to quinone. The distance between the Ru(II) centre and the quencher was varied by changing the length of the bridging peptide. The electron transfer from the Ru(II) chromophore (^{3}MLCT state) to the quinone group (oxidative quencher) was examined by steady-state and time-resolved luminescence experiments [108]. Due to the flexibility of the peptide bridge and interference of residual hydroquinone-containing Ru(II) complexes, multi-exponential emission decays were observed. Nevertheless, a sharp decrease in the electron-transfer rate was found when the peptide bridge was lengthened.

In this chapter, the synthesis, characterisation and the

physical properties of the $Ru(bpy)_2(II)$ complexes containing a ligand $HptH_2Q$ are described.

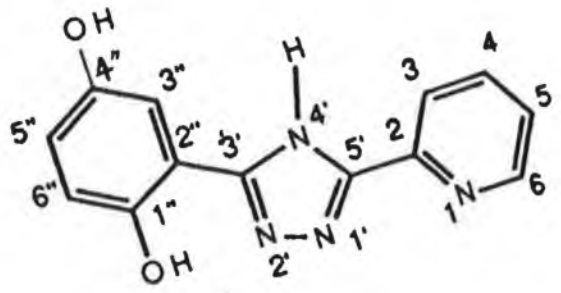

3-(1,4-dihydroxy-2-phenol)-5-(pyridin-2-yl)-1,2,4-triazole. ($HptH_2Q$)

The aim of this study is to prepare complexes which might show some properties similar to those found in photosynthetic reaction centres. As mentioned earlier, in photosynthetic reaction centres ubiquinone serves as an electron acceptor and its reduction process is coupled with protonation. On the other hand, it was reported by Plancherel et al. several years ago [198] that both hydroquinone and quinone can effectively quench the ^{3}MLCT state of $[Ru(bpy)_3]^{2+}$ via a bimolecular process. It might therefore be of interest to prepare a complex containing the $HptH_2Q$ ligand, as the hydroquinone unit in this ligand might serve as a quencher of the ^{3}MLCT state. For the ligand $HptH_2Q$, the electrochemistry shows that its π-accepting ability is weaker compared to bpy (see section VI.2.4). In the

$Ru(bpy)_2$ complex containing the $HptH_2Q$ ligand, any emission originated from the ^3MLCT state will be bpy-based. The quencher, hydroquinone, is attached on the pyridyltriazole ring so that it is directly linked to the $Ru(bpy)_2$ moiety. Possibly the hole transfer [7] between the the $Ru(bpy)_2(II)$ chromophore and the quencher, hydroquinone, might be observed. Moreover, as hydroquinone can be oxidised to quinone, the analogous Ru(II)-quinone complex can also be prepared. So it will be possible to examine whether the intramolecular electron transfer can take place in the complex containing the quinone unit. If electron transfer takes place from the $Ru(bpy)_2(II)$ chromophore, either through space or through the triazole bridging ring, to the quinone unit, then the process would be of some similarity to that observed in the photosynthetic reaction centres: the $Ru(bpy)_2$ unit functions as the "special pair" while the quinone unit functions as the ubiquinone group.

VI.2 Results and discussion.

VI.2.1 General consideration on the possible structures.

As described in Chapter II, refluxing $[Ru(bpy)_2Cl_2].2H_2O$ with the $HptH_2Q$ ligand in ethanol/H_2O (1:1) yields three products, as indicated by HPLC analysis. The three fractions have been separated by

semi-preparative HPLC techniques. The structures of these complexes are elucidated using ^{1}H-NMR and electrochemistry. Before going on with the detailed analysis, some possible structures can be considered.

For the first fraction, $[Ru(bpy)_2(ptH_2Q\text{-}1)]^+$, electrochemistry shows, apart from the redox couple of Ru(II/III), an extra redox couple corresponding to the hydroquinone unit (section VI.2.4). Thus, the possible structures for the first fraction have been reduced to two. This complex has to be bound via one nitrogen of the pyridine ring and another nitrogen (either $N^{1'}$ or $N^{4'}$) of the triazole ring (Fig. VI.1). If the Ru(II) centre is bound via $-H_2Q$ unit then the oxidation of this unit is expected to be absent (vide infra).

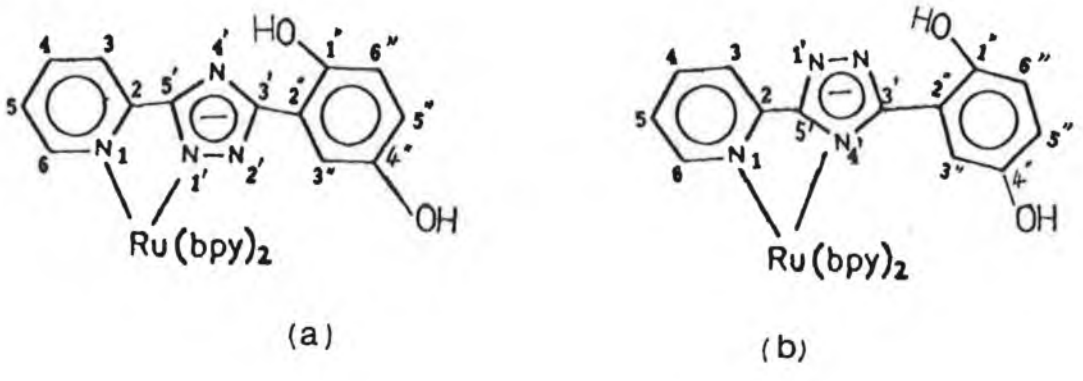

Fig. VI.1 Possible structures for $[Ru(bpy)_2(ptH_2Q\text{-}1)]^+$.

For the second fraction, $[Ru(bpy)_2(ptH_2Q\text{-}2)]^+$, the oxidation of hydroquinone unit is absent (Section VI.2.4). There are two possible reasons for the absence of the hydroquinone oxidation. First, the hydroquinone unit might be oxidised to quinone during the synthesis of the complex; second, the hydroquinone is bound to the Ru(II) centre.

The first reason can be ruled out based on the infra-red spectrum of this complex, where there is no -C=O band observed for uncoordinated quinones (1669 cm^{-1} [199]) or coordinated quinones (1600-1675 cm^{-1} [200]). Therefore, the hydroquinone is most likely involved in coordination.

Further more, in the third fraction, which was found to be a dinuclear complex according to electrochemistry, the hydroquinone oxidation is also absent (section VI.2.4). This further supports that in the second fraction, the hydroquinone unit is coordinated.

Therefore, $[Ru(bpy)_2(ptH_2Q\text{-}2)]^+$ is most likely bound via one of the nitrogens on the triazole ring (either $N^{2'}$ or $N^{4'}$) and the -OH group on the hydroquinone ring. Elemental analysis indicates that this complex carries a charge of 1+, suggesting that the $HptH_2Q$ ligand losts only one proton. The deprotonation may occur either on the triazole ring or on the hydroquinone. Thus, there are four possible structures for this complex (Fig. VI.2).

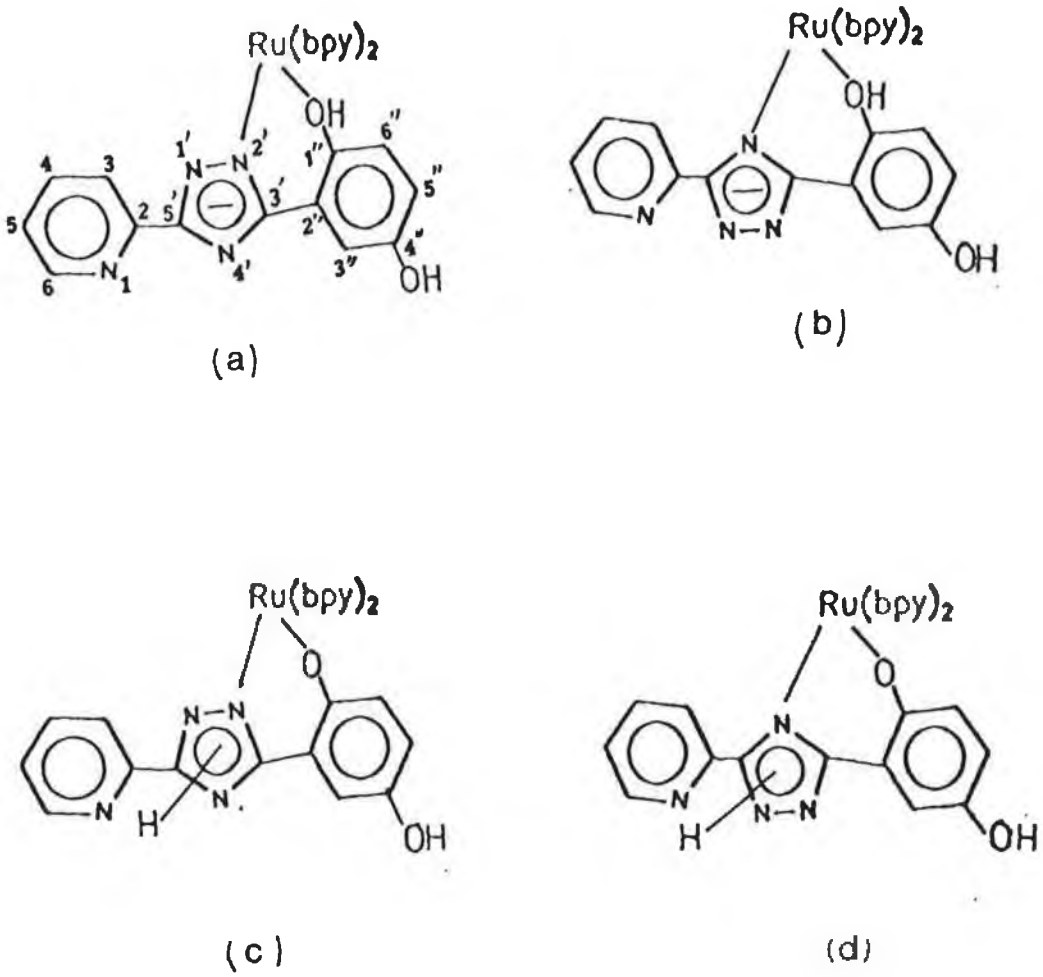

Fig. VI.2 Possible structures for the complex $[Ru(bpy)_2(ptH_2Q\text{-}2)]^+$.

The possible structures of the dinuclear complex will be discussed later when the coordination modes for the two mononuclear complexes are established.

For all three complexes, the structures are analysed using ^{1}H-NMR and electrochemistry, and will be described in the following sections.

VI.2.2 ^{1}H-NMR spectroscopy.

$[Ru(bpy)_2(ptH_2Q\text{-}1)]^+$.

The proton NMR spectrum for the first fraction is presented in Fig. VI.3. By using 2D-COSY techniques and comparing the data with those obtained on the free $HptH_2Q$ ligand, a complete assignment has been made. The chemical shifts have been listed in Table VI.1. The most important observation is that the H^6 proton of the pyridine ring of the ptH_2Q ligand is shifted about 1.20 ppm upfield, a behaviour typically observed for the coordinated pyridine rings [201-202] and caused by the diamagnetic anisotropic magnetic interaction of the H^6 proton with an adjacent bpy ligand. The significant chemical shift of the H^6 also suggests that the hydroquinone unit is not involved in coordination. The other protons on the coordinated ptH_2Q^- ligand are all shifted upfield, which is caused by the negative charge present on the triazole ring [89]. In this complex, all the chemical shifts for the bpy protons fall within the normal

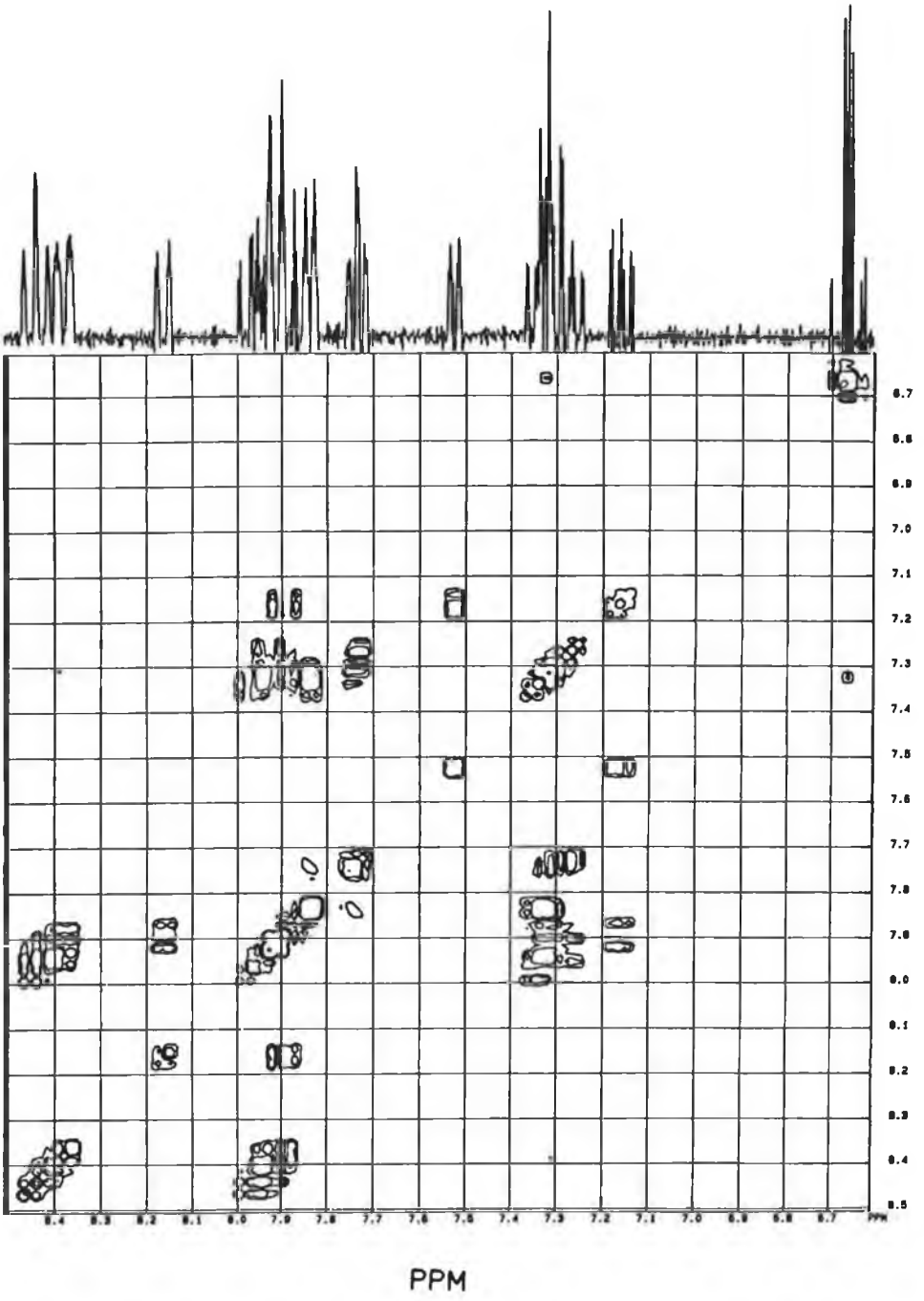

Fig. VI.3 2D-COSY ^{1}H-NMR spectrum of $[Ru(bpy)_2(ptH_2Q\text{-}1)]^+$ in d^6-acetone/D_2O at pH 7.50.

Table VI.1

^{1}H-NMR data for the ptH_2Q^- ligand in $Ru(bpy)_2$ complexes.

The data in parentheses are the difference between the chemical shifts of the coordinated and free ligand ($HptH_2Q$).

	Chemical Shifts (ppm)						Chemical Shifts (ppm)	
	H^3	H^4	H^5	H^6	$H^{3"}$	$H^{4"}$	$H^{5"}$	$H^{6"}$
$[Ru(bpy)_2(ptH_2Q\text{-}1)]^+$	8.16	7.90	7.16	7.52	7.32		6.22-6.70	
	(-0.10)	(-0.05)	(-0.31)	(-1.18)	(-0.32)		(-0.20/-0.16)	
$[Ru(bpy)_2(ptH_2Q\text{-}2)]^+$	8.18	7.90	7.33	8.44	7.90		7.15	7.51
	(-0.08)	(-0.05)	(-0.14)	(-0.26)	(0.26)		(0.33/0.29)	(0.69/0.85)
$[\{Ru(bpy)_2\}_2(ptH_2Q)]^{3+}$	6.60-6.63							
	(-1.61/-1.67)							
$[Ru(bpy)_2(ptOH)]^+$ [83]	8.24	8.04	7.32	7.78	7.98	6.78-6.84	7.15	6.78-6.84
	(+0.04)	(+0.01)	(-0.04)	(-0.97)	(-0.05)	(-0.26/-0.20)	-0.41	(-0.24/-0.28)
$[Ru(bpy)_2(bpt)]^+$ [80]	8.23	8.01	7.26	7.74	8.06	7.74	7.20	8.45
	(+0.08)	(+0.01)	(-0.26)	(-0.97)	(-0.09)	(-0.26)	(-0.32)	(-0.22)

The chemical shifts observed for bpy ligands in the mixed-chelate complexes are:

H^3: 8.3-8.8; H^4: 7.9-8.2; H^5: 7.2-7.6; H^6: 7.6-8.0.

region [80-81, 83-84, 88-89].

It is not straightforward to determine from the NMR spectrum whether the Ru(II) centre is bound via $N^{1'}$ or $N^{4'}$ of the triazole ring. To determine the coordination mode, the chemical shifts of the $-H_2Q$ protons in this complex are compared with those of the phenol protons in another similar complex $[Ru(bpy)_2(ptOH)]^+$ [83] (see Table VI.1).

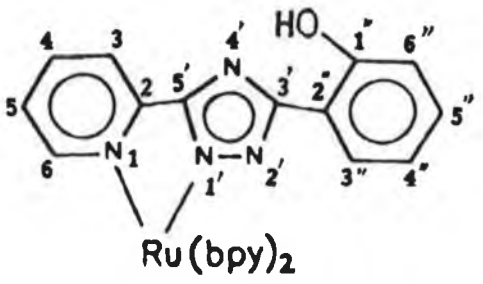

$[Ru(bpy)_2(ptOH)]^+$.

X-ray crystallographic data have shown that in $[Ru(bpy)_2(ptOH)]^+$ the Ru(II) centre is bound via $N^{1'}$ (for crystal structure see Fig. V.2). The absence of the $N^{4'}$ isomer can be explained by the steric hinderance to the phenol group if the Ru(II) is bound via $N^{4'}$.

It can be seen that the NMR data obtained for this complex are in general comparable with those of $[Ru(bpy)_2(ptH_2Q\text{-}1)]^+$

For $[Ru(bpy)_2(ptOH)]^+$, the $H^{5"}$ proton shows the largest shift (upfield 0.41 ppm) amongst the phenol protons. For $[Ru(bpy)_2(ptH_2Q\text{-}1)]^+$, the largest chemical shift observed amongst the $-H_2Q$ protons is $H^{3"}$ (upfield 0.32 ppm). If the Ru(II) centre is bound via $N^{4'}$, larger chemical shifts are expected for the protons on the phenyl ring or on the $-H_2Q$ ring. This is because if the $N^{4'}$ is directed to the Ru(II) centre the steric interaction between the phenol (or the hydroquinone) and the adjacent bpy is expected to be larger. Even for a much smaller methyl group in the complex $[Ru(bpy)_2(3,3'\text{-dimethyl-}5,5'\text{-bis-}1,2,4\text{-triazole})]^{2+}$, a downfield shift of 0.5 ppm is observed when the Ru(II) centre is bound via $N^{4'}$ [203]. The similarity in the chemical shifts observed between $[Ru(bpy)_2(ptH_2Q\text{-}1)]^+$ and $[Ru(bpy)_2(ptOH)]^+$ suggests that the Ru(II) centre is also bound via $N^{1'}$ in the former.

Another comparable complex is $[Ru(bpy)_2(bpt)]^+$ [80]. The crystal structure for this complex is shown in Fig. VI.4. (For the numbering of the atoms on the bpt^- ligand used here see Fig. I.4.)

X-ray crystallographic data reveal that in this complex the Ru(II) centre is also bound via $N^{1'}$ of the triazole ring. The $N^{4'}$ bound isomer is not obtained, again due to the steric reason. If the Ru(II) centre is bound via $N^{4'}$ the coordination environment will be too crowded because of the

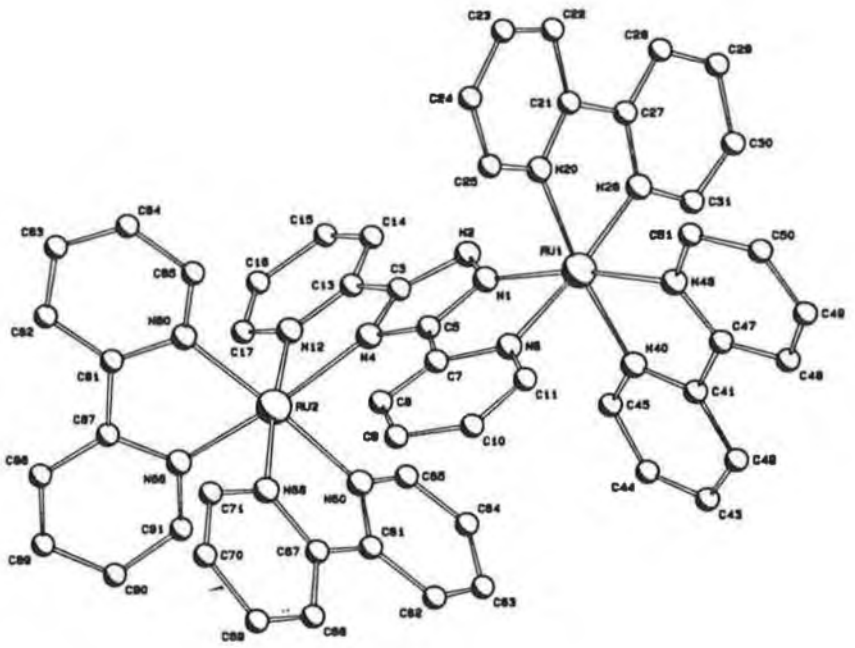

Fig. VI.4 PLUTO drawing of the $[\{Ru(bpy)_2\}_2(bpt)]^{3+}$ cation. All hydrogen atoms are omitted for reasons of clarity [80].

presence of the free pyridine ring (see Fig. VI.4). The NMR data obtained for this complexes are listed in Table VI.1. It is clear that the the chemical shifts for the protons on the free pyridine ring are comparable to those observed for the $-H_2Q$ protons. This suggests that the Ru(II) centre is also bound via $N^{1'}$ in the complex $[Ru(bpy)_2(ptH_2Q\text{-}1)]^+$.

Based on the above analysis, the proposed structure for the complex $[Ru(bpy)_2(ptH_2Q\text{-}1)]^+$ would be structure (a) as shown in Fig. VI.1.

$[Ru(bpy)_2(ptH_2Q\text{-}2)]^+$.

The proton NMR spectrum for this complex is shown in Fig. VI.5. The most direct evidence for the fact that in this complex a different coordination mode is obtained is the chemical shift of the H^6 proton of the ptH_2Q^- ligand.

The change in chemical shift for H^6 is much smaller (-0.26) compared to when the pyridine ring is coordinated (normally > 1 ppm [80-81, 83-84, 201-202]). Also downfield chemical shifts for $H^{3"}$, $H^{5"}$ and $H^{6"}$ are observed in this complex. The changes in chemical shifts are in the following order: $H^{3"}$ (0.26) < $H^{5"}$ (0.33-0.39) < $H^{6"}$ (0.69-0.85), which is expected for a coordinated $-H_2Q$ ring. The chemical shifts for the other protons on the pyridine ring of

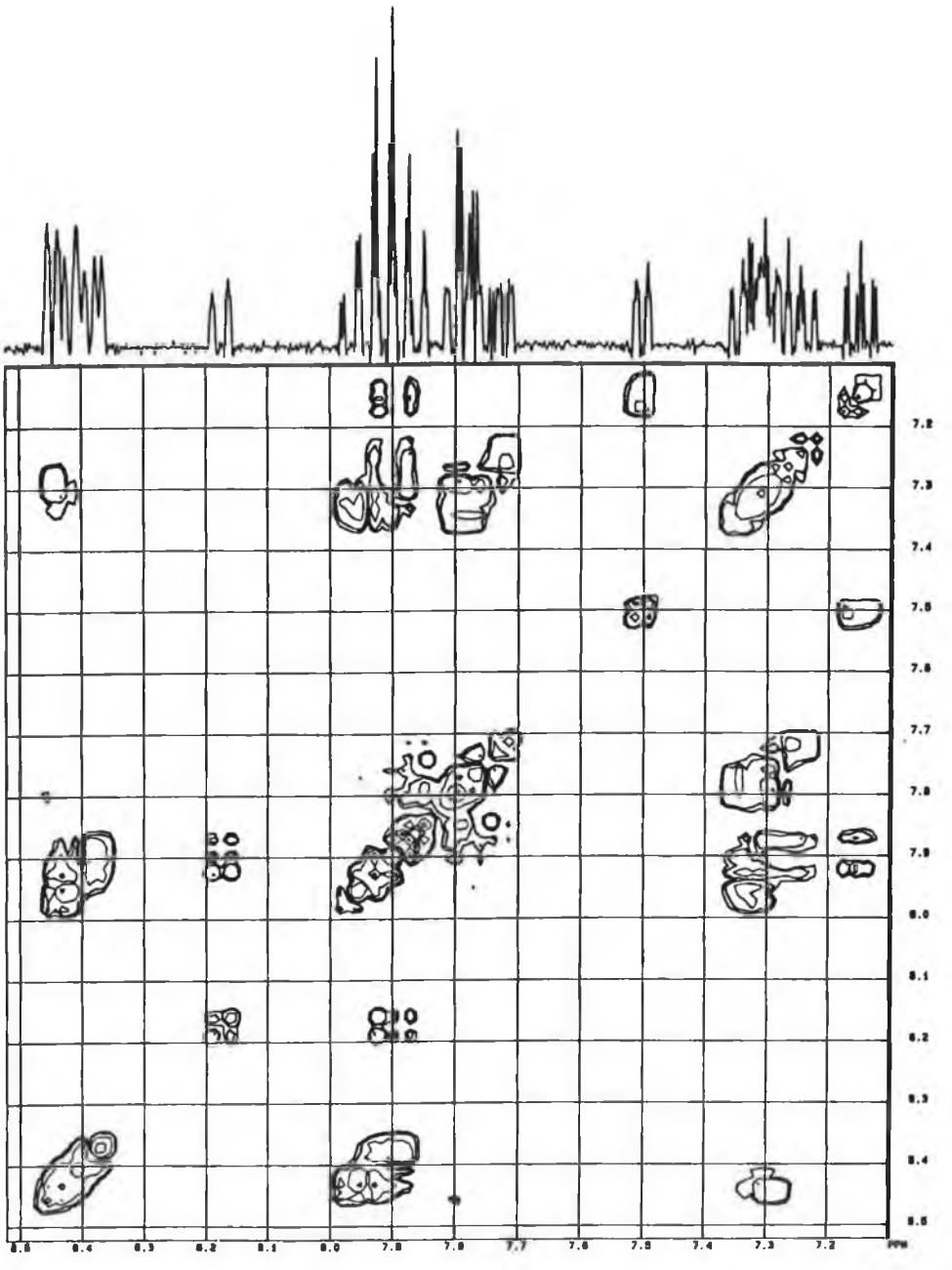

Fig. VI.5 2D-COSY ^{1}H-NMR spectrum of $[Ru(bpy)_2(ptH_2Q\text{-}2)]^+$ in d^6-acetone/D_2O at pH 6.85.

the coordinated ptH_2Q^- ligand are only slightly shifted upfield, which is due to the negative charge present on the triazole ring [89]. The chemical shifts for all the bpy protons fall within the expected region [80-81, 83-84].

The small change in chemical shift for the H^6 proton compared to the free ligand value strongly suggests that the pyridine ring is not coordinated, otherwise an upfield shift at least 1 ppm should be observed. On the other hand, the observed downfield shift for the protons of a coordinated $-H_2Q$ unit is expected, as the the electron density on this ring decreases upon coordination.

Now the next question is: is the Ru(II) centre coordinated via $N^{4'}$ or via $N^{2'}$ in this complex ? From the changes in chemical shift of the uncoordinated pyridine ring compared to the free ligand, it seems most likely the Ru(II) centre is bound via $N^{2'}$. If the Ru(II) centre is bound via $N^{4'}$, then the uncoordinated pyridine ring should feel the ring current of the adjacent bpy ligands more strongly, and the chemical shifts should be changed much more. As mentioned earlier, for $[Ru(bpy)_2(ptOH)]^+$ and $[Ru(bpy)_2(bpt)]^+$ only $N^{1'}$ bound isomers are obtained due to the steric

reason. For $[Ru(bpy)_2(ptH_2Q\text{-}2]^+$, it is also expected that the presence of the free pyridine ring hinders the formation of the $N^{4'}$ isomer. From Table V.1 it can be seen that the NMR data for this complex are comparable to those obtained on $[Ru(bpy)_2(bpt)]^+$ and $[Ru(bpy)_2(ptOH)]^+$. Especially, the chemical shifts for the protons on the pyridine ring are very similar between the coordinated bpt^- and ptH_2Q^- ligands. Thus, it is most likely in $[Ru(bpy)_2(ptH_2Q\text{-}2]^+$ the Ru(II) centre is bound via $N^{1'}$.

Another question is whether the triazole ring or the hydroquinone unit in this complex is deprotonated. The general upfield chemical shifts for the protons on the uncoordinated pyridine ring in this complex seem to suggest that the triazole ring is deprotonated [80-81, 83-84, 89]. Again it can be seen from the data on $[Ru(bpy)_2(bpt)]^+$, where the triazole ring is certainly deprotonated, that the resonance for the protons of the uncoordinated pyridine ring are all upfield shifted compared to those of the free bpt ligand (Table VI.1).

It is also known that for the deprotonation of H_2Q to HQ^- the pK_a is 9.85, while the pK_a for the deprotonation of HQ^- to Q^{2-} is 11.4 [198]. Preliminary acid-base chemistry has been carried out for the $HptH_2Q$ ligand. The first and second deprotonation steps for the $-H_2Q$ unit are

not resolved spectroscopically, but the deprotonation certainly occurs above pH 8 with an approximate pK_a value of 10. The pK_a for deprotonation of the triazole ring is found to be around 6. Therefore, the deprotonation of the triazole ring is expected to be easier, and coordination of the -OH group of the hydroquinone unit directly to the Ru(II) centre without deprotonation is possible. If this is true then another free -OH group is also likely protonated. In another similar complex $[Ru(bpy)_2(ptOH)]^+$, deprotonation of the HptOH ligand during the synthesis of the complex is also found to occur on the triazole ring and the phenol group remains protonated. For the free ligand HptOH, deprotonation of the triazole ring has a pK_a of 6 and that of the phenol group has pK_a of 11.8 [83].

Based on the above analysis, the proposed structure for $[Ru(bpy)_2(ptH_2Q\text{-}2)]^+$ would be structure (a) in Fig. VI.2. That the coordinated -OH group remains protonated in this complex is rather unusual, but several compounds in similar coordination fashions have also been reported [204-207].

$[\{Ru(bpy)_2\}_2(ptH_2Q)]^{3+}$.

The ^{1}H-NMR results obtained on the first and second fractions suggest that in none of the two mononuclear complexes the Ru(II) centre is bound via $N^{4'}$. Thus, as long as any one of the two mononuclear complexes is formed,

the second $Ru(bpy)_2$ moiety has to be bound via $N^{4'}$. Elemental analysis indicates that the complex carries a charge of 3+. Assuming the triazole ring is deprotonated while the hydroquine remains protonated, as established for $[Ru(bpy)_2(ptH_2Q\text{-}2)]^+$, then two coordination modes are possible for this dinuclear complex (Fig. VI.6). For each of

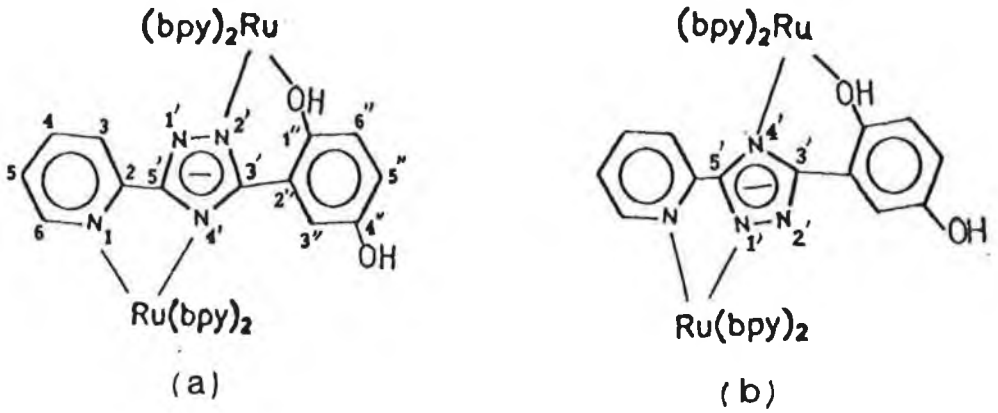

Fig. VI.6 Possible structure for $[\{Ru(bpy)_2(ptH_2Q)\}]^{3+}$.

the isomers, conformational isomers (or optical isomers) can also exist, although the optical isomers are not expected to complicate the NMR spectrum further [80]. The ^{1}H-NMR for this complex is presented in Fig. VI.7. Because of the possibility for the presence of both isomers, no unambiguous assignment can be made at this stage. Nevertheless, bpy protons can be found, of which the chemical shifts are comparable to another dinuclear complex $[\{Ru(bpy)_2\}_2(bpt)]^{3+}$ [80]. In addition, the two peaks

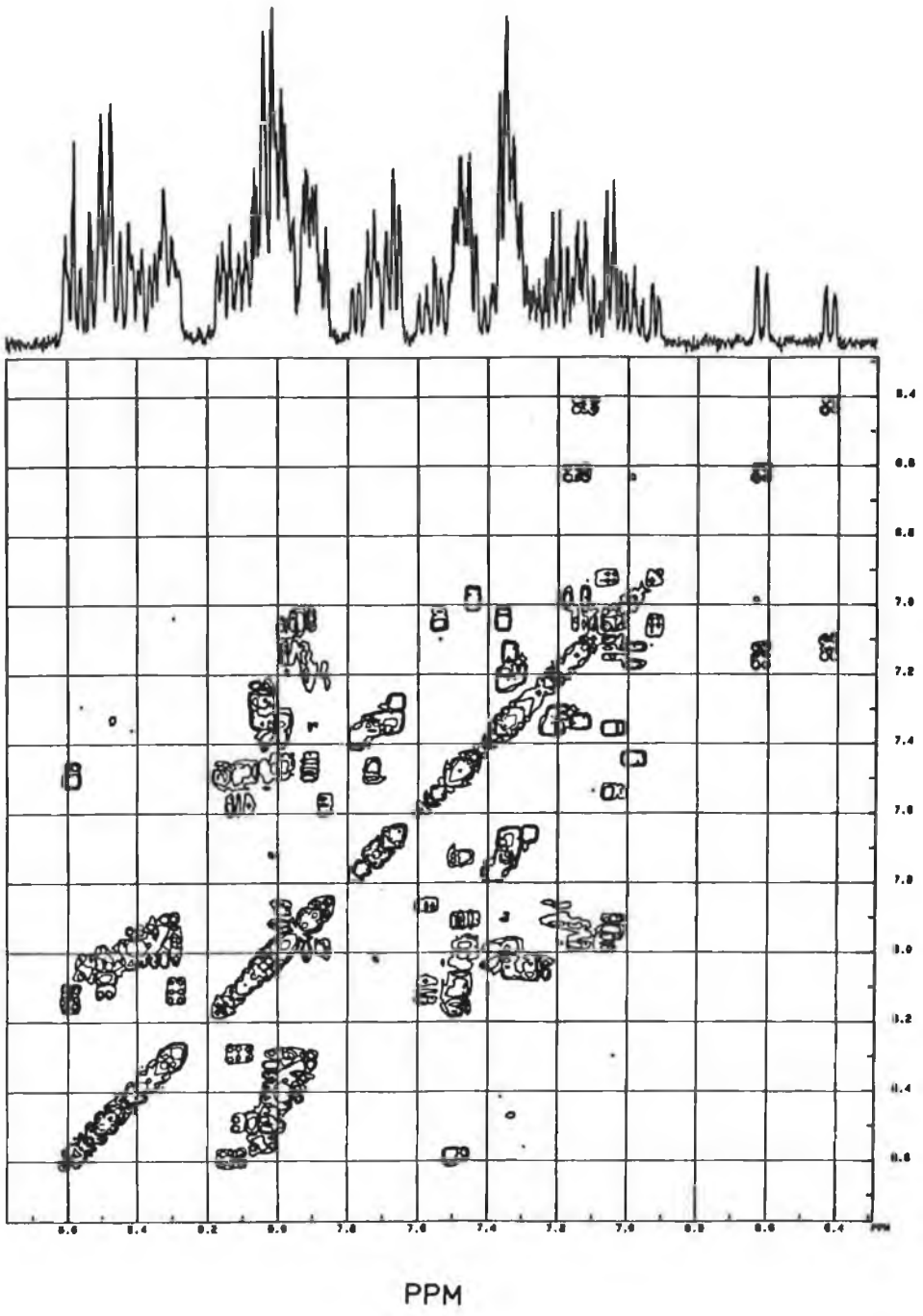

Fig. VI.7 2D-Cosy ^{1}H-NMR spectrum of $[\{Ru(bpy)_2\}_2(ptH_2Q]^{3+}$ in d^6-acetone.

(all doublet) at 6.62 and 6.42 ppm most likely represent the H^3 protons of the two conformational isomers [80]. The large changes in the chemical shift (-1.64 and -1.82) upon coordination of the ligand is due to that the H^3 is directed to the ajacent bpy ligand when $N^{4'}$ is coordinated. This effect is also observed for $[\{Ru(bpy)_2\}_2(bpt)]^{3+}$ [80].

VI.2.3 Electronic spectra.

UV-vis absorption spectra.

The UV-visible absorption and emission energies are listed in Table VI.2. The UV-vis absorption spectra for all three complexes are presented in Fig. VI.8. There are no significant differences in the lowest ^{1}MLCT absorption band between the two mononuclear complexes. In the deprotonated form, both complexes have ^{1}MLCT maxima at around 475 nm; while upon protonation of the triazole ring the absorption maxima shift to about 430 nm. The protonation of the ptH_2Q^- ligand causes a decrease in the σ-donating ability but an increase in π-accepting ability. The Ru(II) based t_{2g} levels are stabilised and the t_{2g}-^{1}MLCT gap is thus increased, which leads to the blue shift of the absorption maxima. The absorption maxima obtained on the two mononuclear complexes are comparable to those obtained for other related pyridyltriazole-containing $Ru(bpy)_2$(II) complexes (Table VI.2).

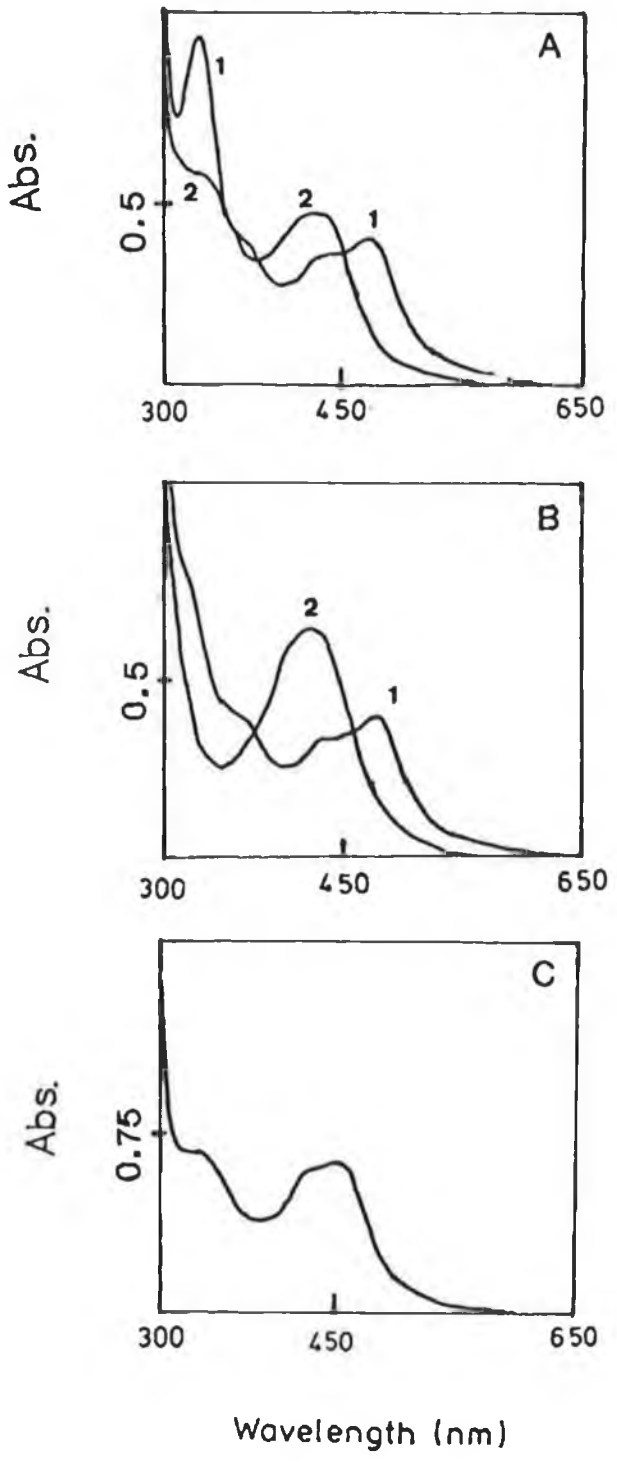

Fig. VI.8 UV-vis absorption spectrum for

A --- (1) $[Ru(bpy)_2(ptH_2Q\text{-}1)]^{+}$.

(2) $[Ru(bpy)_2(HptH_2Q\text{-}1)]^{2+}$.

B --- (1) $[Ru(bpy)_2(ptH_2Q\text{-}2)]^{+}$.

(2) $[Ru(bpy)_2(HptH_2Q\text{-}2)]^{2+}$.

C --- (3) $[\{Ru(bpy)_2\}_2(ptH_2Q\text{-}1)]^{3+}$.

Table VI.2

UV-visible and emission energies of the $Ru(bpy)_2$ complexes containing the $HptH_2Q$ ligand and some related compounds.

	abs.($10^{-4}\epsilon$)[a] λ_{max}, nm	E_{em}[a] 298 K, nm	E_{em}[b] 77 K, nm
$[Ru(bpy)_2(HptH_2Q\text{-}1)]^{2+}$	430	647	583
$[Ru(bpy)_2(ptH_2Q\text{-}1)]^{+}$	475(1.01)	678	622
$[Ru(bpy)_2(HptH_2Q\text{-}2)]^{2+}$	427	656	588
$[Ru(bpy)_2(ptH_2Q\text{-}2)]^{+}$	477(1.08)	682	614
$[\{Ru(bpy)_2\}_2(ptH_2Q)]^{3+}$	454	649	610
$HptH_2Q$	280, 310-330(sh.)		
ptH_2Q^- [c]	276, 310-330(sh.)		
$[Ru(bpy)_2(HptOH)]^{2+}$ [83]	435(1.31)	616	580
$[Ru(bpy)_2(ptOH)]^{+}$ [83]	463(1.05)	664	620
$[Ru(bpy)_2(Hptr\text{-}2)]^{2+}$	444(1.29)	611	577
$[Ru(bpy)_2(ptr\text{-}2)]^{+}$	484(1.10)	677	607
$[Ru(bpy)_2(Hbpt)]^{2+}$ [89]	429(1.56)		
$[Ru(bpy)_2(bpt)]^{+}$ [80]	475(1.13)	678	628
$[\{Ru(bpy)_2\}_2(bpt)]^{3+}$ [80]	453(2.26)	648	608

a. Measured in CH_3CH.

b. Measured in 4:1 ethanol/methanol.

c. Measured in Buffer at pH 7.

It is worth noting that around 330 nm, an very intense transition is observed for the complex $[Ru(bpy)_2(ptH_2Q\text{-}1)]^+$. When the triazole ring is protonated, this band decreases dramatically. In $[Ru(bpy)_2(ptH_2Q\text{-}2)]^+$, this band is not present. As mentioned earlier, in $[Ru(bpy)_2(ptH_2Q\text{-}2)]^+$, the hydroquinone group is bound to the Ru(II) centre. Thus, the uncoordinated $-H_2Q$ unit might be responsible for this intense π--->π^* electron transition in $[Ru(bpy)_2(ptH_2Q\text{-}2)]^+$.

The ^{1}MLCT maximum for the dinuclear complex $[\{Ru(bpy)_2\}_2(ptH_2Q)]^{3+}$ is around 450 nm, similar to that of $[\{Ru(bpt)_2\}_2(bpt)]^{3+}$ (Table VI.2). The blue shift of the MLCT band relative to the parent mononuclear complexes is due to the reduced electron density on the ptH_2Q^- ligand upon coordination to the two $Ru(bpy)_2$(II) units.

Emission spectra.

The emission energies for all three complexes are also listed in Table VI.2. These values are comparable to those of the other similar Ru(II) complexes (Table VI.2). For the two mononuclear complexes, the ^{3}MLCT emission maxima shift to higher energies in the protonated forms. The reason given for the blue shift of the absorption maxima upon protonation is also applicable here. There is no substantial difference

in peak shapes between the room temperature emission spectra. But slight differences are observed between the 77 K emission spectra of the two mononuclear complexes in the protonated form (Fig. VI.9). For $[Ru(bpy)_2(ptH_2Q\text{-}1)]^+$, vibrational structures are present in the spectra in both deprotonated and protonated forms. This behaviour is also observed for other Ru(II) similar pyridyltriazole complexes [88-89], and is attributed to the contribution of bpy-based vibrations in the relaxation of the ^{3}MLCT state [208-209]. The emission spectrum for the deprotonated complex $[Ru(bpy)_2(ptH_2Q\text{-}2)]^+$ has a similar shape as that for $[Ru(bpy)_2(ptH_2Q\text{-}1)]^+$; while for the protonated complex, $[Ru(bpy)_2(HptH_2Q\text{-}2)]^{2+}$, the spectrum does not show a resolved vibrational structure (Fig. VI.9). The different coordination environment for the two complexes is probably responsible for the difference in the emission spectra.

For the dinuclear complex, $[\{Ru(bpy)_2\}_2(ptH_2Q)]^{3+}$, the room temperature and 77 K emission spectra are presented in Fig. VI.10. The emission energies are comparable to those of another complex $[\{Ru(bpy)_2\}_2(bpt)]^{3+}$ (Table VI.2). The emission maxima of the dinuclear compounds are shifted to higher energies relative to their deprotonated parent mononuclear complexes. This is again caused by the reduced electron density of the bridging ligand when coordinated to two metal centres.

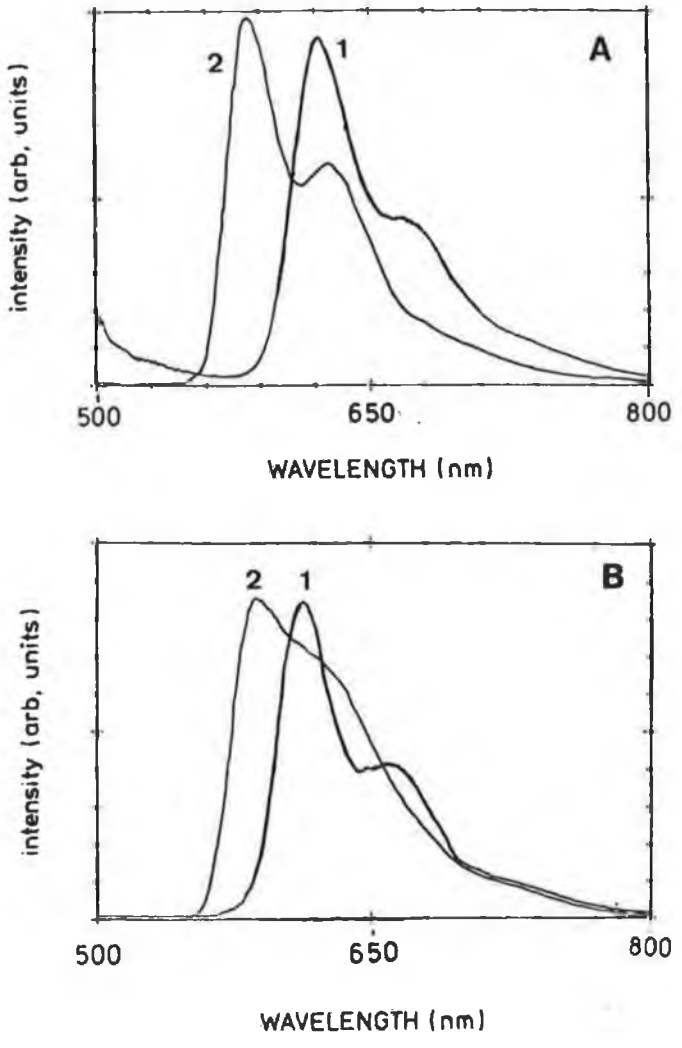

Fig. VI.9 77 K emission spectra measured in 4:1 ethanol/methanol.

A: 1. $[Ru(bpy)_2(ptH_2Q\text{-}1)]^+$.

2. $[Ru(bpy)_2(HptH_2Q\text{-}1)]^{2+}$.

B. 1. $[Ru(bpy)_2(ptH_2Q\text{-}2)]^+$.

2. $[Ru(bpy)_2(HptH_2Q\text{-}2)]^{2+}$.

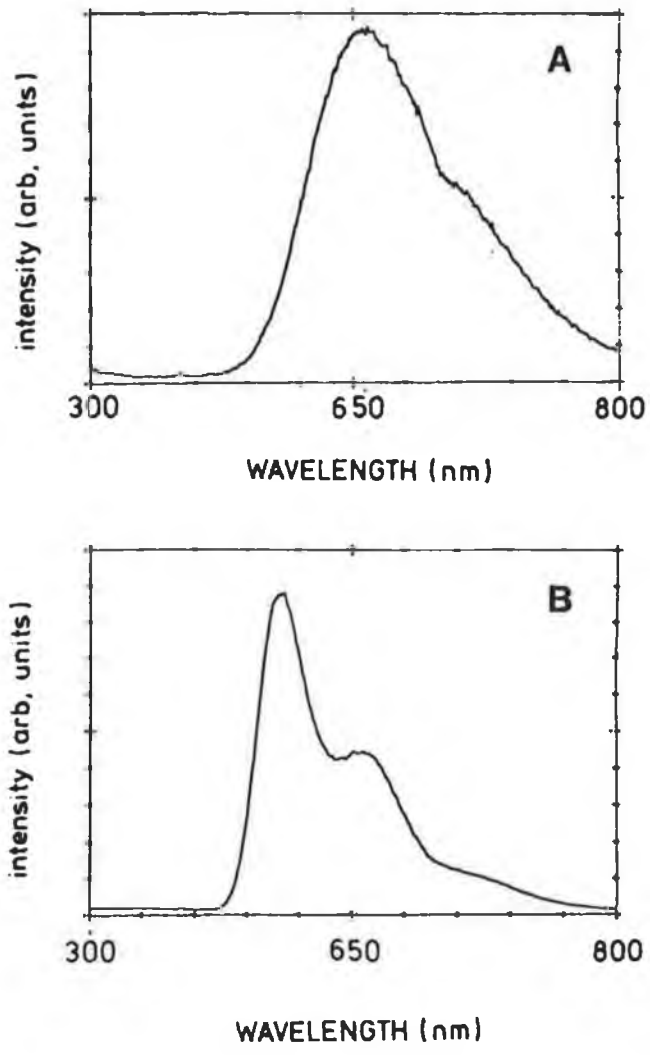

Fig. VI.10 Room temperature (CH_3CN) and 77 K (4:1 ethanol/methanol) emission spectra of $[\{Ru(bpy)_2\}_2(ptH_2Q)]^{3+}$.

VI.2.5 Electrochemical properties.

The electrochemical potentials for the complexes and for the free ligand $HptH_2Q$ are listed in Table VI.3.

The free $HptH_2Q$ ligand shows a quasi-reversible oxidation of the $-H_2Q$ unit. When extra acid is added into the solution the oxidation peak is shifted to a more positive potential. These redox potentials and the pH dependent behaviour are similar to those reported on other hydroquinones [197]. The reduction of the $HptH_2Q$ ligand shows a very broad and irreversible peak between -1.57 to -2.30 V.

In all three complexes, the irreversible reduction of the coordinated ptH_2Q^- (or $HptH_2Q$) does not occur until the potential reaches about -2.3 V. This suggests that the $HptH_2Q$ ligand is a weaker π-acceptor than bpy, as found for other pyridyltriazole ligands [88-89]. Thus in the three complexes the LUMO is bpy based, and the emission observed from these complexes most likely originates from bpy-based ^{3}MLCT states.

For the two mononuclear complexes, in both protonated and deprotonated forms, the Ru(II/III) oxidation potential is lower than that of $[Ru(bpy)_3]^{2+}$ (see Table VI.3). This is the result of the combination of the stronger σ-donating

Table VI.3

Electrochemical potentials of the $Ru(bpy)_2$ complexes containg the $HptH_2Q$ ligand.

	$E_{1/2}$, Volt vs. Ag/AgCl[a]		
	Ru(II/III)	H_2Q/Q	ligand based reduction
$[Ru(bpy)_2(HptH_2Q\text{-}1)]^{2+}$[f]	1.18(0.05)	0.64(0.72)	-1.51(0.06), -1.75(0.05), -2.3[b]
$[Ru(bpy)_2(ptH_2Q\text{-}1)]^{+}$	1.06[c], 1.25[d](0.07)	0.41(0.46)	-1.47(0.06), -1.71(0.06), -2.3[b]
$[Ru(bpy)_2(HptH_2Q\text{-}2)]^{2+}$	1.02(0.06)	absent	-1.49(0.07), -1.74(0.06), -2.3[b]
$[Ru(bpy)_2(ptH_2Q\text{-}2)]^{+}$	0.85(0.07), 0.99[e]	absent	-1.53(0.05), -1.74(0.05), -2.3[b]
	Ru(II)Ru(II)-Ru(II)Ru(III)		
$[\{Ru(bpy)_2\}_2(ptH_2Q)]^{3+}$	1.05(0.04)		-1.45(0.08), -1.69(0.15), -2.3[b]
	Ru(II)Ru(III)-Ru(III)Ru(III)		
	1.36(0.05)		
$HptH_2Q$		0.40(0.42)	-1.57 to -2.3
$HptH_2Q$[f]		0.60(0.32)	
$[Ru(bpy)_3]^{2+}$ [69]	1.26		-1.35, -1.55, 1.80

a. Measured by cyclic voltammetry in 0.1 M TEAP/CH_3CN. Scan rate 100 mV/sec. $E_{1/2} = (E_{pa} - E_{pc})/2$; data in parentheses are peak-to-peak separations $\Delta E = E_{pa} - E_{pc}$.

b. Irreverible.

c. No corresponding reductive peak observed; see text.

d. See text.

e. See text.

f. CF_3COOH was added to the electrolyte except for measuring ligand-based reductions.

and weaker π-accepting properties of the ptH_2Q^- (or $HptH_2Q$) ligand compared to bpy.

For $[Ru(bpy)_2(ptH_2Q\text{-}1)]^+$ and its protonated analogue, apart from the Ru(II/III) oxidation, another redox couple due to the $-H_2Q$ unit is clearly observed. This suggests that the hydroquinone is not bound to the Ru(II) centre but remains as a free unit. The electrochemical data are therefore consistent with the ^{1}H-NMR data. A very interesting observation is that after $-H_2Q$ oxidation, the complex is partially protonated. This is reflected by the two peaks corresponding to Ru(II/III) oxidations of both deprotonated and protonated species, respectively (see Table VI.3). This electrochemically induced proton transfer process will be discussed in detail in Chapter VII.

For $[Ru(bpy)_2(ptH_2Q\text{-}2)]^+$ and its protonated analogue, the most important observation is that the redox couple corresponding to the $-H_2Q$ unit is absent. This strongly suggests that the hydroquinone group is bound to the Ru(II) centre, as also suggested by the ^{1}H-NMR data. It will be seen later that in the dinuclear complex $[\{Ru(bpy)_2\}_2(ptH_2Q)]^{3+}$, where the $-H_2Q$ unit has to be bound to the Ru(II) centre, the redox couple corresponding to the $-H_2Q$ unit is also absent. This further supports that in $[Ru(bpy)_2(ptH_2Q\text{-}2)]^+$ the hydroquinone group is involved in coordination.

The cyclic voltammograms of $[Ru(bpy)_2(ptH_2Q\text{-}2]^+$ and its protonated analogues are presented in Fig. VI.11. For the protonated complex, only one clean redox couple coorsponding to Ru(II/III) was observed (Fig. VI.11B). For the deprotonated complex (Fig. VI.11A), however, the process is less clear. During oxidative scan, only one peak was detected at 0.88 V, which can be assigned to Ru(II) ---> Ru(III) oxidation. During the reductive scan, two peaks, at 0.81 V and 0.99 V repectively, were observed. The peak at 0.81 V is corresponding to Ru(III) ---> Ru(II) reduction. Another peak at 0.99 V, is at present not understood.

It can been seen from Fig. VI.11B that the reductive peak for the protonated complex is also at 0.99 V. This might suggest that for the deprotonated complex, after Ru(II) ---> Ru(III) oxidation, protonation of the triazole ring takes place. A possible proton source would be the coordinated -OH group. After Ru(II) centre is oxidised to Ru(III), the -OH group will denote more electron density to the Ru(III) centre thus becomes more acidic. The coordinated -OH group is then deprotonated and the released proton subsequently protonates the triazole ring. If this is true the the process would be considered as an electrochemically induced proton transfer process. However, this assumption is challenged by the fact that if the -OH group is deprotonated the increased -donor ability of this group should lead to a Ru(III) ---> Ru(II) reduction more difficult. In other words, it should occur at

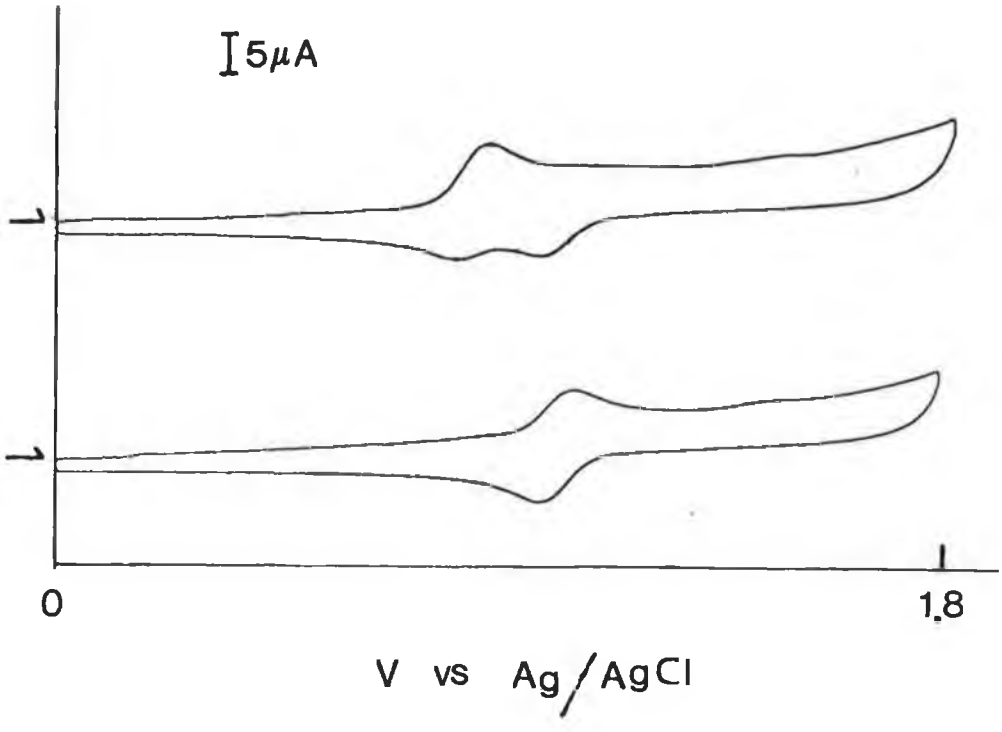

Fig. VI.11 Cyclic voltammogram of the complex $[Ru(bpy)_2(ptH_2Q\text{-}2)]^+$ (A), and of its protonated form $[Ru(bpy)_2(HptH_2Q\text{-}2)]^{2+}$ (B) in 0.1 M TEAP/CH_3CN. Scan rate 100 mV/sec.

a potential at least less positive than 0.99 V, where the Ru(III) ---> Ru(II) for $[Ru(bpy)_2(HptH_2\text{-}2)]^{2+}$ occurs (Fig. VI.11B).

In a separate experiment, 10% strong base diethylamine was added into a solution containing the deprotonated complex $[Ru(bpy)_2(ptH_2Q\text{-}2)]^{+}$. In this strong basic solution it is expected that the -OH group should be deprotonated. But this causes no changes in the absorption spectrum of the complex. This may suggest that even when the -OH group is deprotonated, the t_{2g} level of the ruthenium centre is not affected significantly. Thus the reductive peak at 0.99 V observed for $[Ru(bpy)_2(ptH_2Q\text{-}2)]^{+}$ might be due to the species of which the triazole ring is protonated and the coordinated -OH group is deprotonated. Further studies are certainly needed for understanding this electrochemical process.

It is also important to note that for the protonated complex, $[Ru(bpy)_2(HptH_2Q\text{-}2)]^{2+}$, the Ru(II/III) oxidation potential occurs at 1.02 V, about 160 mV lower than that of $[Ru(bpy)_2(HptH_2Q\text{-}1)]^{2+}$ (1.18 V). From the structures (Fig. VI.1a and Fig. VI.2a) it is clear that for the two complexes the $N^{1'}$ and $N^{2'}$ are essentially equivalent. Thus the coordinated pyridine ring and $-H_2Q$ unit in the two complexes respectively are probably responsible for the difference in the electrochemical potentials. The proton NMR

data seem to suggest that in $[Ru(bpy)_2(HptH_2Q\text{-}2)]^{2+}$ the coordinated -OH is protonated, so that the σ-donating ability of this group is expected to be similar to the nitrogen on the pyridine ring. The low Ru(II/II) oxidation potential of $[Ru(bpy)_2(HptH_2Q\text{-}2)]^{2+}$ might be due to the decreased π-accepting ability when the complex is bound in such a coordination fashion.

For the dinuclear complex, $[\{Ru(bpy)_2\}_2(ptH_2Q)]^{3+}$, cyclic voltammetry shows two clearly resolved redox couples corresponding to Ru(II)Ru(II) ---> Ru(III)Ru(II) (1.06 V) and Ru(III)Ru(II) ---> Ru(III)Ru(III) (1.36 V), repectively. The first and second oxidation potentials are separated by 300 mV. (Fig. VII.12). This result is very similar to that of $[\{Ru(bpy)_2\}_2(bpt)]^{3+}$, where a separation of 300 mV between the two oxidations is also observed [80].

There are three possible reasons for the separation of the oxidation potentials for the two metal centres. First, the coordination environment is not equivalent for the two Ru(II) centres in the dinuclear complexes. The Ru(II) centres are coordinated via the different nitrogens on the triazole ring; furthermore the pyridine and $-H_2Q$ units are quite different coordinating groups. Second, electrostatic effects, arise as soon as the first metal centre is oxidised. The increased positive charge built up within the complex will cause the oxidation of the second Ru(II) centre to be more difficult.

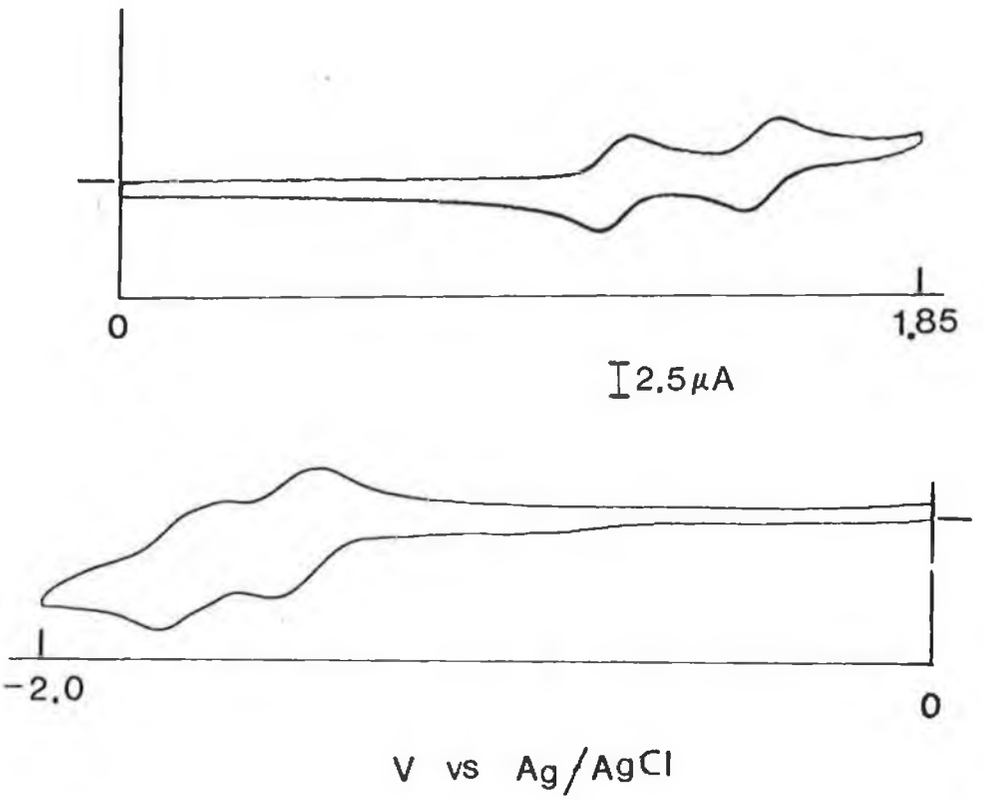

Fig. VI.12 Cyclic voltammograms of $[\{Ru(bpy)_2\}_2(ptH_2Q)]$ in 0.1 M TEAP/CH_3CN.

Finally, the electron density of the second Ru(II) centre might be more delocalised after the first Ru(II) centre is oxidised. Therefore the t_{2g} level of the second Ru(II) centre is stabilised and oxidation becomes more difficult. However, such a delocalisation effect alone is probably too small to account for the large separation (300 mV) between the two oxidation potentials [210].

The first oxidation potential of the dinuclear complex is similar to that of $[Ru(bpy)_2(ptH_2Q\text{-}1)]^+$ while about 300 mV higher than that of $[Ru(bpy)_2(ptH_2Q\text{-}2)]^+$. In general, coordination of the bridging triazole ligand to the Ru(II) centre leads to the decrease of the electron density on the triazole ring. The oxidation potential is thus expected to be higher compared to the corresonding mononuclear complex [210]. Therefore the first oxidation potential in the dinuclear complex is probably corresponding to the $Ru(bpy)_2$(II) unit where the triazole and hydroquinone group is bound to Ru(II) centre in structure (b) (Fig. VI.6). The very clean oxidation potentials observed for the dinuclear complex (Fig. VI.12) suggest that most likely only one coordination isomer is formed. The presence of the optical isomers can however not be ruled out, as they normally do not affect the redox properties to a large extent [89].

No evidence of the oxidation of the hydroquinone group is

detected. This supports that in the complex $[Ru(bpy)_2(ptH_2Q\text{-}2)]^+$ the Ru(II) center is indeed bound to the hydroquinone group.

The two resolved ligand-based reductions, in comparison with the mononuclear complexes, can be assigned as bpy-based (Fig. VI.12). They are not split, although the peaks are rather broad. This strongly suggests that the two $Ru(bpy)_2$(II) units have the similar ^{3}MLCT level. The last reduction peak at -2.3 V, which is irreversible, is again explained by the reduction of the ptH_2Q^- ligand. This suggests that the LUMO in this complex is bpy based, and the ptH_2Q^- serves as an bridging and spectator ligand. Thus, the emission observed from this complex most likely originates from bpy-based ^{3}MLCT states.

VI.2.4 Excited-state lifetimes.

The excited-state lifetime values for all three complexes are listed in Table VI.4. Single exponential decay was observed for all the complexes. At 77 K, the two mononuclear complexes show the common excited-state behaviour which is governed by the energy gap law [52]. The protonated complexes are longer lived, due to their higher emission energies. At room temperature, however, the excited-state behaviour is less clear.

Table VI.4

Excited-state lifetimes of the $Ru(bpy)_2$ complexes containing the $HptH_2Q$ ligand and some related compounds.

	$\tau_{298\ K}$[a] ns	$\tau_{77\ K}$[b] ns
$[Ru(bpy)_2(HptH_2Q\text{-}1)]^{2+c}$	9	4221
$[Ru(bpy)_2(ptH_2Q\text{-}1)]^{+}$	140	2716
$[Ru(bpy)_2(HptH_2Q\text{-}2)]^{2+c}$	351	4164
$[Ru(bpy)_2(ptH_2Q\text{-}2)]^{+}$	152	2991
$[\{Ru(bpy)_2\}_2(ptH_2Q)]^{3+}$	91	4102
$[Ru(bpy)_2(HptOH)]^{2+c}$	10	4847
$[Ru(bpy)_2(ptOH)]^{+}$	163	2823
$[Ru(bpy)_2(Hptr\text{-}2)]^{2+c}$	5	3635
$[Ru(bpy)_2(ptr\text{-}2)]^{+}$	145	2436
$[Ru(bpy)_2(bpt)]^{+}$ [82]	160	2800
$[\{Ru(bpy)_2\}_2(bpt)]^{3+}$ [82]	100	3600

a. Measured in CH_3CN. N_2 degassed for 10 min. before each measurement.

b. Measured in 4:1 ethanol/methanol.

c. Protonation is ensured by adding CF_3COOH to the solutions.

For $[Ru(bpy)_2(ptH_2Q\text{-}1)]^+$, the emission lifetime is about 140 ns in CH_3CN. This value is very similar to those observed for other related mononuclear complexes (Table VI.3). This observation suggests that the intramolecular quenching of the ^{3}MLCT state by the hydroquinone group is at best very inefficient. The possible reasons for the lack of the reductive quenching might be: 1) the rate of the back electron transfer process is comparable to that of the forward process; 2) the negative charge present on the triazole ring hinders the electron migration (hole transfer) from the hydroquinone unit to the Ru^{III} centre (the ^{3}MLCT state is bpy based and the electron excited from the Ru(II) centre is localised on one of the bpy ligand so that the Ru(II) becomes virtually oxidised to Ru(III) in the excited state [45].)

When the triazole ring is protonated, the lifetime is decreased to less than 10 ns, but this cannot be taken as direct evidence that reductive quenching is taking place. Protonation of the complex will reduce the ^{3}MLCT - ^{3}MC gap, and as a result at room temperature the ^{3}MC state becomes much easier to populate thermally. This will also lead to a decrease in the emission lifetime, as already found for other related pyridyltriazole-containing complexes (Chapter IV and V).

For $[Ru(bpy)_2(ptH_2Q\text{-}2)]^+$, a remarkable observation is

that at room temperature the emission lifetime is increased upon protonation. The electronic spectra and energies of this complex are similar to those of $[Ru(bpy)_2(ptH_2Q\text{-}1)]^+$, and this remains true when both complexes are protonated. It should be noted in $[Ru(bpy)_2(ptH_2Q\text{-}2)]^+$ the Ru(II) centre is bound via the hydroquinone unit, of which the coordination environment is quite different compared to $[Ru(bpy)_2(ptH_2Q\text{-}1)]^+$. But how this coordination environment affects the excited-state properties in this complex is not understood at this stage, and more detailed studies including temperature dependent lifetime measurements are needed to for such unique excited-state behaviour.

For the dinuclear complex, $[\{Ru(bpy)_2\}_2(ptH_2Q)]^{3+}$, the emission lifetimes both at room temperature and at 77 K are similar to those for $[\{Ru(bpy)_2\}_2(bpt)]^{3+}$ (see Table VI.4). The room temperature value, 100 ns, is lower than that observed for the two parent mononuclear complexes (Table VI.4). This might result from the decreased o-donating ability of the ptH_2Q^- ligand when bound to the two Ru(II) centres, as a consequence the ^3MC level is lowered and easier to populate at room temperature from the emitting ^3MLCT state [45].

VI.2.6 Temperature dependent emission lifetime measurements and photostability of the complex $[Ru(bpy)_2(ptH_2Q\text{-}1)]^+$.

The temperature dependence of the emission lifetime for the complex $[Ru(bpy)_2(ptH_2Q\text{-}1)]^+$ and for its protonated form are presented in Fig. VI.13.

The protonated complex shows a dramatic decrease of the emission lifetime when the temperature exceeds 200 K. For the deprotonated complex, the temperature dependence of the emission lifetimes is much smaller. The emission decays can be satisfactorily fit as single exponential in the whole temperature range examined. The calculated kinetic and thermodynamic data using eq. IV.4 [$1/\tau = k_0 + k'(-E_a/RT)$] for both protonated and deprotonated forms are listed in Table VI.5.

For the deprotonated complex, a small activation energy (435 cm^{-1}) and small prefactor of 1.1×10^8 were found. These are values characteristic for the thermal activation of the MLCT states at slightly higher energy which are largely singlet in character [45]. Complexes showing this type behaviour are mostly photoinert. In Chapter IV, it has been described that the two isomers of $[Ru(bpy)_2(ptr)]^+$ have small activation paramaters, and they are indeed photochemically stable.

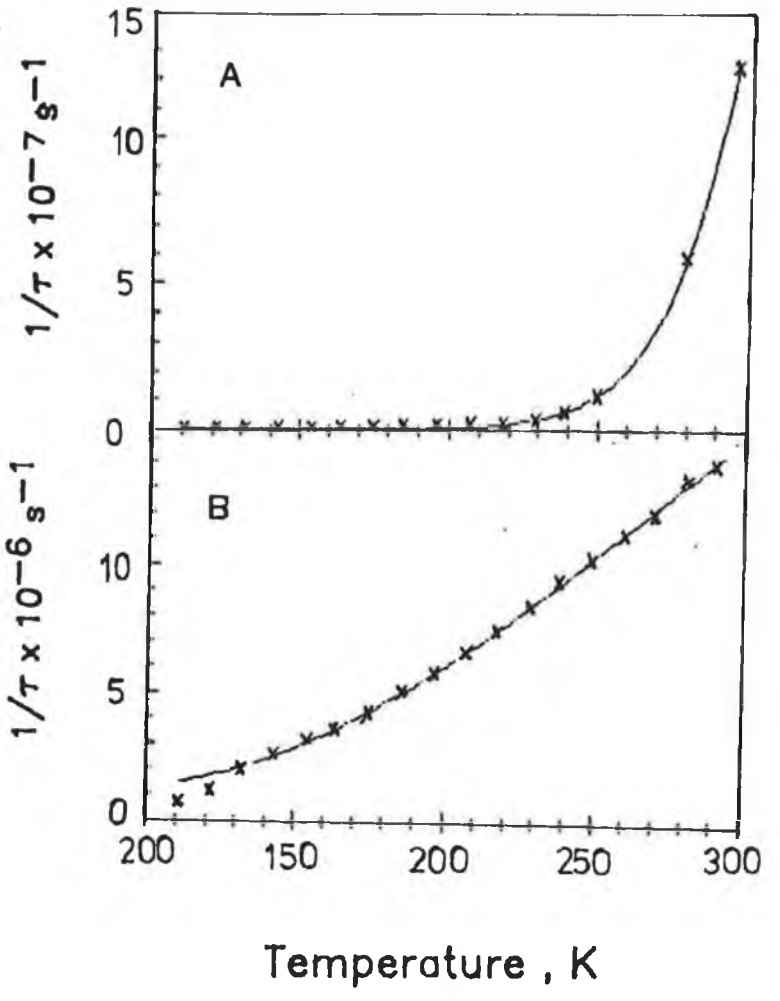

Fig. VI.13 Emission lifetime as a function of temperature in 4:1 ethanol/methanol.

A --- $[Ru(bpy)_2(HptH_2Q\text{-}1)]^{2+}$.

B --- $[Ru(bpy)_2(ptH_2Q\text{-}1)]^{+}$.

Note the different scale for $1/\tau$ in A and B.

Table VI.5 Activation parameters from the temperature dependent emission lifetime measurements.[a,b]

	k_0, s^{-1}	k', s^{-1}	E_a, cm^{-1}
$[Ru(bpy)_2(HptH_2Q\text{-}1)]^{2+}$	$5.4x10^5$	$4.4x10^{13}$	2638
$[Ru(bpy)_2(ptH_2Q\text{-}1)]^{+}$	$1.1x10^6$	$1.1x10^8$	435
$[Ru(bpy)_2(Hptr\text{-}4)]^{2+}$	$6.1x10^6$	$9.2x10^{13}$	2860
$[Ru(bpy)_2(ptr\text{-}4)]^{+}$	$1.6x10^6$	$3.1x10^7$	600
$[Ru(bpy)_2(Hptr\text{-}2)]^{2+}$	$1.6x10^6$	$6.0x10^{10}$	1710
$[Ru(bpy)_2(ptr\text{-}2)]^{+}$	$1.7x10^6$	$4.7x10^7$	550

a. Measured in 4:1 ethanol/methanol. Protonation and deprotonation were ensured by adding CF_3COOH and Et_2NH (~2%) to the solution.

b. Activation parameters are obtained by fitting the emission lifetimes into eq. IV.4.

For $[Ru(bpy)_2(ptH_2Q\text{-}1)]^+$, preliminary photolysis in 3mM TBAB/CH_2Cl_2 has shown that the complex is much more stable than $[Ru(bpy)_3]^{2+}$ but less stable than the two isomers of $[Ru(bpy)_2(ptr)]^+$. Irradiation for three hours yields less than 20% decomposition of the starting material. Under the same condition, the photosubstitutional reaction for $[Ru(bpy)_3]^{2+}$goes to completion within 30 minutes. The activation parameters and photochemical behaviour for this complex are similar to the other Ru(II) diimine complexes such as those reported by Balzani, Zelewsky and co-workers [56] and Meyer and co-workers [61].

As expected based on its strong temperature dependence on the emission lifetime, the protonated complex, $[Ru(bpy)_2(HptH_2Q\text{-}1)]^{2+}$, is photochemically labile, and the photosubstitutional reaction rate is comparable to $[Ru(bpy)_3]^{2+}$.

VI.2.7 Emission spectroelectrochemistry of the complex $[Ru(bpy)_2(ptH_2Q\text{-}1)]^+$.

One of the interesting features of the complex $[Ru(bpy)_2(ptH_2Q\text{-}1)]^+$ is that the hydroquinone unit can be oxidised to quinone before the Ru(II) center is oxidised. Therefore, it is possible to prepare the complex containing the quinone group in-situ by fixed-potential electrolysis, and then measure the emission lifetimes. As mentioned

earlier, the hydroquinone unit does not quench the ^{3}MLCT state very efficiently in this complex. It would be interesting to see whether an oxidative quenching of the bpy-based ^{3}MLCT emission can be observed after the hydroquinone unit is oxidised to the quinone.

As mentioned in the Introduction (section VI.1), Schanze and Sauer have examined the intramolecular quenching of the ^{3}MLCT emission of the Ru(II) trisdiimine complexes linked with the quinone group via peptide chains. The quinone group serves as an effective oxidative quencher and electron transfer from photoexcited Ru(II) center to the quinone are through the peptide chains. Also, in a recent study [136], it is found that for a dinuclear complex $[Ru(bpy)_2(bpt)Os(bpy)_2]^{3+}$, effective energy transfer and charge transfer are been observed between the two metal centers. The electron- or energy-transfer pathway is best explained as via the bridging bpt^- ligand. Due to the weaker π-accepting ability of the bpt^- ligand relative to bpy, the energy or excited electron are not trapped by the triazole ring during migration [136]. Based on these observations, it is expected that similar intramolecular electron transfer would be observed for the quinone-containing complex.

The emission lifetime as a function of the electrochemical potential has been measured in 0.1 M TBAP/CH_3CN. The

results are presented in Table VI.6. It is clear that, along with the increase of the applied potential, a double exponential decay behaviour was observed. The long component, with a lifetime of around 70 ns, corresponds to the unquenched hydroquinone-containg complex. The short component, unfortunately, can not be directly attributed to a quenching process. This is because as soon as the hydroquinone unit is oxidised, the released proton in turn protonates the negatively charged triazole ring (see section VI.2.4 and Chapter VII). The protonation of the ptH_2Q^- ligand also leads to the decrease in the emission lifetime of this complex due to the reduced ^{3}MLCT - ^{3}MC gap. Therefore, the possible oxidative quenching of the ^{3}MLCT state by the quinone group is obscared by the protonation effect. It can also be seen from Table VI.6 that the spectroelectrochemical process is reversible within this potential range. Thus, the elctrochemically formed quinone group can be re-reduced during the reduction process. This implies that the protonated triazole ring "returns" the proton taken during the reduction process ! This behaviour is even more clearly observed in the UV-vis spectroelectrochemistry, and will be discussed further in Chapter VII.

Further studies using faster spectroscopical techniques (e.g. time-resolved emission spectroscopy on the picosecond scale)

Table VI.6 Emission lifetimes as a function of electrochemical potential for the complex $[Ru(bpy)_2(ptH_2Q\text{-}1)]^+$.[a]

potential[b] (V vs. Ag/AgCl)	lifetime[c] τ_1, ns	τ_2, ns
oxidation:		
none	62	
0.4	62	
0.45	62	
0.5	16 (6544)	68 (25659)
0.55	11 (10607)	70 (20688)
0.6	10 (14163)	71 (15561)
0.7	7 (13873)	75 (14574)
Reduction (reversed process):		
0.5	8 (12950)	76 (12004)
0.3	9 (15699)	74 (12501)
0.2	9 (8489)	69 (21910)
0.1	30 (9237)	74 (21495)
0.0	63	

a. Measured in 0.1 M TEAP/CH_3CN.

b. Lifetimes were measured after holding each potential for 20 min.

c. Data in parentheses are prefactors for each components.

are needed to differenciate the quenching process and protonation effect. The direct observation of an oxidative quenching of the ^{3}MLCT state by the quinone group might alternatively be achieved by synthetic modification of the ptH_2Q^- ligand. For instance, by adding a methyl group onto the triazole ring so that protonation can be eliminated.

VI.3 Concluding remarks.

The three products obtained from synthesis have been separated and isolated using HPLC techniques. Elemental analysis, ^{1}H-NMR, and electrochemistry reveal that the first and second fractions are mononuclear species while the third fraction is a dinuclear complex.

For the first fraction, $[Ru(bpy)_2(ptH_2Q\text{-}1)]^+$, ^{1}H-NMR and electrochemistry provide clear evidence that the Ru(II) center is bound via the pyridine ring and the $N^{1'}$ on the triazole ring.

For the second fraction, $[Ru(bpy)_2(ptH_2Q\text{-}2)]^+$, ^{1}H-NMR and electrochemistry suggest that the Ru(II) center is bound via the hydroquinone unit and the $N^{2'}$ on the triazole ring. Although definite conclusions can not be drawn at this stage, available experimental evidence seems to favour the coordination fashion where the -OH group remains protonated when bound to the Ru(II) center.

The excited-state lifetime observed for $[Ru(bpy)_2(ptH_2Q\text{-}1)]^+$ is comparable to other similar complexes such as $[Ru(bpy)_2(ptOH)]^+$ and the two isomers of $[Ru(bpy)_2(ptr)]^+$. This suggests that the intramolecular reductive quenching by the hydroquinone unit via hole transfer is at best inefficient in this complex. The analogous quinone-containing complex can be prepared in-situ electrochemically. However due to the intervening of the electrochemically induced proton transfer process, the oxidative quenching of the ^{3}MLCT state by the quinone group in this complex can not be confirmed.

For the complex $[Ru(bpy)_2(ptH_2Q\text{-}2)]^+$, where the hydroquinone group is coordinated to the Ru(II) center, the most interesting feature is that when the triazole ring is protonated the emission lifetime is increased. The Ru(II/III) oxidation potential of the protonated form is significantly lower than that of $[Ru(bpy)_2(HptH_2Q\text{-}1)]^+$. These properties might result from the unusual coordination mode of this complex.

For the dinuclear complex, $[\{Ru(bpy)_2\}_2(ptH_2Q)]^{3+}$, a 300 mV separation between the oxidation potentials for the two Ru(II) centers might result from the different coordination environment for each of the two Ru(II) centers, the electrostatic effect, and the electron delocalisation effect. This complex might have very closed bpy-based

^{3}MLCT levels for each of the two $Ru(bpy)_2$ units. The expected electronic communication between the two Ru(II) centers, suggested by the nonequivalent oxidation potentials for the two Ru(II) centers, is to be confirmed by measuring the intervalence transition.

Chapter VII

Electrochemically Induced Proton Transfer Processes in $Ru(bpy)_2$ Complexes Containing Pyridyltriazoles

VII.1 Introduction.

As mentioned briefly in chapter V and chapter VI, electrochemically induced proton transfer was observed for the complexes $[Ru(bpy)_2(ptOH)]^+$ and $[Ru(bpy)_2(ptH_2Q\text{-}1)]^+$. Such processes are rather unusual and therefore they deserve a separate chapter for discussion.

Electrochemically induced proton transfer is not a well documented phenomenon [152-154, 211-212]. Of some relavance to the work to be described in this chapter are the following two examples, which are proton-coupled electron transfer processes observed for some Mn and Ru oxo complexes [152-154].

In 1985, Meyer and co-workers [152], observed that reduction of $[(bpy)_2(py)Ru^{IV}O]^{2+}$ by H_2O_2 yields $[(bpy)_2(py)Ru^{III}(OH)]^{2+}$. Kinetic studies reveal that the reduction process is not a process where a simple outer-sphere electron transfer between the oxidant and reductant takes place first to form $[(bpy)_2(py)Ru^{III}(O)]^+$ and the protonation of the product occurs afterwards to form $[(bpy)_2(py)Ru^{III}(OH)]^{2+}$. Rather, the protonation takes place simultaneously with the electrochemical reduction. (The proton is provided by H_2O_2.) Thus, in such a proton-coupled electron transfer process the redox site in

the complex $[(bpy)_2(py)Ru^{IV}O]^{3+}$ acts as not only an electron acceptor but also a proton acceptor. This process might be of relevance to similar redox processes of some biologically redox couples such as $NADH/NAD^+$ [152].

Another example of proton-coupled electron transfer is reported by Thorp et al. [153-154]. For a mixed-valence dimer $[(bpy)_2Mn(O)_2Mn(bpy)_2](ClO_4)_3$, a model for the oxygen-evolving complex of PS II [10], reduction of $Mn^{IV}Mn^{IV}$ to $Mn^{III}Mn^{IV}$ was found to be coupled with the protonation of the di-μ_2-oxo group in the complex. It is known that oxo-bridged clusters of iron and manganese are important structural and functional unit of many redox enzymes, including uteroferrin, hemerythrin, catalase and PS II [30]. In such reactions, the binding of O_2 or the catalysis of the oxidation of water or peroxide by these enzymes involves oxidation or reduction of a metal center and deprotonation or protonation of a bridging oxo ligand.

The above two examples, have the common feature that any protons transferred, accompanying electron transfer, must come from an external source.

In this chapter, a different proton-coupled electron transfer process observed on some pyridyltriazole-containing Ru(II) complexes will be described. The most important feature of the process observed for these two complexes is that the

proton transfer is most likely intramolecular. No extra proton is needed from solvent or from a proton-donor molecule.

V.2 Results and discussion.

VII 2.1 Electrochemical properties of $[Ru(bpy)_2(ptH_2Q\text{-}1)]^+$.

VII 2.2.1 Cyclic voltammetry.

The cyclic voltammagrams for the free ligand $HptH_2Q$ and for the complex $[Ru(bpy)_2(ptH_2Q\text{-}1)]^+$ are presented in Fig. VII.1. The oxidation of the free ligand $HptH_2Q$ ($E_{1/2}$ = 0.46 V) appears to be a quasi-reversible process, as indicated by a large separation (700 mV) between the oxidative and reductive peaks (Fig. VII.1A). Upon addition of acid, the oxidation shifts to a more positive potential (Fig. VII.1B). By comparison with the literature value [198], the redox couple observed for the free ligand can be assigned to $-H_2Q$ ---> $-Q$ oxidation.

For the complex $[Ru(bpy)_2(ptH_2Q\text{-}1)]^+$ (Fig. VII.1C), where the triazole ring is deprotonated, the oxidation of the hydroquinone group still occurs at a similar potential ($E_{1/2}$=0.41 V) compared to the free ligand.

At 1.06 V, a small irreverible oxidation peak is observed,

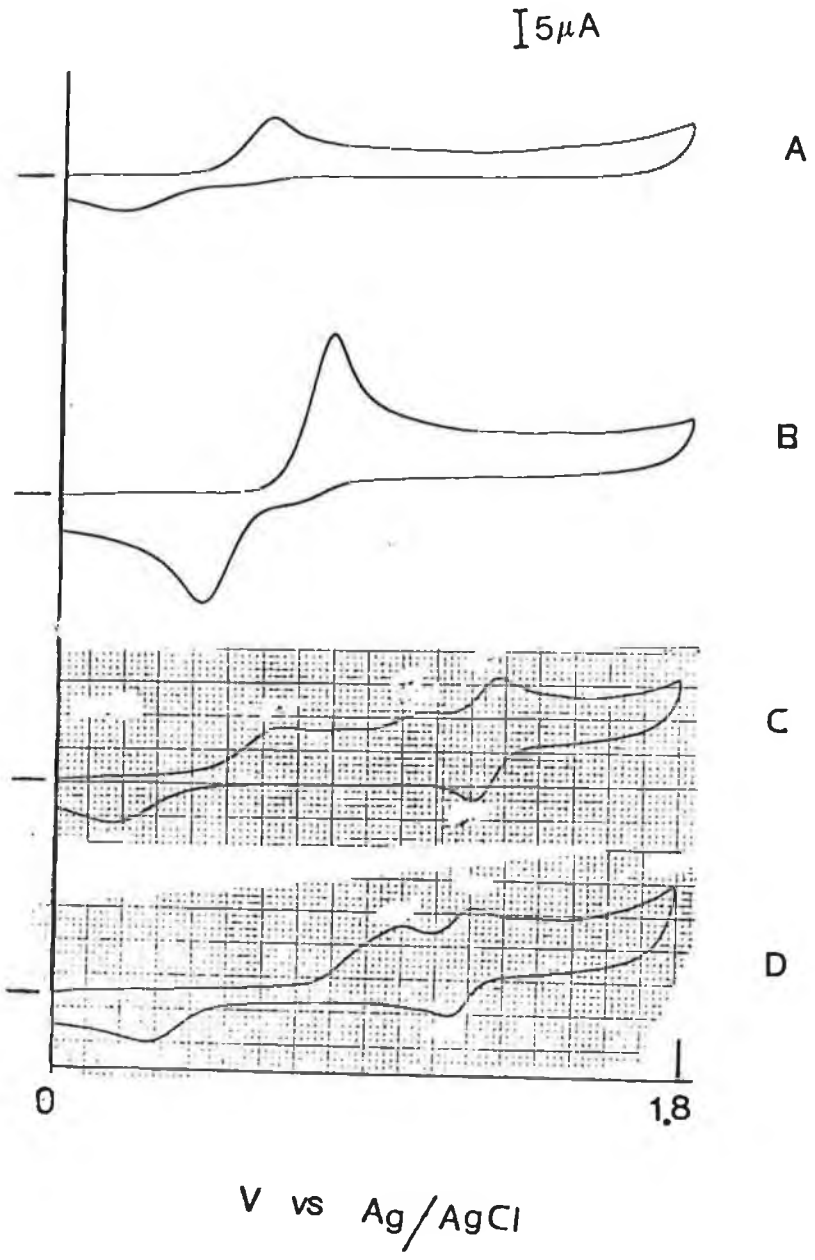

Fig. VII.1 Cyclic Voltammograms of the free ligand $HptH_2Q$ (A and B) and of the complexes $[Ru(bpy)_2(ptH_2Q\text{-}1)]^+$ and $[Ru(bpy)_2(HptH_2Q\text{-}1)]^{2+}$. (C and D) in 0.1 M TEAP/CH_3CN. Scan rate: 100 mV/sec.

followed by a reversible redox couple ($E_{1/2}$ = 1.25 V, ΔEp = 70 mV). The peak at 1.06 V, compared to other similar pyridyltrazole complexes [79-80, 83-85], can be assigned as due to the oxidation of Ru(II) to Ru(III). Assignment for the reversible redox couple at 1.25 V, however, needs a comparison with the results observed for the protonated complex $[Ru(bpy)_2(HptH_2Q\text{-}1)]^{2+}$.

The cyclic voltammogram obtained for $[Ru(bpy)_2(HptH_2Q\text{-}1)]^{2+}$, where the triazole ring is protonated, suggests that the Ru(II) oxidation occurs at a formal potential 1.18 V (Fig. VII.1D). This suggests that for the deprotonated ccomplex, $[Ru(bpy)_2(ptH_2Q\text{-}1)]^{+}$, the triazole ring is most likely protonated after the oxidation of the hydroquinone group. This means the proton released from the hydroquinone group due to oxidation subsequently protonates the triazole ring. Thus, the reversible redox couple with a formal potential 1.25 V is most likely due to the protonated quinone-containing complex.

It should be pointed out that for measuring $[Ru(bpy)_2(HptH_2Q\text{-}1)]^{2+}$ about 5% CF_3COOH was added to solution to ensure the protonation. The lower formal potential (1.18 V) observed for this protonated complex might be due to the added acid in the solution which activates the electrode and thus redcues the overpotential for the Ru(II) ---> Ru(III) oxidation [213].

The proposed mechanism for the electrochemically induced proton transfer process for the deprotonated complex, $[Ru(bpy)_2(ptH_2Q\text{-}1)]^+$, is depicted in Fig VII.2. As the oxidation of hydroquinone group appears as a board peak, it is not clear whether the semiquinone group is formed as an intermediate. However, if any semiquinone group is formed, then the protonation of triazole ring can also be directly induced. If the semiquinone is stabilised, then the process might follow the mechanism shown in Fig. VII.3. At present we can not differentiate between these two possibilities. The formation of the semiquinone could in principle be detected by using in-situ electrochemical ESR techniques.

VII. 2.2.2 UV-vis spectroelectrochemistry.

The protonation of the triazole ring as results of the oxidation of the hydroquinone group was further investigated by UV-vis spectroelectrochemistry. As shown by cyclic voltammetry, the hydroquinone group can be oxidised before the Ru(II) center. Therefore, if the protonation of the triazole ring does occur after hydroquinone oxidation, the MLCT maximum of this complex should shift to a higher energy.

The UV-vis spectrum as a function of electrochemical potential for $[Ru(bpy)_2(ptH_2Q\text{-}1)]^+$ is presented in Fig. VII.4. The results clearly show that along with the increase of the applied potential, the MLCT maximum shifts from 475 nm

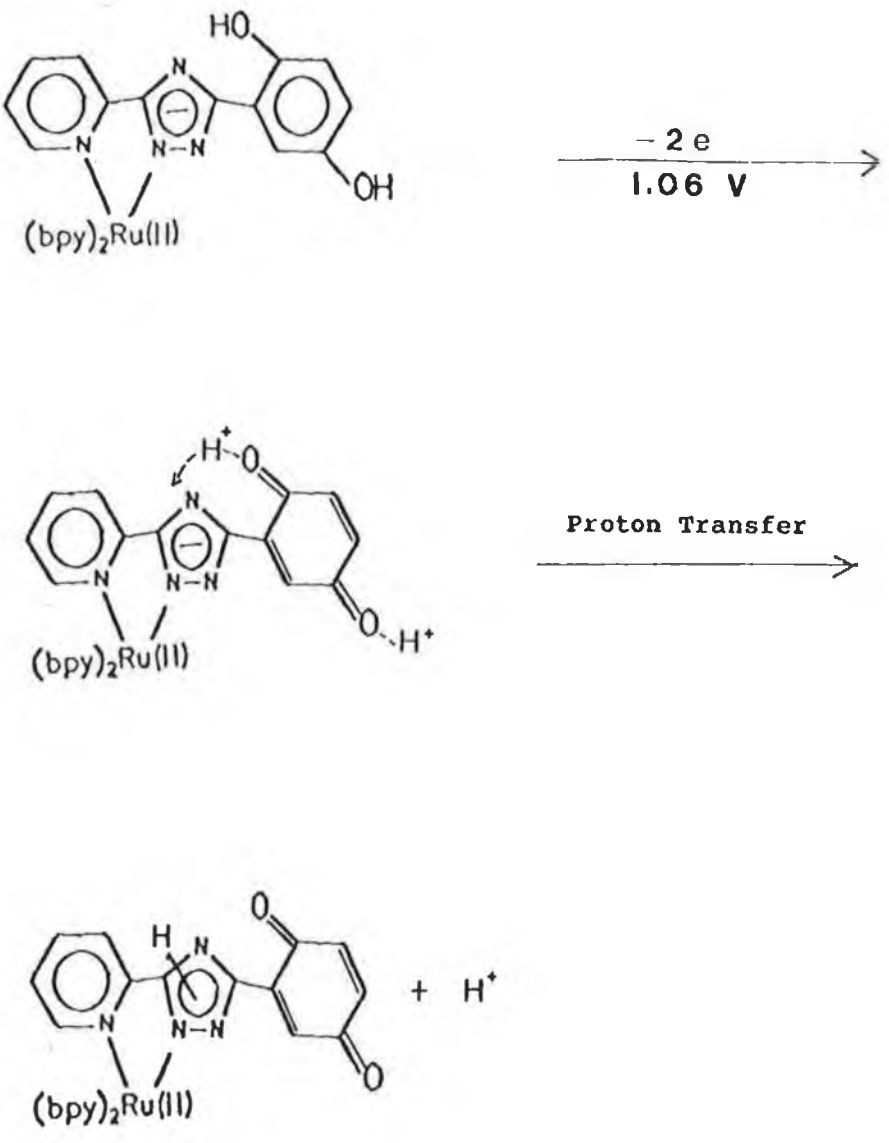

Fig. VII.2 Proposed mechanism for the electrochemically induced proton transfer process in $[Ru(bpy)_2(ptH_2Q\text{-}1)]^+$.

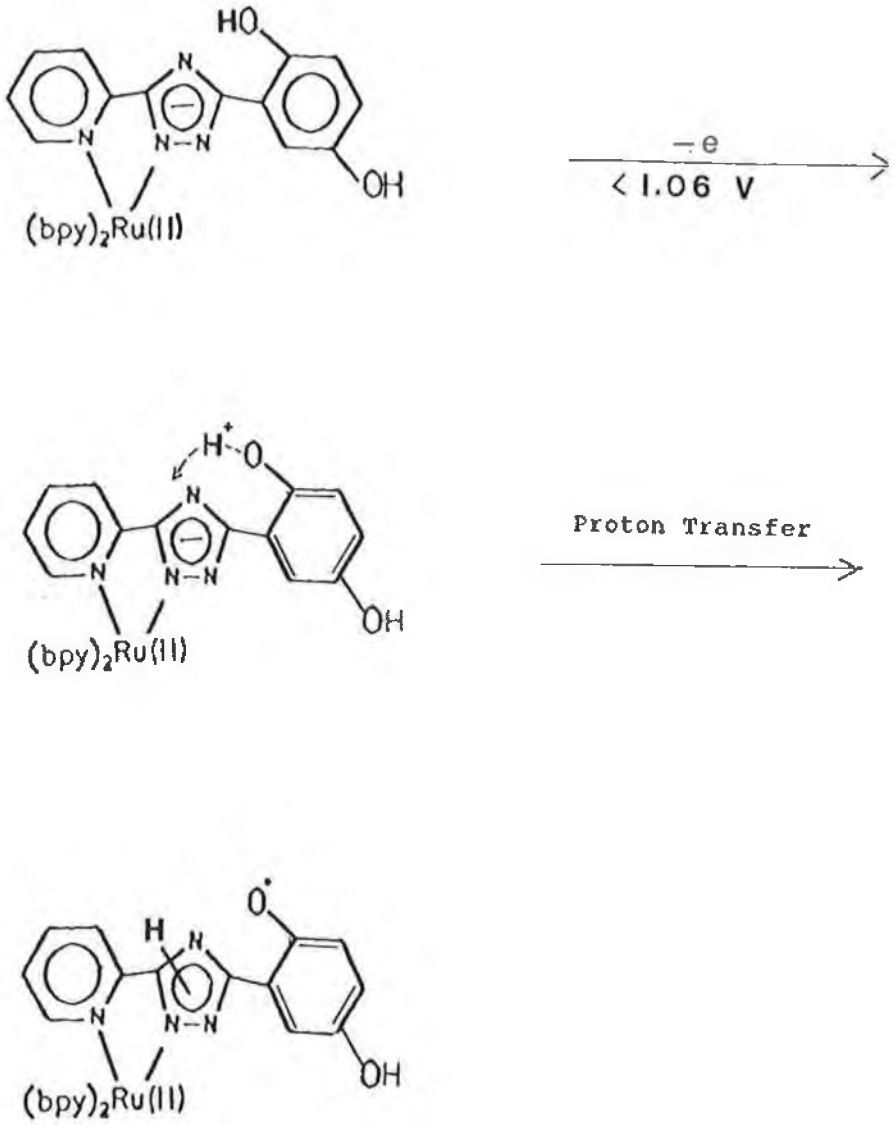

Fig. VII.3 Proposed mechanism for the electrochemically induced proton transfer process in $[Ru(bpy)_2(ptH_2Q\text{-}1)]^+$, assuming semiquinone is formed and stabilised during the process.

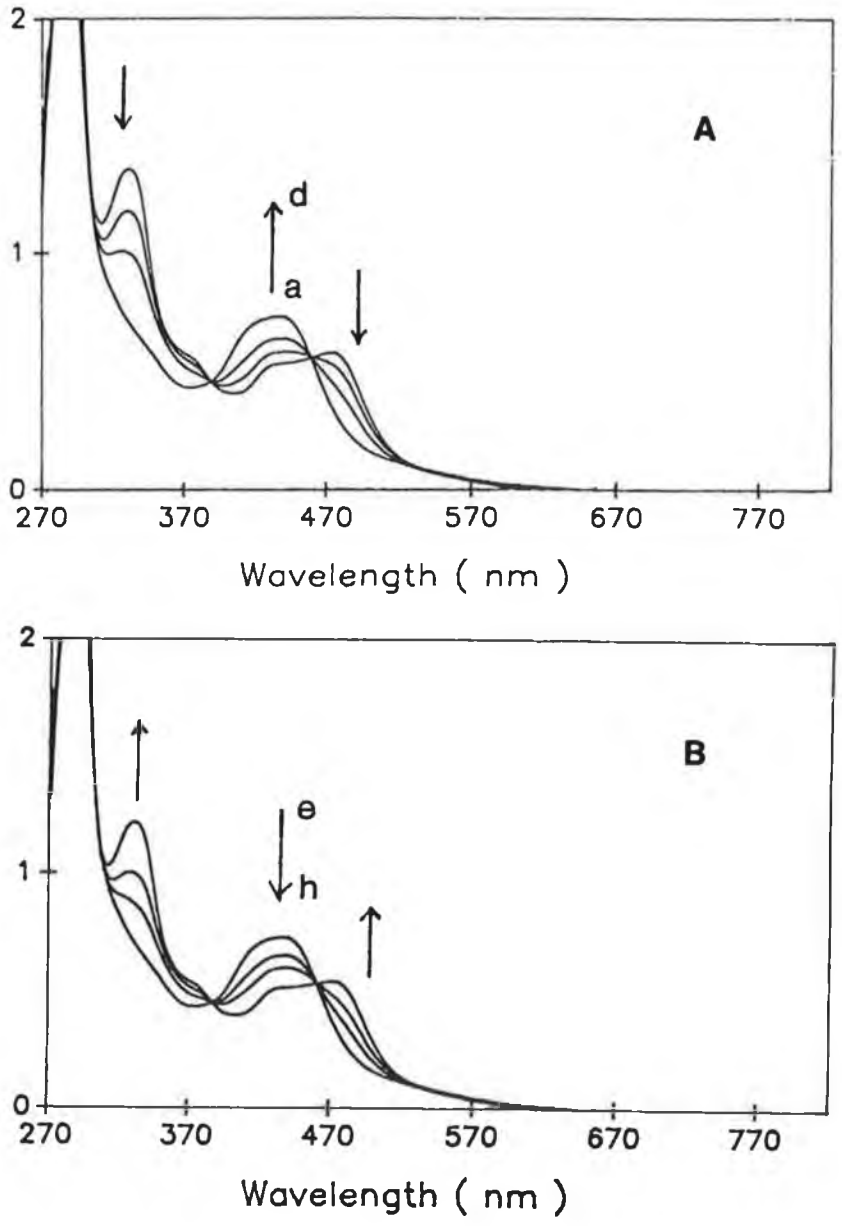

Fig. VII.4 UV-vis absorption spectrum as a function of electrochemical potential for the complex $[Ru(bpy)_2(ptOH)]^+$.
A: Oxidation; for a-d applied potential = 0, 0.50, 0.55 and 0.75 V. B: Reduction; for e-h applied potential = 0.75, 0.25, 0.20, 0.0 V. (vs. Ag/AgCl).

to 440 nm. In the meantime, the π---> π^* transition at about 330 nm which corresponds to the hydroquinone group decreases upon oxidation. It is interesting that between 0 to 0.7 V, the electrochemically induced proton transfer between the hydroquinone and triazole rings is reversible (Fig. VII.4).

VII.2.2 Electrochemical properties of $[Ru(bpy)_2(ptOH)]^+$.

VII.2.2.1 Differential pulse voltammetry.

The oxidation process of the $[Ru(bpy)_2(ptOH)]^+$ complex is presented in Fig. VII.5A. The Ru(II/III) oxidation potential occurs at 0.89 V. The two peaks at 1.26 and 1.43 V can be assigned to the oxitation of the phenol group, by comparison with data obtained for the free ligand and literature values obtained for the phenols [214]. When the complex is protonated, the Ru (II/III) oxidation potential shifts to a higher potential, 1.1 V, while the phenol oxidation potential remains unchanged. Upon protonaton, $ptOH^-$ becomes HptOH and its σ-donating ability is decreased while its π-accepting ability is increased. As a result, the Ru(II)-based t_{2g} level is stabilised so that the Ru(II) center becomes more difficult to oxidise. The oxidation of the phenol group appears insensitive to the protonation of the triazole ring, which is not surprising. The oxidation of phenols is usually very complex which involves stepwise

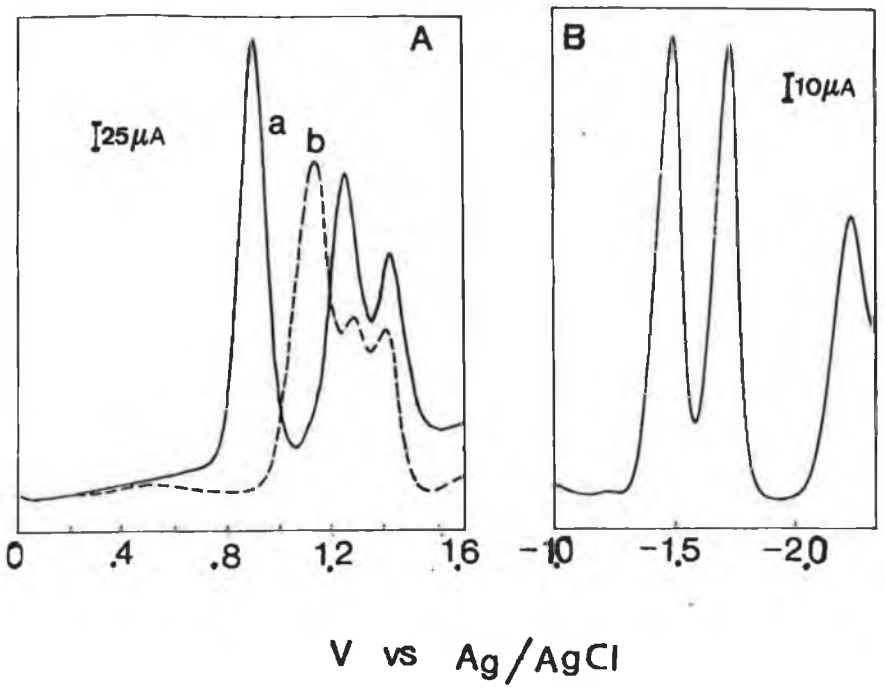

Fig. VII.5 A --- differential pulse voltammogram of $[Ru(bpy)_2(ptOH)]^+$ in 0.1 M TEAP without (a) and with (b) CF_3COOH.
B --- differential pulse voltammogram (ligand based reduction) of $[Ru(bpy)_2(ptOH)]^+$.

multi-electron transfer processes [213-214]. No attempts are made in order to identify the each of the two peaks of the phenol oxidation in $[Ru(bpy)_2(ptOH)]^+$.

The oxidation potentials for both Ru(II) and the phenol group have a strong solvent dependence. Detailed description of such behaviour can be found in a related publication [83], and the discussion to be given here will focus on the electrochemically induced proton transfer process.

The reduction process for $[Ru(bpy)_2(ptOH)]^+$ is presented in Fig. VII.8B. The peak at about -2.3 V, is assigned to the reduction of the $ptOH^-$ ligand, compared to the data obtained on the free ligand. The bpy-based reductions were observed at -1.42 and -1.68 V. This suggests the LUMO is bpy-based in this complex, which is consistent with the results obtained from acid-base chemistry (Chapter V).

VII.2.2.2. Cyclic voltammetry and square wave voltammetry.

The cyclic voltammograms of $[Ru(bpt)_2(ptOH)]^+$ and $[Ru(bpy)_2(HptOH)]^{2+}$ are presented in Fig. VII.6.

When scanning between 0 and 1.0 V, a reversible redox couple corresponding to Ru(II) ---> Ru(III) is observed at $E_{1/2}$ = 0.83 V. The peak-to-peak separation is of 75 mV.

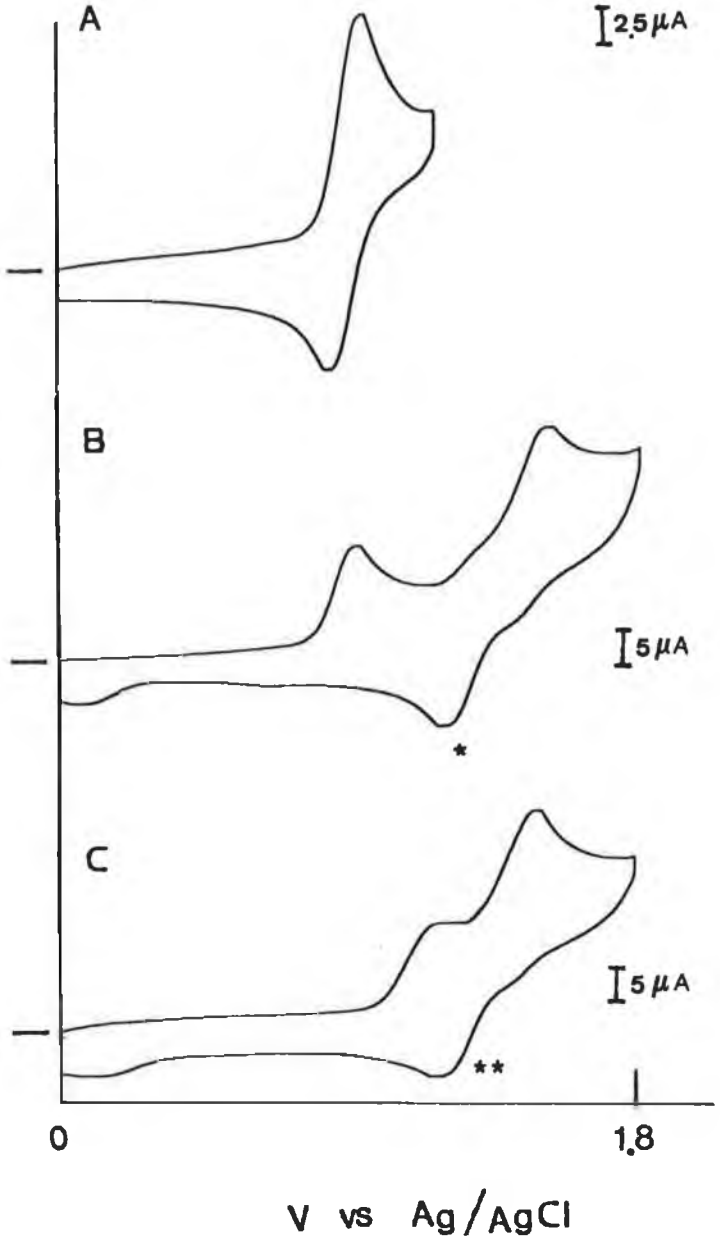

Fig. VII.6 Cyclic voltammogram of $[Ru(bpy)_2(ptOH)]^+$ (A and B) and $[Ru(bpy)_2(HptOH)]^{2+}$ (C).

When scanning from 0 V to 1.8 V (Fig. VII.6B), the first oxidation peak remains at the same potential, 0.87 V, but now a second oxidation peak at 1.43 V is present, which can be assigned to the oxidation of the phenol group. During the reductive scan, a peak (*) at 1.12 V was observed. However the expected peak at a potential lower than 0.87 V corresponding to the reduction of Ru(III) -> Ru(II) seems to disappear.

Peak (*) cannot be due to the reduction of the oxidised phenol group. Instead, the small reductive peak at about 0.2 V is most likely corresponding to the reduction of the oxidised phenol compared with the results obtained for the free ligand. (From Fig. VII.6A it can be seen in the potential range where the phenol group can not be oxidised, then that small reduction peak at 0.2 V is absent.) Peak (*) cannot be due to the Ru(III/II) reduction of the deprotonated $[Ru(bpy_2(ptOH)]^+$ either, as it should occur at least at a potential less positive than 0.87 V (oxidation). So what is peak (*) and where is the reduction of Ru(III) ---> Ru(II) for $[Ru(bpy)_2(ptOH)]^+$?

The answer can be obtained if the results are compared to those obtained for the protonated complex (Fig. VII.6C). For the protonated complex, $[Ru(bpy)_2(HptOH)]^{2+}$, the Ru(II) ---> Ru(III) oxidation occurs at 1.15 V. During the reductive scan, the only reduction peak is peak (**) at the

potential 1.12 V, which is almost at the same potential as for peak (*). Thus both Peak (*) and Peak (**) can be assigned to Ru(III) ---> Ru(II) reduction. This implies that for the deprotonated complex $[Ru(bpy)_2(ptOH)]^+$, after the oxidation of the phenol group the released proton protonates the triazole ring.

A possible mechanism for the electrochemically induced proton transfer in this complex is presented in Fig VII.7.

The above results were further clarified by the use of square wave voltammetry (Fig VII.8). The advantage of this technique compared to CV is that it can provide a higher sensitivity at the same scan rate. From Fig. VII.8 it can be seen that two peaks were detected during the reductive scan from 1.7 to 0.1 V (Fig. VII.8B). A small reduction peak at ca. 0.86 V, which was not seen from CV at the same scan rate, is most likely due to the reduction of some residual complex where the triazole ring remains deprotonated. The reductive peak at ca. 1.13 V is caused by Ru(III) ---> Ru(II) for the protonated complex. The peak 1 and peak 2 are comparable in peak area, suggesting that most of the Ru(III) species has been protonated before any reduction takes place.

Concluding remarks.

The results described in this chapter suggest that

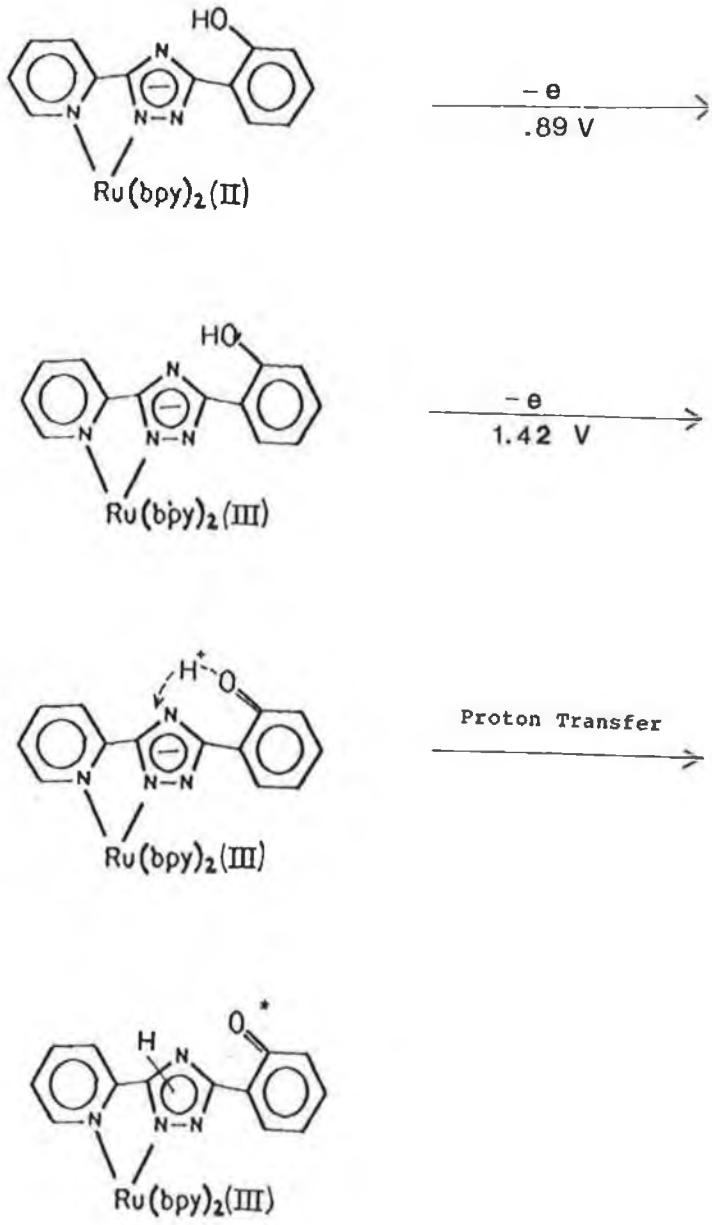

Fig. VII.7 Proposed mechanism for the electrochemically induced proton transfer process in the complex $[Ru(bpy)_2(ptOH)]^+$. * presumed product of phenol oxidation.

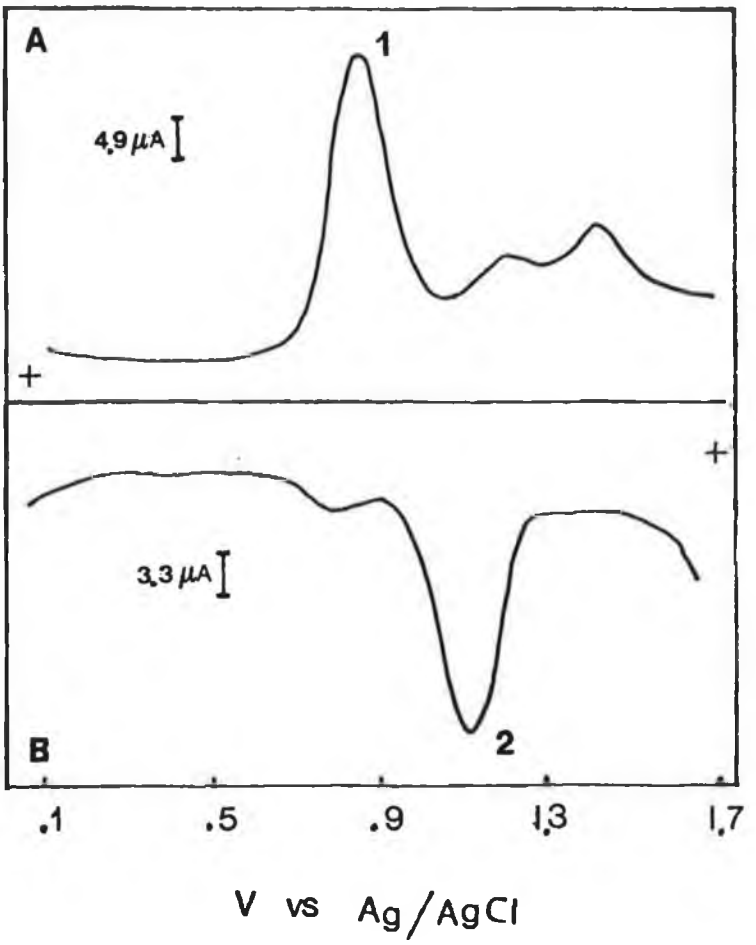

Fig. VII.8 Square wave voltammogram of the complex $[Ru(bpy)_2(ptOH)]^+$ in 0.1 M $TEAP/CH_3CN$.

A ---- oxidative scan. B ---- reductive Scan. Pulse height 50 mV. Potential increment 4 mV. Frequency 25 Hz (which yields a scan rate 100 mV/sec.)

electrochemically induced proton transfer occurs for the complexes $[Ru(bpy)(ptH_2Q\text{-}1)]^+$ and $[Ru(bpy)_2(ptOH)]^+$. The most interesting feature of the proton transfer process observed for these two complexes is that it does not need an extra proton pool or proton donor. A proton can be directed from one functional group to another within the same molecule or between the same type of molecules. This process is different from that reported by Meyer and co-workers [152] and by Thorp and co-workers [153-154]. In their cases, the proton-coupled electron transfer needs protons from other proton-donor molecules [152] or from solvent [153-154].

Chapter VIII

Final Remarks and Future Work

In this work, the photophysical, photochemical and electrochemical properties of a wide range of Ru(II) diimine complexes containing substituted 1,2,4-triazoles have been investigated. Several new Ru(II) complexes containing a pyridyltriazole ligand linked to a hydroquinone group have been synthesised and characterised. Their photophysical properties are studied. The most interesting results obtained in this work are the following:

The Photostability of several Ru(II) complexes containing triazoles.

Photostability has been observed for a number of Ru(II) complexes containing triazoles. These complexes include the two isomers of $[Ru(bpy)_2(ptr)]^+$, $[Ru(bpy)_2(3Mptr)]^+$, $[Ru(bpy)_2(ptOH)]^+$, and the two isomers of $[Ru(phen)_2(ptr)]^+$. This is interesting not only for the potential application of these complexes as photosensitisers in energy conversion systems, but also for the fundamental interest. Numerous Ru(II) diimine complexes have been synthesised in past few years and only about 10 of them were reported to be photostable. Most of those observed photoinert complexes contain at least one ligand which is a good π-acceptor and a weak σ-donor. The four new photostable complexes described in this thesis are all based on triazoles which are known as strong σ-donors and weaker π-acceptors. Such systems are relatively rare. It is also interesting that for these triazole complexes the

photoreactivity can be controlled simply by controlling the deprotonation/protonation of the triazole ring.

The photoinduced linkage isomerism.

The photoinduced linkage isomerism has been observed for the two isomers of $[Ru(bpy)_2(Hptr)]^{2+}$ and for $[Ru(bpy)_2(H3Mptr)]^{2+}$. Such behaviour has not been found from literature for other Ru(II) diimine complexes. The only similar case is the photoracemesation of $[Ru(bpy)_3]^{2+}$.

pH control of the nature of the emitting state.

For a series of Ru(II) complexes containing pyrazyltriazoles, it is found the LUMO is located on the bpy when the traizole ring is deprotonated. However, when the triazole ring is protonated, the LUMO is switched to pyrazyltriazole based π^* orbitals. This is a typical case, among few others, where the origin of the emitting ^{3}MLCT state can be altered by "second-sphere" perturbations.

Electrochemically induced proton transfer processes.

Electrochemically induced proton transfer has been observed for the complexes $[Ru(bpy)(ptH_2Q\text{-}1)]^+$ and $[Ru(bpy)_2(ptOH)]^+$. The most interesting feature of such processes, which differs from those reported for other systems, is that external proton source is not required. A proton can be transferred from one site to another within the same molecule or between the same type of molecules.

The long emission lifetime, photostablity and oxygen quenching effect observed for the two isomers of $[Ru(phen)_2(ptr)]^+$.

The emission lifetimes for the two isomers of $[Ru(phen)_2(ptr)]^+$ are about 6-7 times longer than their bpy and dmb based analogues in degassed CH_3CN and 3-4 times longer in aqueous buffer. The lifetime values for the $[Ru(phen)_2(ptr)_2]^+$ complexes are comparable to $[Ru(bpy)_3]^{2+}$. The advantage of the former is that, unlike $[Ru(bpy)_3]^{2+}$, they are photochemically stable.

A number of questions arising in this thesis have not been clarified at this stage. For instance:

Why are the emission lifetimes for the two isomers of $[Ru(phen)_2(ptr)]^+$ much longer compared to their bpy or dmb based analogues ?

Although it has been suggested that for these photoinert complexes the energy gap law might be the dominant factor which governs the excited-state relaxation, temperature dependent lifetime measurements for phen- and dmb- based complexes, combined with those obtained for the bpy-based two isomers, are needed to confirm the validity of this assumption.

The coordination mode of the complex $[Ru(bpy)_2(ptH_2Q\text{-}2)]^+$ is unclear.

The NMR data seem to prefer the coordination fashion where the coordinated -OH group on the hydroquinone ring remains protonated. This is a rather unusual coordination mode, although a few other similar complexes have been reported in literature. With the lack of X-ray crystallographic data, no definite conclusion can be drawn concerning its structure. It is also peculiar that for this complex the protonated form has a longer lifetime in CH_3CN than its deprotonated analogue. The electrochemistry of this complex is also unclear at present.

Why does the solvent have such significant effect on the emission lifetimes for the pyrazyltriazole complexes ?

The lifetimes for these complexes are usually 10 times longer in CH_3CN than in aqueous buffer. Such significant solvent effect has not been found for other triazole-containing complexes. The origin of the solvent effect on the emission energies and emission lifetimes of Ru(II) complexes is in general an unsolved question in ruthenium chemistry.

More detailed investigations are needed in order to find possible answers for the above questions. Besides, the work described in this thesis, especially on the hydroquinone-containing complexes, is to to be extended.

The quenching by electrochemically formed quinone groups is obscured by the electrochemically induced proton transfer process. The quenching process is possible to isolate by modification of the $HptH_2Q$ ligand. For instance, by substitution of a methyl group on the triazole ring, the protonation of this group can be eliminated. The mechanism of the electrochemically induced proton transfer for $[Ru(bpy)_2(ptH_2Q\text{-}1)]^+$ might also be interesting to study in more detail. Whether semiquinone is involved in this process can be investigated using in-situ electrochemical ESR techniques.

The unique excited-state lifetime behaviour observed for $[Ru(bpy)_2(ptH_2Q\text{-}2)]^+$ might be better understood from the temperature dependent lifetime measurements and photolysis experiments. A single crystal structure is crucial for confirming the coordination mode for this complex.

For the dinuclear complex $[\{Ru(bpy)_2\}_2(ptH_2Q)]^{3+}$, the 300 mV separation between the oxidation potential for the two Ru(II) centres suggests that electronic communucations between the Ru(II) sites most probably exist. Such communications can be confirmed by investigating the intervalence transition for this complex. This can be done fairly easily using spectroelectrochemical techniques.

The significant oxygen quenching effect found for the two

isomers of $[Ru(phen)_2(ptr)]^+$ might be extended towards the construction of oxygen sensors. The long emission lifetime and photostability of these two complexes make them interesting for further investigations. For instance, more insight into the excited-state properties of these complexes might be obtained by studying the electric field effect on their electronic transitions (especially MLCT) using Stark effect spectroscopy.

References:

1. D. Voet and J.G. Voet, Biochemistry, John Wiley & Sons, Inc., 1990, New York, p586-617.
2. J.R. Norris and M. Schiffer, Chem. & Chem. Eng. News, July 30, 1990, p23.
3. L. Palminsano, V. Augugliaro, A. Sclafani, and M. Schiavello, J. Phys. Chem., 1988, 92, 6710.
4 A. Mills, S. Giddings, N. McMurphy, and G. Williams, Inorg. Chim. Acta, 1989, 159, 7.
5. T.J. Meyer, Acc. Chem. Res., 1989, 22, 163.
6. H.B. Gray, Chem. & Chem. Eng. News, April 15, 1990, p39.
7. V. Balzani and F. Scandola, Supramolecular Photochemistry, Ellis Horwood, 1991.
8. K. Kalyanasundarum, Coord. Chem. Rev., 1982, 46, 159.
9. J.A. Basshan and M. Calvin, The Path of Carbon in Photosynthesis, Prentice-Hall, New Jersey, 1957.
10. G.W. Brudvig and R.H. Crabtree, Prog. Inorg. Chem., S.J. Lippard (Ed.), 1989, 36, 99.
11. J. Deisenhofer, O. Epp, K. Miki, R. Huber, and H. Michel, Nature (London), 1985, 318, 618.
12. S. Borman, Chem. & Chem. Eng. News, Oct. 8, 1990, p27.
13. G.L. Closs and J.R. Miller, Science, 1988, 240, 440.
14. D. Gust, T.A. Moore, P.A. Liddell, G. Nemeth, L.R. Makings, A.L. Moore, D. Barrett, P.J. Pessiki, R.V. Bensasson, M. Rougee, C. Chachaty, F.C. De Schryer, M.

Van der Auweraer, A.R. Holtzwarth, and J.S. Connolly, J. Am. Chem. Soc., 1987, 109, 846.

15. J.R. Norris and P. Gast, J. Photochem., 1985, 29, 185.

16. D.J. Lockhart, S.L. Hammes, S. Franzen, and S.G. Boxer, J. Phys. Chem., 1991, 95, 2217.

17. D.J. Lockhart, C. Kirmaier, D. Holten, and S.G. Boxer, J. Phys. Chem., 1990, 94, 6987.

18. D.B. Knaff, TIBS, 1988, 13, 460.

19. B. Lagoutte and P. Mathis, Photochem. and Photobiol., 989, 49, 833.

20. P. Joliot, G. Barbieri, and R. Chabaud, Photochem. Photobiol., 1969, 10, 309.

21. B. Kok, B. Forbush, and M. McGloin, Photochem. Photobiol., 1970, 11, 457.

22. B. Forbush, B. Kok, and M. McGloin, Photochem. Photobiol., 1971, 14, 307.

23 G.T. Babcock, New Comprehensive Biochemistry: Photosynthesis, J. Amesz (Ed.), Elsevier, Armsterdam, 1987, pl25.

24. G.W. Brudvig, J. Bioenerg. Biomembran., 1987, 19, 91.

25. P. Joliot and B. Kok, Bioenergetics of Photosynthesis, Govindjee (Ed.), Academic Press, New York, 1975, P.387.

26. J.A. Kirby, A.S. Tompson, S.R. Cooper, and M.P. Klein, J. Am. Chem. Soc, 1981, 103, 5529.

27. V.K. Yachandra, R.D. Guiles, A.E. McDermott, R.D. Britt, S.L. Dexheimer, K. Sauer, and M.P. Klein,

Biochim. Biophys. Acta, 1986, 850, 324.

28. V.K. Yachandra, R.D. Guiles, A.E. McDermott, J.L. Cole, R.D. Britt, S.L. Dexheimer, K. Sauer, and M.P. Klein, Biochemistry, 1987, 26, 3974.

29. G.N. George, R.C. Prince, and S.P. Cramer, Science, 1989, 243, 789.

30. K. Wieghardt, Angew. Chem. Int. Ed. Engl., 1989, 28, 1153.

31. K.S. Hagen, W.H. Armstrong, and H. Hope, Inorg. Chem., 1988, 27, 967.

32. G. Christou, Acc. Chem. Res., 1989, 22, 328.

33. R.J. Kulawiec, R.H. Crabtree, G.W. Brudvig, and G.K. Schulte, Inorg. Chem., 1988, 27, 1039.

34. G.W. Brudvig and R.H. Crabtree, Proc. Natl. Acad. Sci., (U.S.A.), 1986, 83, 4586.

35. M.K. Chan and W.H. Armstrong, Inorg. Chem., 1990, 112, 4985.

36. D.W. Low, D.M. Eichhorn, A. Draganescu, and W.H. Armstrong, Inorg. Chem., 1991, 30, 878.

37. K. Kalyanasundaram, M. Gratzel, and E. Pelizzetti, Coord. Chem. Rev., 1986, 69, 57.

38. N. Serpone (Ed.), Photochemical Energy Conversion, Elsevier, Armsterdam, 1989.

39. D. Gust and T.A. Moore, J. Photochem., 1985, 29, 173.

40. E.A. Seddon and K.R. Seddon, The Chemistry of Ruthenium, Elsevier, Armsterdam, 1984.

41. A. Juris, V. Balzani, F. Barigelleti, A. von Zelewsky,

Coord. Chem. Rev., 1988, 84, 85.

42. J.P. Paris and W.W. Brandt, J. Am. Chem. Soc., 1959, 81, 5001.

43. H.D. Gafney and A.W. Adamson, J. Am. Chem. Soc., 1973, 94, 8238.

44. T.N. Demas and A.W. Adamson, J. Am. Chem. Soc., 1973, 95, 5159.

45. T.J. Meyer, Pure & Appl. Chem., 1986, 58, 1193.

46. E.M. Kober and T.J. Meyer, Inorg. Chem., 1982, 21, 3967.

47. E.M. Kober and T.J. Meyer, Inorg. Chem., 1983, 22, 1614.

48. E.M. Kober and T.J. Meyer, Inorg. Chem., 1984, 23, 3877.

49. H. Yersin and E. Gallhuber, J. Am. Chem. Soc., 1984, 106, 6582.

50. K. Kalyanasunduram and M. Gratzel, Andew. Chem. Internat. Ed. Engl., 1979, 18, 781.

51. K.F. Freed and J. Jortner, J. Chem. Phys., 1970, 52, 6272.

52. T.J. Meyer, Prog. Inorg. Chem., S.J. Lippard (Ed.), 1983, 30, 389.

53. E.C. Constable and P.J. Steel, Coord. Chem. Rev., 1989, 93, 205.

54. C.A. Bignozzi, C. Chiorboli, M.T. Indelli, M.A. Scandola, G. Varani, and F. Scandola, J. Am. Chem. Soc., 1986, 7872.

55. R.P. Thummel, F. Lefoulon, and S. Chirayil, Inorg. Chem., 1987, 26, 3072.

56. G.H. Allen, R.P. White, D.P. Rillema, and T.J. Meyer, J. Am. Chem. Soc., 1984, 106, 2613.

57. S.D. Ernst and W. Kaim, Inorg. Chem., 1989, 28, 1520.

58. F. Barigelletti, A. Juris, V. Balzani, P. Belser and A. von Zelewsky, Inorg. Chem., 1987, 26, 4115.

59. A. Juris, S. Campagna, V. Balzani, G. Gremaud, and A. von Zelewsky, Inorg. Chem., 1988, 27, 3652.

60. A. Juris, P. Belser, F. Barigelletti, A. von Zelewsky, and V. Balzani, Inorg. Chem., 1986, 25, 256.

61. F. Barigelletti, A. Juris, V. Balzani, P. Belser, and A. von Zelewsky, Inorg. Chem., 1983, 26, 3335.

62. L. De Cola and F. Barigelletti, Inorg. Chim. Acta, 1989, 159, 169.

63. D.P. Rillema, G. Allen, T.J. Meyer, and D. Conrad, Inorg. Chem., 1983, 22, 1618.

64. D.P. Rillema, D.G. Taghdiri, D.S. Jones, C.D. Keller, L.A. Worl, T.J. Meyer and H.A. Levy, Inorg. Chem., 1987, 26, 578.

65. D.P. Rillema and K.B. Mack, Inorg. Chem., 1982, 21, 3849.

66. R. Hage, J.H. v. Dieman, G. Ehrlich, J.G. Haasnoot, D.J. Stufkens, T.L. Soneck, J.G. Vos, and J. Reedijk, Inorg. Chem., 1990, 29, 988.

67. R.P. Thummel and S. Chirayil, Inorg. Chim. Acta, 1988, 154, 77.

68. R.P. Thummel and Y. Decloitre, Inorg. Chim. Acta, 1987, 128, 245.

69. Y. Kawanishi, N. Kitamura, and S. Tazuke, Inorg. Chem., 1989, 28, 2968.

70. M. Haga, T. Matsumura-Inoue, K. Shimizu, and G.P. Sato, J. Chem. Soc., Dalton Trans., 1989, 371.

71. M. Haga, Inorg. Chim. Acta, 1983, 75, 29.

72. M. Haga and A. Tsunemitsu, Inorg. Chim. Acta, 1989, 164, 137.

73. A.M. Bond and M. Haga, Inorg. Chem., 1986, 25, 4507.

74. P.J. Steel, F. Lahouse, D. Lerner, and C. Marzin, Inorg. Chem., 1983, 22, 1488.

75. C. Marzin, F. Budde, P.J. Steel, and D. Lerner, Nouv. J. Chim., 1987, 11, 33.

76. P.J. Steel and E.C. Constable, J. Chem. Soc., Dalton Trans., 1990, 1389.

77. J.G. Vos, J.G. Haasnoot, and G. Vos, Inorg. Chim. Acta, 1983, 71, 155.

78. R. Hage, J.G. Haasnoot, J. Reedijk and J.G. Vos, Inorg. Chim. Acta, 1986, 118, 73.

79. R. Hage, P. Prins, J.G. Haasnoot, J. Reedijk, and J.G. Vos, J. Chem. Soc., Dalton Trans., 1987, 1389.

80. R. Hage, A.H.J. Dijkhuis, J.G. Haasnoot, R. Prin, J. Reedijk, B.E. Buchanan, and J.G. Vos, Inorg. Chem., 1988, 27, 2185.

81. R. Hage, J.G. Haasnoot, D.J. Stufkens, T.J. Snoeck, J.G. Vos, and J. Reedijk, Inorg. Chem., 1989, 28,

1413.

82. F. Barigelleti, L. De Cola, V. Balzani, R. Hage, J.G. Haasnoot, J. Reedijk, and J.G. Vos, Inorg. Chem., 1989, 28, 4344.

83. R. Hage, J.G. Haasnoot, J. Reedijk, R. Wang, E.M. Ryan, J.G. Vos, A.L. Spek, and A.J.M. Duisenberg, Inorg. Chim. Acta, 1990, 174, 77.

84. B.E. Buchanan, R. Wang, J.G. Vos, R. Hage, J.G. Haasnoot, and J. Reedijk, Inorg. Chem., 1990, 29, 3263.

85. B.E. Buchanan, J.G. Vos, M. Kaneko, W.J.M. van der Putten, J.M. Kelly, R. Hage, R.A.G. de Graaff, R. Prins, J.G. Haasnoot, and J. Reedijk, J. Chem. Soc., Dalton Trans., 1990, 2425.

86. R. Hage, J.G. Haasnoot, J. Reedijk, R. Wang, and J.G. Vos, Inorg. Chem., in press.

87. R. Wang, J.G. Vos, R.H. Schmehl, and R. Hage, Submitted to J. Am. Chem. Soc..

88. B.E. Buchanan, Ph. D. Thesis, Dublin City University, 1989.

89. R. Hage, Ph. D. Thesis, Leiden University (The Netherlands), 1990.

90. P.J. Giordano, C.R. Bock, and M.S. Wrighton, J. Am. Chem. Soc., 1978, 100, 6960.

91. P.J. Giordano, C.R. Bock, M.S. Wrighton, L.V. Interrant, and R.F.X. Williams, J. Am. Chem. Soc., 1977, 99, 3187.

92. R.J. Crutchley, N. Kress, A.B.P. Lever, J. Am. Chem. Soc., 1983, 105, 1170.

93. A. Kirsch-De Mesmeaker, L. Jacquet, and J. Nasielski, Inorg. Chem., 1988, 27, 4451.

94. T. Shimizu, T. Iyoda, and K. Tzak, J. Phys. Chem., 1985, 89, 642.

95. S.H. Peterson and J.N. Demas, J. Am. Chem. Soc., 1979, 101, 6571.

96. S.H. Peterson and R.E. Shepherd, Inorg. Chem., 1983, 22, 1117.

97. P. Ford, D.E.P. Rudd, R. Gaunder, and H. Taube, J. Am. Chem. Soc., 1968, 90, 1187.

98. K. Kalyanasundaram, Inorg. Chem., 1989, 28, 4251.

99. M.K. Nazeeruddin and K. Kalyanasundaram, Inorg. Chem., 1989, 28, 4251.

100. J. Davila, C.A. Bignozzi, and F. Scandola, J. Phys. Chem., 1989, 93, 1373.

101. C. Long and J.G. Vos, Inorg. Chim. Acta, 1983, 71, 155.

102. H.A. Nieuwenhuis, J.G. Haasnnot, R. Hage, J. Reedijk, T.L. Snoeck, D.J. Stufkens, and J.G. Vos, Inorg. Chem., 1991, 30, 48.

103. R. Hage, J.G. Haasnoot, H.A. Nieuwenhuis, J. Reedijk, R. Wang, and J.G. Vos, J. Chem. Soc., Dalton Trans., in press.

104. F. Barigelleti, L. De Cola, V. Balzani, P. Belser, A. von Zelewsky, F. Vogtle, F. Ebmeyer, and S.

Grammenudi, J. Am. Chem. Soc., 1989, 111, 4662.

105. L. De Cola, F. Barigelletti, V. Balzani, P. Belser, A. von Zelewsky, F. Vogtle, F. Ebmeyer, and S. Grammenudi, J. Am. Chem. Soc., 1988, 110, 7210.

106. V. Balzani, J. Photochem. Photobiol., A: Chemistry, 1990, 51, 55.

107. L.F. Cooley, C.E.L. Headford, C.M. Elliot, and D.F. Kelly, J. Am. Chem. Soc., 1988, 110, 6673.

108. K.S. Schanze and K. Sauer, J. Am. Chem. Soc., 1988, 110, 1180.

109. G. McLendon, Acc. Chem. Res., 1988, 21, 160.

110. T. Gauarr and G. McLendon, Coord. Chem. Rev., 1985, 68, 1.

111. A.B. Tossi and J.M. Kelly, Photochem. Photobiol., 1989, 49, 545.

112. H.Y. Mei and J.K. Barton, Proc. Natl. Acad. Sci., (U.S.A.), 1988, 85, 1339.

113. R.S. Davidson and M.M. Hilchenbach, Photochem. and Photobiol., 1990, 52, 431.

114. S. Anderson, E.C. Constable, M.P. Dare-Edwards, J.B. Goodenough, A. Hamnett, K.R. Seddon, and R.D. Wright, Nature (London), 1979, 280, 571.

115. N. Vlachopoulos, P. Liska, J. Augustynski, and M. Graztel, J. Am. Chem. Soc., 1988, 110, 1216.

116. M. Gratzel, in Ref. 38.

117. B. O'Regan, J. Moser, M. Anderson, and M. Gratzel, J. Phys. Chem., 1990, 94, 8720.

118. C. Creutz and H. Taube, J. Am. Chem. Soc., 1973, 95, 1086.

119. C.A. Bignozzi, S. Roffia, C. Chiorboli, J. Davia, M.T. Indelli, and F. Scandola, Inorg. Chem., 1989, 28, 4350.

120. J.C. Curtis, J.S. Bernstein, and T.J. Meyer, Inorg. Chem., 1985, 24, 385.

121. B.P. Sullivan and T.J. Meyer, Inorg. Chem., 1980, 19, 752.

122. E.M. Kober, K.A. Goldsby, D.N.S. Narayana, and T.J. Meyer, J. Am. Chem. Soc., 1983, 105, 4303.

123. J.T. Hupp and T.J. Meyer, Inorg. Chem., 1987, 26, 2332.

124. R. Sahai, L. Morgan, and D.P. Rillema, Inorg. Chem., 1988, 27, 3495.

125. J.T. Hupp, J. Am. Chem. Soc., 1990, 112, 1563.

126. W. Kaim, S. Ernst, S. Kohlmann, and P. Welkerling, Chem. Phys. Lett., 1985, 118, 431.

127. W. Kaim and S. Kohlmann, Chem. Phys. Lett., 1987, 139, 365.

128. R.H. Schmehl, R.A. Auerbach, W.F. Wacholtz, C.M. Elliot, R.A. Freitag, and J.W. Merkert, Inorg. Chem., 1986, 25, 2440.

129. W.F. Wacholtz, R.A. Auerbach, and R.H. Schmehl, Inorg. Chem., 1987, 26, 2989.

130. R.H. Schmehl, R.A. Auerbach, and W.F. Wacholtz, J. Phys. Chem., 1988, 92, 6202.

131. J.W. Shaw, R.T. Webb, and R.H. Schmehl, J. Am. Chem. Soc., 1990, 112, 1117.

132. C.K. Ryu and R.H. Schmehl, J. Phys. Chem., 1989, 93, 7961.

133. H.E. Toma, P.R. Auburn, E.S. Dodsworth, M.N. Golovin, and A.B.P. Lever, Inorg. Chem., 1987, 26, 4257.

134. M. Haga, T. Matsumura-Inoue, and S. Yamabe, Inorg. Chem., 1987, 26, 4148.

135. R. Hage, J.G. Hassnoot, H.A. Nieuwenhuis, J. Reedijk, D.J.A. De Ridder, and J.G. Vos, J. Am. Chem. Soc., 1990, 112, 9245.

136. L. De Cola, F. Berigelleti, V. Balzani, R. Hage, J.G. Haasnoot, J. Reedijk, and J.G. Vos, Chem. Phy. Lett., 1991, 178, 491.

137. J.M. de Wolf, R. Hage, J.G. Haasnoot, J. Reedijk, and J.G. Vos, New J. Chem., 1991, 15, 501.

138. R. Hage, J.G. Haasnoot, J. Reedijk, R. Wang, and J.G. Vos, Inorg. Chem., in press.

139. N.S. Hush, Prog. Inorg. Chem., S.J. Lippard (Ed.), 1967, 8, 391.

140. N.S. Hush, Electrochim. Acta, 1968, 13, 1005.

141. J.-M. Lehn, A. Rigault, J. Siegel, J. Harrowfield, B. Chevirier, and D. Moras, Proc. Natl. Acad. Sci. (U.S.A.), 1987, 84, 2565.

142. J.-M. Lehn and A. Rigault, Angew. Chem. Int. Ed. Engl., 1988, 27, 1095.

143. U. Koert, M.M. Harding, and J.-M. Lehn, Nature

(London), 1990, 346, 339.

144. E.C. Constable, M.D. Ward, and D.A. Tocher, J. Chem. Soc., Dalton Trans., 1991, 1675.

145. E.C. Constable, M.G.B. Drew, amd M.D. Ward, J. Chem. Soc., Chem. Comm., 1987, 1610.

146. M. Barley, E.C. Constable, S.A. Corr, R.C.S. Mcqueen, J.C. Nutkins, M.D. Ward, and M.G.B. Drew, J. Chem. Soc., Dalton Trans., 1988, 2655.

147. E.C. Constable, S.M. Elder, J. Healy, M.D. Ward, and D.A. Tocher, J. Am. Chem. Soc., 1990, 112, 4590.

148. E.C. Constable, M.D. Ward, and D.A. Tocher, J. Am. Chem. Soc., 1990, 112, 1256.

149. C.J. Cathy, E.C. Constable, M.J. Hannon, D.A. Tocher, and M.D. Ward, J. Chem. Soc., Chem. Comm., 1990, 621.

150. A.W. Axup, M. Albin, S.L. May, R.J. Crutchley, and H.B. Gray, J. Am. Chem. Soc., 1988, 110, 435.

151. T.J. Meade, H.B. Gray, and J.R. Winkler, J. Am. Chem. Soc., 1989, 111, 4353.

152. J.A. Gilbert, D.S. Eggleston, W.R. Murphy, D.A. Geselowitz, D.J. Hodgson, and T.J. Meyer, J. Am. Chem. Soc., 1985, 107, 3855.

153. H.H. Thorp, J.E. Sarneski, G.W. Brudvig, and R.H. Crabtree, J. Am. Chem. Soc., 1984, 111, 9249.

154. H.H. Thorp, G.W. Brudvig, and E.F. Bowden, J. Electroanal. Chem., 1990, 290, 293.

155. R.A. Marcus and N. Sutin, Biochim. Biophys. Acta, 1985, 811, 265.

156. R.A. Marcus, J. Chem. Phys., 1956, 24, 966.

157. J.R. Miller, L.T. Calcaterra, and G.L. Closs, J. Am. Chem. Soc., 1984, 106, 3047.

158. E.M. Ryan, Ph. D. Thesis, Dublin City University, 1991.

159. B.P. Sullivan, D.J. Salmon, T.J. Meyer, and J. Peedin, Inorg. Chem., 1978, 18, 3369.

160. J.M. Calvert, J.V. Caspar, R.A. Binstead, T.D. Westmoreland, and T.J. Meyer, J. Am. Chem. Soc., 1982, 104, 6620.

161. D.W. Marquardt, Soc. Ind. Appl. Math., 1963, 11, 431.

162. J. Sipior, M. Sulkes, R.A. Auerbach, and M. Boivineau, J. Phys. Chem., 1987, 91, 2016.

163. C.K. Ryu, R. Wang, and R.H. Schmehl, unpublished results.

164. A. Casoli, A. Mangia, G. Predieri, E. Sappa, and M. Volante, Chem. Rev., 1989, 89, 407.

165. H. Veening, J.M. Greenwood, W.H. Shanks, and B.R.J. Willeford, J. Chem. Soc., Chem. Comm., 1969, 1305.

166. S.J. Valenty and P.E. Behinken, Anal. Chem., 1978, 50, 835.

167. J.W. O'Laughlin, Anal. Chem., 1982, 54, 178.

168. J.W. O'Laughlin and R.S. Hanson, Anal. Chem., 1980, 52, 2263.

169. L. Roecker, W. Kutner, J.A. Gilbert, M. Simmons, R.W. Murray, and T.J. Meyer, Inorg. Chem., 1985, 24, 3784.

170. P.K. Ghosh, B.S. Brunschwig, M. Chou, C. Creutz, and

N. Sutin, J. Am. Chem. Soc., 1984, 106, 4772.

171. B.E. Buchanan, E. Mc Govern, P. Harkin, and J.G. Vos, Inorg. Chim. Acta, 1988, 154, 1.

172. E. Mc Govern, M. Sc. Thesis, Dublin City University, 1988.

173. B.E. Buchanan, H. Hughes, J.H. van Diemen, R. Hage, J.G. Haasnoot, J. Reedijk, and J.G. Vos, J. Chem. Soc., Chem. Comm., 1991, in press.

174. L.R. Synder, J.J. Kirkland, An Introduction to Modern Liguid Chromatography, Wiley, 2nd ed., 1979.

175. J. Van Houten, R.J. Watts, J. Am. Chem. Soc., 1976, 98, 4853.

176. B. Durham, J.V. Caspar, K.K. Nagle, and T.J. Meyer, J. Am. Chem. Soc., 1982, 104, 4803.

177. J.N. Demas and G.A. Grosby, J. Am. Chem. Soc., 1971, 93, 2841.

178. J. Davila, C.A. Bignozzi, and F. Scandola, J. Phys. Chem., 1987, 93, 1373.

179. G.B. Porter and R.H. Sparks, J. Photochem., 1980, 13, 123.

180. V. Balzani, N. Sabbatini, and F. Scandola, Chem. Rev., 86, 319.

181. S.H. Peterson and J.N. Demas, J. Am. Chem. Soc., 1976, 98, 7880.

182. P. Belser, A.von Zelewsky, A. Juris, F. Barigelleti, and V. Balzani, Gazz. Chim. Ital., 1985, 115, 723.

183. S. Lumpkin and T.J. Meyer, J. Phys. Chem., 1986, 90,

5307.

184. G.H. Allen, M.A. Thesis, The University of North Carolina, 1983.

185. C.A. Bignozzi, S. Roffia, and F. Scandola, J. Am. Chem. Soc., 1985, 107, 1644.

186. A.J. Bolton and A. Mckillop, Comprehensive Heterocyclic Chemistry, Vol 5, A.R. Katrinsky and C.W. Rees (eds.), Pergamon Press, Oxford, 1984.

187. J.F. Ireland and P.A.H. Wyatt, Adv. Phys., Org. Chem., 1976, 12, 32.

188. J.V. Caspar and T.J. Meyer, J. Am. Chem. Soc., 1983, 105, 5583.

189. J.V. Caspar and T.J. Meyer, Inorg. Chem., 1983, 22, 2444.

190. Y. Kawwanishi, N. Kitamura, Y. Kim, and S. Tazuke, Riken Q, 1987, 78, 212.

191. B.L. Hauenstein, Jr., W.J. Dressick, S.L. Buell, J.N. Demas, and B.A. Degraff, J. Am. Chem. Soc., 1983, 105, 4251.

192. J.I. Cline III, W.J. Dressick, J.N. Demas, and B.A. Degraff, J. Phys. Chem., 1989, 93, 4116.

193. E.R. Carraway, J.N. Demas, B.A. Degraff, and J.R. Bacon, Anal. Chem., 1991, 63, 337.

194. C.J. Timpson, C.C. Carter, and J. Olmsted III., J. Photochem., 1989, 93, 4116.

195. P. Chen, R. Duesing, D.K. Graff, and T.J. Meyer, J. Phys., Chem., 1991, 95, 5850.

196. J.M. Lehn, Angew. Chem. Int. Edit. Engl., 1988, 27, 89.

197. V. Balzani and R. Ballaradini, Photochem. & Photobiol., 1990, 52, 409.

198. D. Plancheral, J.G. Vos, and A. von Zelewsky, J. Photochem., 1987, 36, 267.

199. Vogel's Textbook of Practical Organic Chemistry, B.S. Furniss, A.J. Hannaford, P.W.G. Smith, and A.R. Tatchell, (eds.), 5th Ed., Longman Scientific and Technical, 1989.

200. A.B.P. Lever, P.R. Auburn, E.S. Dodsworth, M.Haga, W. Liu, M. Mlink, and W.A. Nevin, J. Am. Chem. Soc., 1988, 110, 8076.

201. P. Belser, A. von Zelewsky, Helv. Chim. Acta, 1971, 57, 239.

202. E.C. Constable and J. Lewis, Inorg. Chim. Acta, 1983, 70, 251.

203. D.J.R. Fennema, J.G. Haasnoot, R. Hage, J. Reedijk, and J.G. Vos, Inorg. Chem. Acta, 1990, 171, 223.

204. A.R. Middleton, J.R. Thornback, and G. Wilkinson, J. Chem. Soc., Dalton Trans., 1980, 174.

205. V.E. Alvarez, R.J. Allen, T. Masubara and P. Ford, J. Am. Chem. Soc., 1974, 96, 7686.

206. B.S. Tovorog, S.E. Diamond, and F. Mares, J. Am. Chem. Soc., 1979, 101, 5067.

207. T. Dougherty, T.B. Lauber, and D.L. Sedney, Inorg. Chem. Acta, 1984, 86, 51.

208. P.S. Lumpkin, Ph. D. Thesis, The University of North Carolina, Chapel Hill, 1985.

209. T.D. Westmoreland, Ph. D. Thesis, The University of North Carolina, Chapel Hill, 1985.

210. K.A. Goldsby and T.J. Meyer, Inorg. Chem., 1985, 23, 3002.

211. S.W. Gersten, G.J. Sammels, and T.J. Meyer, J. Am. Chem. Soc., 1982, 104, 4029.

212. W.K. Seok and T.J. Meyer, J. Am. Chem. Soc., 1988, 110, 7558.

213. G.E. Cabaniss, A.A. Diamantis, W.R. Murphy, Jr., R.W. Linton, and T.J. Meyer, J. Am. Chem. Soc., 1985, 107, 1845.

214. O. Hammerich, Organic Electrochemistry, M.M. Baizer and H. Lund, (eds.), 1983, 2nd. Ed., Marcel Dekker, Inc., New York, p485, and references therein.

Electrochimica Acta, Vol. 35, No. 6, pp. 985–988, 1990.
Printed in Great Britain.

Appendix II

0013–4686/90 $3.00 + 0.00
Pergamon Press plc.

ELECTRODEPOSITION OF SILVER ONTO ELECTRODES COATED WITH $[Os(bipy)_2(PVP)_{10}Cl]Cl$

R. WANG, R. J. FORSTER, A. CLARKE, and J. G. VOS

School of Chemical Sciences, Dublin City University, Dublin 9, Ireland

(*Received* 30 *May* 1989; *in revised form* 7 *August* 1989)

Abstract—Silver has been deposited electrochemically onto glassy carbon electrodes modified with the redox polymer $[Os(bipy)_2(PVP)_{10}Cl]Cl$, where bipy = 2,2'-bipyridyl and PVP = poly-4-vinylpyridine. The electrodeposition process has been studied using cyclic voltammetry. For electrodes coated with the analogous ruthenium containing polymer $[Ru(bipy)_2(PVP)_{10}Cl]Cl$ no electrodeposition was observed. These results suggest a mediated electrodeposition in the case of the osmium polymer. Chronocoulometry experiments show that the charge transport behaviour of the osmium coatings does not change upon deposition of silver.

Key words: silver, electrodeposition, osmium, poly-4-vinylpyridine, redox polymer.

INTRODUCTION

In recent years it has been recognised that modified electrodes can be further modified by introducing metal particles into the polymer matrix[1–9]. A number of investigations have focused on the electrodeposition of metals onto conducting polymers. Kao and Kuwana[1] found that Pt particles dispersed into poly (vinylacetic acid) electrocatalyse hydrogen evolution and oxygen reduction. More recenty, Kuwana *et al.* reported that Pt electrodeposited into polyaniline films catalyses the reduction of hydrogen and the oxidation of methanol[2]. The electrodeposition of palladium particles within poly(thiophene) modified electrodes and their electrocatalytic activity for the reduction of oxygen was investigated by Yassar *et al.*[4].

Less attention has been paid to metal electrodeposition onto redox polymers. However, the first example of metal deposition onto polymer coatings was reported by Wrighton's group using a redox polymer[6, 7]. In this investigation Pt(IV) and Pd(II) complexes were introduced into surface bound *N*,*N*'-dialkyl-4, 4'-bipyridinium layers and then reduced to Pt(0) and Pd(0) by electrochemical or photochemical techniques. It was demonstrated that the efficiency of hydrogen evolution at a semiconductor photocathode was improved by this modification. Wrighton and coworkers also reported catalytic generation of hydrogen by deposited Rh and Pd in a cobaltacenium redox polymer on a semiconductor electrode[8]. The electrodeposition of metal particles in the redox polymer poly-$[Ru(bipy)_2(4\text{-vinylpyridine})_2]^{2+}$ has been reported by Pickup *et al.*[9].

The modification of redox polymer modified electrodes with metal particles is interesting, not only because of the aforementioned catalytic activity, but also because of other potential applications. For instance, copper deposition was used to study the microstructure of Nafion films containing conducting crystals[10]. Also, "sandwich" modified electrodes, *ie* polymer coated electrodes coated with a metal layer, have been proposed for the study of charge transport processes in redox polymers[11] whereas the application of such assemblies in electronic devices has also been proposed[12].

In this paper, we report the electrodeposition of silver onto a glassy carbon electrode coated with the redox polymer $[Os(bipy)_2PVP_{10}Cl]Cl$ (Fig. 1). To obtain information about how the electrodeposition is initiated, experiments were also carried out with the corresponding ruthenium polymer.

EXPERIMENTAL

Materials

$[Os(bipy)_2PVP_{10}Cl]Cl$ and $[Ru(bipy)_2PVP_{10}Cl]Cl$ were prepared as described elsewhere[13, 14]. All the reagents were of AR grade and used without further purification.

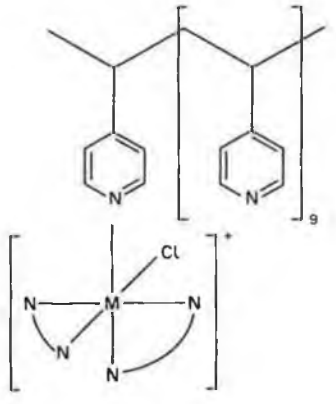

Fig. 1. Molecular structure of redox polymers $[M(bipy)_2PVP_{10}Cl]Cl$, M = Os(II), Ru(II), N–N = 2,2'-bipyridyl (bipy).

Apparatus and methods

Cyclic voltammetry was conducted using an EDT ECP133 potentiostat and galvanostat. Chronocoulometry was carried out using an EG&G PAR 175 universal programmer and 363 potentiostat, combined with a 397 digital coulometer. A Philips 3311 digital storage oscilloscope interfaced to a BBC microcomputer was used for transient data acquisition and analysis. Transient coulometric measurements were made in the 20 ms range while the potential was stepped from −0.2 to 0.8 V. By microcomputer typically three signals were averaged and background signals were subtracted. The surface coverage of the electrode surfaces was estimated from cyclic voltammograms obtained at a scan rate of 1 mV s^{-1}. As the actual swelling of the polymer in the different electrolytes is not known, it is not possible to obtain an accurate measure for the layer thickness. An estimate can be made from the density of the dry polymer (1.2 g cm^{-3}), if swelling is ignored a typical surface coverage of 1.5×10^{-8} mol cm^{-2}, has a calculated thickness of about 200 nm. The electrochemical cell used was a conventional three electrode cell. All the electrochemical potentials are referenced to *sce*. In cyclic voltammetry experiments, agar–KNO_3 salt bridges were used for separating the working solution and reference electrode. Pt foil with an area of *ca* 1.6 cm^2 was used as auxiliary electrode. Working electrodes were Teflon shrouded glassy carbon disc electrodes with a diammeter of 0.7 cm. The supporting electrolyte used for electrodeposition was 0.1 M H_2SO_4. Silver was electrodeposited using the perchlorate salt. All the experiments were performed in 20 ±2°C. Experiments on $[Ru(bipy)_2PVP_{10}Cl]Cl$ coated electrodes were conducted in the dark to avoid photochemically induced ligand exchange reactions [15, 16].

RESULTS AND DISCUSSION

Earlier experiments with the osmium containing polymer have shown the material to be very stable in a range of electrolytes. The redox potential of the Os(II/III) redox couple of interest in these studies is around +200 mV *vs sce*, depending on the electrolyte used[17]. When a $[Os(bipy)_2PVP_{10}Cl]Cl$ coated electrode in 0.1 M H_2SO_4 containing 1 mM $AgClO_4$ was held at +0.22 V for a few minutes or cycled between +0.7 and −0.2 V *vs sce*, the formation of a clear silver coating could be observed. Under these experimental conditions the redox potential of the polymer coating is +200 mV *vs sce*. This suggests that at the deposition potential used, mediation of the reduction of Ag^+ by the surface bound redox couple, as in reactions (1) and (2), is thermodynamically possible:

$$Ag^+ + Os^{2+} \rightarrow Ag^0 + Os^{3+}, \quad (1)$$

$$Os^{3+} + e^- \rightarrow Os^{2+}. \quad (2)$$

However, it is also possible that Ag^+ ions permeate from solution through the polymer and are then electrodeposited directly onto the glassy carbon surface. Further deposition on this directly deposited silver can then also result in the formation of a silver coating throughout the film. To obtain information about the nature of the electrodeposition process cyclic voltammetry was employed. On bare glassy carbon, the electrodeposition starts at about +160 mV (Fig. 2a). In the first scan, a slight hysteresis is seen, indicating the overpotential for electrodeposition of silver onto glassy carbon. This overpotential is eliminated as soon as nucleation has started (Fig. 2b). During the positive scan, a very sharp anodic wave reflects the stripping of silver from the electrode surface. In the second scan, the electrodeposition starts at a more positive potential relative to the first scan. A permanent silver coating on glassy carbon cannot be obtained using cyclic voltammetry as the deposit is stripped off during the positive scan.

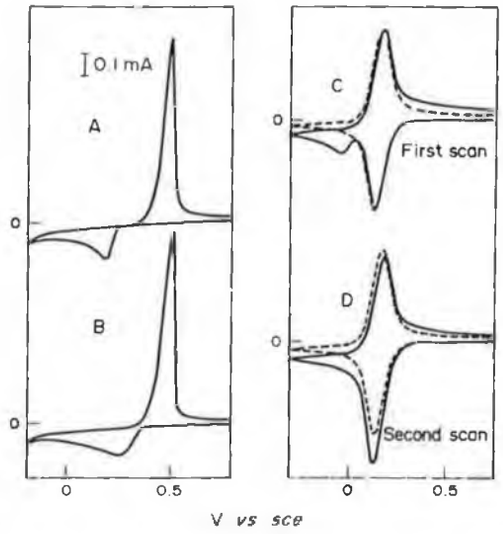

Fig. 2. Cyclic voltammograms of bare glassy carbon electrode (A, B) and $[Os(bipy)_2PVP_{10}Cl]Cl$ coated electrode (C, D) in 0.1 M H_2SO_4 + 1 mM $AgClO_4$(--- in 0.1 M H_2SO_4), scan rate 100 mV s^{-1}, surface coverage = 2.2×10^{-8} mol cm^{-2}. the current scale is the same in 2A–2D.

A $[Os(bipy)_2PVP_{10}Cl]Cl$ polymer coated electrode was first cycled in background electrolyte until the cyclic voltammogram became stable. Then the electrode was transferred to a Ag^+-containing solution and cyclic voltammograms were recorded (Fig. 2). During the first scan of the polymer coated electrode, in addition to the polymer reduction wave, a small cathodic wave appears at a potential of about +100 mV *vs sce* (Fig. 2c). During the positive scan, instead of very sharp anodic wave observed in the bare glassy carbon electrode experiment, only a small shoulder on the polymer oxidation wave is present. From the second scan on, the wave at +100 mV no longer appears, but the reductive wave of the polymer is enhanced and a small cathodic plateau current is observed. (Fig. 2d) at the same time the anodic plateau becomes lower. At slower scan rates, two slightly separated reduction peaks are seen and an anodic stripping wave is observed at + 400 mV (Fig. 3). If the scanning potential is limited to more positive potentials, where the small wave in the first scan was not reached, the reduction wave of the polymer still increases gradually and stabilises after a few minutes, indicating that also under these conditions deposition

of silver is taking place. The effect of the silver ion concentration, scanning limits and of the film thickness is shown in Fig. 4. This figure shows that at higher substrate concentration and for thin films the cathodic plateau is increased, but that there is also evidence for anodic stripping, as evidenced by a wave at +400 mV *vs sce* (compare Figs 4a and 4b). Figure 4c shows that by scanning to less negative potentials the direct deposition can be reduced considerably, so that no stripping wave is observed.

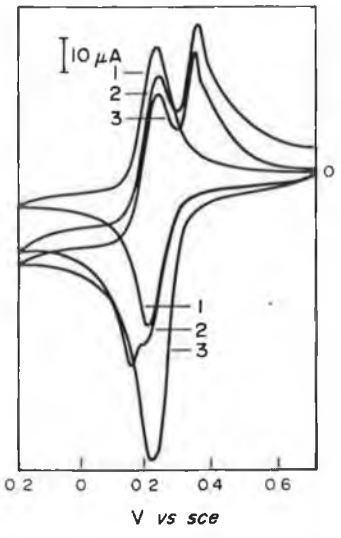

Fig. 3. Cyclic voltammetry of $[Os(bipy)_2PVP_{10}Cl]Cl$ coated electrode in 0.1 M H_2SO_4 (1) and in 0.1 M H_2SO_4 containing 1 mM $AgClO_4$. 2 and 3 are respectively the first and second scan in the silver containing solution; scan rate 5 mV s^{-1}, surface coverage 2.7×10^{-8} mol cm^{-2}

The results obtained so far clearly indicate the large influence of the polymer coating on, especially, the stripping process. It appears that the electrodeposition is, at least in part, mediated by the polymer coating and not just arising from a direct deposition of silver on the underlaying electrode surface. To further investigate the relative importance of direct and mediated electrodeposition, the analogous redox polymer $[Ru(bipy)_2PVP_{10}Cl]Cl$ was investigated. The ruthenium containing polymer is expected to have a very similar structure as the osmium containing polymer. However, the ruthenium polymer is thermodynamically unable to mediate the reduction of Ag^+ as its formal potential is more positive (about 640 mV *vs sce*) than that of the $Ag^{+/0}$ couple (590 mV *vs sce*). Therefore only electrodeposition directly on the underlaying glassy carbon surface is possible for an electrode coated with this polymer. Electrodes coated with the ruthenium containing polymer were scanned over the same potential range as used for the above described experiments with the osmium coatings. In contrast with the results obtained for the osmium coatings (Fig. 2) no reduction wave was observed at +100 mV and no differences between the first and subsequent scans was observed (Fig. 5). In the positive scan, a very small stripping wave was observed at about +400 mV indicating some electrodeposition onto the glassy carbon. It is important to note here that contrary to what is observed for the osmium polymer, the stripping process can be mediated by the polymer coating. However, when the scanning range was extended past the ruthenium redox couple, only a very small increase of the ruthenium oxidation wave, that could be interpreted as a stripping of silver, was observed (Fig. 5).

So the results obtained for the ruthenium polymer support the suggestion made before that the electrodeposition is mediated by the osmium polymer and that the osmium centres are involved in the electrodeposition process. As is also observed for the

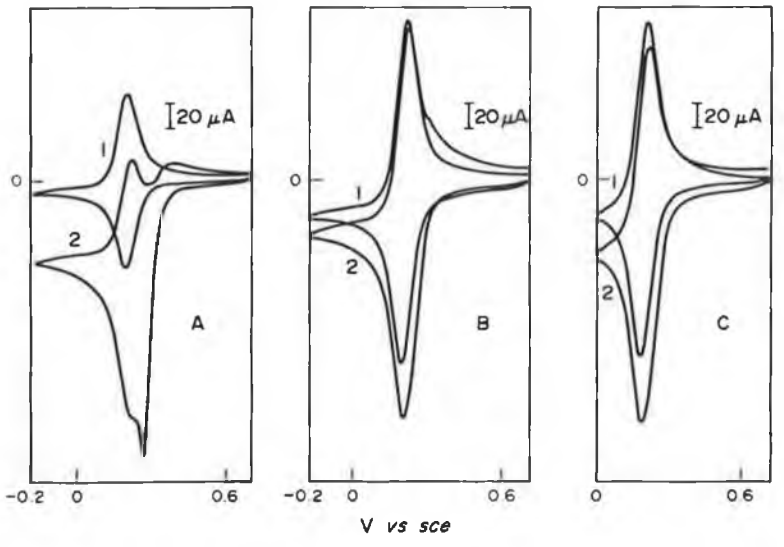

Fig. 4. Cyclic voltammetry of $[Os(bipy)_2PVP_{10}Cl]Cl$ coated electrodes in 0.1 M H_2SO_4 without (1) and with (2) $AgClO_4$, scan rate: 10 mV s^{-1}, Ag(I) concentration; (A) 3 mM and (B, C) 2 mM, surface coverage $= 1.5 \times 10^{-8}$ mol cm^{-2} for (A) and 7×10^{-8} mol cm^{-2} for (B, C); negative scan limit −200 mV *vs sce* for A and B, 0.00 mV *vs sce* for C.

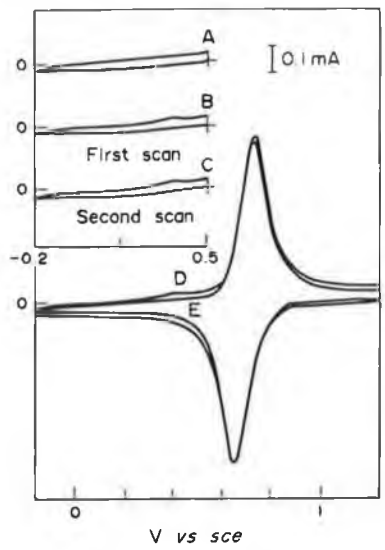

Fig. 5. Cyclic voltammetry of a $[Ru(bipy)_2(PVP)_{10}Cl]Cl$ coated electrode in 0.1 M H_2SO_4 (A, E) and in 0.1 M H_2SO_4 +1 mM $AgClO_4$ (B, C, D,) scan rate 100 mV s^{-1}, Surface coverage 1.5×10^{-8} mol cm^{-2}.

bare electrode, the mediation of the Ag(I) reduction by Os(II) is initially slow, but as soon as any nucleation occurs the subsequent deposition becomes easier. The location of this nucleation process is at this stage unclear. That direct deposition on the glassy carbon surface occurs can be seen clearly from the stripping current observed at about +400 mV *vs sce*. The magnitude of the direct deposition can be controlled by adjusting variables such as substrate concentration, layer thickness and scanning range (Fig. 4). Deposition might occur either at the underlying glassy carbon surface or in the polymer layer. However the results obtained from the ruthenium polymer suggest that even if initially direct deposition on the electrode occurs, the presence of osmium centres is needed to propagate the process through the whole layer. As stripping of the silver deposit by the osmium polymer is thermodynamically not possible, any stripping current observed must come from silver deposited directly onto the glassy carbon.

Potential-step chronocoulometry were carried out for the Os(II/III) oxidation wave using glassy carbon electrodes with a surface coverage of $2 \pm 1 \times 10^{-8}$ mol cm^{-2}. From an Anson type analysis[18] of the transient data, apparent diffusion coefficients of $6.0 \pm 1 \times 10^{-9}$ $cm^2 s^{-1}$ for the coating containing metal particles and $5.6 \pm 1 \times 10^{-9}$ $cm^2 s^{-1}$ for the polymer coating before deposition were estimated. This clearly shows that the overall charge transport properties of the layer have not been effected by the presence of the silver particles.

CONCLUSION

This study shows that it is possible to introduce metal particles into the osmium containing redox polymer *via* mediation at quite positive potentials. As anodic stripping of the silver from the polymer layer is thermodynamically unfavourable, the metal deposits can be maintained on the polymer. In this manner metal deposits with specific catalytic properties can be obtained without destroying the redox activity of the polymer itself.

Acknowledgements—The financial assistance of EOLAS for this project is gratefully acknowledged. The authors thank Johnson Matthey for a generous loan of ruthenium trichloride.

REFERENCES

1. W-H Kao and T. Kuwana, *J. Am. chem. Soc.* **106,** 473 (1984).
2. K. M. Kost, D. E. Bartak, B. Kazee and T. Kuwana, *Anal. Chem.* **60,** 2379 (1988).
3. M. D. Imisides and G. G. Wallace, *J. electroanal. Chem.* **246,** 181 (1988).
4. A. Yassar, J. Roncali and F. Garnier, *J. electroanal. Chem.* **255,** 53 (1988).
5. G. K. Chandler and D. Pletcher, *J. appl. Electrochem.* **16,** 62 (1986).
6. R. N. Dominey, N. S. Lewis, J. A. Bruce, D. C. Bookbinder, and M. S. Wrighton, *J. Am. chem. Soc.* **104,** 467 (1982).
7. J. A. Bruce, T. Murahashi and M. S. Wrighton, *J. phys. Chem.* **86,** 1552 (1982).
8. R. A. Simon, T. E. Mallouk, K. A. Daube and M. S. Wrighton, *Inorg. Chem.* **24,** 3119 (1985).
9. P. G. Pickup, K. N. Kuo and R. W. Murray, *J. electrochem. Soc.* **130,** 2205 (1983).
10. T. P. Henning, H. S. White and A. J. Bard, *J. Am. chem. Soc.* **104,** 5862 (1982).
11. P. G. Pickup and R. W. Murray, *J. Am. chem. Soc.* **105,** 4510 (1983).
12. P. G. Pickup and R. W. Murray, *J. electrochem. Soc.* **131,** 833 (1984).
13. J. M. Clear, J. M. Kelly, C. M. O'Connell and J. G. Vos, *J. Chem. Res.* (M) 3037, (1981).
14. R. J. Forster and J. G. Vos, to be published.
15. O. Haas, M. Kriens and J. G. Vos, *J. Am. chem. Soc.* **103,** 1318, (1981).
16. O. Haas, J. G. Vos and H. R. Zumbrunnen, *Electrochim. Acta* **30,** 1551 (1985).
17. R. J. Forster, A. J. Kelly, J. G. Vos and M. E. G. Lyons, *J. electroanal. Chem.* **270,** 365 (1989).
18. F. C. Anson, T. Ohsaka, and J. M. Saveant, *J. Am. chem. Soc.* **105,** 4883 (1983).

Appendix III

Selected Computer Programs

a. Program for Square Wave Voltammetry

```
 10 REM SQUARE WAVE VOLTAMMETRY (REDUCTION)
 15 REM by RENYI WANG, 1989
 20 CLS:PRINT:PRINT:PRINT
 30 PRINT"     SQUARE WAVE VOLTAMMETRY (REDUCTION)"
 40 PRINT
 50 PRINT"     DR. J.G.VOS'S RESEARCH GROUP"
 60 PRINT:PRINT:PRINT:PRINT:PRINT:PRINT:PRINT:PRINT:PRINT:PRINT
 70 INPUT"     PLEASE PRESS RETURN TO CONTINUE";Y$
 80 CLS
 90 PRINT:PRINT:PRINT:PRINT
100 PRINT"                        SQUARE WAVE VOLTAMMETRY"
110 PRINT"                              (REDUCTION)"
120 PRINT:PRINT:PRINT:PRINT:PRINT:PRINT:PRINT:PRINT:PRINT
130 PRINT"    1)                      NEW MEASUREMENT"
140 PRINT:PRINT:
150 PRINT"    2)               RECONSTRUCTION OF SAVED DATA"
160 PRINT
170 PRINT:PRINT:PRINT
180 CLEAR
190 DIM OUTPUT$(2048)
200 DIM HI$(40)
210 DIM PAR$(12)
220 DIM F$(10)
230 INPUT CHOOSE$
240 IF CHOOSE$="1" THEN CLS:GOTO260
250  IF CHOOSE$="2" THEN PRINT:PRINT:GOTO1830
260 REM EXPERIMENT SETUP
270 PRINT
280 BZ=0:AZ=1
290 PRINT"ENTER PARAMETERS"
300 PRINT
310 INPUT"INITIAL E (+/-1900mV)";INIT
320 PRINT
330 INPUT"FINAL E (+/-1900mV)";FINAL
340 PRINT
350 INPUT"SCAN INCREMENT (1-10 mV)";INCREM
360 PRINT
370 INPUT"PULSE HIGHT (1-100 mV)";PULSEMAG
380 PRINT
390 INPUT"FREQUENCY (1-1000 HZ)";T
400 PRINT
410 INPUT"CURRENT RANGE EXPONENT";RI
420 PRINT
430 INPUT"CYCLES";C
440 PRINT
450 INPUT"FILTER ON (Y/N)";Q$
460 IF Q$="Y" THEN F9=1 ELSE F9=0
470 IF Q$<>"N" THEN 450
480 PRINT
490 INPUT"TEMPERATURE IN CENTIGRADE";TEMP
500 PRINT
```

```
510 INPUT"ELECTRODE AREA IN CENTIMETER SQURE";AREA
530 INPUT"ELECTROLYTE TYPE AND CONCENTRATION";COMMENT$
550 INPUT"RUN EXPERIMENT (Y/N)";Q$
560 IF Q$="Y" THEN 600
570 IF Q$<>"N" THEN 550
580 PRINT"END PROGRAM"
590 END
600 REM RUN EXPERIMENT
610 PRINT"NOTE: TO SIMPLYFY PROGRAM, THE ONLY ERROR CHECK IS #POINTS"
620 PRINT"USE LF TERMINATOR"
630 C$="DD 10":GOSUB 1250
640 PRINT"COMPUTING PARAMETERS"
660 REM NUMBER OF POINTS
670 LET POINT=INT(ABS(FINAL-INIT)*2/INCREM)+2
680 IF POINT>2047 THEN PRINT"ERROR: >2048 POINTS":GOTO 580
690 REM PULSE HEIGHT DAC COUNTS
700 PULSEMAG=ABS(PULSEMAG)
710 IF FINAL<INIT THEN PULSEMAG=-PULSEMAG
720 PULSEMAG1=PULSEMAG*4
730 REM SCAN Inc DAC COUNTS
740 INCREM=ABS(INCREM)
750 IF FINAL<INIT THEN INCREM=-INCREM
760 INCREM1=INCREM*4
770 REM TIMEBASE (TMB) AND
780 REM SAMPLES/POINT (S/P)
790 REM FREQ=1/(TMB*S/P*2)
800 REM HIGH FREQUENCY CASE
810 IF T>500 THEN T2=1:T1=INT(10^6/(2*T)):GOTO840
820 T2=1
830 T1=INT(10^6/2/T/T2):IF T1>10000 THEN T2=T2+1:GOTO830
840 REM CALCULATE WAVEFORM PTS
850 OUTPUT$(0)=STR$(INIT*4):REM INITIAL E
860 OUTPUT$(1)=STR$(INIT*4+PULSEMAG1)
870 OUTPUT$(2)=STR$(INIT*4-PULSEMAG1)
880 FOR X=3 TO POINT
890 OUTPUT$(X)=STR$(VAL(OUTPUT$(X-2))+INCREM1)
900 NEXT X
910 REM RUN EXP & GET DATA
920 PRINT"SENDING COMMONDS TO M273"
930 PRINT
940 REM CONFIGUURE MOD DAC
950 C$="DCL;MM 2; MR 2;INTRP 0; MOD "+OUTPUT$(0)
960 GOSUB 1340
970 REM CONFIGURE MEMORY USAGE
980 C$="DCV 0;SCV 2;PCV 2;FP 0;LP "+STR$(POINT)
990 GOSUB 1340
1000 INPUT"GO ON (Y/N)";H$
1010 IF H$="Y" THEN 1030
1020 IF H$="N" THEN END ELSE 1000
1030 REM SEND WAVEFORM
1040 GOSUB 1610
1050 REM CONFIGURE ACQUISITION
1060 C$="PAM 0;SAM 1;DT 2000;SWPS "+STR$(C)+";TMB "+STR$(T1)
```

```
)
1070 GOSUB 1340
1080 C$="S/P "+STR$(T2)+";I/E "+STR$(RI)
1090 GOSUB 1340
1100 REM START EXPERIMENT
1110 PRINT"STARTING EXPERIMENT"
1120 PRINT
1130 C$="NC;CELL 1"
1140 GOSUB 1340
1150 TIME=0:REM DEAD TIME 2 SEC.
1160 IF TIME>=200 THEN 1170
1170 C$="TC;NCD;CELL 0"
1180 GOSUB 1340
1190 PRINT"EXPERIMENT COMPLETE"
1200 PRINT"GETTING DATA"
1210 PRINT
1220 C$="PCV 0;DC 1 "+STR$(POINT)
1230 GOSUB 1340
1240 GOTO1730
1250 REM IEEE ROUTINES
1260 *IEEE
1270 cmd%=OPENIN("COMMAND")
1280 data%=OPENIN("DATA")
1290 PRINT#cmd%,"BBC DEVICE NO",7
1300 PRINT#cmd%,"CLEAR"
1310 PRINT#cmd%,"REMOTE ENABLE"
1320 PRINT#cmd%,"END OF STRING",CHR$(13)+CHR$(10)
1330 pot%=OPENIN("12")
1340 PRINT#cmd%,"LISTEN",pot%,"EXECUTE"
1350 REM DEVICE DRIVER
1360 GOSUB 1390:REM SEND
1370 GOSUB 1460:REM RECEIVE
1380 RETURN
1390 REM SEND COMMAND
1400 GOSUB 1570:REM SERIAL POLL
1410 IF (ASC(serpoll$) AND 1)=1 THEN 1420 ELSE 1400
1420 PRINT#cmd%,"LISTEN",pot%,"EXECUTE"
1430 PRINT#data%,C$
1440 PRINT#cmd%,"UNLISTEN"
1450 RETURN
1460 REM RECEIVE RESPONSES
1470 I9=0:REM COUNTER
1480 GOSUB 1570:REM SERIAL POLL
1490 IF (ASC(serpoll$) AND 128)=128 THEN 1500 ELSE 1540
1500 I9=I9+1
1510 PRINT#cmd%,"TALK",pot%
1520 INPUT#data%,OUTPUT$(I9)
1530 PRINT#cmd%,"UNTALK"
1540 IF (ASC(serpoll$) AND 1)=1 THEN 1550 ELSE 1400
1550 IF (ASC(serpoll$) AND 2)=2 THEN PRINT"ERROR":END
1560 RETURN
1570 REM SERIAL POLL
1580 PRINT#cmd%,"SERIAL POLL",pot%,1
1590 INPUT#cmd%,serpoll$
1600 RETURN
```

```
1610 REM LOAD CURVE
1620 REM N=# POINTS-1 (LP)
1630 C$="LC 0 "+STR$(POINT+1)
1640 GOSUB 1390:REM SEND
1650 REM SEND ONLY   RECEIVE AFTER RECEIVING DC COMMAND
1660 PRINT#cmd%,"LISTEN",pot%,"EXECUTE"
1670 FOR X=0 TO POINT
1680 PRINT#data%,OUTPUT$(X)
1690 NEXT X
1700 PRINT#cmd%,"UNLISTEN"
1710 RETURN
1720 REM LIST DATA
1730 I=0
1740 FOR X=1 TO POINT
1750 PRINTOUTPUT$(X)
1760 I=I+1
1770 NEXT X
1780 MODE 128
1790 VDU 28,0,5,60,0
1800 PRINT"NUMBER OF DATA "; I
1810 *DISK
1820 GOTO2170
1830 REM THIS PROGRAM FOR OBTAINING DATA FROM SQWCV AND DRAW THE DATA
1840 REM ON THE SCREEN AND ON THE HI-80 PRINTER
1850 *DISK
1860 *.
1870 PRINT
1880 BZ=1:AX=0
1890 INPUT"NAME OF DATA FILE";File$
1900 PRINT:PRINT"DATA TRANSFER FROM DISK TO HOST COMPUTER"
1910 PRINT:PRINT"APPROXIMATE 20 SECONDS, PLEASE WAIT"
1920 Y=OPENIN(File$)
1930 FOR M=1 TO 10
1940 INPUT#Y,F$(M)
1950 NEXT M
1960 X=1
1970 REPEAT
1980 INPUT#Y,OUTPUT$(X)
1990 X=X+1
2000 UNTIL OUTPUT$(X-1)="STOP"
2010 CLOSE#Y
2020 POINT=VAL(F$(1))
2030 INIT=VAL(F$(2))
2040 PULSEMAG=VAL(F$(3))
2050 INCREM=VAL(F$(4))
2060 FINAL=VAL(F$(5))
2070 TEMP=VAL(F$(6))
2080 T=VAL(F$(7))
2090 RI=VAL(F$(8))
2100 AREA=VAL(F$(9))
```

```
2110 COMMENT$=F$(10)
2120 MODE 128
2130 VDU 28,0,5,60,0
2140 PRINT:PRINT"DATA TRANSFER COMPLETE"
2150 PRINT:PRINT"NUMBER OF DATA  ";X-2:PRINT
2160 PRINT"PLEASE WAIT FOF DATA DRAWING ON THE SCREEN":GOTO2220
2170 PRINT:PRINT"DATA CONVERTING IN PROGRESS"
2180 FOR X=1 TO POINT
2190 OUTPUT$(X)=STR$(-VAL(OUTPUT$(X)))
2200 NEXT X
2210 CLS:PRINT"DATA CONVERTING COMPLETE"
2220 PRINT:PRINT"DATA DRAWING IN PROGRESS"
2230 FT=1:HIFT=1:CX=FT
2240 REM BASELINE DRAWING ***********************************
2250 BASEH=500
2260 MOVE ABS(PULSEMAG),BASEH
2270 AX=ABS(FINAL-INIT+PULSEMAG)
2280 DRAW AX,BASEH
2290 REM FORWARD CURRENT ************************************
2300 MOVE AX,BASEH
2310 VOLT=AX+PULSEMAG
2320 FOR X=1 TO POINT STEP 2
2330 FX=VOLT
2340 FY=(VAL(OUTPUT$(X)))*FT+BASEH
2350 DRAW FX,FY
2360 VOLT=VOLT+INCREM
2370 NEXT X
2380 REM BACKWARD CURRENT
2390 MOVE AX,BASEH
2400 VOLT=AX-PULSEMAG
2410 FOR X=2 TO POINT STEP 2
2420 BX=VOLT
2430 BY=(VAL(OUTPUT$(X)))*FT+BASEH
2440 DRAW BX,BY
2450 VOLT=VOLT+INCREM
2460 NEXT X
2470 REM DIFFERENCE CURRENT
2480 MOVE AX,BASEH
2490 VOLT=AX+PULSEMAG
2500 FOR X=1 TO POINT STEP 2
2510 CNT1=VAL(OUTPUT$(X))
2520 CNT2=VAL(OUTPUT$(X+1))
2530 CNT=CNT1-CNT2
```

```
}
2540 DX=VOLT
2550 DY=CNT*FT+BASEH
2560 DRAW DX,DY
2570 VOLT=VOLT+INCREM
2580 NEXT X
2590 PRINT
2600 INPUT"ENTER FACTOR FOR CURRENT AXIS OR RETURN TO CONTINUE";FT
2610 IF FT=0 THEN FT=1:GOTO2640
2620 HIFT=FT:C%=FT
2630 IF FT>1 THEN CLG:GOTO2260
2640 PRINT
2650 INPUT"PRINT ON HI-80 PRINTER (Y/N)";Y$
2660 IF Y$="Y" THEN 2680 ELSE 2670
2670 IF Y$="N" THEN END ELSE 2650
2680 IF POINT>1000 THEN 2690 ELSE 2720
2690 PRINT:PRINT"DATA POINTS>1000, RETRANSFER BEFORE PRINTING, PLEASE WAIT"
2700 File$="CCCC":GOTO3800
2710 REM SET UP STARTING PARAMETERS FOR DRAWING ******************
2720 A=0:R=1
2730 DRST=INIT-FINAL
2731 DRST=ABS(DRST)
2740 REPEAT
2750 HI$(R)=STRING$(180,"*")
2760 FOR X=1 TO 40 STEP 2
2770 Y=40*A+X
2780 IF Y>POINT THEN FINISH=1:GOTO 2900 ELSE FINISH=0
2790 IF R=1 THEN 2800 ELSE 2820
2800 IF X=1 THEN HI$(R)="AM 0":GOTO 2830
2810 GOTO 2830
2820 IF X=1 THEN HI$(R)="AM 0"+","+VOLT$+","+CNT$
2830 CNT=VAL(OUTPUT$(Y))
2840 VOLT=PULSEMAG+(Y-1)/2*INCREM+DRST
2850 CNT$=STR$(CNT*HIFT)
2860 VOLT$=STR$(VOLT)
2870 HI$(R)=HI$(R)+","+VOLT$+","+CNT$
2880 NEXT X
2890 A=A+1:R=R+1
2900 UNTIL FINISH=1
2910 VDU2
2920 PRINT"HO"
2930 HIBASE=1100
2940 PRINT"MA !00,"+STR$(HIBASE)
2950 PRINT"OR"
2960 DRST$="MA "+STR$(DRST)+",0"
2970 PRINT DRST$
2980 PRINT"AM 0"
2990 GOSUB3710
3000 VDU3
3010 A=0:R=1
3020 REPEAT
3030 FOR X=2 TO 40 STEP 2
3040 Y=40*A+X
3050 IF Y>POINT THEN FINISH=1:GOTO 3170 ELSE FINISH=0
3060 IF R=1 THEN 3070 ELSE 3090
3070 IF X=2 THEN HI$(R)="AM 0":GOTO 3100
```

```
)
3080 GOTO 3100
3090 IF X=2 THEN HI$(R)="AM 0"+","+VOLT$+","+CNT$
3100 CNT=VAL(OUTPUT$(Y))
3110 VOLT=-PULSEMAG+(Y-2)/2*INCREM+DRST
3120 CNT$=STR$(CNT*HIFT)
3130 VOLT$=STR$(VOLT)
3140 HI$(R)=HI$(R)+","+VOLT$+","+CNT$
3150 NEXT X
3160 A=A+1:R=R+1
3170 UNTIL FINISH=1
3180 VDU2
3190 GOSUB3710
3200 VDU3
3210 A=0:R=1
3220 REPEAT
3230 FOR X=1 TO 40 STEP 2
3240 Y=40*A+X
3250 IF Y>POINT THEN FINISH=1:GOTO 3390 ELSE FINISH=0
3260 IF R=1 THEN 3270 ELSE 3290
3270 IF X=1 THEN HI$(R)="AM 0":GOTO 3300
3280 GOTO 3300
3290 IF X=1 THEN HI$(R)="AM 0"+","+VOLT$+","+CNT$
3300 CNT1=VAL(OUTPUT$(Y))
3310 CNT2=VAL(OUTPUT$(Y+1))
3320 CNT=CNT1-CNT2
3330 VOLT=PULSEMAG+(Y-1)/2*INCREM+DRST
3340 CNT$=STR$(CNT*HIFT)
3350 VOLT$=STR$(VOLT)
3360 HI$(R)=HI$(R)+","+VOLT$+","+CNT$
3370 NEXT X
3380 A=A+1:R=R+1
3390 UNTIL FINISH=1
3400 VDU2
3410 GOSUB 3710
3420 POTFS=10^RI
3430 LABEL$="LA"+STR$((INT(POTFS/(HIFT*204.8)*1E8+0.5))/10)+"uA"
3440 PRINT"MA 0,"+STR$(-HIBASE+300)
3450 REM ****************************************************
3460 PRINT"AX 3,1600,8,0,200,1000,50,0"
3470 PRINT"HO"
3480 REM ****************************************************
3490 PRINT"MA 500,"+STR$(-HIBASE+100)
3500 PRINT"CS3"
3510 PRINT"SI 40,25"
3520 PRINT"LA POTENTIAL mVs"
3530 PRINT"AM 0,0,200,0,300"
3540 PRINT"MA 10,230"
3550 PRINTLABEL$
3560 REM PARAMETERS STRING PRINTING ******************
3570 PAR$(1)="LA SQUARE WAVE VOLTAMETRY"
3580 PAR$(2)="LA (REDUCTION)"
3590 PAR$(3)="LA INIT. V "+STR$(INIT)+" mV"
3600 PAR$(4)="LA FINAL V "+STR$(FINAL)+" mV"
3610 PAR$(5)="LA INCREM. "+STR$(INCREM)+" mV"
```

```
3620 PAR$(6)="LA PULSE MAG. "+STR$(PULSEMAG)+" mV"
3625 PAR$(7)="LA FREQ. "+STR$(T)+" HZ"
3626 PAR$(8)="LA M273 I SETTING "+STR$(10^RI)+" A"
3627 PAR$(9)="LA SAMPLE:"
3628 PAR$(10)="LA ELECTROLYTE:"
3629 PAR$(11)="LA ELECTRODE:"
3630 PAR$(12)="LA DATE:"
3635 PABASE=1600
3640 PRINT"SI 40,20"
3641 FOR X=1 TO 12
3642 PRINT"MA 1900,"+STR$(-HIBASE+PABASE)
3643 PRINTPAR$(X)
3644 IF X=2 OR X=8 THEN PABASE=PABASE-300 ELSE PABASE=PABASE-80
3645 NEXT X
3650 PRINT"HO"
3660 PRINT"MA -100,"+STR$(-HIBASE)
3670 PRINT"OR"
3680 PRINT"IN"
3690 VDU3
3700 GOTO3750
3710 FOR Z=1 TO R
3720 PRINTHI$(Z)
3730 NEXT Z
3740 RETURN
3750 INPUT"OUTPUT TO DATA FILE (Y/N)";Y$
3760 IF Y$="Y" THEN 3770 ELSE END
3770 REM SEND DATA TO DISC
3780 *DISK
3790 INPUT"ENTER DATA FILE NO MORE THAN 7 LETTERS AND  NOT A PREVIOUSLY NAMED";File$
3800 H=OPENOUT File$
3810 PRINT#H,STR$(POINT)
3820 PRINT#H,STR$(INIT)
3830 PRINT#H,STR$(PULSEMAG)
3840 PRINT#H,STR$(INCREM)
3850 PRINT#H,STR$(FINAL)
3860 PRINT#H,STR$(TEMP)
3870 PRINT#H,STR$(T)
3880 PRINT#H,STR$(RI)
3890 PRINT#H,STR$(AREA)
3900 PRINT#H,COMMENT$
3910 FOR X=1 TO POINT
3920 PRINT#H, OUTPUT$(X)
3930 NEXT X
3940 PRINT#H,"STOP"
3950 CLOSE#H
3960 IF POINT>1000 THEN CHAIN"DRRECOM" ELSE END
```

```
 10 REM SQWCV DATA (REDUCTION) PRINTING ON HI-80 PRINTER
 20 DIM F$(10)
 30 DIM OUTPUT$(2048)
 40 DIM HI$(52)
 50 File$="CCCC"
 60 Y=OPENIN(File$)
 70 FOR M=1 TO 10
 80 INPUT#Y,F$(M)
 90 NEXT M
100 X=1
110 REPEAT
120 INPUT#Y,OUTPUT$(X)
130 X=X+1
140 UNTIL OUTPUT$(X-1)="STOP"
150 CLOSE#Y
160 POINT=VAL(F$(1))
170 INIT=VAL(F$(2))
180 PULSEMAG=VAL(F$(3))
190 INCREM=VAL(F$(4))
200 FINAL=VAL(F$(5))
210 TEMP=VAL(F$(6))
220 T=VAL(F$(7))
230 RI=VAL(F$(8))
240 AREA=VAL(F$(9))
250 COMMENT$=F$(10)
260 PRINT
270 PRINT:PRINT"DATA TRANSFER COMPLETE"
275 PRINT:INPUT"HARDCOPY ONTO HI-80 PLOTER (Y/N)";HDCO$
276 IF HDCO$="Y" THEN 280 ELSE 277
277 IF HDCO$="N" THEN 1214 ELSE 275
280 HIFT=C%
290 PRINT:PRINT"FORWARD CURRENT DATA PROCESSING"
295 REM SET UP PARAMETERS FOR DRAWING **********************
300 A=0:R=1:DRST=FINAL-INIT
310 REPEAT
320 HI$(R)=STRING$(170,"*")
330 FOR X=1 TO 40 STEP 2
340 Y=40*A+X
350 IF Y>POINT THEN FINISH=1:GOTO 470 ELSE FINISH=0
360 IF R=1 THEN 370 ELSE 390
370 IF X=1 THEN HI$(R)="AM 0":GOTO 400
380 GOTO 400
390 IF X=1 THEN HI$(R)="AM 0"+","+VOLT$+","+CNT$
400 CNT=VAL(OUTPUT$(Y))
410 VOLT=PULSEMAG+(Y-1)/2*INCREM+DRST
420 CNT$=STR$(CNT*HIFT)
430 VOLT$=STR$(VOLT)
440 HI$(R)=HI$(R)+","+VOLT$+","+CNT$
450 NEXT X
460 A=A+1:R=R+1
470 UNTIL FINISH=1
```

```
480 VDU2
490 PRINT"HO"
500 PRINT"MA 300,1300"
510 PRINT"OR"
520 PRINT"MA DRST,0"
530 PRINT"AM 8"
540 GOSUB1170
550 VDU3
560 PRINT:PRINT"BACKWARD CURRENT DATA PROCESSING"
570 A=0:R=1
580 REPEAT
590 FOR X=2 TO 40 STEP 2
600 Y=40*A+X
610 IF Y>POINT THEN FINISH=1:GOTO 730 ELSE FINISH=0
620 IF R=1 THEN 630 ELSE 650
630 IF X=2 THEN HI$(R)="AM 0":GOTO 660
640 GOTO 660
650 IF X=2 THEN HI$(R)="AM 0"+","+VOLT$+","+CNT$
660 CNT=VAL(OUTPUT$(Y))
670 VOLT=-PULSEMAG+(Y-2)/2*INCREM+DRST
680 CNT$=STR$(CNT*HIFT)
690 VOLT$=STR$(VOLT)
700 HI$(R)=HI$(R)+","+VOLT$+","+CNT$
710 NEXT X
720 A=A+1:R=R+1
730 UNTIL FINISH=1
740 VDU2
750 GOSUB1170
760 VDU3
770 PRINT:PRINT"DIFFERENCE CURRENT DATA PROCESSING"
780 A=0:R=1
790 REPEAT
800 FOR X=1 TO 40 STEP 2
810 Y=40*A+X
820 IF Y>POINT THEN FINISH=1:GOTO 960 ELSE FINISH=0
830 IF R=1 THEN 840 ELSE 860
840 IF X=1 THEN HI$(R)="AM 0":GOTO 870
850 GOTO 870
860 IF X=1 THEN HI$(R)="AM 0"+","+VOLT$+","+CNT$
870 CNT1=VAL(OUTPUT$(Y))
880 CNT2=VAL(OUTPUT$(Y+1))
890 CNT=CNT1-CNT2
900 VOLT=PULSEMAG+(Y-1)/2*INCREM+DRST
910 CNT$=STR$(CNT*HIFT)
920 VOLT$=STR$(VOLT)
930 HI$(R)=HI$(R)+","+VOLT$+","+CNT$
940 NEXT X
```

```
)
  950 A=A+1:R=R+1
  960 UNTIL FINISH=1
  970 VDU2
  980 GOSUB 1170
  990 POTFS=10^RI
 1000 LABEL$="LA"+STR$((INT(POTFS/(HIFT*2048)*1E6*100*10+0.5))/10)+"uA"
 1010 PRINT"MA 0,-1000"
 1020 PRINT"AX 3,1000,9,0,0,1000,50,0"
 1030 PRINT"HO"
 1040 PRINT"MA 600,-1200"
 1050 PRINT"CS3"
 1060 PRINT"SI 40,25"
 1070 PRINT"LA POTENTIAL mVs"
 1080 PRINT"AM 0,0,200,0,300"
 1090 PRINT"MA 10,230"
 1100 PRINTLABEL$
 1110 PRINT"HO"
 1120 PRINT"MA -300,-1100"
 1130 PRINT"OR"
 1140 PRINT"IN"
 1150 VDU3
 1160 GOTO1210
 1170 FOR Z=1 TO R
 1180 PRINTHI$(Z)
 1190 NEXT Z
 1200 RETURN
 1210 IF AZ=1 THEN 1211 ELSE END
 1211 INPUT"OUTPUT TO DATA FILE (Y/N)";Y$
 1212 IF Y$="Y" THEN 1214 ELSE 1213
 1213 IF Y$<>"N" THEN 1211 ELSE END
 1214 REM SAVE DATA TO DISC
 1215 *DISK
 1220 INPUT"ENTER DATA FILE NO MORE THAN 7 LETTERS AND NOT PREVIOUSLY USED";File$
 1230 H=OPENOUT(File$)
 1240 PRINT#H,STR$(POINT)
 1250 PRINT#H,STR$(INIT)
 1260 PRINT#H,STR$(PULSEMAG)
 1270 PRINT#H,STR$(INREM)
 1280 PRINT#H,STR$(FINAL)
 1290 PRINT#H,STR$(TEMP)
 1300 PRINT#H,STR$(T)
 1310 PRINT#H,STR$(RI)
 1320 PRINT#H,STR$(AREA)
 1330 PRINT#H,COMMENT$
 1340 FOR X=1 TO POINT
 1350 PRINT#H,OUTPUT$(X)
 1360 NEXT X
 1370 PRINT#H,"STOP"
 1380 CLOSE#H
 1390 END
```

b. pK_a and pK_a^* data analysis.

```
 10 MODE 128
 20 REM COPYRIGHT BY RENYI WANG AND BORIS FENNEMA
 30 CLS
 40 PRINT"THIS PROGRAM CALCULATES THE PKA OR PKA* BY USING THE INTENSITY"
 50 PRINT:PRINT
 60 PRINT"DIFFERENCE METHOD [P%=INTENSITY(I)-INTENSITY(MAX)/DIFFERENCE OF"
 70 PRINT:PRINT
 80 PRINT"MINIMUM AND MAXIMUN INTENSITY] BASED ON EMMISION OR ABSORPTION "
 90 PRINT:PRINT
100 PRINT"EXPERIMENTS. FOR EMMISION PLEASE USE FIXED SCALE VALUES AND FOR "
110 PRINT:PRINT
120 OLDFILE=0
130 PRINT"ABSORPTION USE THE ABSORPTION DATA. IF YOU WANT TO USE "
140 PRINT:PRINT
150 PRINT"THE PEAK HEIGHT FROM THE EMISSION MEASUREMENTS PLEASE"
160 PRINT:PRINT
170 PRINT"TYPE A FOR ADSORPTION AND GIVE THE PEAK HEIGHT WHEN"
180 PRINT:PRINT
190 PRINT"ASKED FOR INTENSITY DATA."
200 PRINT:PRINT
210 PRINT"ALL OPTIONS HAVE A DEFAULT SETTING SHOWN IN [],"
220 PRINT:PRINT
230 PRINT"IF YOU USE THIS SETTING AS WELL JUST TYPE RETURN."
240 PRINT:PRINT
250 REM RESERVING SPACE FOR VARIABLES//////////////////////////////
260 DIM PRC(50)
270 DIM WEN(50)
280 DIM PH(50)
290 DIM PH$(50)
300 DIM EN(50)
310 DIM WENN(50)
320 DIM PHN(50)
330 DIM DIF(50)
340 INPUT"ARE YOU USING EMMISION (E) OR ABSORPTION (A) DATA :[E]"; MEAS$
350 IF MEAS$<>"A" THEN MEAS$="E"
360 PRINT:PRINT:PRINT:
370 INPUT"DO YOU WANT TO ENTER NEW DATA (N) OR EDIT OLD DATA FROM A FILE (O):[N]";L$
380 IF L$<>"O" THEN L$="N"
390 REM OPENING OLD DATAFILE IN 1510//////////////////////////
400 IF L$="O" THEN 1610
410 CLS
420 PRINT"PLEASE ENTER A (/) FOR THE PH AT THE END OF DATA"
430 PRINT:PRINT:PRINT
440 I=1
450 REPEAT
460 INPUT"ENTER PH       "; PH$(I)
470 IF PH$(I)="/" THEN 510
480 PH(I)=VAL(PH$(I))
490 INPUT"ENTER INTENSITY DATA";"        "; EN(I)
500 I=I+1
```

```
510 UNTIL PH$(I)="/"
520 REM FINISHING NEW DATA INPUT//////////////////////////////
530 DA=I-1
540 CLS
550 PRINT
560 REM TRANSFER OF FIXSCALE INTO INTENSITY//////////////////////
570 FOR I=1 TO DA
580 IF MEAS$<>"A" THEN WEN(I)=1/EN(I)  ELSE WEN(I)=EN(I)
590 NEXT I
591 PRINT" ----------------------------------------"
600 PRINT"  NO         PH           INTENSITY"
610 PRINT" ----------------------------------------"
611 PRINT
620 FOR I=1 TO DA
630 PRINT"  ";I,"  ";PH(I),"        ";WEN(I)
640 NEXT I
650 PRINT
651 PRINT" ----------------------------------------"
652 PRINT:PRINT:
660 INPUT"DO YOU WANT TO EDIT THIS DATA (Y/N):[N]";M$
670 PRINT:PRINT:PRINT
680 IF M$<>"Y" THEN M$="N"
690 IF M$="Y" THEN 700 ELSE 1080
700 PRINT
710 INPUT"DO YOU WANT TO CHANGE (C), DELETE (D) OR ADD (A) DATA:";DD$
720 IF DD$="C" THEN 750
730 IF DD$="D" THEN 840
740 IF DD$="A" THEN 960
750 PRINT:PRINT:PRINT
760 INPUT"GIVE NUMBER OF THE DATAPOINT";DP
770 PRINT
780 INPUT"(NEW) PH VALUE FOR THIS POINT";PH(DP)
790 PRINT
800 INPUT"(NEW) INTENSITY DATA FOR THIS POINT";WEN(DP)
810 IF MEAS$<>"A" THEN WEN(DP)=1/WEN(DP)
820 GOTO 1040
830 REM DELETING DATA//////////////////////////////////////////////////
840 PRINT:PRINT:PRINT
850 INPUT"GIVE THE NUMBER OF THE DATA POINT YOU WANT TO DELETE:";DP
860 FOR X=1 TO DA
870 IF X>DP-1 THEN WENN(X)=WEN(X+1) ELSE WENN(X)=WEN(X)
880 IF X>DP-1 THEN PHN(X)=PH(X+1) ELSE PHN(X)=PH(X)
890 NEXT X
900 DA=DA-1
910 FOR X=1 TO DA
920 WEN(X)=WENN(X)
930 PH(X)=PHN(X)
940 NEXT X
950 GOTO 1040
960 REM ADDING A DATA POINT////////////////////////////////////////////
970 PRINT:PRINT:PRINT
980 DA=DA+1
990 OLDFILE=1
1000  INPUT" PH VALUE FOR THIS POINT,PLEASE";PH(DA)
1010 PRINT
```

```
1020 INPUT" INTENSITY DATA FOR THIS POINT";WEN(DA)
1030  IF MEAS$()"A" THEN WEN(DA)=1/WEN(DA)
1040 FOR X=1 TO 1000
1050 NEXT X
1060 CLS
1070 GOTO 600
1080 FOR X=1 TO DA
1090 IF MEAS$()"A" THEN EN(X)=1/WEN(X)  ELSE EN(X)=WEN(X)
1100 NEXT X
1110 REM CALCULATING THE DIFFERENCE AND PERCENTAGE//////////////////////
1120 ENMAX=0
1130 ENMIN=1000
1140 FOR I=1 TO DA
1150 IF WEN(I)>ENMAX THEN ENMAX=WEN(I)
1160 NEXT I
1170 FOR I=1 TO DA
1180 IF WEN(I)<ENMIN THEN ENMIN=WEN(I)
1190 NEXT I
1200 BOT=ENMAX-ENMIN
1210 FOR I=1 TO DA
1220 DIF(I)=ENMAX-WEN(I)
1230 PRC(I)=100-((DIF(I)/BOT)*100)
1240 NEXT I
1250 PRINT"DO YOU WANT A HARDCOPY OF THE CALCULATED DATA (Y/N):[Y]"
1260 PRINT:PRINT:PRINT
1270 INPUT"(SWITCH ON PRINTER PLEASE)                              ";Z$
1280 REM PREPARING FOR HARDCOPY//////////////////////////////////////
1290 CLS
1300 IF Z$()"N" THEN VDU2
1310 PRINT "  PH(I)";"       INTENSITY(I)";"     PERCENTAGE(I)";
1320 PRINT:PRINT
1330 FOR I=1 TO DA
1340 PRINT
1350 PRINT "   ";PH(I)"               ";WEN(I)"              ";PRC(I)
1360 NEXT I
1370 IF Z$()"N" THEN VDU3
1380 PRINT:PRINT:PRINT
1390 INPUT"DO YOU WANT THE CALCULATED DATA IN A FILE (Y/N):[Y]"; K$
1400 REM FILING NEW DATA//////////////////////////////////////////////
1410 IF K$()"N" THEN K$="Y" ELSE  1560
1420 IF OLDFILE=1 THEN PRINT:PRINT:PRINT:PRINT"PLEASE CHOOSE A DIFFERENT FILE NAME"
1430 PRINT:PRINT:PRINT
1440 INPUT"PLEASE GIVE A FILE NAME (NOT MORE THAN 7 SYMBOLS):";File$
1450 H=OPENOUT(File$)
1460 PRINT#H,DA
1470 FOR I=1 TO DA
1480 PRINT#H, EN(I)
1490 PRINT#H, PH(I)
1500  PRINT#H, PRC(I)
1510 IF I=DA THEN 1530
1520 PRINT#H, DIF(I)
```

```
1530 NEXT I
1540 PRINT#H,"STOP"
1550 CLOSE#H
1560 REM PREPARING FOR CHAINING PLOT PRG//////////////////////////
1570 PRINT:PRINT:PRINT
1580 INPUT"DO YOU WANT TO MAKE A GRAPH OF THE DATA(Y/N):[Y]";P$
1590 IF P$<>"N" THEN CHAIN"PLOTPRW" ELSE END
1600 REM OPENING OLD FILE//////////////////////////////////////
1610 PRINT:PRINT:INPUT"GIVE FILE NAME PLEASE:";File$
1620 Y=OPENIN(File$)
1630 INPUT#Y,DA
1640 FOR I=1 TO DA
1650 INPUT#Y, EN(I)
1660 INPUT#Y, PH(I)
1670 INPUT#Y, PRC(I)
1680 IF I=DA THEN 1700
1690 INPUT#Y, DIF(I)
1700 NEXT I
1710 CLOSE#Y
1720 GOTO 540
```

```
 10 MODE 128
 20 CLS
 30 PRINT"THIS PROGRAM PLOTS THE DATA FROM THE CALCULATIONS MADE IN BORIS. "
 40 PRINT:PRINT:PRINT
 50 PRINT"IT IS NECESSARY TO LOAD THE EXTRA PRINT PROGRAM FOR DRAWING THE GRAPH."
 60 PRINT:PRINT:PRINT
 70 PRINT"SO BE SURE THAT R.RAMPRNT 8000 W Q IS LOADED."
 80 PRINT:PRINT:PRINT
 90 PRINT"IF NOT,TYPE CTRL BREAK,FOLLOWED BY *SRLO.R.RAMPRNT 8000 W Q "
100 PRINT:PRINT:PRINT
110 PRINT"AGAIN FOLLOWED BY CTRL BREAK."
120 PRINT:PRINT:PRINT
130 PRINT:PRINT:PRINT
140 PRINT"PRESS <RETURN> TO CONTINUE"
150 WAIT$="WAIT"
160 REPEAT
170 INPUT WAIT$
180 UNTIL WAIT$<>"WAIT"
190 TITLE$=""
200 REM *** by Barbara B. Kebbekus,1983 //REVISED BY B.FENNEMA 1989 FOR PKA
```

```
210  REM *** CALCULATIONS
220  MODE1:@%=&600
230 XLO=0 :XHI=10 :YLO=0:YHI=100:NX=10:NY=10
240 LABX$="PH":LABY$="PERCENTAGE"
250DIM X(60),Y(60)
260 DIM EN(50)
270 DIM DIF(50)
280GOTO290
290CLS
300 REM Recall data from disk
310 PRINT:PRINT"GIVE FILE NAME PLEASE TO RECOVER "
320 PRINT:PRINT: INPUT"DATA FROM DISC:";FILE$
330 Z=OPENIN(FILE$)
340 INPUT#Z,DA
350 FOR I=1 TO DA
360 INPUT#Z,EN(I)
370 INPUT#Z,X(I)
380 INPUT#Z,Y(I)
390 IF I=DA THEN 410
400 INPUT#Z,DIF(I)
410 NEXT I
420 CLOSE#Z
430 CT=DA
440CLS: REM Set up graph
450PRINT"X-AXIS MINIMUM ";XLO;:INPUT TXLO$
460 IF TXLO$<>"" THEN XLO=VAL(TXLO$)
470PRINT"X-AXIS MAXIMUM ";XHI;:INPUT TXHI$
480 IF TXHI$<>"" THEN XHI=VAL(TXHI$)
490PRINT"# OF DIVISIONS ON X-AXIS ";NX;:INPUT TNX$
500 IF TNX$<>"" THEN NX=VAL(TNX$)
510PRINT"Y-AXIS MINIMUM ";YLO;:INPUT TYLO$
520 IF TYLO$<>"" THEN YLO=VAL(TYLO$)
530PRINT"Y-AXIS MAXIMUM ";YHI;:INPUT TYHI$
540 IF TYHI$<>"" THEN YHI=VAL(TYHI$)
550  PRINT"# OF DIVISIONS ON Y-AXIS ";NY;:INPUT TNY$
560 IF TNY$<>"" THEN NY=VAL(TNY$)
570 PRINT"X-AXIS LABEL ",LABX$:INPUT LINE TLABX$: IF TLABX$<>"" THEN LABX$=TLABX$
580PRINT"Y-AXIS LABEL ",LABY$ :INPUT LINE TLABY$: IF TLABY$<>"" THEN LABY$=TLABY$
590 REM Draw graph
600 XSC=(XHI-XLO)/NX:YSC=(YHI-YLO)/NY
610  XINT=INT(1000/NX)
620  YINT=INT(700/NY)
630 MODE0
640VDU5
650MOVE200,200:DRAW1200,200
660 MOVE200,200
670 FORK=1TONX
680   PLOT0,XINT,-10
690 PLOT1,0,10
700NEXTK
710MOVE200,200:DRAW200,900
```

```
720 MOVE200,200
730 FORK=1TONY
740  PLOT0,-10,YINT
750PLOT1,10,0
760NEXTK
770  LX=XLO
780FORK=0TONX
790   MOVE180+K*XINT,170
800 PRINT LX
810LX=LX+XSC
820NEXTK
830  LY=YLO
840FORK=0TONY
850    MOVE100,200+K*YINT
860PRINT LY
870LY=LY+YSC
880NEXTK
890FORK=1TOCT
900X=(XINT *(X(K)-XLO)/XSC)+200
910Y=(YINT *(Y(K)-YLO)/YSC)+200
920PROCCROSS(X,Y)
930 NEXTK
940 MOVE 620-7*LEN(TITLE$),1000:PRINTTITLE$
950 MOVE620-8*LEN(LABX$),125:PRINT LABX$
960 FORK=0 TO LEN(LABY$)-1:MOVE0,(500+16*LEN(LABY$))-32*K:PRINT MID$(LABY$,1+K,1):NEXTK
970  GOSUB 1030
980 ZZ$=GET$
990 *FX6,0
1000 IF ZZ$="P" THEN CLS:*GDUMP 1 0 3 1
1010 XX=INSTR(" P",ZZ$):IF XX=0 GOTO980
1020 VDU4:GOTO1070
1030VDU4:VDU28,0,31,39,29
1040PRINT"<P> For Printer, <SPACE> To Continue"
1050 RETURN
1060 REM Display menu
1070VDU26: CLS:PRINT TAB(5,3)"<1> RETURN TO DATA EDITING":PRINT TAB(5,5)"<2> REDO GRAPH":PRINTTAB(5,7)"<3> END PROGRA
1080 INPUTQQ:IF QQ<1 OR QQ>3 GOTO1080
1090 IF QQ=1 THEN CHAIN"BORISWA"
1100 IF QQ=2 THEN 440
1110 IF QQ=3 THEN 1120
1120 CLS:CLOSE#0:END
1130 DEF PROCCROSS(X,Y)
1140  MOVEX,Y-6
1150  PLOT1,0,13
1160  MOVEX-6,Y
1170  PLOT1,13,0
1180 ENDPROC
```

Publication List

1. R. Wang, R.J. Forster, A. Clarke and J.G. Vos, "Electrodeposition of Silver onto Electrodes Coated with $[Os(bpy)_2PVP_{10}Cl]Cl$", Electrochim. Acta, 1990, 35, 985.

2. R. Wang, J.G. Vos, R.H. Schmehl and R. Hage, "pH Control of Photoreactivity of Ru(II) Pyridyltriazole Complexes: Photoinduced Linkage Isomerism and Photoanation", submitted to J. Am. Chem. Soc..

3. R. Hage, J.G. Haasnoot, J. Reedijk, R. Wang, E. Ryan, J.G. Vos, A.L. Spek, and A.J.M. Duisenberg, "Synthesis, Spectroscopic and Electrochemical Properties and X-ray Studies of Bis(2,2'-bipyridyl)(3-(2-hydroxy-phenyl)-5-(pyridin-2-yl)-1,2,4-triazole)ruthenium(II)hexafluro-phosphate", Inorg. Chim. Acta, 1990, 74, 77.

4. B.E. Buchanan, R. Wang, J.G. Vos, R. Hage, J.G. Haasnoot and J. Reedijk, "Chromatographic Separation and Charaterisation of Linkage Isomers of the 3-(pyridin-2-yl)-1,2,4-triazole Complex of Ruthenium(II) bis(2,2'-bipyridyl)", Inorg. Chem., 1990, 29, 3263.

5. R. Hage, J.G. Haasnoot, J. Reedijk, R. Wang and J.G. Vos, "The Effect of the Coordination Mode on the Acid-Base Properties of Pyrazyltriazole Ligands Bound to Ruthenium(II)bis(2,2'-bipyridyl) Moities", J. Chem. Soc. Dalton Trans., in press.

6. J.H. van Dieman, J.G. Haasnoot, R. Hage, J. Reedijk, J.G. Vos and R. Wang, "Orthometalated Rh(II) Complexes Containing Substituted Triazoles. Synthesis, Struture, Electrochemical, and Electronic Properties. X-ray Structure of [3-(pyridin-2-yl)-5-phenyl-1,2,4-triazole-bis(2-(2-phenylato)pyridine)rhodium(II) Hexaflurophosphate.monoacetone", submitted to Inorg. Chem..

7. R. Hage, J.G. Haasnoot, J. Reedijk, Renyi Wang, and J.G. Vos, "Mononuclear and Dinuclear Ruthenium Complexes with Triazole Containing Ligands; Fine-tuning of the Spectroscopic Properties", Inorg. Chem., in press.